

Low Power Loss Gears: Influence of Design, Materials and Oil Formulation

DEMec

CETRIB – INEGI

Rui Manuel Lino da Silva

Dissertação do MIEM

Orientador no CETRIB: Eng. Luís Magalhães

Orientador na FEUP: Prof. Jorge Seabra



FEUP

Faculdade de Engenharia da Universidade do Porto

Mestrado Integrado em Engenharia Mecânica

Julho 2010

Dissertation submitted to the “Faculdade de Engenharia da Universidade do Porto” within the “Dissertação” course

**Low Power Loss Gears:
Influence of Design, Materials and Oil
Formulation**

Rui Silva

DEMec – Mechanical Engineering Department

Engineering Faculty

Oporto University

Oporto, July 2010

To my Parents and Fiancée

Resumo

As crescentes necessidades energéticas e o aparecimento de uma consciência ambiental no seio da indústria, levou à procura de componentes mecânicos mais eficientes e óleos lubrificantes com menos impacto na natureza, ou seja, lubrificantes com uma alta taxa de biodegradabilidade.

Sendo as transmissões por engrenagens, um dos componentes mais comuns na indústria automóvel e nas máquinas industriais, surgiu a necessidade de melhorar a sua eficiência recorrendo ao conceito de engrenagens de baixa perda de potência, (“Low Loss Gears”) as quais não são mais do que engrenagens de alto rendimento que podem ser fabricadas com ferramentas standard presentes em qualquer empresa do ramo. A este conceito de engrenagens de elevado rendimento acrescenta-se o uso de lubrificantes biodegradáveis com um pacote de aditivos satisfazendo ao mesmo tempo o decréscimo nas perdas de energia combinado com um menor impacto para a natureza por parte dos lubrificantes.

Neste trabalho foram usadas três geometrias “Low Loss” em aço de cementação (20MnCr5) e ADI (ferro nodular austemperado) e lubrificadas com dois lubrificantes diferentes, um éster altamente saturado e de baixa toxicidade (E2) e um óleo de base polialfaolefínica sintético de alta performance (P1). Ambas as engrenagens e respectivos óleos foram submetidos a ensaios de perda de potência numa máquina FZG. Uma versão alternativa do mesmo ensaio de perda de potência com um nível de óleo reduzido, foi também executado para estudar a influência do nível de óleo na perda de potência da engrenagem.

Após a análise e discussão de todos os ensaios verifica-se que em média o rendimento do engrenamento aumenta quando:

- o módulo diminui e as correcções x_1 e x_2 são fortemente positivas;
- é utilizado o óleo E2 ao invés do P1 especialmente a baixas e médias velocidades;
- são utilizadas engrenagens em aço, pois libertam consideravelmente menos partículas que o ADI, mas o ADI tem um comportamento superior ao do aço na maioria dos casos, podendo ser uma óptima alternativa ao aço pois é mais barato e fácil de maquinar.
- O nível de óleo é mais baixo, atingindo diminuições de temperatura até 40% em alguns casos.

Low Power Loss Gears – Design and Experimental Evaluation

Abstract

The growing energy needs and the appearance of an environmental awareness among industrial world lead to the search of more efficient mechanical components and lubricant oils with less impact into nature, in other words, lubricant oils with a high level of biodegradability.

Being gear transmissions some of the most common components in automotive industries and industrial machines, arose the need to improve their efficiency using the “Low Loss Gears” concept, which are high efficiency gears manufactured with standard cutting tools. Associated with this concept is the use of biodegradable lubricants with a additives package serving at the same time the need of less energy dissipation combined with a lower environmental impact.

In this work three “Low Loss” gear geometries manufactured in carburized steel (20MnCr5) and ADI (Austempered Ductile Iron) and lubricated with two different lubricants, a highly saturated biodegradable low toxicity ester base oil(E2) and a fully synthetic polyalphaolefine high performance industrial gear oil (P1), Both gears and respective lubricants were submitted to a power loss test in a FZG test rig. An alternative version of the power loss test with a reduced oil level was also performed to assess oil level influence in gear power losses.

After the analysis and discussion of all tests could be concluded that in average, the gearing efficiency increased when:

- The modulus m decreases and x_1 and x_2 are strongly positive;
- E2 oil is used instead of P1 oil, specially at slow and medium speeds;
- Steel gears are used, because they release much less particles to the lubricant oil than the ADI ones, but ADI has in general better behavior to the steel ones, being a good alternative due to the fact it's cheaper and easy to manufacture than the steel.
- The oil level is lower, reaching temperature decreases up to 40% in some cases.

ACKNOWLEDGMENTS

This work could not have been done without the help of a wide group of people from all kinds of personal relationship levels.

First I would like to express my immense gratitude and love to my parents that have made a huge sacrifice to support all these years of college education without asking anything in return and also their supportive and understanding behavior during those times when things didn't go as planned.

Second of all, I would like to thank the unconditional support of my fiancée Silvia, who never let me lay down my hands and encourage me to fight for my goals and to be a better student and person. Also a word of recognition for the countless weekends spent away from her, studying, passing our relationship for a second plan, which she handles with grace.

A sincere word of appreciation goes to Prof. Jorge Seabra, person that much contributed to my evolution as a student, and in this new world of scientific research. I would like to thank him also for his help putting together this thesis, his enormous patience, the time and dedication he invested in me so that I could do a good work, and his effort to provide me with great work conditions and environment.

My appreciation goes also to all the CETRIB/INEGI team, that always provide me with a fantastic work environment with a constant feeling of fellowship and friendship. In the CETRIB unit I would like to thank the precious help of Dr. Ramiro Martins that patiently guide me through all the different processes involved in the experimental testing and result analysis performed along this work. Another important person I would like to thank is Engineer Beatriz Graça for her help with the huge amount of oil analysis necessary for this work and the result corresponding analysis.

A word of appreciation is also directed to my project leader in CETRIB Dr. Luís Magalhães, for his constant availability to enlighten me in all aspects of my experimental investigation, and also all the other colleagues from CETRIB Tiago Cousseau, José Brandão, Armando Campos and Jorge Castro, for their friendship and for providing me with a great work environment.

I would also like to thank FEUP (Faculdade de Engenharia da Universidade do Porto) and INEGI (Instituto de Engenharia e Gestão industrial) for the conditions provided to the realization of this dissertation. I would like to thank also to INEGI and FCT (Fundação para a Ciência e Tecnologia) for the scholarship provided that helped covering my financial expenses during this time.

Table of Contents

Resumo	iii
Abstract	v
ACKNOWLEDGMENTS	vii
Figure Index.....	xiii
Table Index.....	xvii
Nomenclature	xix
Introduction.....	xxiii
1. GEAR TRIBOLOGY	3
1.1. Tribology	3
1.2. Tribology of the contact between gear teeth	3
1.2.1. Teeth contact force.....	4
1.2.2. Curvature radius	6
1.2.3. Contact Pressure	7
1.2.4. Contacting teeth sub-surface stress state	8
1.2.5. Surfaces velocities.....	11
1.2.6. Lubricant film thickness	13
1.2.7. Inlet shear heating in an EHD contact.....	15
1.2.8. Specific lubricant film thickness.....	16
1.2.9. Lubrication Regimes	17
1.2.10. Friction coefficient in gear teeth	20
1.2.11. Teeth flank temperature	23
1.2.12. Lubricant temperature.....	24
1.3. Lubricant oils	26
1.3.1. Vegetable and animal lubricant oils.....	26
1.3.2. Mineral based lubricant oils.	26
1.3.3. Synthetic base lubricant oils	27
1.3.4. Additives.....	27
1.3.5. Lubricant classification – Viscosity Grades	28
1.4. Gear lubrication.....	32
1.5. Gear failure modes.....	33
1.5.1. Current wear.....	34
1.5.2. Scoring and scuffing.....	35
1.5.3. Pitting (spalling)	36

1.5.4.	Micro-Pitting (Gray Staining).....	36
1.6.	Gear power loss.....	37
1.6.1.	Load dependent power losses.....	38
1.6.2.	No Load dependant power losses	39
1.6.3.	Heat removal	40
2.	Gears, Materials and Oils.....	45
2.1.	Low loss gears	45
2.2.	Gears geometry	47
2.2.1.	Geometry of low loss gears 311, 411 and 611	48
2.2.2.	Geometry of low loss gears 312, 412 and 612	50
2.3.	Gears Material.....	52
2.3.1.	ADI (Austempered Ductile Iron)	52
2.3.2.	Carburized steel (DIN 20MnCr5).....	54
2.4.	Tested gear oils	56
3.	Test Machines and Procedures.....	59
3.1.	FZG test rig.....	59
3.2.	Pressure pads	61
3.3.	Power loss test procedure.....	62
3.4.	Churning loss test procedure.....	64
3.5.	Surface Roughness and Topography Measurement	64
3.6.	Mass loss procedure	67
3.7.	Oil Analysis Procedures	68
3.7.1.	Direct Reading Ferrometry: Equipment and procedure.....	68
3.7.2.	Analytic Ferrography: Equipment and procedure	70
4.	Experimental results.....	75
4.1.	Ester base (E2) lubricant oil gear test	75
4.1.1.	Stabilization temperatures – Ester gear oil (E2), high oil level and steel gears..	75
4.1.2.	Stabilization temperatures – Ester gear oil E2, high oil level and ADI gears ..	77
4.1.3.	Oil analysis wear particles – Ester gear oil E2, high oil level, steel and ADI...	79
4.1.4.	Surface roughness – Ester gear oil E2, high oil level, steel and ADI.....	80
4.1.5.	Gear mass loss – Ester gear oil E2, high oil level, steel and ADI	82
4.2.	PAO base (P1) lubricant oil gear tests	83
4.2.1.	Stabilization temperatures – PAO gear oil P1, high oil level and steel gears	83

4.2.2.	Stabilization temperatures – PAO gear oil P1, high oil level and ADI gears.....	85
4.2.3.	Oil analysis wear particles – PAO gear oil P1, high oil level, steel and ADI	87
4.2.4.	Surface roughness – PAO gear oil (P1), High oil level, steel and ADI.....	88
4.2.5.	Gear mass loss – PAO gear oil E2, high oil level, steel and ADI	90
4.3.	Steel vs. ADI gears and Ester vs. PAO gear oils.....	92
4.4.	PAO based gear oil (P1) with low oil level.....	96
4.4.1.	Stabilization temperatures – PAO (P1) gear oil, low oil level and steel gears	96
4.4.2.	Oil analysis wear particles – PAO (P1) gear oil, low oil level and steel gears	101
4.4.3.	Surface roughness – PAO gear oil (P1), low oil level, steel	102
4.4.4.	Mass loss – PAO gear oil (P1), low oil level, steel	103
4.5.	“No load” power loss tests with oil P1	105
4.5.1.	Stabilization temperatures – PAO (P1) gear oil, low and high oil level and steel gears	105
4.5.2.	Oil analysis wear particles – PAO (P1) gear oil, low and high oil level and steel gears	106
5.	Conclusion	111
5.1.	Gear geometries	111
5.1.1.	Temperatures	111
5.1.2.	Mass loss	111
5.2.	20MnCr5 carburized steel vs ADI (Austempered Ductile Iron).....	111
5.2.1.	Temperatures	111
5.2.2.	Mass Loss.....	111
5.3.	Ester base oil E2 vs PAO base oil P1	112
5.3.1.	Temperatures	112
5.3.2.	Mass Loss.....	112
5.4.	Oil level.....	112
5.4.1.	Temperatures	112
5.4.2.	Mass loss	112
5.5.	Churning Losses	112
5.6.	General conclusion.....	113
6.	Future Work Perspectives	117
	References	121
	Appendix A: Power Loss Data Sheets.....	123
	311 Gear Power Loss High Oil – E2.....	125
	411 Gear Power Loss High Oil – E2.....	127

611 Gear Power Loss High Oil – E2.....	129
311 Gear Power Loss High Oil – P1.....	131
411 Gear Power Loss High Oil – P1.....	133
611 Gear Power Loss High Oil – P1.....	135
312 Power Loss High Oil – E2.....	137
412 Power Loss High Oil – E2.....	139
612 Power Loss High Oil – E2.....	141
312 Power Loss High Oil – P1.....	143
412 Power Loss High Oil – P1.....	145
612 Power Loss High Oil – P1.....	147
311 Power Loss Low Oil – P1	149
411 Power Loss Low Oil – P1	151
611 Power Loss Low Oil – P1	153
311 Churning Loss high and Low Oil – E2	155
311 Churning Loss high and Low Oil – P1	157
411 Churning Loss high and Low Oil – P1	159
611 Churning Loss high and Low Oil – P1	161
Appendix B: Stribeck curve with Portuguese nomenclature	163
Appendix C: Oil Reports	167
311 – P1 Churning Loss: High Oil and Low Oil	169
311 – E2 Churning Loss: High Oil and Low Oil	174
412 – E2 Power Loss: High Oil	179
412 – P1 Power Loss: High Oil	186
312 – P1 Power Loss: High Oil	193
311 – P1 Power Loss: Low Oil	200
411 – P1 Churning Loss HO & LO + Power Loss: Low Oil.....	207
611 – P1 Churning Loss HO & LO + Power Loss: Low Oil.....	215
612 – P1 Power Loss: High Oil	223
Appendix D: Hydrostatic and Hydrodynamic Lubrication	231
A. Lubrication: Introduction and Basic Theory	233
i. Introduction.....	233
ii. Basic film Theory.....	234
B. Hydrodynamic Lubrication.....	238
C. Hydrostatic Lubrication	240

Figure Index

Figure 1 – Teeth normal contact force[11]: a) Normal force decomposition in radial and tangential components; b) Normal contact force variation along meshing line.	5
Figure 2 – Normal contact force distribution between FZG type-C gear along meshing line[11].	6
Figure 3- Oscular discs curvature radius.	6
Figure 4 – Equivalent Curvature radius of contact between FZG type-C gear Teeth along meshing line.	7
Figure 5 – Normal stress along OZ, maximum shear stress "isobaric" (τ_{\max}/p_0) and orthogonal shear stress "isobaric" (τ_{xz}/p_0) on contacting teeth sub-surface[11].	8
Figure 6 – Variation of Hertz pressure, maximum orthogonal shear stress and maximum shear stress along meshing line[11].	10
Figure 7 – Variation of Hertz contact half-width, maximum orthogonal shear stress depth and maximum shear stress depth along meshing line[11].	10
Figure 8 – a) P generic point of meshing line velocities V_1 and V_2 ;.....	12
Figure 9 – Variation of tangential velocities U_1 and U_2 and sliding velocity along meshing line[11].	12
Figure 10 – Variation of tangential and sliding velocities along meshing line of a FZG type C gear teeth contact[11].	13
Figure 11 – Film thickness at contact center h_0 and minimum film thickness h_m [11].	15
Figure 12 – Variation of Specific lubricant film thickness (h_{oT}) and thermal corrected film thickness (Λ) along meshing line of a FZG Type C gear teeth contact.	16
Figure 13 – Friction coefficient, μ , vs [(viscosity)(velocity)/load], showing the three lubrication regimes. Regime 1, boundary lubrication; Regime 2, mixed film lubrication; Regime 3, full film lubrication[15].	18
Figure 14 – Gears lubrication regimes: boundary lubrication on top, mixed film lubrication in the middle and thick film lubrication on the bottom[11].	19
Figure 15 – 5 % Gear Breakdown probability curve, function of pitch line velocity and lubricant specific film thickness[13].	20
Figure 16 – Stribeck curve [16] (Also see page 120).....	21
Figure 17 – Variation of sliding rate and friction coefficient according to Michaelis along meshing line on a contact between two FZG type C gear teeth[11].	22
Figure 18 – Variation of flash temperature and surface temperature along meshing line of a contact between two gear teeth [11].	24
Figure 19 – Variation over the meshing line of the sliding rate V_E , the flash temperature, surface temperature, and the lubricant temperature in the contact between two FZG type C gear teeth [11].	25
Figure 20 – Splash oil system [13].	32
Figure 21 – Jet oil lubrication system[16].	32
Figure 22 – Lubrication selection abacus by the rotational speed and gear diameter correlation[16].	33
Figure 23 – Wear in a tooth flank[20].	34
Figure 24 – Scuffing in type A gear tooth flank[20].	35
Figure 25 – Pitting in a tooth flank.	36

Figure 26 – Micro-Pitting in a gear tooth[20].	37
Figure 27 – Forms of power loss and heat dissipation of the FZG test box[8].	39
Figure 28 – Main data of reference gearing model and gear cross section [5]	45
Figure 29 – Power loss composition in the model gearbox [5].	46
Figure 30 – Gear geometries: FZG type-C on the left vs Low Loss on the right.	47
Figure 31 – Pinions teeth geometry for the Low Loss gears 311, 411 and 611.	48
Figure 32 – Austempering thermal cycle [29].	53
Figure 33 – ADI Microstructure (100x and 1000x magnification)[24].	53
Figure 34 – ADI surface (50x magnification)[7].	53
Figure 35 – FZG test rig schematic view.	59
Figure 36 – FZG test rig real view.	60
Figure 37 – Model of the pressure pads mounted on the sides of the pinion.	61
Figure 38 – Oil flow caused by pressure pads during meshing cycle.	62
Figure 39 – Oil samples collected after each power loss load stage.	63
Figure 40 – Photograph of a Hommelwerke TK300 measurement rig.	65
Figure 41 – Roughness measurement and Digital filtering sheet of the Turbowave software from Hommelwerke.	65
Figure 42 – TK300 gear program datasheet, used in the roughness measure filtering.	66
Figure 43 – Roughness measurement location (FZG Type A pinion tooth).	67
Figure 44 – Weighing scale with 0.001g accuracy.	68
Figure 45 – Direct Reading Ferrogafer scheme.[33].	69
Figure 46 – Picture of the Direct Reading Ferrogafer.	69
Figure 47 – Analytic ferrografy schematic view[33].	70
Figure 48 – Picture of the Analytic Ferrogafer.	70
Figure 49 – Bi-chromatic microscope.	71
Figure 50 – Ferrogram taken of a P1 oil sample after k1 load stage of a power loss test with 311 gear geometry (Appendix A:Power Loss Data Sheets) 1000x.	71
Figure 51 – Maximum oil temperature and stabilization temperature of gear 311: 20MnCr5 steel, E2 gear oil and high oil level.	75
Figure 52 – Maximum oil temperature and stabilization temperature of gear 411: 20MnCr5 steel, E2 gear oil and high oil level.	75
Figure 53 – Maximum oil temperature and stabilization temperature of gear 611: 20MnCr5 steel, E2 gear oil and high oil level.	76
Figure 54 – Stabilization temperatures of 20MnCr5 steel gears: geometries 311, 411 and 611, E2 gear oil and high oil level.	76
Figure 55 – Stabilization temperatures of ADI gears: geometries 312, 412 and 612, E2 gear oil and high oil level.	77
Figure 56 – Stabilization temperatures of 20MnCR5 steel vs. ADI gears: E2 gear oil and high oil level.	78
Figure 57 – Oil analysis wear particle indexes for 20MnCr5 steel gears: geometries 311, 411 and 611, E2 gear oil and high oil level.	79
Figure 58 – Oil analysis wear particle indexes for ADI gears: geometries 311, 411 and 611, E2 gear oil and high oil level.	80
Figure 59 – Pinion mass loss of 20MnCr5 steel vs. ADI gears: E2 gear oil and high oil level.	82
Figure 60 – Maximum oil temperature and stabilization temperature of gear 311: 20MnCr5 steel, E2 gear oil and high oil level.	83

Figure 61 – Maximum oil temperature and stabilization temperature of gear 411: 20MnCr5 steel, E2 gear oil and high oil level.	83
Figure 62 – Maximum oil temperature and stabilization temperature of gear 611: 20MnCr5 steel, E2 gear oil and high oil level.	84
Figure 63 – Stabilization temperatures of 20MnCr5 steel gears: geometries 311, 411 and 611, P1 gear oil and high oil level.	84
Figure 64 – Stabilization temperatures of ADI gears: geometries 312, 412 and 612, P1 gear oil and high oil level.	85
Figure 65 – Stabilization temperatures of 20MnCr5 steel vs. ADI gears: P1 gear oil and high oil level.	86
Figure 66 – Oil analysis wear particle indexes for 20MnCr5 steel gears: geometries 311, 411 and 611, P1 gear oil and high oil level.	87
Figure 67 - Oil analysis wear particle indexes for ADI gears: geometries 312, 412 and 612, P1 gear oil and high oil level.	88
Figure 68 – Pinion mass loss of 20MnCr5 steel vs. ADI gears: PAO gear oil and high oil level.	91
Figure 69 – Variation of stabilization temperatures with Input Power for 311 steel and 312 ADI gears with E2 and P1 high oil level.	92
Figure 70 – Variation of stabilization temperatures with Input Power for 411 steel and 412 ADI gears with E2 and P1 high oil level.	93
Figure 71 – Variation of stabilization temperatures with Input Power for 611 steel and 612 ADI gears with E2 and P1 high oil level.	94
Figure 72 – Pinion mass loss of 20MnCr5 steel vs. ADI gears: PAO and Ester gear oil and high oil level.	95
Figure 73 – CPUC Ferrometric Index values for all Steel and ADI gears in the end of k9 High oil Power loss test.	95
Figure 74 – Stabilization temperatures of steel gears: geometries 311, 411 and 611, P1 gear oil and low oil level.	96
Figure 75 – Resume of stabilization temperature differences between the three gear geometries for high oil and low oil FZG Power Loss test, with P1 lubricant oil.	97
Figure 76 – Variation of stabilization temperatures with Input Power for 311 steel gear with E2 and P1 high oil level and P1 Low oil level.	98
Figure 77 – Variation of stabilization temperatures with Input Power for 411 steel gear with E2 and P1 high oil level and P1 Low oil level.	99
Figure 78 – Variation of stabilization temperatures with Input Power for 611 steel gear with E2 and P1 high oil level and P1 Low oil level.	100
Figure 79 – Oil analysis wear particle indexes: steel gears lubricated with P1 gear oil and low oil level.	101
Figure 80 – CPUC Ferrometric Index values for Steel gears in the end of k9 High oil and Low oil Power loss tests.	102
Figure 81 – Pinion mass loss in FZG power loss test for the Steel gear geometries with high and low P1 Lubricant oil level.	104
Figure 82 – Stabilization temperature for 311, 411 and 611 steel gears: gear oil P1, low and high oil levels.	105
Figure 83 - Oil analysis wear particle indexes at high and low oil levels: “no load” power loss tests and steel gears lubricated with P1 gear oil.	106

Figure 84 – Stribeck Curve with Portuguese nomenclature[11].	165
Figure 85 – Axis system[10].	235
Figure 86 – Wedging film action in a hydrodynamic slider. a) Velocity profiles at inlet and outlet region in wedge shape load. b) Pressure distribution beneath the wedge[15].	239
Figure 87 – Squeeze film action in a hydrodynamic slider. a) Equal velocity profiles generated at each end of a flat slider that moves downward due to a squeeze velocity in a normal direction to the slider surface. b) Pressure distribution beneath flat slider[15].	239
Figure 88 – schematics showing the key parameters that determine the operation of a hydrostatic bearing. Nomenclature: p_s , supply pressure; p_r , recess pressure; h_0 , film thickness; b , bearing pocket diameter; l , bearing load thickness[15].	241

Table Index

Table 1 – Geometric characteristics and working conditions of FZG Type-C gear.....	4
Table 2 – Engine oil classification: SAE J300 [5]	29
Table 3 – Axle and manual transmission lubricant viscosity classification: SAE J306 [5].	30
Table 4 - Viscosity system for industrial fluid lubricants[5].....	30
Table 5 – Viscosity equivalents[5].	31
Table 6 – Standard FZG Type-C and “Low Loss” gears [19, 20].....	46
Table 7 – Geometrical parameters of gears 311, 411 and 611.	49
Table 8 – Tooth width safety factor for 20MnCr5 gears.....	49
Table 9 – Safety coefficients and working parameter for ADI and Case hardened steel gears. .	51
Table 10 – ADI chemical composition (%).....	52
Table 11 – Properties of ADI.	54
Table 12 – Chemical composition (weight %) of the 20MnCr5 carburized steel.	54
Table 13 – Physical properties (average values) at ambient temperature of the 20MnCr5 carburized steel.....	55
Table 14 – Average thermal expansion coefficient between 20°C and X°C [in 10^{-6} m/(m.K)]. .	55
Table 15 – Heat treatment steps for the 20MnCr5 carburizing steel.....	55
Table 16 – Gear oils Properties.	56
Table 17 – Test conditions for power loss test.	63
Table 18 – Test conditions for churning loss test.....	64
Table 19 – Tooth flank surface roughness of 20MnCr5 steel gear 311: E2 gear oil and high oil level.	81
Table 20 – Tooth flank surface roughness of 20MnCr5 steel gear 411: E2 gear oil and high oil level.	81
Table 21 – Tooth flank surface roughness of ADI gear312: E2 gear oil and high oil level.	81
Table 22 – Tooth flank surface roughness of ADI gear412: E2 gear oil and high oil level.	82
Table 23 – Tooth flank surface roughness of steel gear 311: P1 gear oil and high oil level.	89
Table 24 – Tooth flank surface roughness of steel gear 411: P1 gear oil and high oil level.	89
Table 25 – Tooth flank surface roughness of steel gear 312: P1 gear oil and high oil level.	89
Table 26 – Tooth flank surface roughness of steel gear 412: P1 gear oil and high oil level.	90
Table 27 – 311 Steel Gear Geometry roughness parameters for the wheel and pinion before and after the Standard FZG power loss test with low level of P1 lubricant oil.....	102
Table 28 – 411 Steel Gear Geometry roughness parameters for the wheel and pinion before and after the Standard FZG power loss test with low level of P1 lubricant oil.....	103
Table 29 – 611 Steel Gear Geometry roughness parameters for the wheel and pinion before and after the Standard FZG power loss test with low level of P1 lubricant oil.....	103
Table 30 – Nomenclature of the thin viscous fluid mechanics equation.	237

Nomenclature

Symbol	Designation	Units
A_{base}	Base support area	m^2
A_h	Horizontal surface area of case	m^2
A_i	Immersed area	m^2
A_{Rad}	Radiation surface area of case	m^2
A_v	Vertical surface area of case	m^2
CPUC	Ferrometric index for the concentration of wear particles	/
D	Bearing mean diameter	m
DL	Ferrometric index for the amount of large particles	/
DS	Ferrometric index for the amount of small particles	/
E^*	Equivalent young modulus	Pa
F_a	Axial force	N
F_{bt}	Tooth normal force, transverse section	N
F_r	Radial force	N
F_R	Froud number	/
ISUC	Ferrometric index for the severity of wear large particles	/
K_f	Lubricant thermal conductivity	W/(m.°K)
K_{FZG}	FZG load stage	/
L	Thermal parameter	/
L_{ca}	Characteristic horizontal length	m
L_t	Total roughness measurement length	mm
M_{r1}	Peak material ratio	%
M_{r2}	Valley material ratio	%
M	Input rotating speed	rpm
P_0	Contact pressure	Pa
P_{fr}	Gear friction loss	W
P_{in}	Input power	W
P_{M0}	Bearing load dependant losses	W
P_{M1}	Bearing no load dependant losses	W
P_{sl}	Seal losses	W
P_{spl}	Gear churning losses	W
Q_{cn}	Heat removal by conduction	W
Q_{rad}	Heat removal by radiation	W

Q_{ncn}	Heat removal by natural convection	W
R_a	Roughness average (according to DIN 4768, ISO 4287)	μm
Re	Reynolds number	/
R_k	Core roughness depth (DIN 4776)	μm
R_{max}	Maximum peak-to-valley height(DIN 4768)	μm
R_{pk}	Reduced peak height(DIN 4776)	μm
R_{vk}	Reduced valley depth (DIN 4776)	μm
R_q	RMS roughness average(DIN 4768, ISO 4287)	μm
R_x	Equivalent radius	m
R_{Z-D}	Mean peak-to-valley height	μm
T	Distance from contact point to pitch point of contact line	m
T_0	Oil bath temperature	$^{\circ}\text{C}$
T_a	Ambient temperature	$^{\circ}\text{K}$
T_{CR}	Critical lubricant temperature	$^{\circ}\text{C}$
T_w	Wall temperature	$^{\circ}\text{K}$
T_{wheel}	Wheel torque	N.m
U_1	Pinion surface speed	m/s
U_2	Wheel surface speed	m/s
VI	Lubricant viscosity index	/
V_{oil}	Oil volume	m^3
V_S	Sliding rate	m/s
X_L	Lubricant factor	/
b	Face width	mm
d	Dilution factor	/
d_p	Pitch diameter	m
d_i	Shaft diameter	m
$f_{0,1}$	Coefficient for bearing losses	/
f_{cn}	Conduction factor	/
g_a	Length of recess path	m
g_f	Length of approach path	m
h_0	Lubricant film thickness	μm
h_{0T}	Corrected lubricant film thickness	μm
h_{ca}	Height of case	m
h_h	Natural convection coefficient, horizontal surface	$\text{W}/(\text{m}^2\text{K})$

h_v	Natural convection coefficient, vertical surface	$W/(m^2 \cdot K)$
p_b	Base pitch	m
z_1	Pinion teeth number	$/$
z_2	Wheel teeth number	$/$
α	Piezoviscosity coefficient	Pa^{-1}
α_{rad}	Radiation heat transfer coefficient	$/$
α_v	Thermal expansion	$g/(cm^3 \cdot ^\circ C)$
β	Thermoviscosity	$cSt/^\circ C$
ε	Case surface emissivity	$/$
η	Dynamic viscosity	$mPa \cdot s$
Λ	Specific lubricant film thickness	$/$
λ_c	Cut-off filter	mm
μ	Friction coefficient	$/$
μ_m	Average friction coefficient	$/$
ν	Kinematic viscosity	mm^2/s
$v_{\Sigma c}$	Sum velocity at pitch point	m/s
ρ	Specific weight	Kg/m^3
ρ_c	Equivalent curvature radius at pitch point	mm
σ	Equivalent roughness	μm
ϕ	Thermal correction factor	$/$

Introduction

Current energy consumption all around the world is setting records, and with the announced end of fossil fuels in a medium short time arises the need to develop more efficient devices and machines to help decrease this massive energy consumption.

Industry as well as common citizen developed an environmental awareness that drives the search for more efficient mechanical components and lubricants, lubricants and lubrication methods are no different. Research works [1-3] indicate that if during gear design, not only load factors but also power dissipation is taken into account, power losses might be minimized and better gearbox efficiency will be obtained together with lower operating temperature. If in addition to gear design improvements, a new biodegradable base oil with low toxicity is used[4], two previously incompatible aspects are met. Energetic efficiency combined with a lower environmental impact.

In order to reach these goals, high efficiency gears, entitled “Low Loss Gears”[5] were developed, allowing power loss reduction. Such gears might be manufactured using standard tools available in all manufacturing shops, without involving any expensive modification of production tools and procedures.

Also a careful choice of gear materials and corresponding heat treatments can have a significant impact on gearbox power losses, in particular in the friction power losses between gear teeth[6].

The main objectives of this work are to study the influence on power losses of:

- Gear design (311/312, 411/412 and 611/612 gears);
- Gear material (carburized steel and ADI);
- Gear base lubricant oils(E2 – ester and P1 – polyalphaolefine);
- Oil level (Standard and reduced).

These geometries were previously calculated with the help of specialized computer software that allow the development of the three geometries with progressive degrees of friction reduction, being this achieved among other parameters, by manipulating the modulus and the profile shifts[7].

Also two different fully formulated gear oils were tested, a Ester-based oil, biodegradable and containing low toxicity additives (E2) and a high performance fully synthetic Polyalphaolefine base oil (P1)[8].

These different gear geometries and lubricant oils where submitted to power loss tests performed in the FZG test rig. Oil samples were collected at the end of each test load stage in order to perform a wear particle analysis, and tooth flank roughness measurements were made before and after the power loss test, to observe the evolution of the surfaces degradation for the different gear materials and lubricating oils. Finally, mass loss measurements were performed before and after each power loss test, to assess the mass loss corresponding to each gear material / gear oil combination.

After the analysis and discussion of all tests could be concluded that in average, the gearing efficiency increased when:

- The modulus m decreases an x_1 and x_2 are strongly positive;
- Is used E2 oil instead of P1 oil, specially at slow and medium speeds;
- Are used steel gears, because they release much less particles to the lubricant oil that the ADI ones, but ADI has in general a best behavior to the steel ones, being a good alternative due to the fact it's cheaper and easy to manufacture than the steel.
- The oil level is lower, reaching temperature decreases up to 40% in some cases.

1 – GEAR TRIBOLOGY

1. GEAR TRIBOLOGY

1.1. Tribology

Tribology is the study of the interaction between contacting surfaces in relative motion and it is spread to a large range of disciplines, from chemistry to physics passing through mechanical engineering and materials science, being a science of major technological importance[9]. Tribology is the science and technique of friction, wear and its consequences having, therefore a great significance in energy and raw materials saving [10]. The origin of the name tribology adopted by OECD (Organization for Economical Cooperation and Development) in 1968, come from the Greek “Tribos”, which means friction and “logos” which means science. Tribology has a major importance in machine design, project and maintenance, but can be applied to any field of science that involves friction and wear, for example, the medical and biomedical field leads with tribology through the study of wear in human artificial joints and heart valves, can also be applied to study the wear in a pavement, etc.

A fundamental aspect where tribology and lubrication are directly connected are in increasing the life of and maintain mechanical components in good conditions, because if a mechanical part breaks down it will force the equipment to stop for repair and that not only cost the price of the new part but also the cost of not being producing. This is the main reason because a proper use of tribology in the conception and maintenance of the mechanical parts is vital and represents near 70% of total breakdown control based on surfaces, leading to a lower cost in equipment maintenance[10].

1.2. Tribology of the contact between gear teeth

A wide range of phenomena occurs between gear teeth, involving contact mechanics and ElastoHydrodynamic lubrication (EHD). In this section will be mentioned a Spartan view of the basic concepts of EHD Contact and Lubrication Mechanics applied to the teeth of a cylindrical gear, in order to calculate contact stress and pressure and their variation along the meshing line. A FZG Type -C gear set as the one in Figure 30 with the working conditions present in Table 1, was used as example for this description.

Table 1 – Geometric characteristics and working conditions of FZG type-C gear.

Parameter	Symbol	Units	Pinion	Wheel
Module	m	[mm]	4.5	
Pressure angle	α	[°]	20	
Teeth number	Z	[/]	16	24
Gear ratio	u	[/]	1.5	
Pitch diameter	d	[mm]	72	108
Base diameter	d_b	[mm]	67.66	101.49
Base pitch	p_b	[mm]	13.28	
Center distance	a	[mm]	90	
Addendum diameter	d_a	[mm]	81	117
Working center distance	a_w	[mm]	91.5	
Addendum modification coefficient	x	[/]	0.182	0.171
Addendum shortening coefficient	k^*	[/]	0.019	0.019
Working pressure angle	α_w	[°]	22.44	
Working modulus	m_w	[mm]	4.575	
Working pitch diameter	d_w	[mm]	73.2	109.80
Working addendum	h_{aw}	[mm]	4.72	4.37
Working tip diameter	d_{aw}	[mm]	82.64	118.54
Tooth flank roughness	R_a	[μ m]	0.3±0.1	0.3±0.1
Power	P	[w]	50800	
Torque	c	[N.m]	215.6	323.4
Rotational velocity	n	[rpm]	2250	1500

1.2.1. Teeth contact force

Teeth contact force F_N works in the meshing line direction and never changes direction as shown in Figure 1. The normal force can be expressed by the following equation in order to torque T and base radius r_b [11]:

$$F_N = \frac{T_1}{r_{b1}} = \frac{T_2}{r_{b2}} \quad (\text{Eq. 1})$$

Or in order to power P, pitch radius and angular velocity,

$$F_N = \frac{P}{r_1 w_1 \cos \alpha'} = \frac{P}{r_2 w_2 \cos \alpha'} \quad (\text{Eq. 2})$$

Normal contact force can be decomposed into two components, the radial F_R and the tangential F_T , as can be seen in Figure 1 a), being defined by

$$F_R = F_N \cos \alpha' \quad (\text{Eq. 3})$$

$$F_T = F_N \sin \alpha' \quad (\text{Eq. 4})$$

The number of teeth geared vary along the meshing line as can be seen in Figure 1 b) being geared two teeth pair at the same time between points A and C and the points D and B and therefore only one teeth pair geared between points C and D, explaining this way why the load is two time bigger between points C and D, being the force carried only by a single pair of teeth between these two points, unlike what happens between points A and C and points D and B.[11] In helical gears where the pinion has a minimum number of teeth, load can be supported by 1, 2 or 3 pairs of teeth, being tooth correction also able to make the load applied to contact stop being discontinuous and be more progressive. A good example of the case mentioned above is the FZG Type-C where the load distribution is more progressive, as presented in Figure 2. Unlike the load distribution in the figure above (1/2,1) the FZG Type-C load distribution is 1/3,2/3,1, implicating that only one third of the load is supported between points A to C and D to B being the remaining two thirds supported between points C and D.

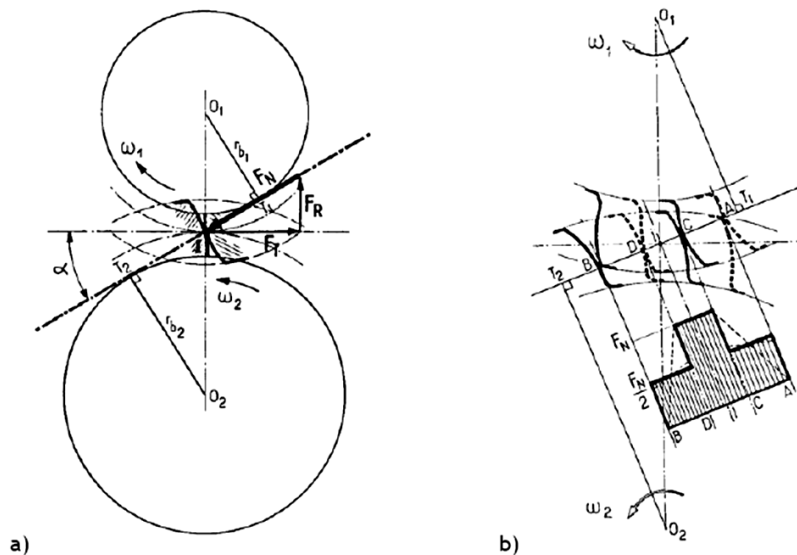


Figure 1 – Teeth normal contact force[11]: a) Normal force decomposition in radial and tangential components; b) Normal contact force variation along meshing line.

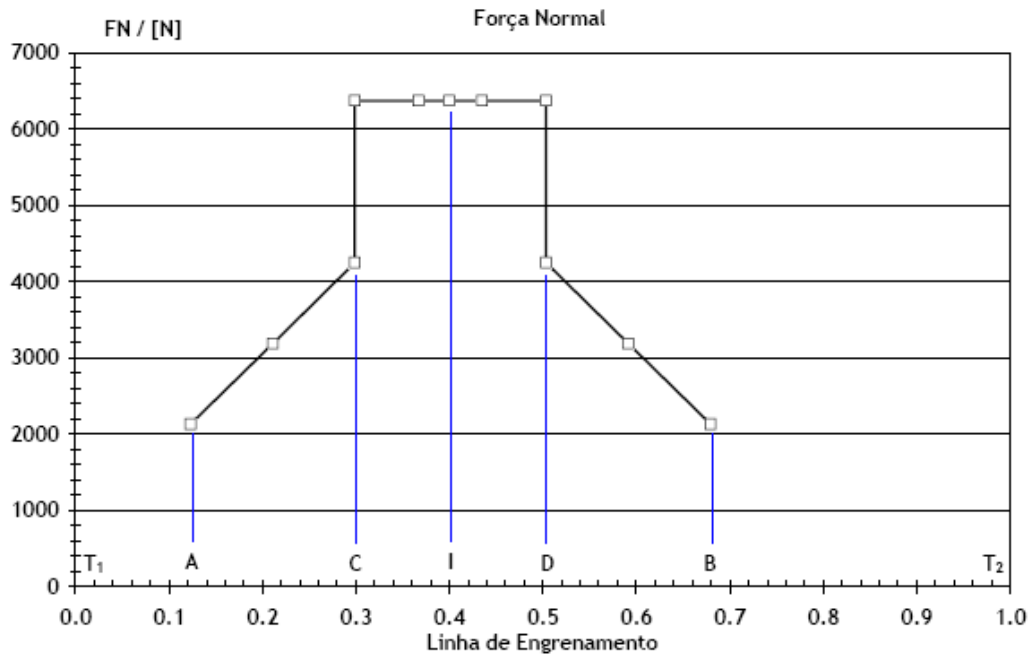


Figure 2 – Normal contact force distribution between FZG type-C gear along meshing line[11].

1.2.2. Curvature radius

The curvature radius of the circle evolut can be defined in the notable meshing line points because they are equivalent to the oscular discs radius (seen entire deduction in chapter 2 of the reference [11]). Known the curvature radius of the oscular discs (Figure 3) is possible to define the equivalent curvature radius at any point R_M , by the following equation.

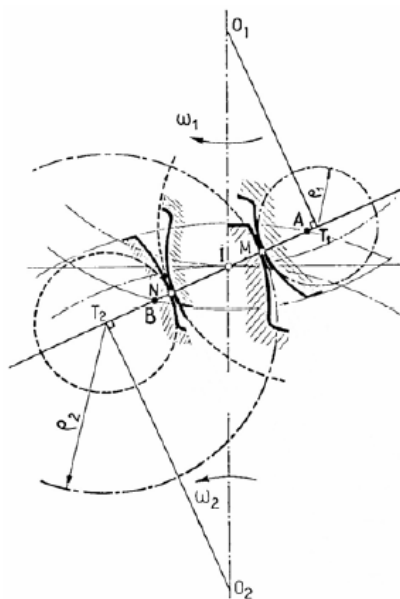


Figure 3- Oscular discs curvature radius.

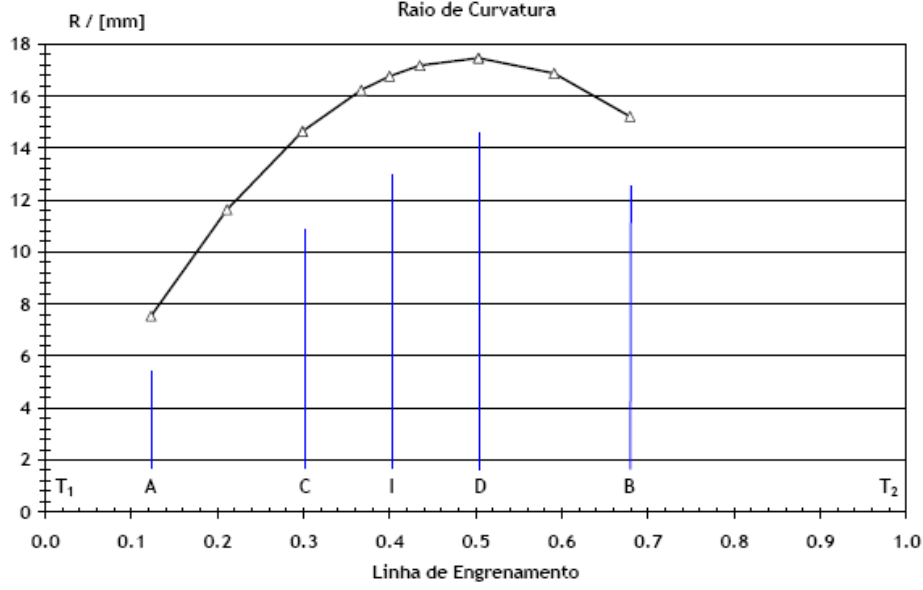


Figure 4 – Equivalent Curvature radius of contact between FZG type-C gear Teeth along meshing line.

$$\frac{1}{R_M} = \frac{1}{2} \left(\frac{1}{T_1 M} + \frac{1}{T_2 M} \right) = \frac{1}{2} \left(\frac{1}{R_{1M}} + \frac{1}{R_{2M}} \right) \quad (\text{Eq. 5})$$

Figure 4 presents the evolution of FZG Type C gear equivalent contact curvature radius along meshing line, being one of the interesting aspects to observe the fact that the curvature radius in the end of the meshing line is nearly twice the one in the beginning. In general the equivalent curvature radius is fairly high, which benefits the tribological gear behavior because the loads will be distributed along a wider area decreasing this way the maximum pressure on tooth surfaces.

1.2.3. Contact Pressure

Hertz pressure or contact pressure (P_0 or P_H) at any point of contact along the meshing line can be calculated through the Hertz theory, considering a linear contact between two solid elastic discs, i. e.,

$$P_0 = P_H = \sqrt{\frac{2 F_N E^*}{\pi b R}} \quad (\text{Eq. 6})$$

where F_N is the normal contact force, b is the gear face width, R is the equivalent curvature radius and E^* is the equivalent young modulus for two contacting solids, defined by

$$\frac{1}{E^*} = \frac{1 - \nu_1^2}{E_1} + \frac{1 - \nu_2^2}{E_2} \quad (\text{Eq. 7})$$

The materials young modulus and the poison coefficients of the oscular discs are respectively E_1 , ν_1 and E_2 , ν_2 .

A rectangular contact area is created by teeth contact and is defined by $2a$ and b , respectively being a the hertzian contact half width defined by:

$$a = \sqrt{\frac{2 F_N R}{\pi b E^*}} \quad (\text{Eq. 8})$$

1.2.4. Contacting teeth sub-surface stress state

The sub-surface stress state of contacting teeth can be calculated through Hertz theory for two solid contact and Boussinesq theory for the elastic half-space[12].

The σ_{xx} σ_{zz} stress variation along OZ axis, the maximum shear stress “isobaric” and the orthogonal shear stress “isobaric”, in the contacting teeth sub-surface is presented in Figure 5.

σ_{xx} and σ_{zz} stress along OZ have his maximum compression near the surface being equal to maximum Hertz pressure p_0 and the maximum shear stress τ_{max} reaches his higher value over the OZ axis being expressed by[11]:

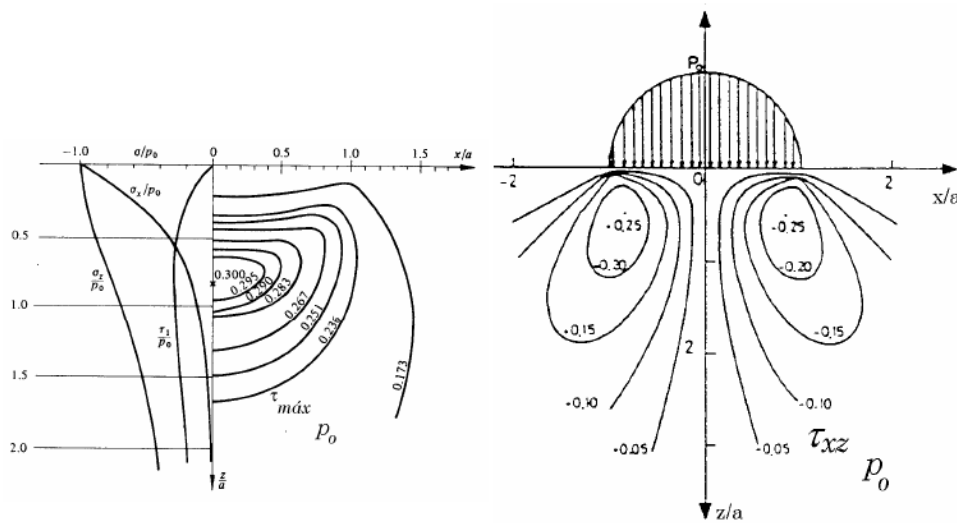


Figure 5 – Normal stress along OZ , maximum shear stress “isobaric” (τ_{max}/p_0) and orthogonal shear stress “isobaric” (τ_{xz}/p_0) on contacting teeth sub-surface[11].

$$\tau_{max} = 0.3p_0 \quad (\text{Eq. 9})$$

Occurring at a depth Z_s defined by

$$Z_s = 0.786a \quad (\text{Eq. 10})$$

The orthogonal shear stress reaches his maximum value at

$$\tau_{xz}^{max} = \tau_0 = 0.25p_0 \quad (\text{Eq. 11})$$

Occurring at a depth Z_0 defined b

$$Z_s = 0.42a \quad (\text{Eq. 12})$$

The largest variation of maximum orthogonal shear stress τ_0 on teeth contact sub-surface along a meshing cycle is expressed by

$$\Delta\tau_0 = 2\tau_0 = 0.5p_0 \quad (\text{Eq. 13})$$

The variation of Hertz pressure, orthogonal shear stress, maximum shear stress and the depth that they respectively occur are presented in Figure 6 and Figure 7

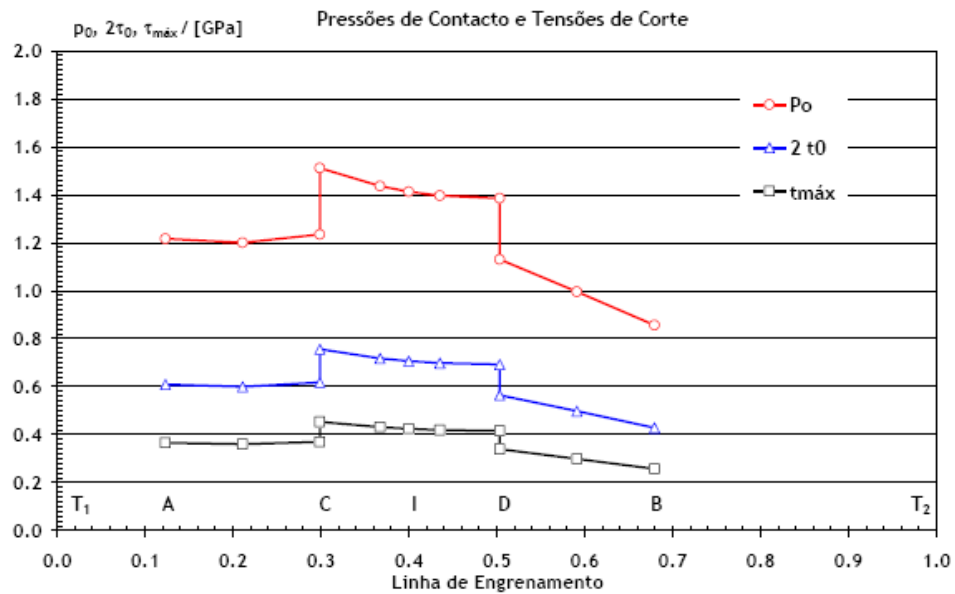


Figure 6 – Variation of Hertz pressure, maximum orthogonal shear stress and maximum shear stress along meshing line[11].

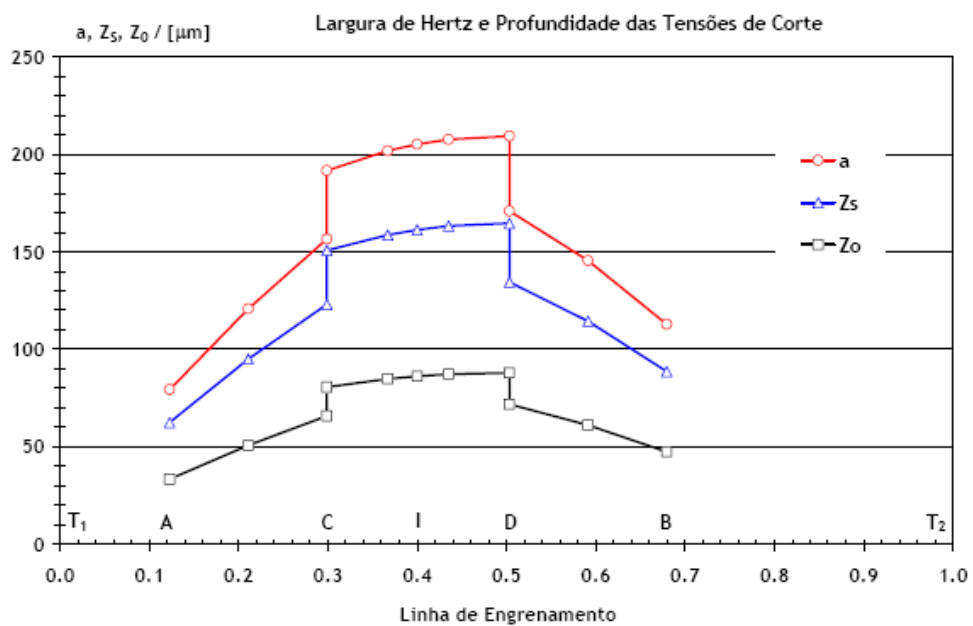


Figure 7 – Variation of Hertz contact half-width, maximum orthogonal shear stress depth and maximum shear stress depth along meshing line[11].

1.2.5. Surfaces velocities

Considering a generic point **P** from the meshing line placed between points **A** and **B**, the absolute velocities of point **P** belonging to each conjugated profile in contact are designated by \mathbf{V}_1 and \mathbf{V}_2 , and their projections in a perpendicular direction to the meshing line respectively U_1 and U_2 , that represent the tangential speed on each one of the conjugated profiles at **P** contact point.

The velocity of the **P** contact point along meshing line is expressed by the projection of \mathbf{V}_1 and \mathbf{V}_2 velocities in the direction of the meshing line, is defined by \mathbf{V} .

Consider now a generic point of the meshing line between points **A** and **B**, as is shown in Figure 8, and being **M** a point located between the length **AI** and **N** point between the length **IB**. The tangential velocities U_1 and U_2 of **M** can be defined by:

$$U_1 = \overline{T_1 M} w_1 = \rho_1 w_1 \quad (\text{Eq. 14})$$

$$U_2 = \overline{T_2 M} w_2 = \rho_2 w_2 \quad (\text{Eq. 15})$$

The sliding velocity can be calculated by the equation

$$V_s = U_2 - U_1 = \rho_2 w_2 - \rho_1 w_1 \quad (\text{Eq. 16})$$

The discs with radius ρ_1 and ρ_2 present in Figure 8 are the oscular discs and can be used to simulate contact between gears teeth, per example; “discs machines” are frequently used in laboratories to conduct studies on gear lubrication, like film thickness in EHD lubrication, etc. In Figure 9 are represented rolling and sliding velocities at each point of meshing line, becoming evident in this figure that the sliding speed is negative in the approximation segment until it reaches the pitch line where there is no sliding and then it changes to the other way and as further we move to the end of contact the sliding velocity becomes higher reaching its maximum in the end of meshing line (point **B**)[11].

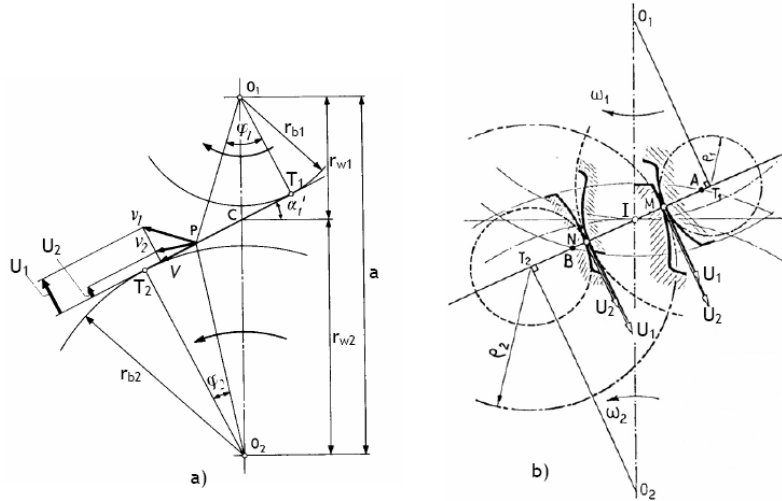


**Figure 8 – a) P generic point of meshing line velocities V_1 and V_2 ;
b) U_1 and U_2 tangential velocities perpendicular to meshing line[11].**

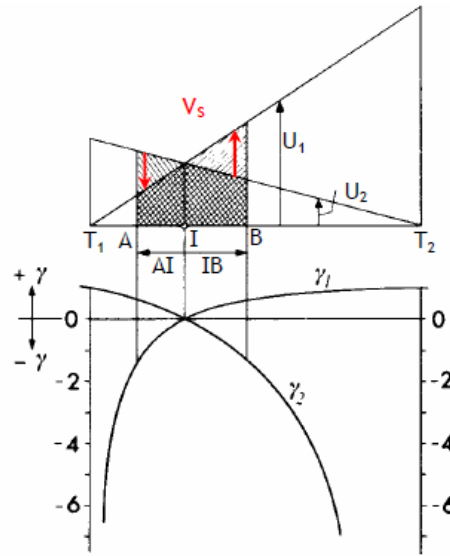


Figure 9 – Variation of tangential velocities U_1 and U_2 and sliding velocity along meshing line[11].

The specific sliding also mentioned in Figure 9 are defined by the following equations,

$$\gamma_1 = \frac{U_1 - U_2}{U_1} \quad (\text{Eq. 17})$$

$$\gamma_2 = \frac{U_2 - U_1}{U_2} \quad (\text{Eq. 18})$$

To finalize, the tangential and sliding velocities variation on a FZG Type C gear along the meshing line is shown in Figure 10 were is once again evident the change in sliding velocity due to the transition from one side to the other of the tooth pitch line.

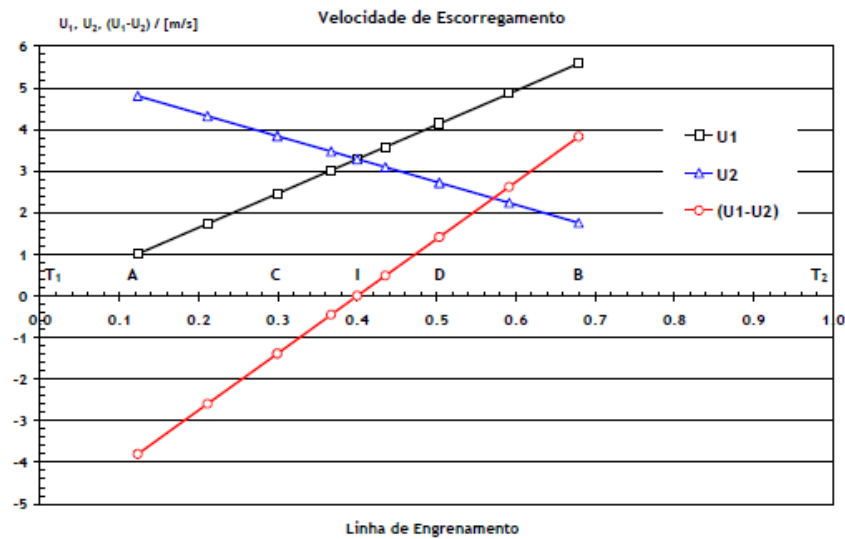


Figure 10 – Variation of tangential and sliding velocities along meshing line of a FZG type C gear teeth contact[11].

1.2.6. Lubricant film thickness

Hydrodynamic and hydrostatic lubrication are usually applied into situations where the contact pressure is relatively low and the contact surfaces are relatively large. Not all mechanical components present this kind of behavior, in some cases the contact surfaces are small and the pressures generated so high that may lead to deformations[13] within an amplitude range that cannot be put aside, given the average film thickness h_m [10], therefore if the solids are considered elastic the contact is hertzian, the lubricant regime is the Elastohydrodynamic.

The most common mechanical components where this type of lubrication can be found are rolling bearings, gears and cams[10].

In elastohydrodynamic contacts lubrication is accessed through the average film thickness that separates the roughness between two surfaces. Nowadays the lubricant film thickness theory between gear teeth follows the D. Dowson and G.R. Higginson [14] which implicates an isothermal contact between smooth surfaces and plenty lubricant[11].

According to Dowson and Higginson [14] the lubricant film thickness inside a Elastohydrodynamic linear contact is presented in Figure 11.

The film thickness in contact center h_0 and minimum lubricant film thickness h_m are defined by the following equations[11]:

$$h_0 = 1.949 \frac{(\eta_0 U)^{0.727} \alpha^{0.77} R_M^{0.364} E^{*0.091}}{\left(F_N/l\right)^{0.091}} \quad (\text{Eq. 19})$$

$$h_m = 1.6 \frac{(\eta_0 U)^{0.7} \alpha^{0.6} R_M^{0.43} E^{*0.03}}{\left(F_N/l\right)^{0.13}} \quad (\text{Eq. 20})$$

Where:

η_0 – Lubricant viscosity at lubricant feeding temperature;

U – Rolling velocity of oscular discs surfaces,

$$U = \frac{1}{2}(U_1 + U_2);$$

α – Lubricant Piezoviscosity coefficient at lubricant feeding temperature;

R – Equivalent curvature radius of oscular discs,

$$\frac{1}{R} = \frac{1}{2} \left(\frac{1}{R_1} + \frac{1}{R_2} \right);$$

E^* - Equivalent young modulus,

$$\frac{1}{E^*} = \left(\frac{1-\nu_1^2}{E_1} + \frac{1-\nu_2^2}{E_2} \right);$$

F_N – Normal solicitation;

l – Gear useful width.

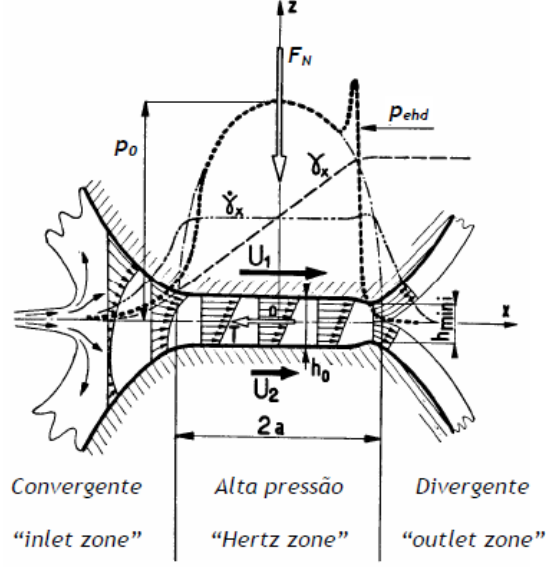


Figure 11 – Film thickness at contact center h_0 and minimum film thickness h_m [11].

1.2.7. Inlet shear heating in an EHD contact

In the beginning of this section was mentioned that the flow inside an EHD contact is isothermal. This assumption is not valid in gears case due to the intense sliding between the contacting surfaces along the meshing line.

An important phenomenon called “inlet shear heating” occurs in the inlet zone where the lubricant is submitted to a high shear deformation caused by the pressure gradient and the rolling and sliding velocities that it’s put up. The shear deformation originates a manifest energy dissipation leading to a increase of the lubricant temperature (ΔT_f), viscosity (η_0) decrease and consequently, lubricant film thickness (h_0) decrease[11]. This decrease of lubricant film thickness is expressed by the factor ϕ_r ,

$$h_{0T} = \phi_T h_0 \quad (\text{Eq.21})$$

$$\phi_T = \{1 + 0.1[(1 + 14.8V_e^{0.83})L^{0.64}]\}^{-1} \quad (\text{Eq.22})$$

$$V_e = \frac{|U_1 - U_2|}{|U_1 + U_2|} \quad (\text{Eq. 23})$$

$$L = \frac{\beta \eta_0 (U_1 + U_2)^2}{K_f} \quad (\text{Eq. 24})$$

Where:

β – Lubricant thermoviscosity coefficient at lubricant feeding temperature;

K_f – Lubricant Thermal conductivity.

The average temperature increase in the inlet zone (ΔT_{inlet}) can be determined using the following equation:

$$\Delta T_{inlet} = \frac{1 - (\phi_T)^{1/0.727}}{K_f} \quad (\text{Eq. 25})$$

1.2.8. Specific lubricant film thickness

Roughness is a factor that cannot be put aside during film thickness calculation in EHD lubrication because real teeth flanks surfaces have roughness that is oriented perpendicularly to the rolling velocities of the oscular discs along the meshing line and can have the same magnitude range of the lubricant film thickness (around $1\mu\text{m}$), therefore the EHD analysis should have this parameter into account. The roughness effect over the lubricant film thickness is made recurring to the *specific lubricant film thickness* Λ defined by:

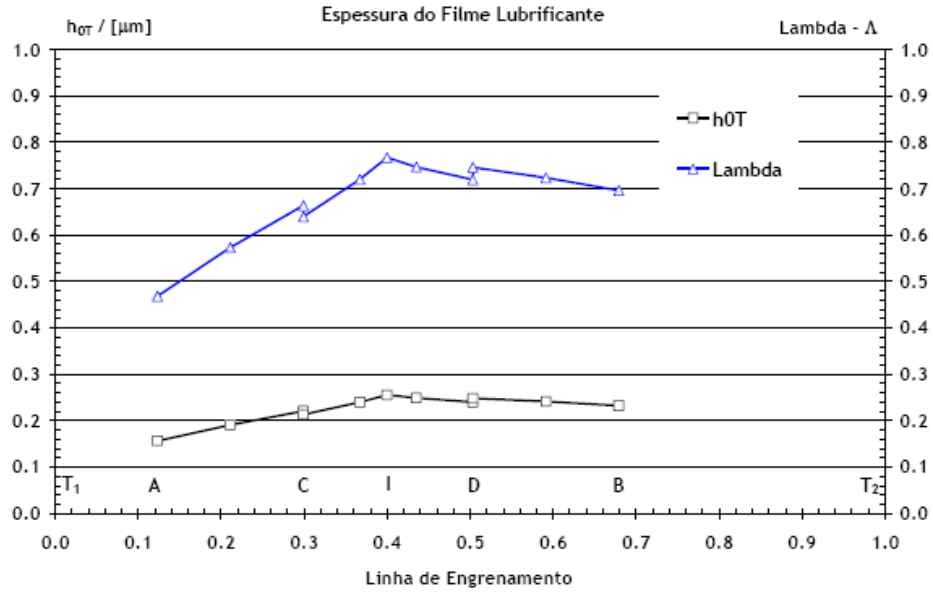


Figure 12 – Variation of Specific lubricant film thickness (h_{0T}) and thermal corrected film thickness (Λ) along meshing line of a FZG Type C gear teeth contact.

$$\Lambda = \frac{h_{0T}}{\sigma} = \frac{h_{0T}}{\sqrt{(R_{q1})^2 + (R_{q2})^2}} \quad (\text{Eq. 26})$$

Where h_{0T} is the lubricant film thickness with the thermal correction and $\sigma = \sqrt{(R_{q1})^2 + (R_{q2})^2}$ is the composed roughness of both contacting flanks.

In Figure 12 is represented the variation of specific film thickness in contact center along meshing life for a FZG Type C gear.

1.2.9. Lubrication Regimes

When two surfaces are in contact the load is carried by the roughness in their surfaces causing an unbearable amount of wear and surface damage, therefore a liquid lubricant is deliberately introduced between the surfaces to separate them totally or partially[15].

When liquids or gases are used as lubricants, it is called *fluid film lubrication*. When the superficial roughness is completely separated by a layer of lubricant several times bigger than the lubricant molecules we are in presence of *thick film lubrication*, in other cases the surfaces roughness is only partially covered by the lubricant allowing metal-metal contact being the load carried partially by the contacting roughness being this way called *mixed film lubrication* or *thin film lubrication*. In more extreme cases the load is entirely carried by the contacting roughness being the film thickness virtually inexistent, and the lubricant is mostly trapped in the roughness valleys, being this regime called *boundary lubrication* or *limit film lubrication*[15]. In Figure 13 is present a stribeck curve where is shown the variation of the lubrication regime with the friction coefficient.

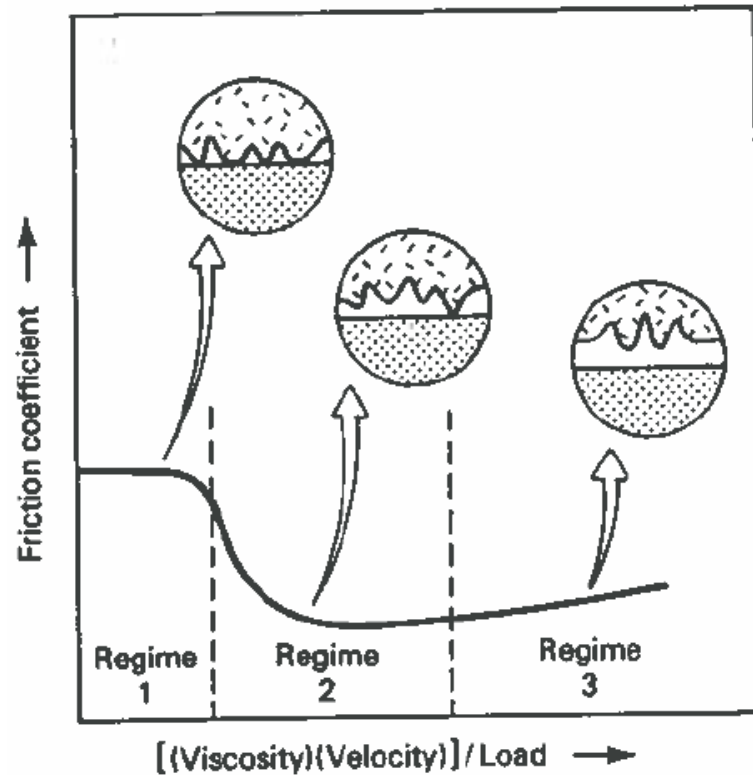


Figure 13 – Friction coefficient, μ , vs $[(\text{viscosity})(\text{velocity})/\text{load}]$, showing the three lubrication regimes. Regime 1, boundary lubrication; Regime 2, mixed film lubrication; Regime 3, full film lubrication[15].

Lubrication regimes can be defined according to a range of specific lubricant film thickness, resulting in the three following regimes also schematically represented in Figure 14:

- ❖ **Boundary Film** $\Lambda < 0.7$
Normal contact force entirely supported by metal-metal contact between surface roughness peaks.
Nonexistence of an hydrodynamic fluid film.
- ❖ **Mixed Film** $0.7 < \Lambda < 2.0$
Normal contact force supported partially by the metal-metal contact and an EHD lubricant film.
- ❖ **Full Film** $\Lambda > 2.0$
Normal contact force entirely supported by the EHD lubricant film which completely separates the surfaces preventing the metal-metal contact.

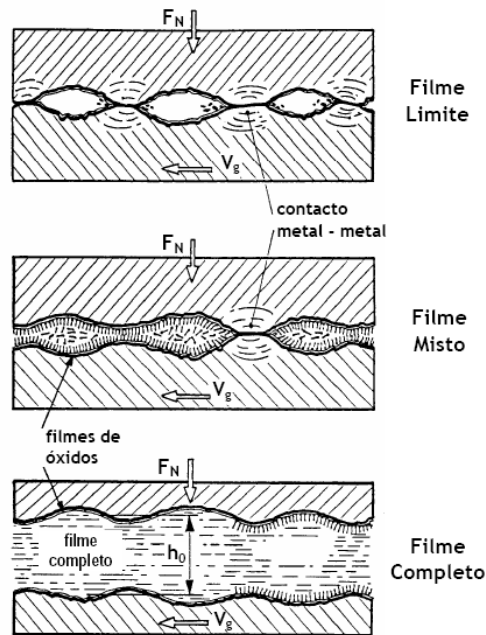


Figure 14 – Gears lubrication regimes: boundary lubrication on top, mixed film lubrication in the middle and thick film lubrication on the bottom[11].

The specific lubricant film thickness changes along the meshing line as exemplified in Figure 12, therefore multiple lubrication regimes may occur along the meshing line.

Looking once again to Figure 12 and keeping in mind the lubrication regimes specific fluid film ranges, we can see that between the points A and C we are in presence of a boundary lubrication regime, being mixed lubrication regime also possible to occur in the area, between the points C and D we are in presence of a mixed lubrication regime, being thick film regime also admissible in this area, and now in between the points D and B there are present two lubrication regimes, a mixed film lubrication regime near point D and as we approach point B the lubrication regime comes closer to a boundary lubrication regime.

It's possible to establish a direct relation between gear breakdown probability by contact fatigue, severe adhesive wear, etc, and the specific lubricant film thickness Λ , function of sliding velocity, lubricant type, etc.[11].

An example can be found in Figure 2 where a curve was traced for a relation between specific film thickness and pitch line velocity.

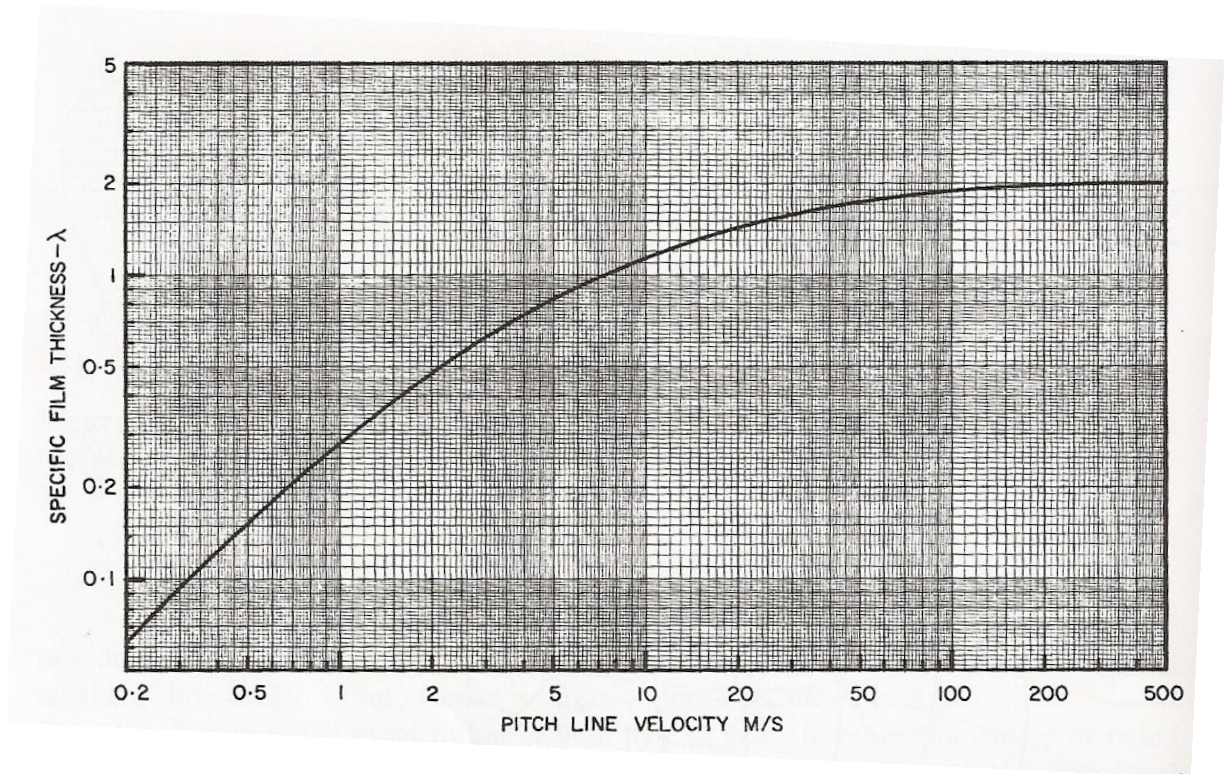


Figure 15 – 5 % Gear Breakdown probability curve, function of pitch line velocity and lubricant specific film thickness[13].

1.2.10. Friction coefficient in gear teeth

Friction is a parameter of extreme importance when we are studying gears and specially, gear teeth because friction controls every aspect of teeth contact, from heat generation, wear, film thickness, etc. Friction is express in the form of a coefficient that establishes a correlation between tangential force F_T and the normal force F_N , being frequently called friction coefficient, and its basic form is defined by

$$\mu = \frac{F_T}{F_N} \quad (\text{Eq. 27})$$

As mentioned before, the friction coefficient is directly related to the film thickness, more specifically to the specific Lubricant film thickness. This relation is usually represented by a group of curves that define the Stribeck curve as seen in Figure 16.

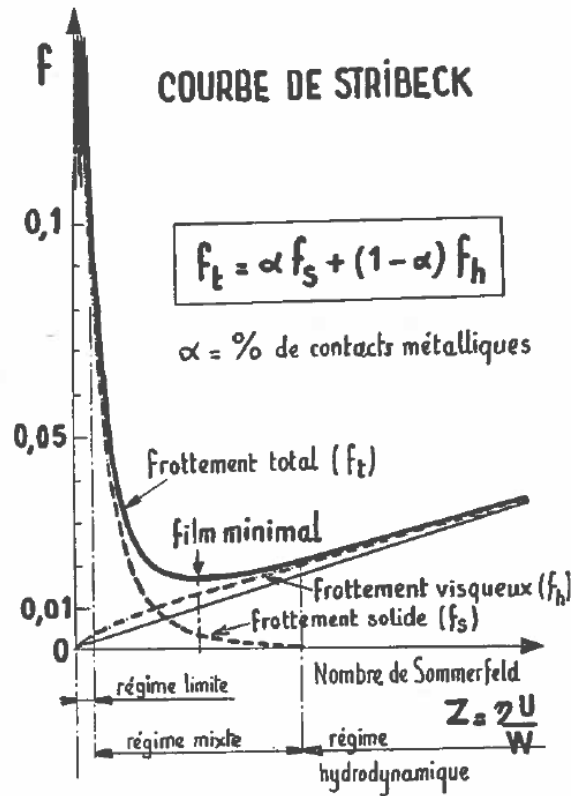


Figure 16 – Stribeck curve [16] (Also see page 163)

The coefficient of friction is a very complex parameter, especially in gears where several lubrication regimes could coexist along the meshing line. Being roughness amplitude and orientation of great influence in the assessment of the coefficient of friction therefore it's common in the empirical formulation of this parameter to have into account experimental results gathered in discs machines or power dissipation gear test[11] being valid for all lubrication regimes.

There are four main formulations that are commonly used, the formulation according to DIN 3990 standard, ISO 6336 standard, Kelly expression and Michaelis expression, being the last one the usual reference expression used to calculate the friction coefficient in the workgroup where the experimental work described ahead was made.

The friction coefficient according to Michaelis[17] is widely used in FZG test Rig tests, and is expressed by the following equation,

$$\mu_{MIC} = 0.048 \left(\frac{W_L}{V_R R_{eq}} \right)^{0.2} \eta_0^{-0.05} R_a^{0.25} \quad (\text{Eq. 28})$$

Where,

$$W_L - \text{specific load (N/mm)} \quad W_L = \frac{F_N}{l \cos \alpha_{wt}}$$

F_N – applied normal force

l – Contact length

η_o – oil dynamic viscosity at oil bath temperature (m.Pa.s)

V_R – rolling velocity (m/s)

$$R_a - \text{equivalent average roughness } (\mu\text{m}) \quad R_a = \frac{1}{2}(R_{a1} + R_{a2})$$

R_{eq} – equivalent curvature radius at each point (mm)

In Figure 17 is presented the variation of the sliding rate and the friction coefficient along the meshing line, where we see intrinsic relation that these two parameters have, the friction coefficient decreases linearly with the decrease of sliding rate near the pitch line place where they are both null.

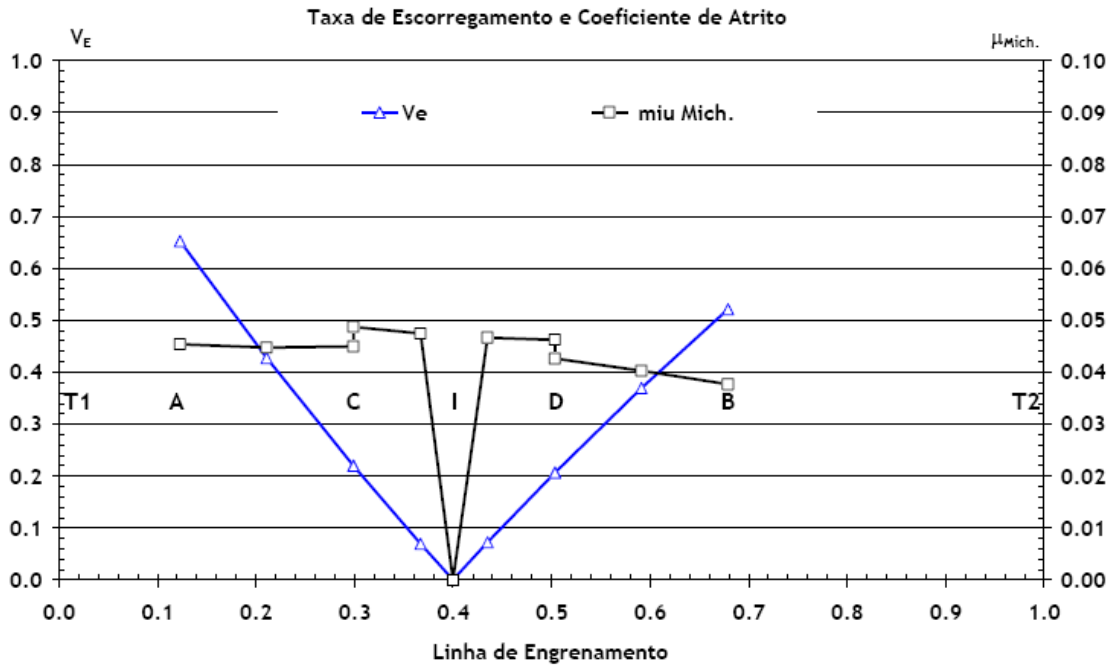


Figure 17 – Variation of sliding rate and friction coefficient according to Michaelis along meshing line on a contact between two FZG type C gear teeth[11].

1.2.11. Teeth flank temperature

The normal forces transmitted through gear teeth contact and high sliding rates between flanks, generate a significant amount of power dissipation in the contact which causes the teeth surfaces and lubricants to rise, and influences the lubricant film thickness[11].

The first analysis performed to determine the maximum temperature achieved in contacting teeth flanks are correlated with gear failure studies [11]. Failures are often results of a brutal rupture of the lubricant film, causing severe wear or teeth scuffing, being directly related to the concept of the lubricant specific film thickness Λ mentioned before, and the critical temperature concept which is also in the base of different failure criteria.

The *Critical Temperature* concept was first formulated by the professor H. Blok from Delft Technical University of Netherland in 1937. The contacting teeth surface temperature is defined by the following expressions[11]:

$$T_S = T_M + T_{flash} \quad (\text{Eq. 29})$$

$$T_M = T_0 + 0.49T_{flash}^{max} \quad (\text{Eq. 30})$$

$$T_{flash} = 0.893 \left(\frac{F_N}{l} \right)^{3/4} \left(\frac{E^*}{R_{eq}} \right)^{1/4} \frac{\mu |U_1 - U_2|}{PT_{S1}\sqrt{U_1} + PT_{S2}\sqrt{U_2}} \quad (\text{Eq. 31})$$

Being

- T_M – the gear mass temperature (gear temperature in point away from the contact point),
- T_{flash} – the localized increase of temperature in each meshing line point,
- T_0 – oil bath temperature,
- μ - friction coefficient,
- PT_{S1} – surface 1 thermal parameter,
- PT_{S2} – surface 2 thermal parameter,

With

$$PT_{S1} = \sqrt{\rho_{S1} C_{S1} K_{S1}}$$

$$PT_{S2} = \sqrt{\rho_{S2} C_{S2} K_{S2}}$$

Which are, the square root of the product of the specific mass by the specific heat and by the thermal conductivity of the surfaces.

The maximum temperature of the contacting surfaces is defined by [11]:

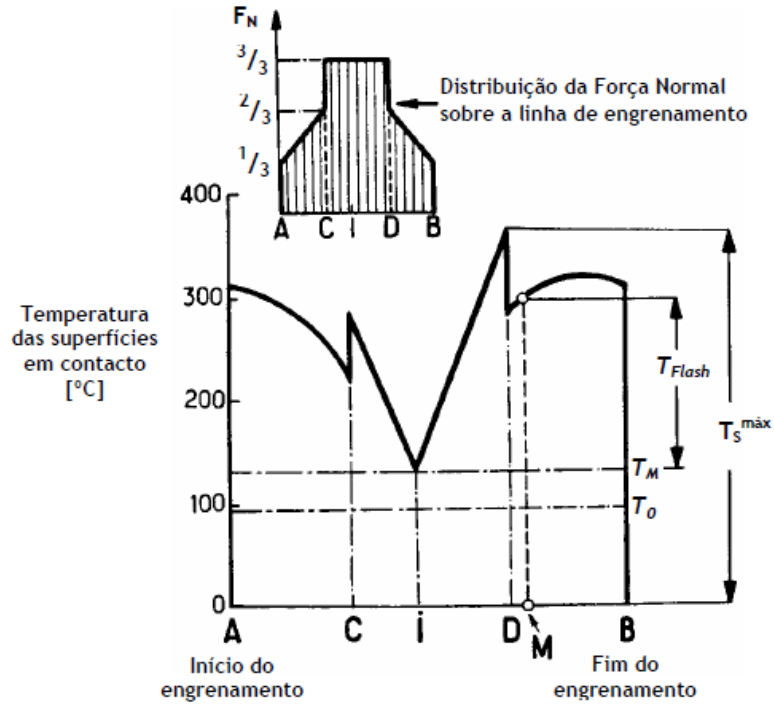


Figure 18 – Variation of flash temperature and surface temperature along meshing line of a contact between two gear teeth [11].

$$T_S^{max} = T_M + T_{flash}^{max} = T_0 + 1.49T_{flash}^{max} \quad (\text{Eq. 32})$$

In Figure 18 we can be seen the variation of contacting teeth surface temperature during the meshing of two corrected gear teeth.

1.2.12. Lubricant temperature

The lubricant fluid temperature T_F inside the contact between gear teeth is defined by the following expression [11]:

$$T_F = T_S + \Delta T_F \quad (\text{Eq. 33})$$

Where T_F represents the fluid temperature, T_S represents the surface temperature and ΔT_F represents the increase of the lubricant temperature above the surface temperature, being this defined by:

$$\Delta T_F = 0.157 \left(\frac{F_N E^*}{l R_X} \right)^{1/2} \frac{\mu |U_1 - U_2| h_0}{k_F} \quad (\text{Eq. 34})$$

Being:

- μ - friction coefficient,
- h_0 – specific film thickness in contact center,
- K_F – thermal conductivity of the lubricant film.

The maximum lubricant temperature along the meshing line is defined by:

$$T_F^{\max} = (T_S + \Delta T_F)^{\max} \quad (\text{Eq. 35})$$

although, in general, the maximum surface temperature and the maximum lubricant temperature occurs in the same point of the meshing line.

In Figure 19 is represented the variation along the meshing line of the maximum lubricant temperature for an FZG Type C gear.

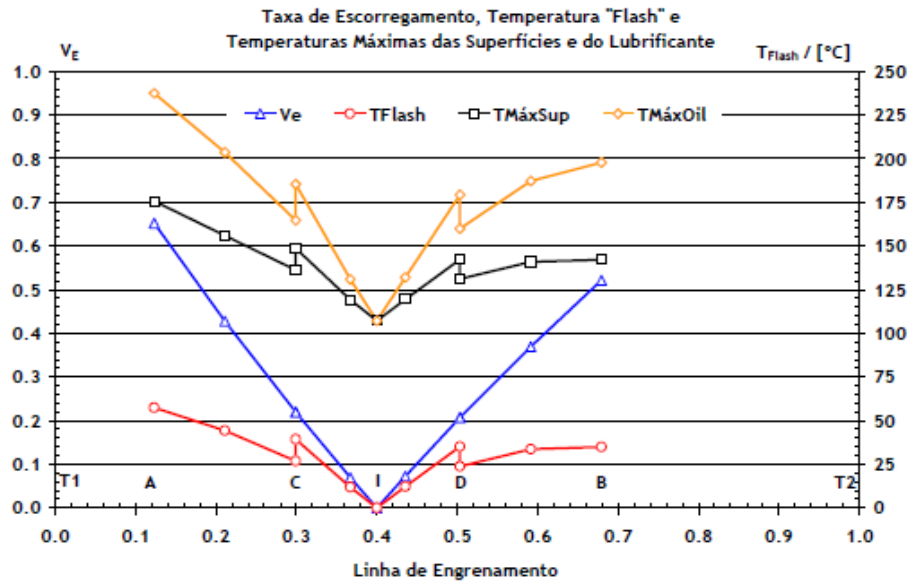


Figure 19 – Variation over the meshing line of the sliding rate V_E , the flash temperature, surface temperature, and the lubricant temperature in the contact between two FZG type C gear teeth [11].

1.3. Lubricant oils

In this section are presented and discussed liquid lubricant oils. Lubricant oils are constituted by a base oil and an additive package to improve specific characteristics according to a determined purpose.

Lubricant oils can have several different origins, such as vegetable, animal, mineral and synthetic.

1.3.1. Vegetable and animal lubricant oils

Vegetable and animal lubricant were the first lubricants used by man, but due to new and more demanding needs this have been put aside by the petroleum and synthetic based lubricants. Nevertheless, the nowadays environmental concerns have brought back the need for vegetable based lubricants, being used almost exclusively by some industries. The reasons to these lubricants to resist are not only driven by an environmental need but also because of its high viscosity index (VI), low evaporation rate, and of course its quick biodegradability. Not everything is perfect with vegetable oils; they oxidize very rapidly and have low resistance to high temperatures[11].

The animal lubricant oils are made out of whales, beavers, etc. being some of these animal oils used not as base oils but rather additives due to their special lubricant properties like greasiness[11].

1.3.2. Mineral based lubricant oils.

Mineral based oils are obtained from petroleum and they are basically hydrocarbons being some of the most common in lubrication applications[11, 18]. The mineral lubricant oils are divided into three categories; paraffinic, naphthenic and aromatic, being the last one not used to lubrication purposes[18].

The paraffinic based mineral oil is characterized by a high fluidity point, also high viscosity index (VI), good oxidation resistance, good oiliness, big amount of carbon residue and very little emulsifiable[18].

The naphthenic based mineral oil is almost the exact opposite of the paraffinic base, it has a low fluidity point, low viscosity index (VI) small oxidation resistance, a large oiliness, a small amount of carbon residue and very emulsifiable[18].

Mineral oils are designated paraffinic or naphthenic according to their composition but there are also oils that are a blend of these two bases, and are widely used as lubricants due to being available in several viscosity grades, they have low volatility, resistant to deterioration, they are corrosion protectors and most of all they have a low cost[11].

1.3.3. Synthetic base lubricant oils

The synthetic lubricants appeared by the need of certain industries like the military and aeronautical industries to develop lubricants able to withstand extreme conditions. Some of these synthetic lubricants can bear extreme temperatures and very large temperature variations, improved oxidation resistance and bigger useful life.

Synthetic oil is in general more expensive but also requires less maintenance and has an extended life period therefore it has a good cost benefit ratio [18]. The synthetic lubricants are also separated by categories, the Polyalphaolephines (PAO), the Polyglycols and Esters.

The PAO's is the most common synthetic base lubricant, having a low fluidity point, good thermal stability, a high viscosity index but is also bad dissolving additives [18].

The polyglycols are characterized mainly by their low friction coefficient, making them ideal for high sliding applications. Its compatibility with seals, paints and oil screens should be carefully analyzed [11].

The ester base oils are a wide group of lubricants being separated in dibasic acids esters, organophosphates esters and silicate esters. Each one of these esters own characteristics that have a great influence in the final lubricant properties.

Some of these esters are rapidly biodegradable, which is a property that is vital in many current applications that need to have a lower impact on nature [11].

1.3.4. Additives

Base lubricant oils have a group of characteristics that differentiate them from each other but due to the extreme demanding in machine operative conditions, is often required for a lubricant to have the base properties of a certain oil type but one or two characteristics typical from other base oil. This problem was solved with the introduction of additives in the lubricant base oils, being these able to add new and better properties to the lubricants or just improve one or more of their natural properties [11, 18].

Additives are in sum a group of chemical compounds that, added to base oils reinforce and improve some of their properties, add them new ones or even remove undesirable properties. We can classify additives in two groups [18]:

- a) Those who modify physical characteristics such as fluidity, foam formation and viscosity index;
- b) And those who have an effect of chemical nature, such as oxidation inhibitors, detergents, extreme pressure agents among others.

Because there are a long list of additives and the objective of this work is not to classify lubricants will be made a summarized approach to the most common additives;

Pour point depressants – These are high molecular weight polymers that restrain the formation of a wax crystal structure that decrease oil flow at low temperatures. They don't stop the crystal formation but rather diminish the temperature at which the crystals form[13].

Viscosity Index (VI) improvers – VI improvers are also polymers that increase the relative viscosity of the oil more at high temperature than at low temperatures[13, 18].

Defoamants – These are most commonly silicone polymers that usually attach to the air bubbles formed in the oil and, rise them to the surface where they collapse preventing this way foam to accumulate.

Oxidation inhibitors – Oxidation occurs in the presence of air, leading to an increase of viscosity and organic acid concentration causing a chain reaction that increases even more the oxidation process. Per example, for temperatures above 93°C metal catalytic effect promote the oxidation process, therefore catalytically inhibitors are used to reduce this effect, reacting with the metal surfaces and forming a protective coating[13].

Antiwear (AW) additive – These additives design to reduce friction, wear, scuffing and scoring under boundary lubrication conditions. Basically these compounds form a protective layer between the surfaces by physical adsorption or a chemical reaction[13].

Extreme pressure (EP) additives - EP additives are used when lubricants are submitted to high temperatures and/or heavy loads where more severe sliding conditions occur, to reduce friction, control wear and prevent severe surface damage. These compounds chemically react with the sliding metal surfaces to form almost insoluble oil films protecting this way the surfaces from excessive wear and eventual surface welding[13, 18].

1.3.5. Lubricant classification – Viscosity Grades

Lubricants may be classified by its viscosity, performance tests, type of mechanism for which is made or the industry where it is used. They can also be classified as automotive, marine, aviation or industrial lubricants[15]. In an lubricant oil selection for any application a primary concern is always the viscosity, because it must be high enough to provide an good film formation but not so high that friction losses become unbearable. Temperature is an important parameter to have into account due to the fact that viscosity varies with temperature, so operating temperature of the oil in the machine and what is the better start in temperature. There are available three numbering systems to identify oils according to their viscosity ranges[13].

The first one is the SAE (society of Automotive Engineers) standard J300 that classifies oil for automotive engines. This classification is made through viscosity determination at low shear rates and high temperatures (100°C) at high shear rates and

high temperature (150°C) and also at high and low shear rates at low temperatures (-5°C to -40°C), being these rates presented in Table 2.

Grades with the suffix *W* are projected primarily for a low ambient temperatures use, while grades without the suffix are projected for more tempered ambient temperatures. In automotive industries is very common to use multi grade oils for a year-round use[13]. Multi grade oils can be formulated per example to reach the low temperature specifications of a 10W grade and at the same time the 100°C limits for the 30 grade, resulting in the following designation of SAE 10W-30 grade. These multi grade oil types frequently require the use of VI additives combined with mineral or synthetic base oil.

The second system is the SAE J306 classification for use in automotive manual transmissions and drive axles by viscosity measured at 100°C and by the maximum temperature at which they reach a viscosity of 150000Pa.s when cooled and measured in accordance with ASM Standard D2983 (Test for apparent viscosity at low temperature using the Brookfiel viscometer)[13]. The lubricant viscosity limits for this system are given in Table 3.

Table 2 – Engine oil classification: SAE J300 [13]

SAE viscosity grade	Low temperature (°C) cranking viscosity (cP, max) ^b	Low temperature (°C) pumping viscosity (cP, max, with no yield stress) ^c	Kinematic viscosity (cSt) at 100°C min ^d	Kinematic viscosity (cSt) at 100°C max ^d	High shear viscosity (cP), at 150°C and 10 ⁶ s ⁻² , min ^e
0W	3250 at -30	60 000 at -40	3.8	—	—
5W	3500 at -25	60 000 at -35	3.8	—	—
10W	3500 at -20	60 000 at -30	4.1	—	—
15W	3500 at -25	60 000 at -25	5.6	—	—
20W	4500 at -20	60 000 at -20	5.6	—	—
25W	6000 at -5	60 000 at -15	9.3	—	—
20	—	—	5.6	< 9.3	2.6
30	—	—	9.3	< 12.5	2.9
40	—	—	12.5	< 16.3	2.9 ^f
40	—	—	12.5	< 16.3	3.7 ^g
50	—	—	16.3	< 21.9	3.7
60	—	—	21.9	< 26.1	3.7

^a All values are critical specifications as defined by ASTM D 3244.

^b ASTM D 5293.

^c ASTM D 4684. Note that the presence of any yield stress detectable by this method constitutes a failure regardless of viscosity.

^d ASTM 445.

^e ASTM D 4683 or ASTM D 4741.

^f 0W-40, 5W-40, and 10W-40 grades.

^g 15W-40, 20W-40, 25W-40 and 40 grades.

The third system was developed by ASTM and the Society of Tribologists and Lubrication Engineers (STLE) to establish definite viscosity levels that could be used as common basis for specifying the viscosity of industrial fluid lubricants, eliminating unjustified intermediate grades. This system is based in 40°C viscosity measurements and is present in on ASTM Standard D2422, Din N° 51519 and International Standards Organization (ISO) Standard 3448[13]. The ISO viscosity grades can be found in Table 4.

A simple way to convert and compare different grades is to use a conversion abacus like the one in Table 5.

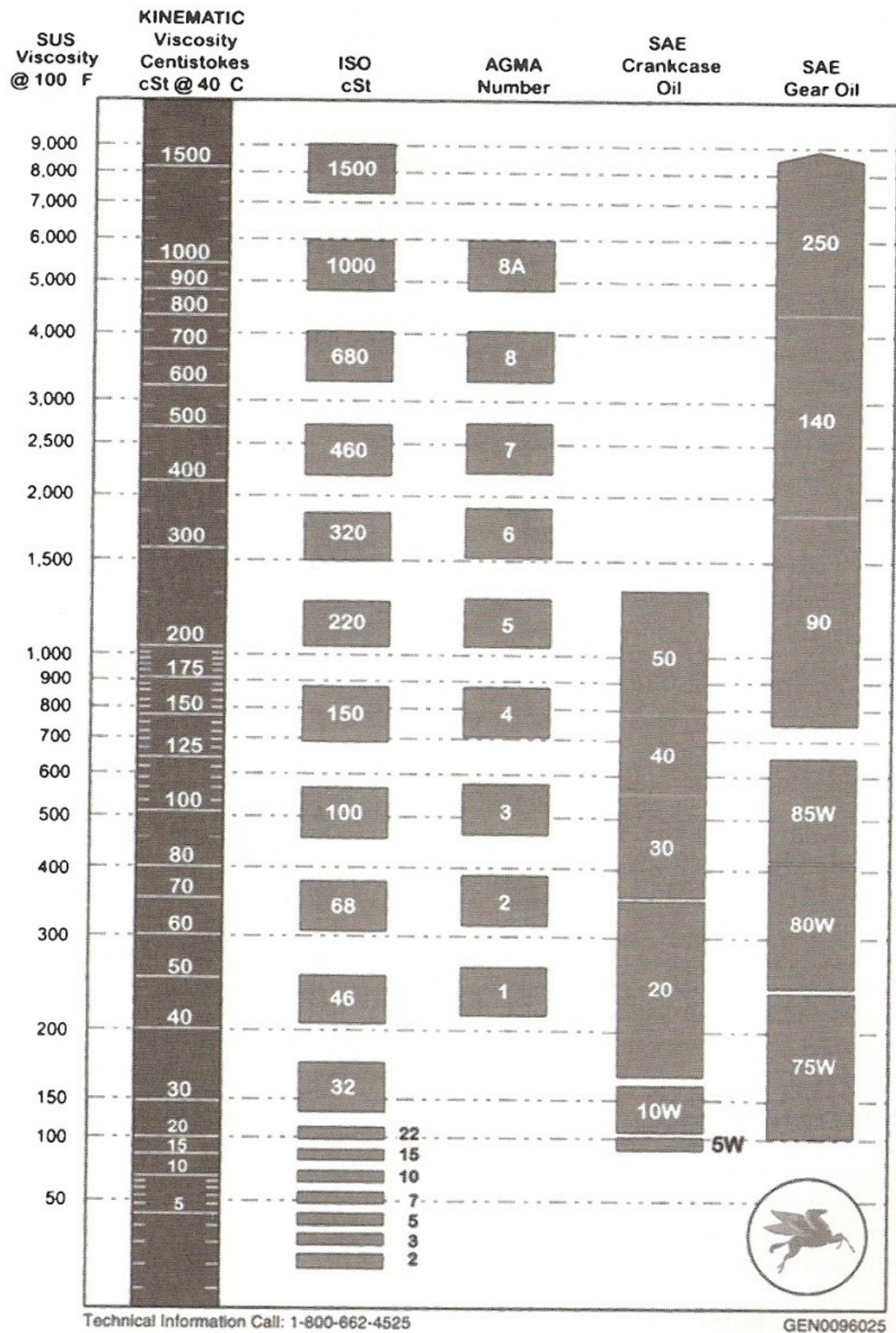
Table 3 – Axle and manual transmission lubricant viscosity classification: SAE J306 [13].

SAE viscosity grade	Maximum temperature for viscosity of 150,000 cP (°C)	(cSt) Viscosity at 100° Celsius	
		Minimum	Maximum
70W	−55	4.1	—
75W	−40	4.1	—
80W	−26	7.0	—
85W	−12	11.0	—
90	—	13.5	24.0
140	—	24.0	41.0
250	—	41.0	—

Table 4 - Viscosity system for industrial fluid lubricants[13]

Viscosity system grade identification	Midpoint viscosity [cSt (mm ² /s)] at 40.0°C	Kinematic viscosity limits [cSt (mm ² /s)] at 40.0°C	
		Minimum	Maximum
ISO VG 2	2.2	1.98	2.42
ISO VG 3	3.2	2.88	3.52
ISO VG 5	4.6	4.14	5.06
ISO VG 7	6.8	6.12	7.48
ISO VG 10	10	9.00	11.0
ISO VG 15	15	13.5	16.5
ISO VG 22	22	19.8	24.2
ISO VG 32	32	28.8	35.2
ISO VG 46	46	41.4	50.6
ISO VG 68	68	61.2	74.8
ISO VG 100	100	90.0	110
ISO VG 150	150	135	165
ISO VG 220	220	198	242
ISO VG 320	320	288	352
ISO VG 460	460	414	506
ISO VG 680	680	612	748
ISO VG 1000	1000	900	1100
ISO VG 1500	1500	1350	1650

Table 5 – Viscosity equivalents[13].



1.4. Gear lubrication

Gears being mechanical components highly sought need efficient lubrication systems. There are several lubrication methods but only two will be referenced in this work due to the fact that only these two are used during this work.

The two lubrication methods are the splash oiling/ oil bath and the oil jet lubrication. In the first method (Figure 20) gears are lubricated by immersion in a oil bath where usually the bigger wheel is partially immersed in the oil, dragging the oil to the contact and splashing it at the same time to other components and the casing walls. This method implicates the need of a good oil level control in order to prevent deficient lubrication and excessive churning[13].

The second lubrication method is the jet oil or circulation lubrication, consisting in pumping oil into the gear teeth near the gearing point[13], being the oil collected in the gearbox bottom, then the oil is filtered and return to the oil reservoir where it's cooled and re-circulated (Figure 21).

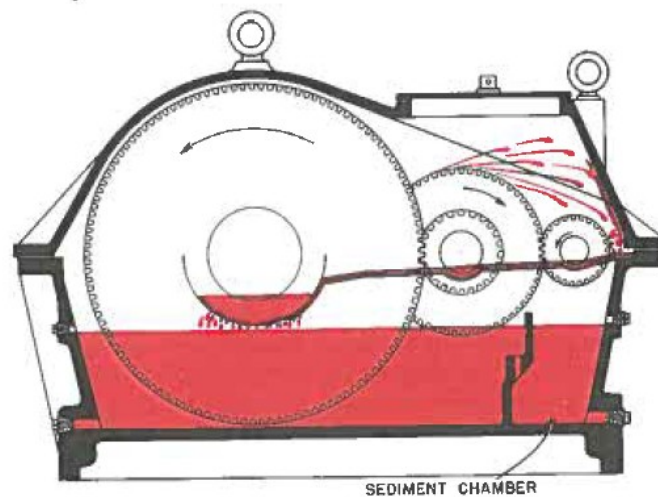


Figure 20 – Splash oil system [13].

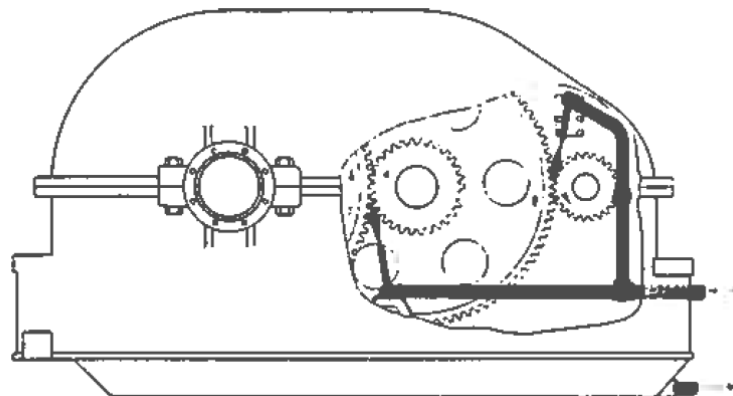


Figure 21 – Jet oil lubrication system[16].

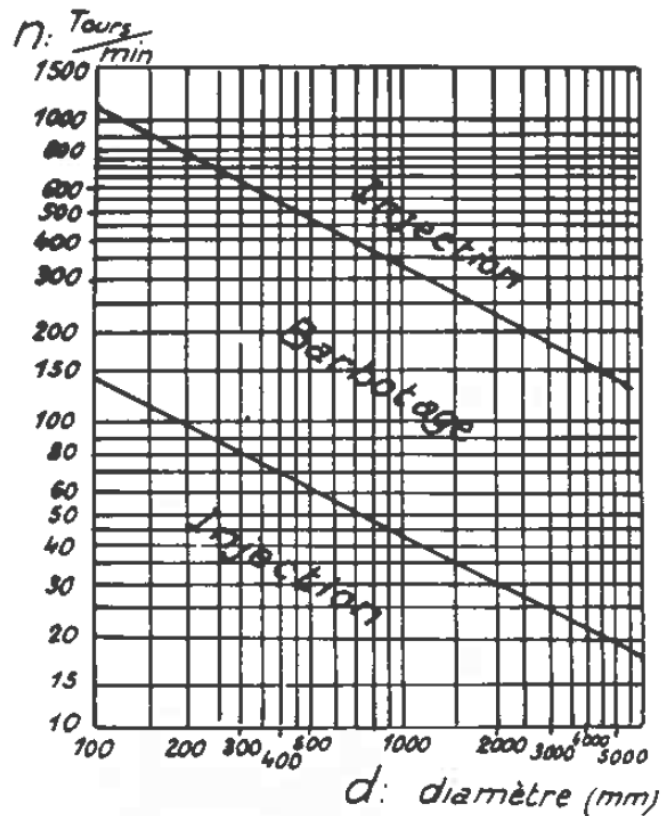


Figure 22 – Lubrication selection abacus by the rotational speed and gear diameter correlation[16].

These two methods are effective but are dependent of some operative and such as gear size rotational speed, etc. In Figure 22 we see an abacus used to choose the most correct lubrication method according to two parameters, the rotational speed n and the gear diameter d . An important aspect is that when the abacus is being used to assess the lubrication method it is important to verify it to the wheel and pinion of the gear pair, because the wheel may be in an oil splash zone but the pinion could be in an oil injection zone leaving the project responsible with a problem to solve.

1.5. Gear failure modes

Gear failure is a serious concern; either you are doing experimental work on lubricants for gears or just gears with a base lubricant or even doing gear design and optimization, a special attention should be paid to the sort of failure mode that could occur during the normal working cycles. The failure mode involved could indicate what changes you might need to do in your lubricant choice or in the gear correction to stop it from happening or in most practical cases, to make the adjustments to decrease the intensity of the failure increasing the life time of the gear sets and the lubricant.

The failure modes in gear tooth can be divided into two major groups: the ones connected to the lubricants and lubrication and the ones connected to the material resistance [19]. The major failure modes associated to the lubricants are the Abrasive and the adhesive wear, scuffing, superficial fatigue most commonly called pitting and

micro-pitting, etc, being this phenomenon's directly related to loss of lubricant film thickness, fast increase in contact temperature and excessive foreign particles in the lubricant[9]. The failures associated to the material resistance are the “Plastic flow” and the fatigue or overload cracks[19].

1.5.1. Current wear

Common wear is basically metallic particle removal from gears tooth constantly along working time due to contact and sliding between active tooth surfaces normally under thin film thickness and slow pitch line velocities[20]. Generally wear occurs during the initiation and stopping of gears and also in gears working at slow velocities, situations where lubrication can be momentarily deficient, causing the marks that could be seen in Figure 23.

The wear rates depends on the roughness contact temperatures which determines the amount of unlubricated area being the most rough asperities of the flanks usually caused by the tooling during the manufacturing process is slowly corroded and abraded away specially during running in and also during gear useful working life, leaving a smooth and polished surface[9, 19]. This phenomenon occurs mainly in high sliding areas located in the tip and root of the tooth and away from the pitch line.

Wear and its intensity depends directly on the working conditions, like lubrications and mechanical solicitations as well as the surfaces finishing, like medium roughness and geometrical profile perfection, but also on material characteristics. A good example of a low wear rate can be found in cemented steel gears or with an hardened surface[19].

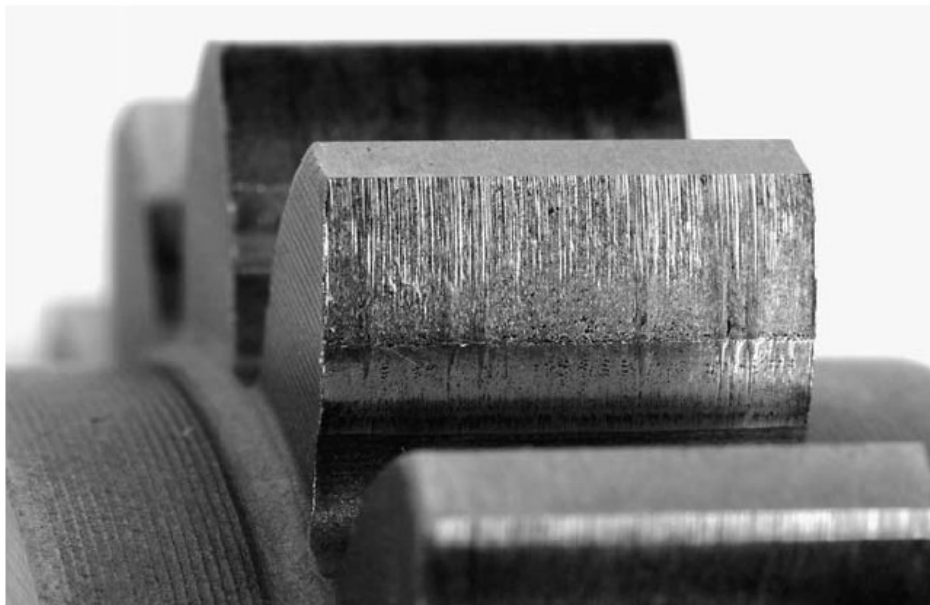


Figure 23 – Wear in a tooth flank[20].

1.5.2. Scoring and scuffing

Scoring and scuffing are different types of wear, both characterized by a sudden weld of both active contacting tooth flanks, and when this phenomenon occurs under low speed and low temperature conditions it's called *Scoring* and when it occurs at medium or high temperatures and high speed it's called *Scuffing*.

Scoring usually occurs due to the appearance of contact stresses superior to the ones bearable by the surfaces, happening mostly when there's a fluid film rupture, which is one of the basic conditions that promote the metal-metal contact. This type of failure initiates with the appearance of small craters or wear striations that rapidly progress to all active tooth flanks.

Scuffing often results from overheating due to a lubricant film rupture causing metal-metal contact allowing localized surfaces adhesion. Preceding this failure phenomenon is identifiable an increase of noise and vibration, a sudden increase of friction and occasionally smoke release[19]. In most common cases the gear teeth surface would present evident marks of a generalized adhesion process and in the case of superficially hardened gear teeth, might occur a sudden crack propagation causing one or more tooth to rupture(Figure 24).

Resuming, this type of failure happens due to an accidental lubrication failure, or an equipment overload, on the other hand, if it happens during the start of the equipment the cause might be the gear conception, bad lubricant choice or miss performed running.



Figure 24 – Scuffing in type A gear tooth flank[20].

1.5.3. Pitting (spalling)

Pitting phenomenon that could appear virtually anywhere along tooth facing but is mostly found in sliding areas near pitch line of spur and helical gears. It's a fatigue failure originated from surface cracks, nicks and furrows on the surface that have been submitted to high surface stress or intense subsurface shear stress. Pitting suffers strong influence from Hertzian stress and surface shear stress therefore fluid film formation[20]. In some cases the crack initiates in the subsurface and propagates towards the surface originating the type of failure seen in Figure 25 which can have dimensions near hertzian contact size[9].

The subsurface pitting is not very affected by the lubrication however the inclusions size, density and material characteristics affect it substantially but surface pitting is directly connected to lubrication because it affects the intensity on the near surface stresses[9].

1.5.4. Micro-Pitting (Gray Staining)

Micro-pitting usually appears when there is a lubrication failure in gear teeth contact leaving the load transfer to be done essentially through roughness contact. It's a fatigue failure characterized by appearing mostly at micro cracking in the negative sliding areas below pitch line[20], leading to the surface material to break (Figure 26), happening more frequently in good quality or nearly inclusion-free materials[9].

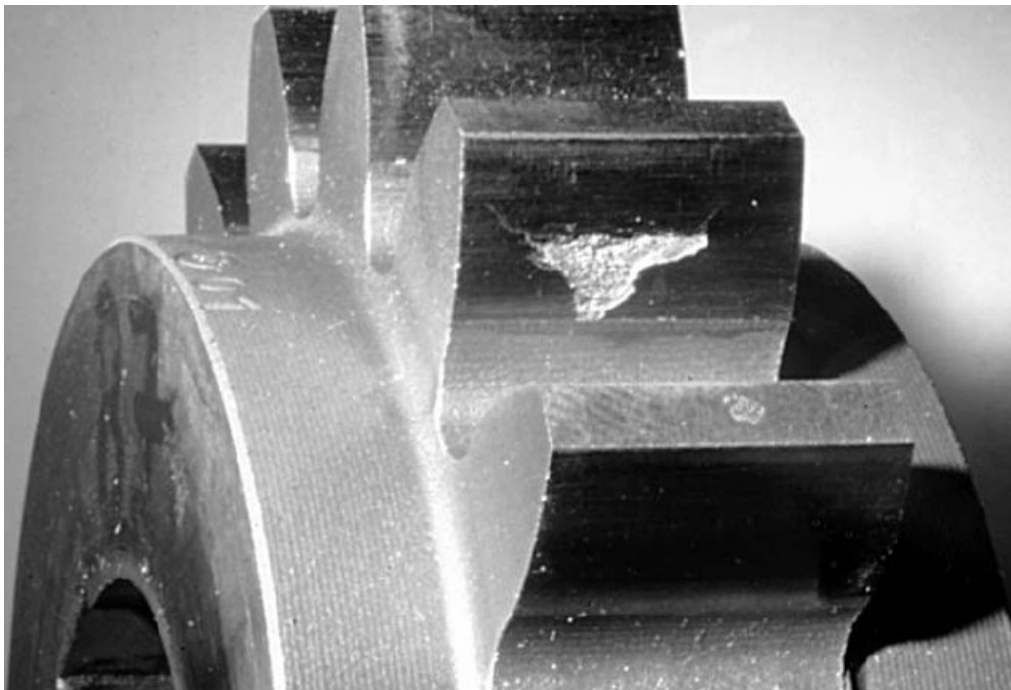


Figure 25 – Pitting in a tooth flank.



Figure 26 – Micro-Pitting in a gear tooth[20].

Micro-pitting is influenced by the relative film thickness λ as the relation of film thickness to surface roughness [20]; it is caused by a fast propagation of a group of cracks originated in the roughness contacts. In a more qualitative view it can be characterized by being shallow small pits measured in the micron range, spread by a large area of the tooth, normally resulting in a gray like patches, being for that reason commonly called “gray staining”. Micro-pitting is considered to be a non-destructive gear failure and can be a slow and progressive degeneration unless it turns into pitting[9].

1.6. Gear power loss

In order to study the influence of gear geometry and material and oil formulation in a power loss test it is necessary to know the origin and type of losses involved.

The most important power dissipation mechanisms inside a gear box, for instance the FZG test rig gearbox, are the churning losses and the frictional losses[8, 21].

The churning losses are associated to the rotational movement of the mechanical components like gears, rolling bearings and seals, immerse in the viscous oil bath. This type of power losses are frequently defined as “No Load Power Loss”, due to their independence from the applied torque [8, 21]. Churning losses inside a gearbox have three preferential origins:

- Churning caused by the rotation of the gear set immersed in the oil bath;
- Churning caused by the rotation of the rolling bearings in the oil bath;
- Friction caused by motion between other parts and the oil bath like seals.

If there is no torque applied, friction between gear teeth is very small not affecting the overall power loss. No Load Power Loss depends mostly on the following parameters [8, 21]:

- Gearbox rotational speed;
- Lubricant oil viscosity at the operating temperature;
- Lubricant oil volume;
- Gearbox geometry and internal parts arrangement;
- Environment temperature in the surroundings influences the heat evacuation.

Frictional losses are associated with friction between moving parts that transmit load, essentially, rolling bearings and gear teeth. These depend on the load transmitted and the friction coefficient between the contacting surfaces[8, 21].

Global power loss is obtained adding the churning and friction losses.

Heat generated inside the gearbox is evacuated by convection, conduction and radiation to the surrounding environment. The final oil bath temperature depends on the balance between heat dissipation and heat generation. After a relatively long operating period, the test rig temperature and the oil temperature tend to a equilibrium state[8, 21].

In Figure 27 we can find the different power loss and heat dissipation mechanisms. FZG test box thermal balance results in an equilibrium temperature, once all the parameters of the equilibrium equation depend directly or indirectly on the oil temperature.

$$P_{fr} + P_{Ml} + P_{spl} + P_{M0} + P_{sl} = Q_{rad} + Q_{cnv} + Q_{cn} \quad (\text{Eq. 36})$$

The temperature dependence of the equilibrium equation terms is non-linear, implicating the use of an interactive solution method.

1.6.1. Load dependent power losses

Gear friction losses (P_{fr}) depend on the geometric conditions of the gearing, the number of teeth, the input power and the friction coefficient[8, 21].

$$P_{fr} = \pi \left(\frac{1}{z_1} + \frac{1}{z_2} \right) \cdot \left(1 - \left(\frac{g_f - g_a}{p_b} \right) + \left(\frac{g_f}{p_b} \right)^2 + \left(\frac{g_a}{p_b} \right)^2 \right) \cdot P_{in} \cdot \mu_m \quad (\text{Eq. 37})$$

The coefficient of friction is a major importance factor in this study, due to be the only parameter affected by the operating conditions. The friction coefficient used in this work is the one proposed by Michaelis et al[21].

$$\mu_M = 0.048 \left(\frac{f_{bt}/b}{v_{\Sigma c} \cdot \rho_c} \right)^{0.2} \eta_0^{-0.05} R_a^{0.25} X_L \quad (\text{Eq. 38})$$

Where $X_L = 1$ for mineral oils.

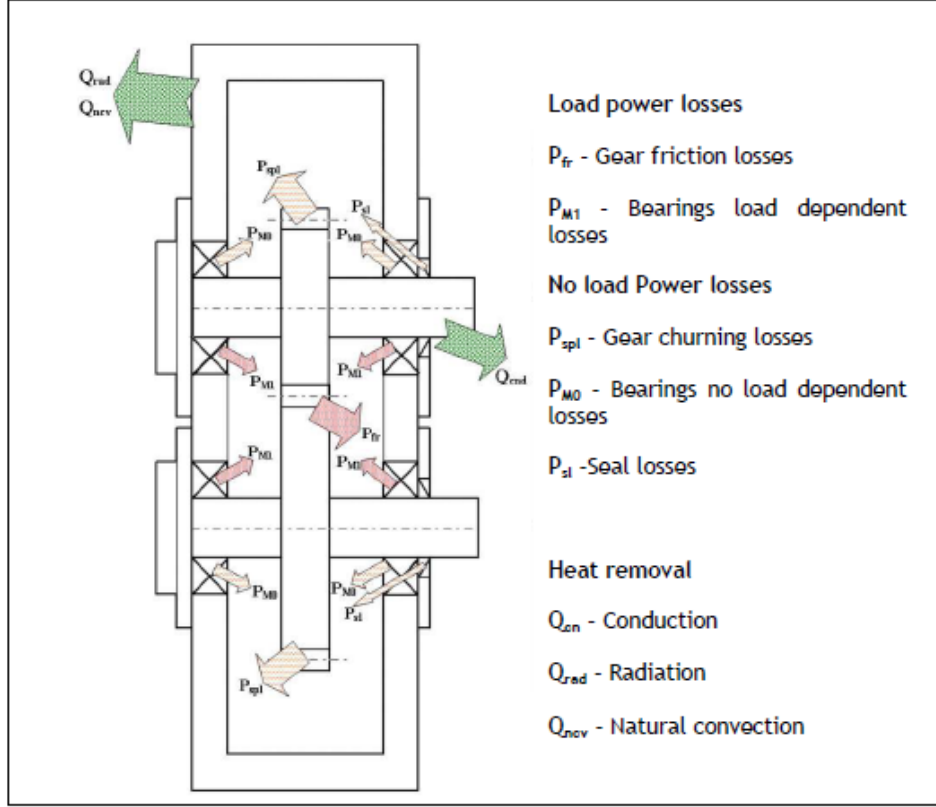


Figure 27 – Forms of power loss and heat dissipation of the FZG test box[8].

Load dependent power losses in bearings depend on the type of bearing, the combined applied load, the bearing diameter and the friction coefficient, being this last one constant for the FZG test box rolling bearings[8].

$$P_{Ml} = \frac{\pi}{30} N \left(\sqrt{F_r^2 + F_a^2} \cdot f_l \cdot D \right) \quad (\text{Eq. 39})$$

1.6.2. No Load dependant power losses

Gear churning losses are independent of load, being the most influent parameters the gear diameter, rotating speed, gears immersion area, gear width, oil viscosity and density. The test box design also has a important influence on the churning losses, as well as the fluid flow regime. An expression was proposed depending on Froud (F_R) and Reynolds (Re) non-dimensional numbers[22].

$$P_{spl} = \frac{\pi}{30} N \left(\frac{1}{2} \rho \left(\frac{\pi N}{30} \right)^2 \cdot A_l \cdot \left(\frac{d_p}{2} \right)^{0.45} \right) \cdot \left(\left(\frac{2h}{d_p} \right)^{0.45} \cdot \left(\frac{V_{oil}}{d_p} \right)^{0.1} F_R^{-0.6} Re^{-0.21} \right) \quad (\text{Eq. 40})$$

No load power loss in bearings depends[22] mainly on the rotating speed, bearing diameter, type of bearing and lubricant viscosity ant operating temperature.

$$P_{M0} = \frac{\pi}{30} N \left(f_0 \cdot 10^{-7} \cdot (N \eta_{oil})^{2/3} \cdot D^3 \right) \cdot 10^{-3}. \quad (\text{Eq. 41})$$

Seals power losses are independent of applied load and represent the friction losses in the contact between seal leaps and shafts, depending mostly on the rotational speed and shaft diameter[21].

$$P_{sl} = 7,69 \cdot 10^{-6} \cdot d_t^2 \cdot N. \quad (\text{Eq. 42})$$

1.6.3. Heat removal

Heat removal from FZG test gearbox depend on the wall temperature that in this case is almost the same as the oil temperature, being this heat dissipated by radiation, free and forced convection and conduction.

The FZG test rig room is equipped with forced ventilation, allowing the temperature too be kept constant, being the air velocity to low to ensure forced convection. Natural convection heat dissipation was separated into two parts referent one to the vertical walls and other to the horizontal ones[22].

The vertical wall convection coefficient is:

$$h_v = 11,06 \cdot h_{ca}^{-0.1} \cdot \left(\frac{Tw - Ta}{Ta} \right)^{0.3} \quad (\text{Eq. 42})$$

where h_{ac} is the height of gearbox.

The convection coefficient for horizontal walls is:

$$h_h = 12,87 \cdot L_{ca}^{-0.04} \cdot \left(\frac{Tw - Ta}{Ta} \right)^{0.32} \quad (\text{Eq. 44})$$

where L_{ca} is the characteristic dimension of the horizontal wall (mean value of width and length).

The power removed by convection in vertical and horizontal walls is:

$$Q_{cnv} = h_v A_v (Tw - Ta) + h_h \cdot A_h \cdot (Tw - Ta) \quad (\text{Eq. 45})$$

The amount of power removed by radiation is determined from the Stefan-Boltzman law, but for simplicity a heat radiation coefficient (α_{rad}) is defined.[21]

$$\alpha_{rad} = 0,23 \cdot 10^{-6} \varepsilon \left(\frac{Tw + Ta}{2} \right)^3 \quad (\text{Eq. 46})$$

The power removed by radiation is determined from the following expression.

$$Q_{rad} = \alpha_{rad} \cdot A_{rad} (Tw - Ta) \quad (\text{Eq. 47})$$

Conduction heat removal calculation in FZG gearbox is to complex due to be bi-directional and the base plate of the fZG test box has a complex shape, therefore

Michaelis et al[17] proposed the substitution of the heat conduction by increasing the test box radiation and convection area by a factor (f_{cn}) of 1.5 to 2.5 times the area of contact between the test box and the base plate.

$$Q_{cn} = (Q_{rad} + Q_{cnv}) \cdot \left(f_{cn} \frac{A_{base}}{A_{rad}} \right) \quad (\text{Eq. 48})$$

The “ f_{cn} ” factor for the used test rig was determined from the result of no load tests resulting in a value of $f_{cn}=2.5$.

2 – GEARS, MATERIALS AND OILS

2. Gears, Materials and Oils

2.1. Low loss gears

The “Low Loss” gears are an especial type of gears, they are designed to achieve low friction between contacting teeth during the meshing cycle in comparison to standard FZG Type C gear. These gears have less power consumption by friction and they can be produced through simple geometric modifications, using standard 20° tools[7].

A good way to better understand the importance of low loss gears is through an example and to do so we will start with the gearing model presented in Figure 28.

Figure 28 shows the main reference gearbox model data and gear shape cross section necessary for the calculations of this example, and applying single modifications we are able to study the influence of a single parameter. In Figure 29 we can see clearly the different types of power loss, but our focus is attached to only two of them, the gear load dependant and no-load dependant power loss. With a closer look at these particular forms of power loss we can rapidly identify that the gear load dependant power losses are dominant relatively to all other forms of power loss and in this case the gear no-load dependant power loss only gains some expression when the pitch line velocity reaches 40 to 60 m/s.[5] Is now clear that the study of Low Loss gears is an important subject, and that the load dependent loads are one of the main sources of power loss in gearboxes.

Gears	Bearings	Operating Conditions
$m_1 = 4 \text{ mm}$	4 ball bearings	$T = 500 \text{ Nm}$
$z_2 : z_1 = 23 : 23$	$d = 30 \text{ mm}$	$p_c = 1180 \text{ N/mm}^2$
$\alpha_n = 20^\circ$	$D = 90 \text{ mm}$	lubricant FVA3A ¹⁾
$\alpha_{wt} = 19.12^\circ$		type injection
$\epsilon_1 : \epsilon_2 = 0.7 : 0.7$		$\theta_{oil} = 60^\circ\text{C}$
$\beta_b = 19^\circ$		
$b = 40 \text{ mm}$		
$a = 91.5 \text{ mm}$		
$x \cdot m = -0.245$		

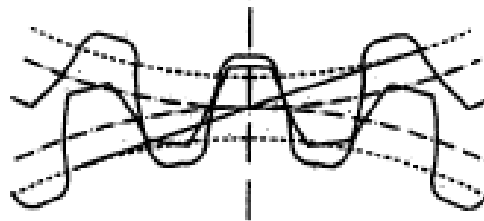


Figure 28 – Main data of reference gearing model and gear cross section [5]

1) mineral oil ISO VG 100 with 4% Sulphur-phosphorus additive (Anglamol 99)

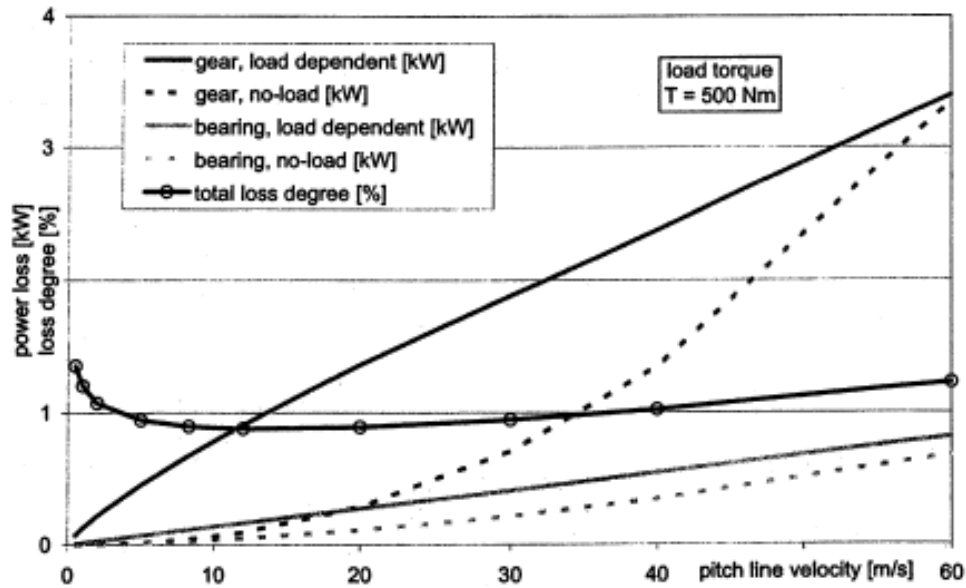


Figure 29 – Power loss composition in the model gearbox [5].

The standard FZG type C gear is a spur gear used as reference in power loss tests and when Hohn et al [5] proposed an equivalent load carrying capacity low loss model of this gear, several improvements were observed, such as, the reduction in the transverse contact ratio that basically is a reduction of the teeth contact along the path line during less time resulting on a reduction of friction. In order to achieve the improvements mentioned above, some changes in the standard Type C gear were made, like introducing an helix angle to guarantee that one or more teeth are always contacting (implying a good total contact ratio), increase the number of teeth and in the particular case of the low loss model presented by Hohn et al. the pressure angle was increased [3]. A resume of the main properties of the Type-C gear and the Low Loss one can be found in the Table 6. To get a better perception of the differences between the FZG Type-C gears and the Low Loss ones check Figure 30 where you can transpose the numbers from the table below to the real geometry.

Table 6 – Standard FZG type-C and “Low Loss” gears [1-2]

	Symbol	Type C	Low Loss
Module (mm)	m	4.5	1.75
Number of teeth	Z1/Z2	16/24	40/60
Pressure angle (°)	α	20	40
Helix angle (°)	β	0	15
Teeth width (mm)	b	14	20
Normal Contact ratio	ε_{α}	1.43	0.55
Complementary contact ratio	ε_{β}	0	0.94
Overall contact ratio	ε_{γ}	1.43	1.49



Figure 30 – Gear geometries: FZG type-C on the left vs Low Loss on the right.

2.2. Gears geometry

In this work were used two base materials to produce the gear sets, a steel alloy and an iron alloy. For each base material were produced several gear sets, being the sets produced in iron slightly different from the ones produced in steel. The main cause for the small difference in geometry is explained by the fact that to achieve the same type of gears using different material is required different manufacturing processes.

The starting point for this study was the elementary FZG Type-C gear design with a 91.5mm of center distance like the one in Table 6, and having into account some previous work on this subject [1, 3, 23], several profiles were developed aiming power loss reduction, and according to the following group of restrictions some of them were targeted of this study[2]:

- (i) Reduce the gear modulus and increase the number of teeth, keeping constant the center distance using high positive profile shifts;
- (ii) Use standard cutting tools with 20° pressure angles available in all manufacturing shops;
- (iii) Impose a minimum value of the normal contact ratio close to 1.0;
- (iv) Impose a total contact ratio close to 2.0;
- (v) Keep constant the gear safety factors against tooth root breakage (SF) and surface pressure (SH).

Following the five objectives presented above were selected 3 different geometries presented in the following chapters.

2.2.1. Geometry of low loss gears 311, 411 and 611

In order to conduct a progressive study of power loss in a test gearbox, 3 different geometries were developed in Carburized steel DIN 20MnCr5 Case Hardened, with a careful set of modifications that starts in the addendum modification coefficients and a helical angle, passing by the increasing of the tooth number, etc. These gear geometries were specially design to be produced by standard 20° rack tools and still be able to present the improvements observed in the “Low Loss” gear model presented by Hohn et al. In Figure 31 – Pinions teeth geometry for the Low Loss gears 311, 411 and 611. can be seen a picture of all three gear geometries and some differences are evident, like the size and number of teeth that vary widely from the 311 to 611.

A summary of all the gears main geometric properties can be found in Table 7. These geometrical properties, security coefficient, contact parameters (Table 8) and friction power loss were calculated with the help of specialized gear calculation software, the Hirnware KISSsoft.

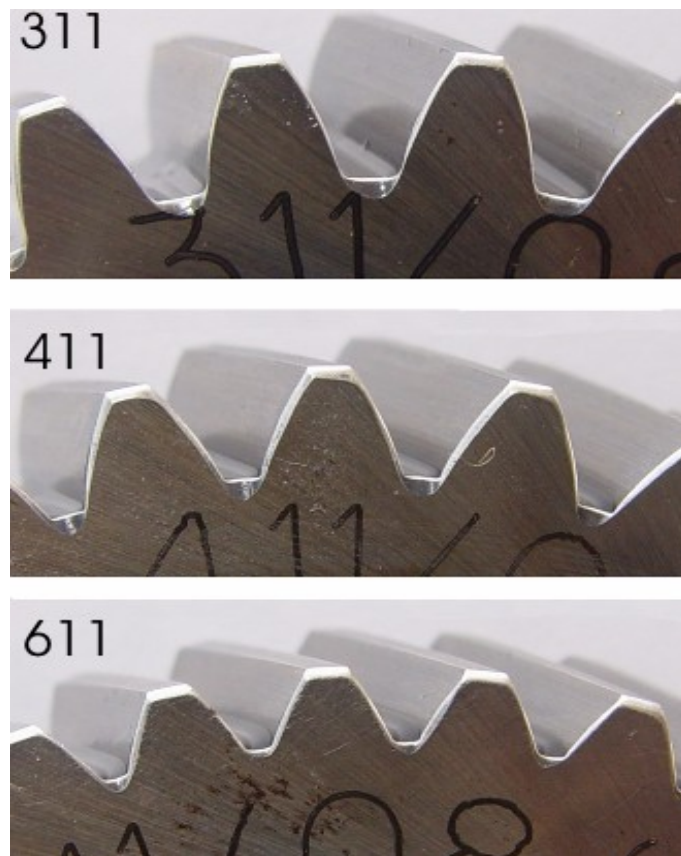


Figure 31 – Pinions teeth geometry for the Low Loss gears 311, 411 and 611.

Table 7 – Geometrical parameters of gears 311, 411 and 611.

Gear Parameters	Symbol	units	311		411		611	
			pinion	wheel	pinion	wheel	pinion	wheel
Module	m	mm	2.5		2.25		1.75	
Number of teeth	Z	-	28	42	30	45	38	57
Teeth width	b	mm			20			
Helical angle	β	°			15			
Working pressure angle	α_{wt}	°	22.12		26.70		28.34	
Addendum mod. Coef.	x	-	0.13	0.25	0.96	1.15	1.74	1.95
Tip diameter	da	mm	78.05	114.89	77.50	113.29	76.41	111.56
Tip diam. Mod. Coef.	k*m	mm	-0.03		-0.61		-1.02	
Pitch diameter	d	mm	72.47	108.70	69.88	104.82	68.85	103.27
Working pitch diameter	d _w	mm	73.20	109.80	73.20	109.80	73.20	109.80
Transverse contact ratio	ε_{α}	/	1.52		1.17		0.93	
Overlap contact ratio	ε_{β}	/	0.66		0.73		0.94	
Total contact ratio	ε_{γ}	/	2.18		1.90		1.87	
Path of contact (length)	g	mm	11.58		8.02		4.97	
<i>Safety coefficients*</i>								
Tooth root stress	SF	/	1.79	1.79	1.49	1.49	1.50	1.49
Surface pressure	SH	/	1.18	1.19	1.16	1.16	1.07	1.08
<i>Contact Parameters*</i>								
Max. Hertz pressure	P ₀	GPa	0.96		0.99		1.07	
Max. sliding speed (tip)	v _{ga}	m/s	2.18	2.37	1.71	1.44	1.24	0.71
<i>Calculated gear friction power loss**</i>								
Gear friction power loss	P _{fr}	W	413		299		240	

*Torque applied to wheel – 323 Nm, wheel rotation – 1500 rpm.

**Considering an ester-based fully saturated gear oil, ISO VG 100.

Table 8 – Tooth width safety factor for 20MnCr5 gears.

Gear Parameters	Symbol	units	311		411		611	
			pinion	wheel	pinion	wheel	pinion	wheel
Tooth width	b	mm	20		22		26	
Safety coefficients*								
Tooth root stress	SF	-	1.79	1.79	1.60	1.60	1.92	1.91
Surface pressure	SH	-	1.18	1.19	1.19	1.21	1.21	1.21
Contact Parameters*								
Max. Hertz pressure	P ₀	GPa	0.96		1.08		0.96	

In Table 8 are presented the safety coefficients and contact parameters for the three geometries and also the real tooth width if there was no width restriction.

2.2.2. Geometry of low loss gears 312, 412 and 612

Three geometries similar to the ones design to the steel gear sets were also manufactured in an iron alloy DIN 1.0Cu-0.5Mn ADI (Austempered Ductile Iron). The main difference between the steel gears and the ADI ones are the manufacturing method because the ADI gears are casted directly in disc shape molds and then transferred to a machine that cuts the teeth shapes and another to finish the superficial layer. The other main difference between the steel and the ADI gears is the most obvious and that is the material they are made of, the ADI has lower Young modulus than steel therefore different elastic response influencing safety factors and the contact parameters. Another big difference is the surface texture that difficult the achievement of equivalent contact conditions specially when mixed lubrication occurs[7]. These differences can be seen on Table 9, where can be found a comparison of the safety factors and contact parameters between the ADI and Steel Gears.

Table 9 – Safety coefficients and working parameter for ADI and Case hardened steel gears.

			311	312	411	412	611	612
<i>Safety Coefficient</i>	<i>Symbol</i>	<i>units</i>	steel	ADI	steel	ADI	steel	ADI
bending	SF	-	1.8	1.0	1.5	1.0	1.5	1.4
Pitting	SH	-	1.2	1.0	1.2	1.0	1.1	0.9
Scuffing	SB	-	3.5	2.58	4.21	2.96	-	-
Working Parameters								
Hertz pressure*	P ₀	GPa	1.17	0.97	1.19	1.01	1.29	1.11
Resonance speed	nE1	rpm	13139	11753	11407	10209	7778	6969
Gear friction Power Loss*	PVZ	kW	0.417	0.624	0.303	0.453	0.243	0.363

*speed=1500rpm, torque=323Nm (applied to wheel), transmitted power=50.8kW

In Table 9 can be seen a couple more parameters that didn't appear in Table 8 like the scuffing safety coefficient and the resonance speed and the reason for that is because those parameters are not an integrant part of the study presented on this thesis despite their importance. These extra parameters are just presented here to reinforce the theoretical advantages of ADI that is one of the major targets of this study.

In general the safety factors in the steel gears are better than the ADI ones for the three geometries except for the scuffing coefficient, this might be explained by the fact of all ADI gears have lower Hertz pressure compared to their analogous steel ones. Also the resonance speed of ADI gears is lower partially because of their smaller specific weight but ADI is not perfect and the major disadvantage is the surface texture that is worse than the steel one, which explains the increase of gear friction power loss in ADI gears relatively to their steel equivalent.

2.3. Gears Material

2.3.1. ADI (Austempered Ductile Iron)

The Austempered Ductile Iron or ADI as is commonly named is an iron alloy that have been used since late 70s of the 20th century and have suffered remarkable improvements since then, being one of the most interesting Fe-C alloy having into account his amazing combination of mechanical properties.

Nowadays ADI can compete with high resistance steel alloys, not only because it has a similar tensile strength but also because its base material[24], the nodular iron costs less than steel and can be casted which means it can be molded into a shape closer to the finished product reducing very significantly the manufacturing process cost when compared to steel [25]. ADI's advantages don't stop here, it's also lighter than steel, reaching less 10% of weight being for instance, very attractive to the automotive companies, and they are also very resistant to wear and scuffing being useful in cases of temporary breakdowns like a lubrication system failure for example [26].

The Iron used to produce the ADI has the chemical composition described in Table 10 [24, 27-29].

The ADI is obtained through an austenitisation during 30 to 40 min at temperatures around 900°C followed by an austenite isothermal transformation during 210 min [7, 24, 29](Simplified process described in Figure 32) in a salt bath crucible furnace in order to ausferritic microstructures to form as shown in Figure 33 and the graphite nodules as shown in Figure 34.

Table 10 – ADI chemical composition (%).

C	Si	Mn	Cu	P	S
3.38	2.43	0.55	1.11	0.01	0.020

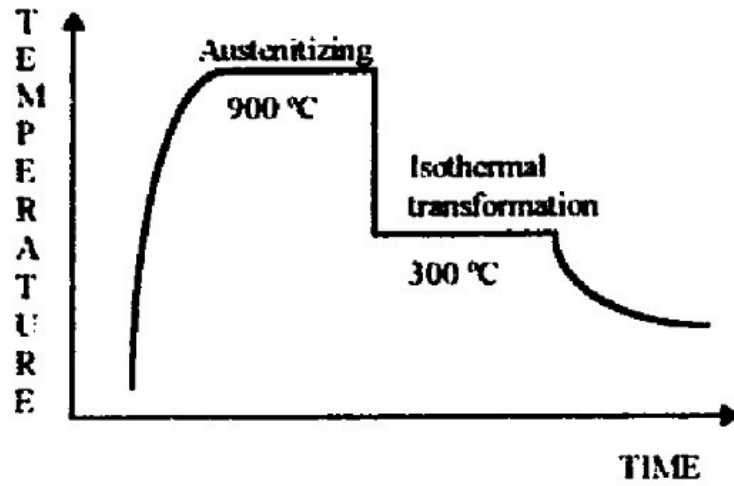


Figure 32 – Austempering thermal cycle [29].

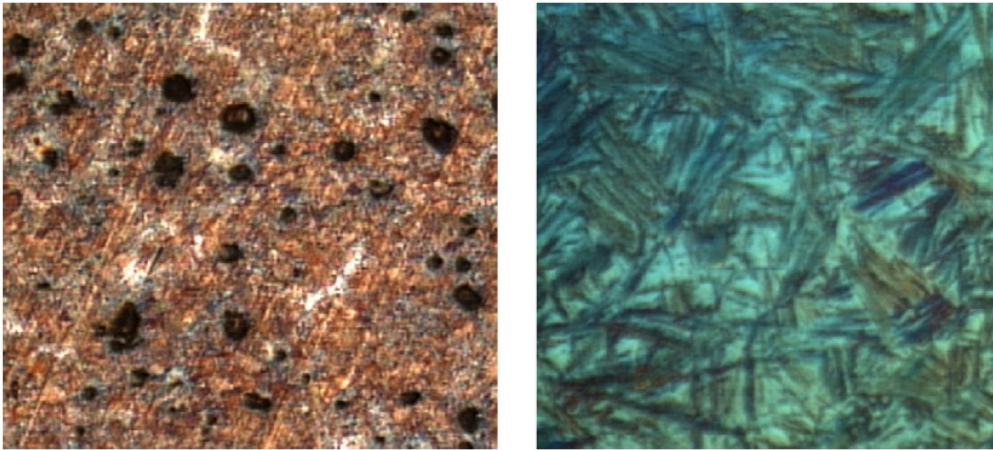


Figure 33 – ADI Microstructure (100x and 1000x magnification)[24].

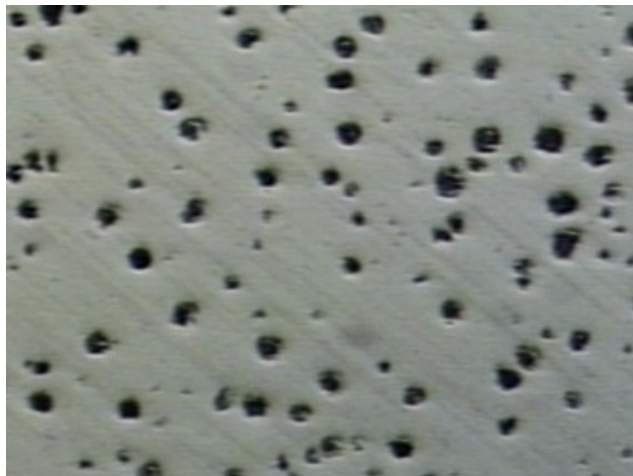


Figure 34 – ADI surface (50x magnification)[7].

Table 11 – Properties of ADI.

Parameter	units	value
Elastic module	GPa	153
Density	g/cm ³	7.06
Poisson ratio	-	0.25
Hardness	HRC	42
Tensile strength	N/mm ²	1313
Yield strength	N/mm ²	1068
Elongation	%	2

The presence of these graphite nodules can have some advantages, being one of them the fact that they originate holes when they fall off during the meshing cycle, being these holes filled with oil behaving this way like a reservoir which is very useful during low lubrication conditions, being the graphite itself also very useful because it decreases the friction avoiding scuffing in limit situations and most important of all ADI seems not to benefit from Extreme pressure and anti-wear lubricant additives enabling the use of lubricants with less additive packages that are less expensive. Despite all this advantages it has also some setbacks like the fact that graphite affects the chemical composition of gear oil especially in the extreme pressure compounds formation and the holes left by graphite alters the fluid film dynamics formation[7]. A resume of ADI properties can be found in Table 11

2.3.2. Carburized steel (DIN 20MnCr5)

Carburized steel is often used to produce highly stressed mechanical components and among them are gears. In this particular work gears were manufactured in DIN 20MnCr5 steel, they were carburized, quenched in oil and annealed before grinding. The steel surface was hard with values around 60 HRC and the core maintain a high strength and a relatively high elongation, being this a common procedure adopted in gear manufacturing[30].

The chemical composition (weight %) of the DIN 20MnCr5 Carburized steel is described in Table 12 and its physical properties are described in Table 13 and Table 14. The thermal expansion coefficient for this material is described in Table 14 for several temperature ranges[30].

Table 12 – Chemical composition (weight %) of the 20MnCr5 carburized steel.

C	Si	Mn	Cr
0.20	0.20	1.25	1.15

Table 13 – Physical properties (average values) at ambient temperature of the 20MnCr5 carburized steel.

Parameter	Units	Value
Modulus of elasticity	10^3 N/mm^2	210
Density	g/cm^3	7.85
Thermal conductivity	W/m.K	42.0
Specific electrical resistivity	$\text{Ohm mm}^2/\text{m}$	0.16
Specific heat capacity	J/g.K	0.46

Table 14 – Average thermal expansion coefficient between 20°C and X°C [in 10^{-6} m/(m.K)].

Temperature Range	100°C	200°C	300°C
Average thermal expansion coefficient	11.1	12.1	-

Table 15 – Heat treatment steps for the 20MnCr5 carburizing steel.

Heat treatment step	Temperature	Time period
Pre-heating	100°C	
Austenitization	900°C	
Carburizing temperature	900-950°C	5h
Diffusion during cooling	From carburizing Temperature to 860°C	2h30
Stabilization before quenching	860°C	00h30
Quenching in oil	60°C	
Tempering temperature	220°C	1h00

The heat treatment applied to 20MnCr5 steel for a carburizing depth of 0.8mm and 58-62 HRC surface hardness is described in Table 15. The main commercial applications of the 20MnCr5 carburized steel are as we've said early, highly solicited parts such as: gears that are the center piece of our study, as well as crankshafts, bushings, etc.

2.4. Tested gear oils

Two industrial gear oils were used in this work, the P1 and E2 formulated with different base oils and both fully saturated, classified as CL gear oils according to DIN 51517, being their main properties presented in Table 16. The P1 and E2 are commercial industrial oils with viscosity grades ISO VG 150 and ISO VG 100 respectively. P1 has a polyalphaolephine (PAO) base oil and E2 has a highly saturated biodegradable ester base oil.

These lubricants have very different properties, being per example, their kinematic viscosities at 100°C 19.4cSt and 14.6cSt for P1 and E2 oils respectively. The piezoviscosity at 100°C is 10.97GPa and 9.51GPa for P1 and E2 oils respectively. The P1 has higher kinematic viscosity and piezoviscosity than the E2 but this has a higher viscosity index, this parameter has influence in the film thickness.

Because these two lubricant oils have such differentiated physical properties, they will generate different friction coefficients between gear teeth and therefore different gear friction power loss, being the operative conditions entirely dependent of the gear oil type.

Table 16 – Gear oils Properties.

Oil Reference		P1	E2
Base Oil		PAO	Ester
Oil properties	units		
Density @ 15°C	g/cm ³	0.848	0.925
Kinematic viscosity @ 40°C - ν_{40}	cSt	151	99.4
Kinematic viscosity @ 100°C - ν_{100}	cSt	19.4	14.6
Viscosity Index - VI	/	147	152
Thermoviscosity @ 40 – β_{40}	cSt/°C	0.0471	0.0443
Thermoviscosity @ 100 – β_{100}	cSt/°C	0.0244	0.0229
Piezoviscosity at 0,2 GPa ($\alpha=s.vt'$)			
Piezoviscosity parameter – s	/	7.382	6.605
Piezoviscosity parameter - t	/	0.1335	0.136
Piezoviscosity @ 40°C – α_{40}	GPa ⁻¹	14.41	12.35
Piezoviscosity @ 100°C – α_{100}	GPa ⁻¹	10.97	9.51

3 – GEAR TESTING PROCEDURES

3. Test Machines and Procedures

In order to do proper investigation work, several specific machines were used. Some of these machines were used to do the first order tests, like for example, the FZG Test Rig, and others used to do a second order test, like the Hommelwerk roughness machine and the direct read ferrometry machine.

3.1. FZG test rig

The FZG test rig is a well known back-to-back spur gear test rig with “power circulation”, shown in Figure 35. The test pinion and the test wheel are connected by two shafts to the driving gears in the slave box. The front shaft is divided in two parts separated by the load clutch. One half of the load clutch can be fixed to the foundation by a locking pin while the other part can be twisted using a load lever and weights. After bolting the clutch together the load can be removed and the shaft unlocked. Now a static torque is applied to the system and can be measured by the torque measuring clutch. The maximum speed of the AC-motor is 3000 rpm. The test gears can be dip lubricated or jet lubricated. When dip lubrication is used, the oil may be heated using the electrical heaters mounted in the test gearbox. The heater and cooling coil allows the settling of a constant oil temperature measured by the temperature sensor[31].

A schematic view of the FZG test rig can be seen in Figure 35 and a real image of the machine can be seen in Figure 36.

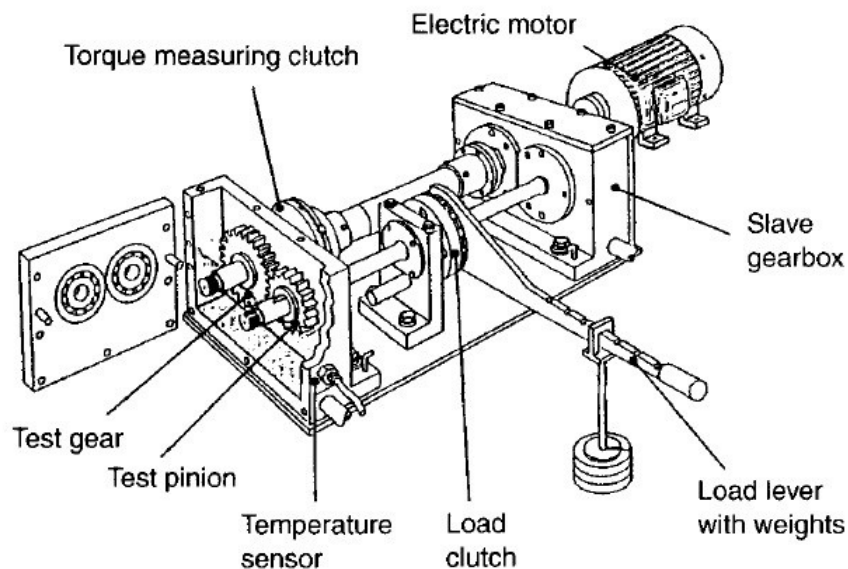


Figure 35 – FZG test rig schematic view.

The FZG test rig allows several gear and oil tests to be performed on it, such as:

- Gear scuffing tests;
- Gear power loss tests;
- Gear pitting tests;
- Gear micropitting test;
- Gear oil scoring test;
- Gear grease scoring and wear test;
- Shear stability test.

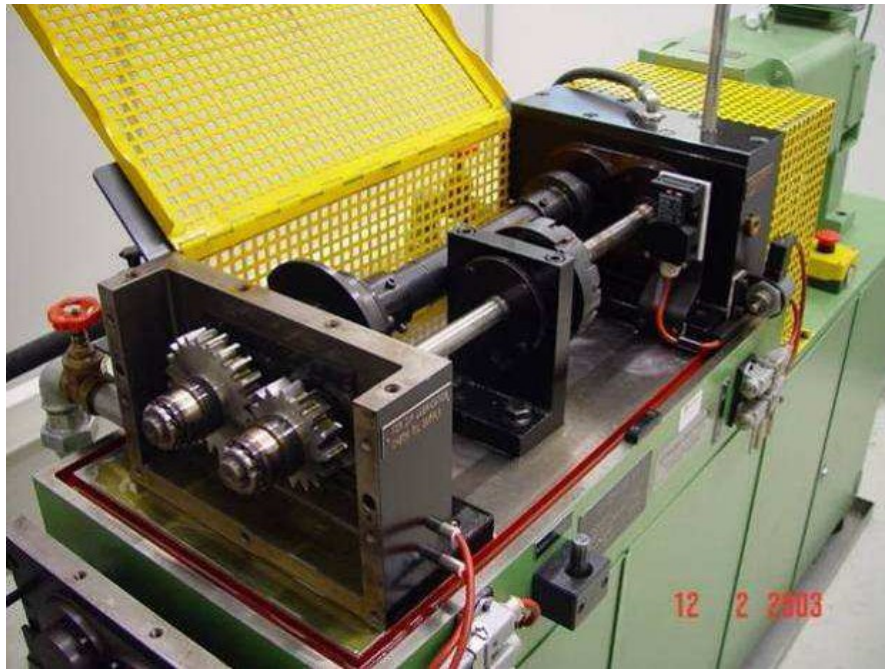


Figure 36 – FZG test rig real view.

3.2. Pressure pads

The pressure pads are a pair of metallic hydrodynamic discs designed to absorb the axial forces produced during the meshing cycle of helical gears sets. These discs are mounted one on each side of the gear set as you can see in Figure 37.

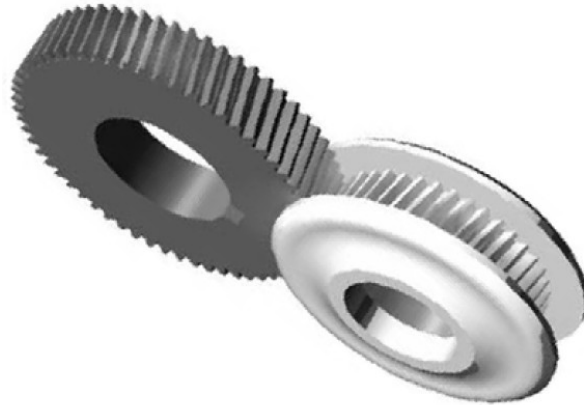


Figure 37 – Model of the pressure pads mounted on the sides of the pinion.

The need to absorb the axial forces generated during the meshing cycle came from the fact that the standard FZG test gearbox is only prepared to test spur gears that generate virtually no axial forces. The pressure pads were the solution found to be able to test the Low Loss gears that are helical in the spur gear test gearbox, transferring almost all the axial forces through the lateral faces of the gear pinion and wheel. Only a residual amount of axial forces is transferred to the cylindrical roller bearings that can only sustain small amounts of axial loads, leaving them free to support only the radial loads generated during the meshing cycle of the helical gears not damaging the test gearbox that could compromise the data gathered during the tests, affecting this way the result and the conclusions of the studies made on the subject [3].

An important fact to be noticed is that, due to the mounting options of the FZG test gearbox and the use of pressure pads the width of the test gears was limited do 20mm. This lead to a decrease of the safety factors of 411 and 611 gears relatively to 311 gear , but this decrease could be avoided if the width limit was not imposed, as you can see in Table 8.

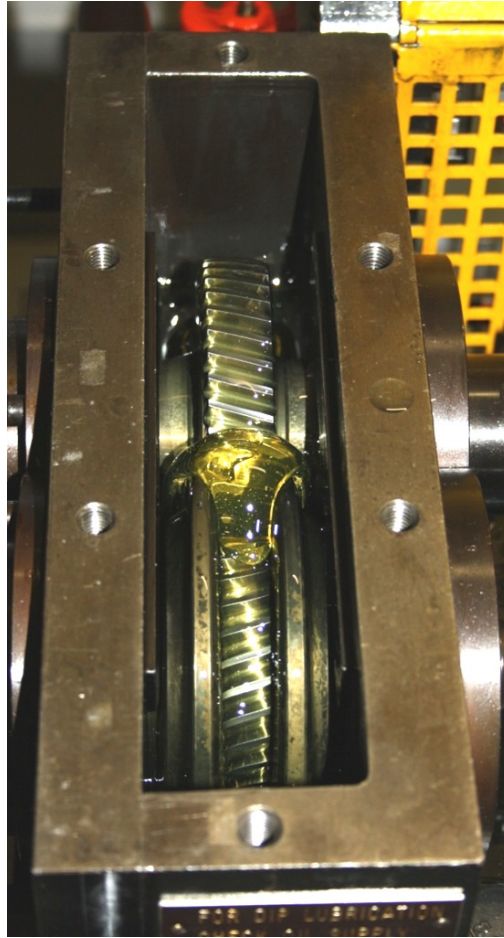


Figure 38 – Oil flow caused by pressure pads during meshing cycle.

3.3. Power loss test procedure

Power loss tests were performed in the FZG machine (Figure 36) using a spur gear test gearbox with pressure pads (see chapter 3.2) for axial loads absorption. The gear tested geometries were the ones described in Table 7 fabricated both in 20MnCr5 case hardened steel and ADI.

The different torques applied correspond to the Standard FZG Load stages, using a 0.35m load arm[31] four load stages were considered, K1, K5, K7 and K9 respectively as referred in Table 17. Every load stage was performed at three different speeds, 500rpm, 1000rpm and 2000rpm respectively

Each load stage speed combination had a 4h operating time in order to achieve an equilibrium energetic state between the power loss inside the FZG gear box and the heat evacuation to the surrounding environment, reaching also a constant oil operating temperature. Every load stage have three 4h operating times one for each speed, performing 120 000 cycles at 500rpm, 240 000 cycles at 1000rpm and 480 000 cycles at 2000rpm, reaching a total of 840 000 cycles per load stage.

Table 17 – Test conditions for power loss test.

Test type	Wheel Torque	Wheel Speed	Input Power	Initial temperature	Operating time	Number of cycles	Lubricant Monitoring
	[Nm]	[rpm]	[kW]	[°C]	[hours]	[x10 ⁶]	Samples
No load tests	4.95 ($k_{FZG}=1$)	500	0.52	Room temperature	4	0.840	40 ml
		1000	1.04		4		
		2000	1.56		4		
Load tests	105.0 ($k_{FZG}=5$)	500	11.00	40≤	4	0.840	40 ml
		1000	21.99		4		
		2000	32.99		4		
	198.8 ($k_{FZG}=7$)	500	20.81	40≤	4	0.840	40 ml
		1000	41.63		4		
		2000	62.44		4		
	323.4 ($k_{FZG}=9$)	500	33.87	40≤	4	0.840	40 ml
		1000	67.73		4		
		2000	101.60		4		
Total	/	/	/	/	48	3.36	/

**Figure 39 – Oil samples collected after each power loss load stage.**

An oil sample is also collected (Figure 39) in the end of each load stage with approximately 40ml, in order to be submitted to a direct ferrometry and an analytic ferrography analysis (seen chapter 3.5).

A low oil version of this test was also made and the results are compared with the standard oil level version in chapter 4.

3.4. Churning loss test procedure

During this work arose the need to study the oil level influence and in order to do so a more extended version of the churning loss test was developed, once the standard churning loss test is coincident with the running in stage (FZG K1 stage) of the standard FZG Power loss test. All gear geometries were submitted to this test described in Table 18 except the ADI gears (see chapter 6).

Besides this difference in the churning loss test, all the other post test analysis procedures like the roughness measurement, oil analysis and mass loss remain the same (Table 18)

Table 18 – Test conditions for churning loss test.

Test type	Wheel Torque	Wheel Speed	Initial temperature	Operating time	Number of cycles	Lubricant Monitoring
	[Nm]	[rpm]	[°C]	[hours]	[x10 ⁶]	Samples
Churning tests	4.95 ($k_{FZG}=1$)	500	Room temperature	4	0.54	40 ml
		750		4		
		1000		4		
		1250		4	1.08	40 ml
		1500		4		
		1750		4		
		2000		4	1.62	40 ml
		2250		4		
		2500		4		
Total	/	/	/	36	3.24	

3.5. Surface Roughness and Topography Measurement

The roughness is a parameter of extreme importance as mentioned before; therefore an accurate measurement of different roughness parameters is critical to a complete study of surfaces submitted to in this case a power loss test. The equipment used in this research is the Hommelwerke test rig (Figure 40) with a TK300 probe covering a total measuring length of $L_t = 4.8\text{mm}$ and a cut-off filter $\lambda_c = 0.8\text{mm}$ with a velocity $V_t = 0.5\text{mm/s}$, being the roughness profile digitally filtered (Figure 41)[32] with the help of the TurboWave software provided by the machine manufacturer, and using the TK300 Gear program.

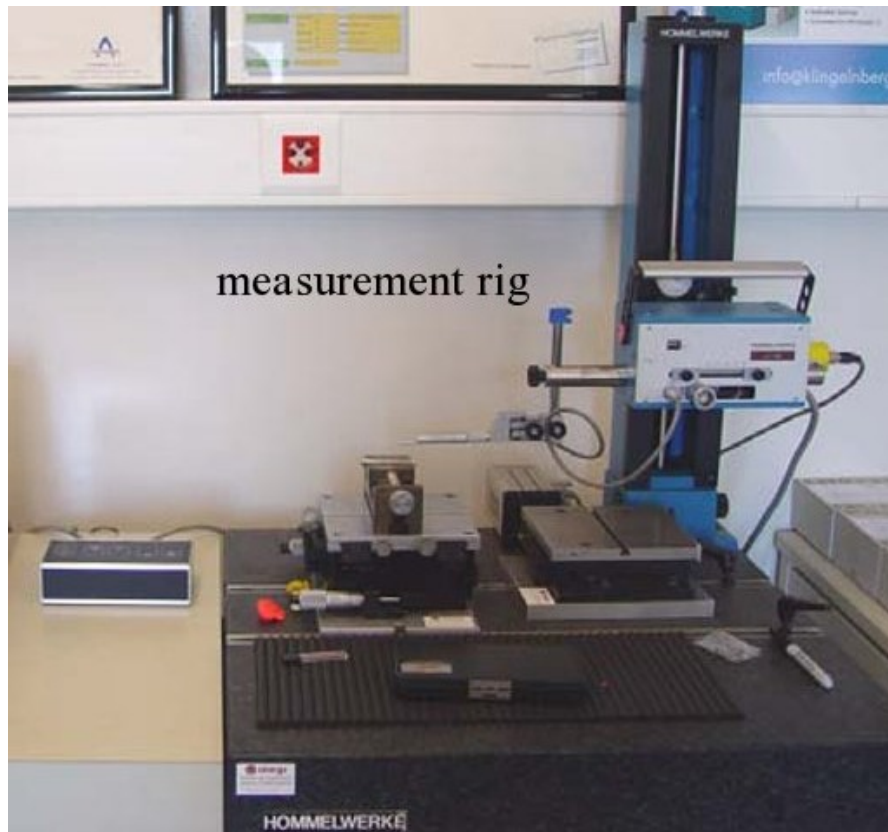


Figure 40 – Photograph of a Hommelwerke TK300 measurement rig.

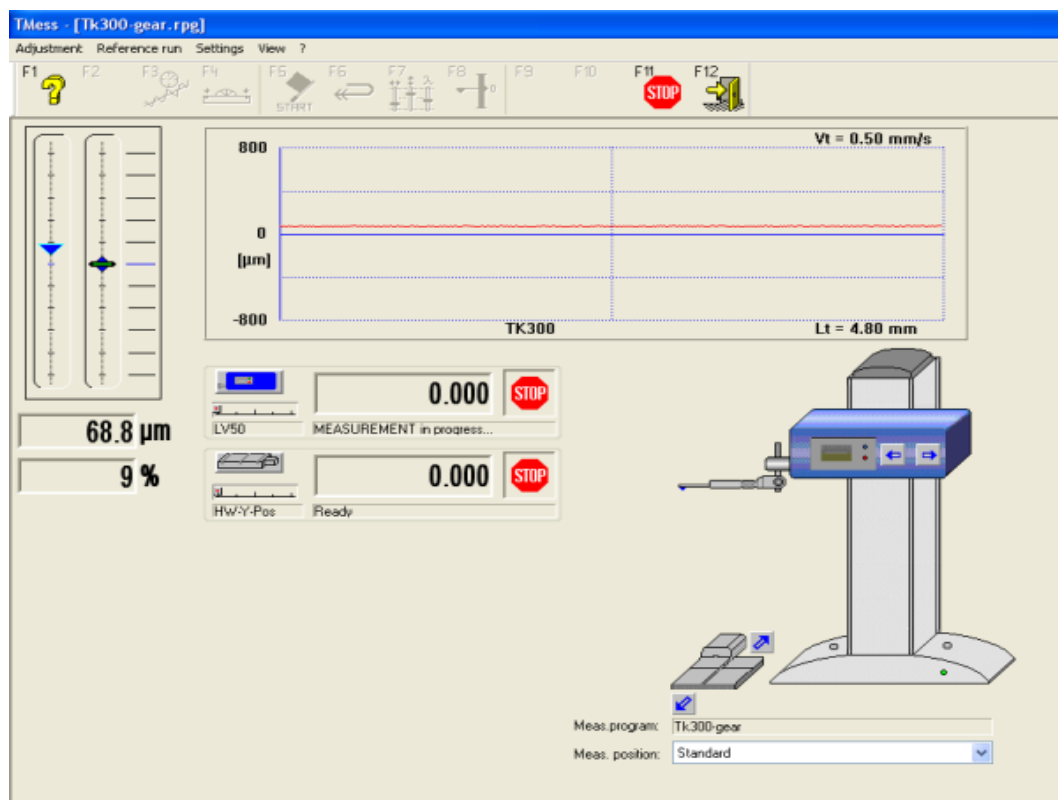


Figure 41 – Roughness measurement and Digital filtering sheet of the Turbowave software from Hommelwerke.

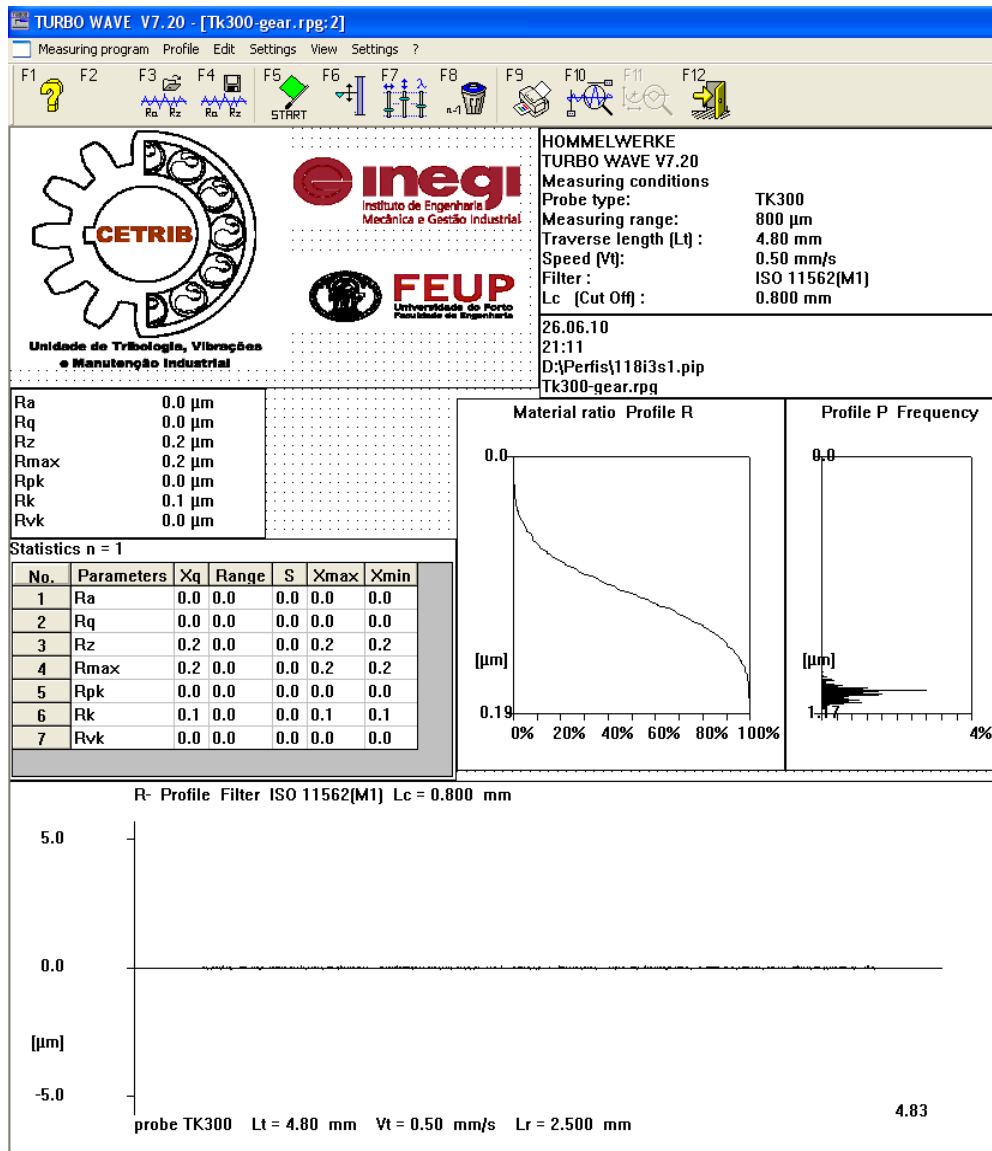


Figure 42 – TK300 gear program datasheet, used in the roughness measure filtering.

The TK300 Gear program calculates a few of the most important roughness parameters mentioned below[32];

- ✓ **The average Roughness, R_a** – used mostly to supervise a production process where gradual changes in the surface finish due to cutting tool wear, may occur;
- ✓ **The root mean-square profile, R_q** – is basically the standard deviation from statistics.
- ✓ **The mean peak to valley height, $R_{z,DIN}$** – gives the description of the amplitude of the roughness that is not too sensitive to freak events, like a single abnormally deep valley in the profile.
- ✓ **The reduced peak height, R_{pk} and the reduced valley depth, R_{vk}** – R_{pk} is the average height of the highest peaks above the core roughness, and R_{vk} is the average depth of the lowest valleys below the core roughness.

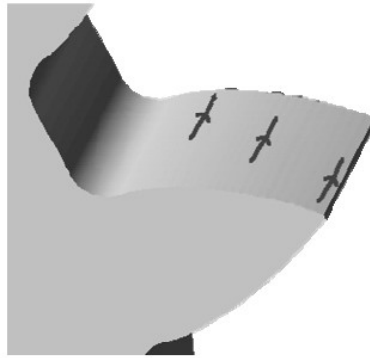


Figure 43 – Roughness measurement location (FZG Type A pinion tooth).

The power loss test procedure is not only the FZG power loss test, a roughness measurement is taken in the first and fifth tooth of each wheel and pinion of the tested gear set in the beginning of the FZG power loss test and another measurement is taken in the end of the test, being both measurements made in the axial direction of the gear teeth. In each tooth are taken three roughness measurements, one below the pitch line, another above the pitch line and the third the close as possible of the pitch line in order to get an accurate representation of the tooth roughness, therefore six roughness measurements are made in each gear. An example of the roughness measuring in a gear tooth is found in Figure 43, being the image representative of a measurement in a FZG type A gear pinion tooth used to exemplification only, due to the fact that this study is conducted only in helical gears, but the measurement technique remains the same and is easy to understand using this example.

3.6. Mass loss procedure

A mass measurement (Figure 44) was also made before and after each complete power loss test, they were weighted with significant accuracy (0.001g) in order to determine the gear mass loss during the FZG power loss test. In order to discard any weighting measurement deviation, a reference pinion was used as comparison for each measurement made.

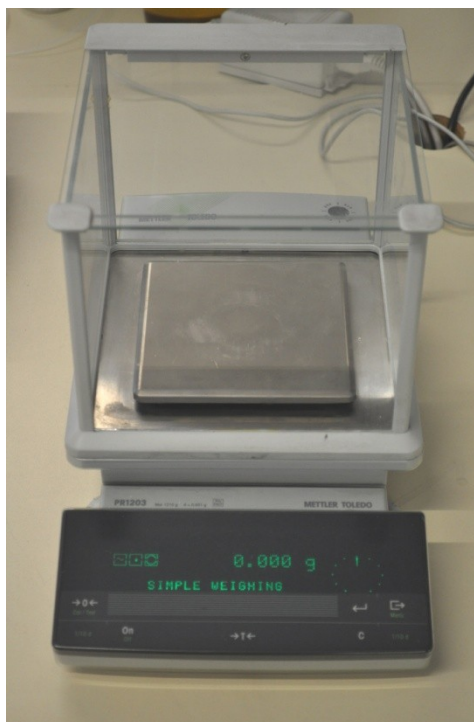


Figure 44 – Weighing scale with 0.001g accuracy.

3.7. Oil Analysis Procedures

Being ferrometry a condition analysis technique, it allows a lubricant assessment in terms of particle contamination and equipment wear. This technique bases itself in the wear particles magnetic separation present in the oil or grease. The ferrography technique has two types of analysis: Direct read Ferrometry (DR III) and Analytic Ferrography (FM III)[33].

3.7.1. Direct Reading Ferrometry: Equipment and procedure

The Direct reading Ferrogafer (DR) measures quantitatively the ferrous particles concentration contained in the lubricant.

A 1ml sample is passed through a capillary tube submitted to a strong magnetic field and two light beams (Figure 45). Particles bigger than $5\mu\text{m}$ are deposited first and the smaller ones deposit themselves 5mm below the tube, being the density of the deposit measured by an optical system that quantifies the intensity of light that passes through the tube, which is directly proportional to the density of the deposited particles.

By this process are obtained the D_L and D_S indexes which represent the large particles and small particles amount respectively. From the knowledge of these two indexes is possible to calculate the wear particle concentration index (CPUC) and the wear severity index (ISUC):

$$CPUC = \frac{D_L + D_S}{d} \quad (\text{Eq. 49})$$

$$ISUC = \frac{D_L^2 + D_S^2}{d^2} \quad (\text{Eq. 50})$$

Where “d” represents the dilution factor of the sample in cases of excessive contamination. A photography of the real equipment present in the oil and lubricants laboratory of CETRIB is shown in Figure 46.

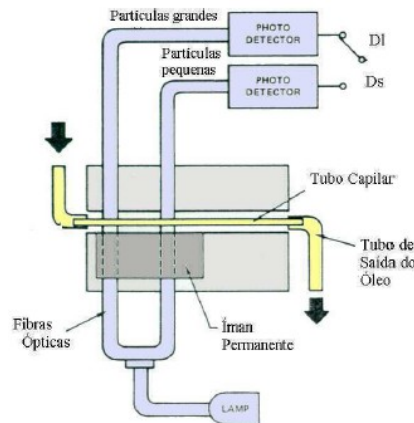


Figure 45 – Direct Reading Ferrogafer scheme.[33]

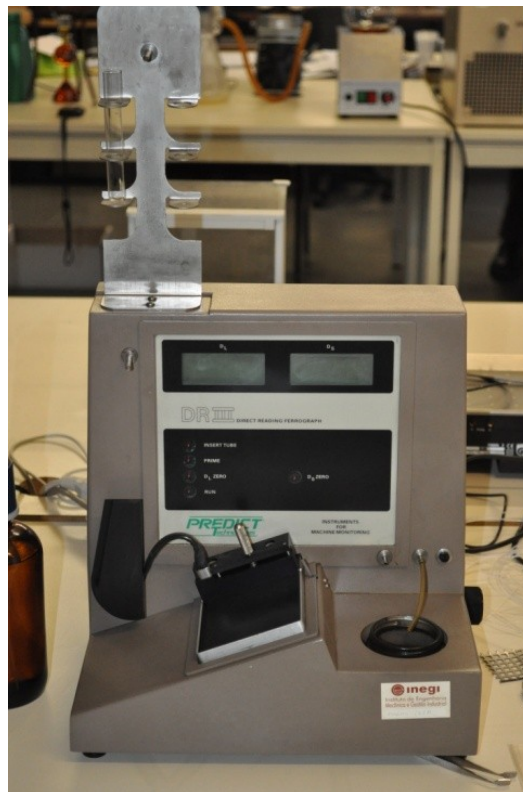


Figure 46 – Picture of the Direct Reading Ferrogafer.

3.7.2. Analytic Ferrography: Equipment and procedure

Analytic Ferrography is used to obtain more detailed information of the lubricant contaminant particles. The particles are deposited and fixated using the same principle as the direct read ferrometer, but over a glass substrate as you can see in the schematic view present in Figure 47. The larger particles deposit in the entrance of the ferrogafer and progressively decrease in size along the time. A photograph of the real equipment present in the laboratory is shown in Figure 48.

After the ferrogram is ready, we move to the analytic part that is made using a Bi-chromatic microscope (Figure 49) (with transmitted light and reflected light), where several particle characteristics are observed, such as: Dimension, morphology, color, bright, surface type, etc.

Some of these characteristics are associated to several types of wear and others to the identification of the material that is being worn.

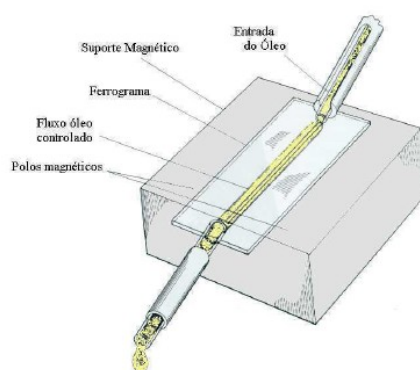


Figure 47 – Analytic ferrography schematic view[33].



Figure 48 – Picture of the Analytic Ferrogafer.



Figure 49 – Bi-chromatic microscope.

An image of a ferrography observed in the microscope can be seen in Figure 50 where are present, ferrous laminar particles typical from fatigue and with large dimensions.

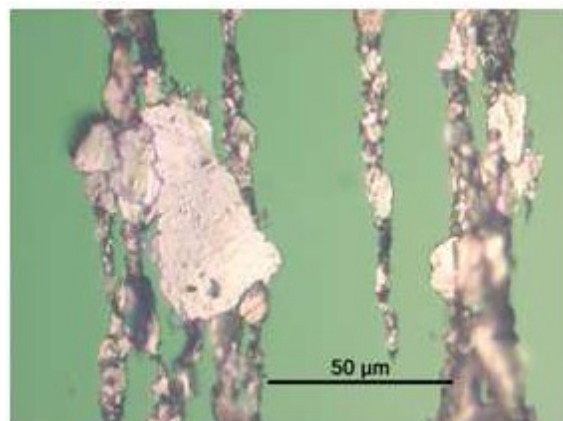


Figure 50 – Ferrogram taken of a P1 oil sample after k1 load stage of a power loss test with 311 gear geometry (Appendix A: Power Loss Data Sheets) 1000x.

4 – Experimental Results

4. Experimental results

The results of the stabilization temperatures measured during the gear power loss tests are presented in this chapter, for all gear geometries, gear oils, gear materials and oil levels. The corresponding results for surface roughness analysis and gear mass loss are also presented. Finally a general discussion of those results is presented.

4.1. Ester base (E2) lubricant oil gear test

4.1.1. Stabilization temperatures – Ester gear oil (E2), high oil level and steel gears

Figure 51, Figure 52 and Figure 53, show the oil maximum temperatures as well as the stabilization temperatures of gears 311, 411 and 611, respectively, lubricated with the ester based gear oil E2, for all the combinations of applied torque and operating speed for high oil level.

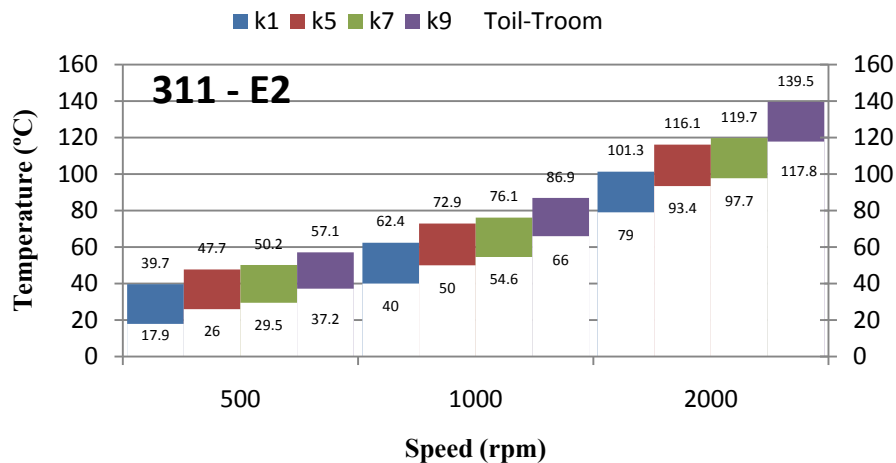


Figure 51 – Maximum oil temperature and stabilization temperature of gear 311: 20MnCr5 steel, E2 gear oil and high oil level

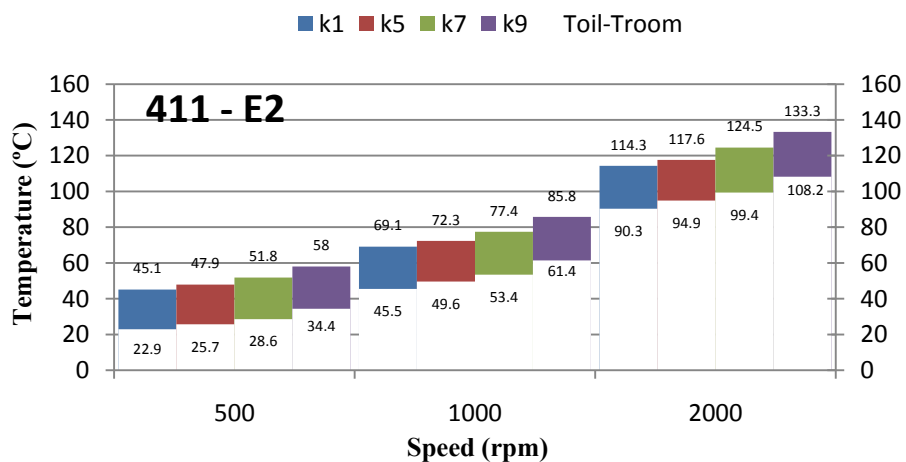


Figure 52 – Maximum oil temperature and stabilization temperature of gear 411: 20MnCr5 steel, E2 gear oil and high oil level.

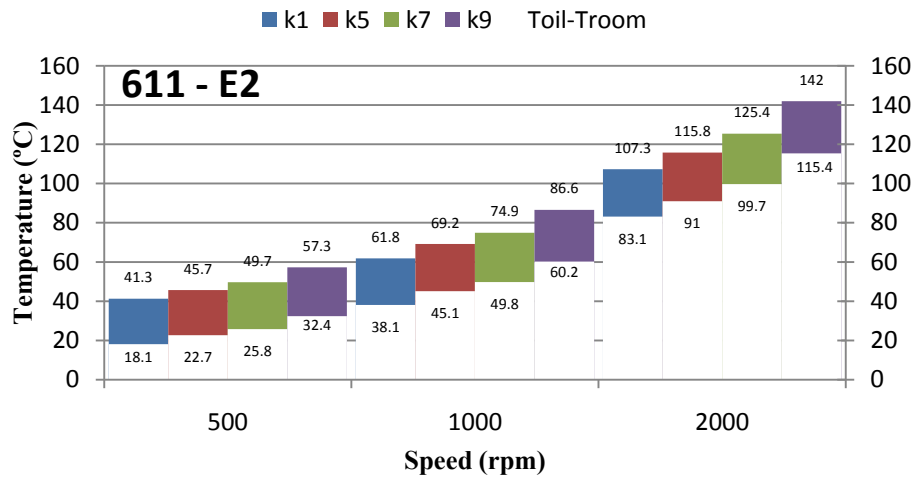


Figure 53 – Maximum oil temperature and stabilization temperature of gear 611: 20MnCr5 steel, E2 gear oil and high oil level.

A summary of the stabilization temperatures can be found in Figure 54 below for each load stage, comparing the different geometries.

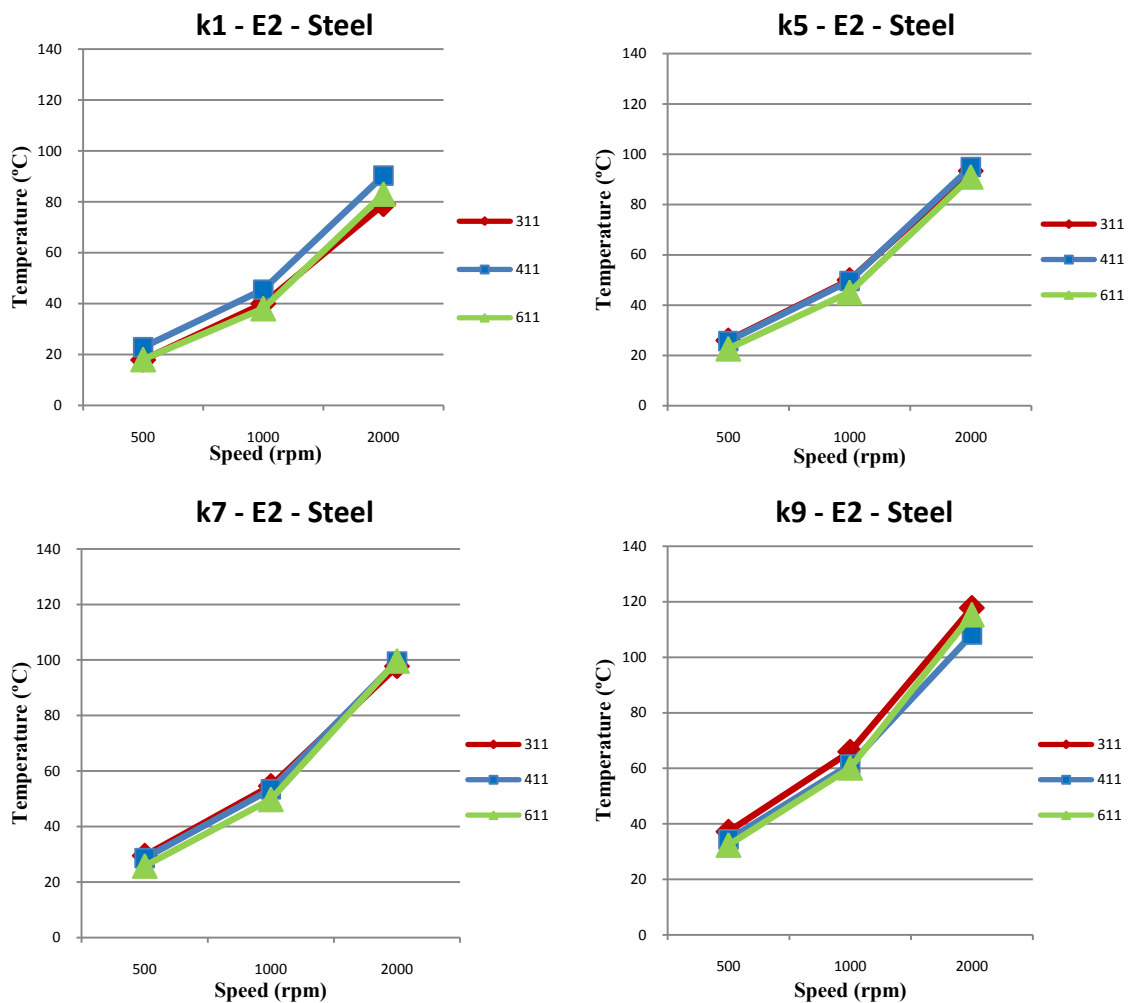


Figure 54 – Stabilization temperatures of 20MnCr5 steel gears: geometries 311, 411 and 611, E2 gear oil and high oil level.

At 500 rpm and 1000 rpm, 611 gear always generates lower stabilization temperatures, whatever the applied torque. At 2000 rpm, the churning losses are very high (higher than the friction losses) and it is not possible to establish a clear difference between the different geometries.

4.1.2. Stabilization temperatures – Ester gear oil E2, high oil level and ADI gears

The stabilization temperatures charts for the ADI gears are identical to those of the steel gears (see Figure 51, Figure 52 and Figure 53). In Figure 54 a summary of the stabilization temperatures is provided. In the case of the ADI gears the results are very clear: whatever the operating torque and speed gear 612 always generates lower stabilization temperature than gear 412, and this one lower values than gear 312, except at very low torque (no-load conditions) where gear 312 generates lower stabilization temperatures than gear 412.

An assessment of the main differences between steel and ADI gears when submitted to the FZG gear power loss test, lubricated with gear oil E2 and a high oil level is given in Figure 56.

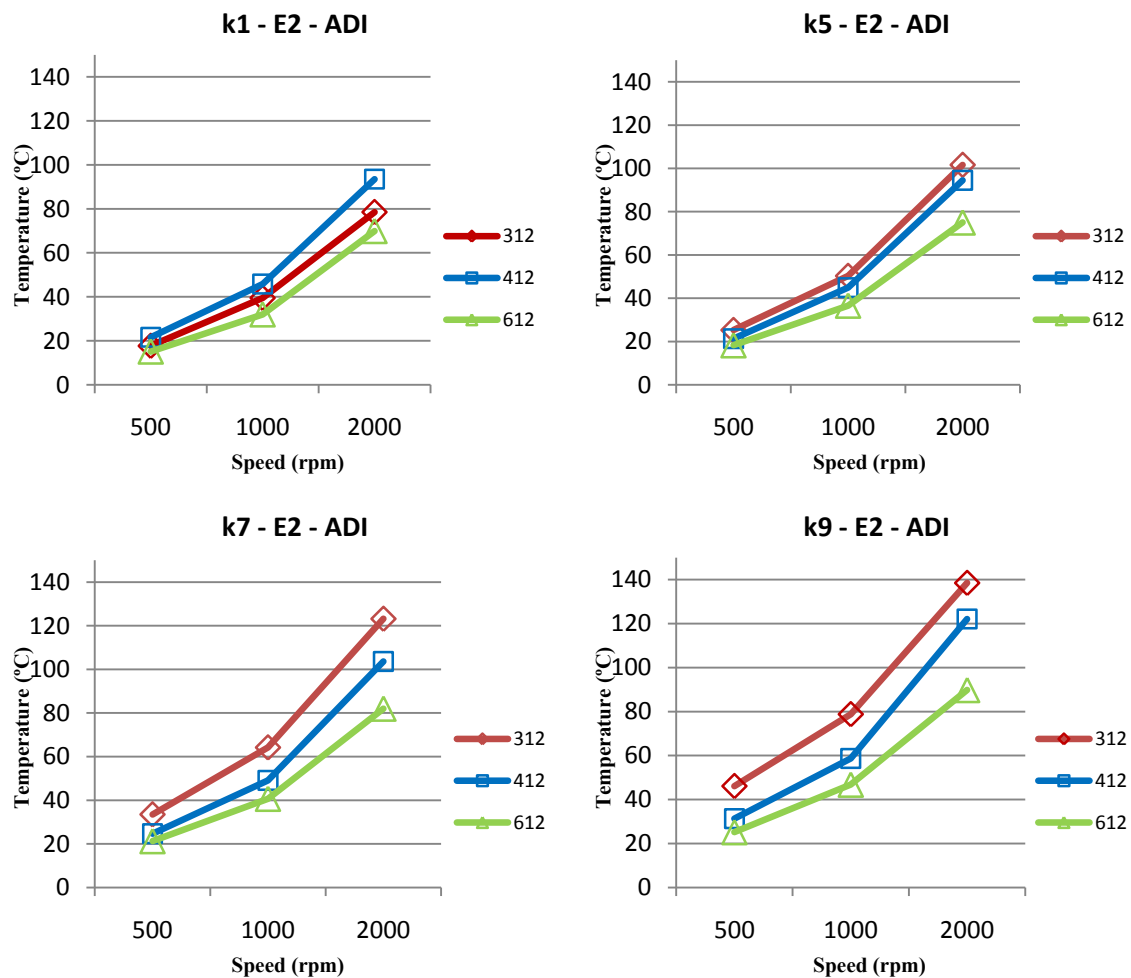


Figure 55 – Stabilization temperatures of ADI gears: geometries 312, 412 and 612, E2 gear oil and high oil level.

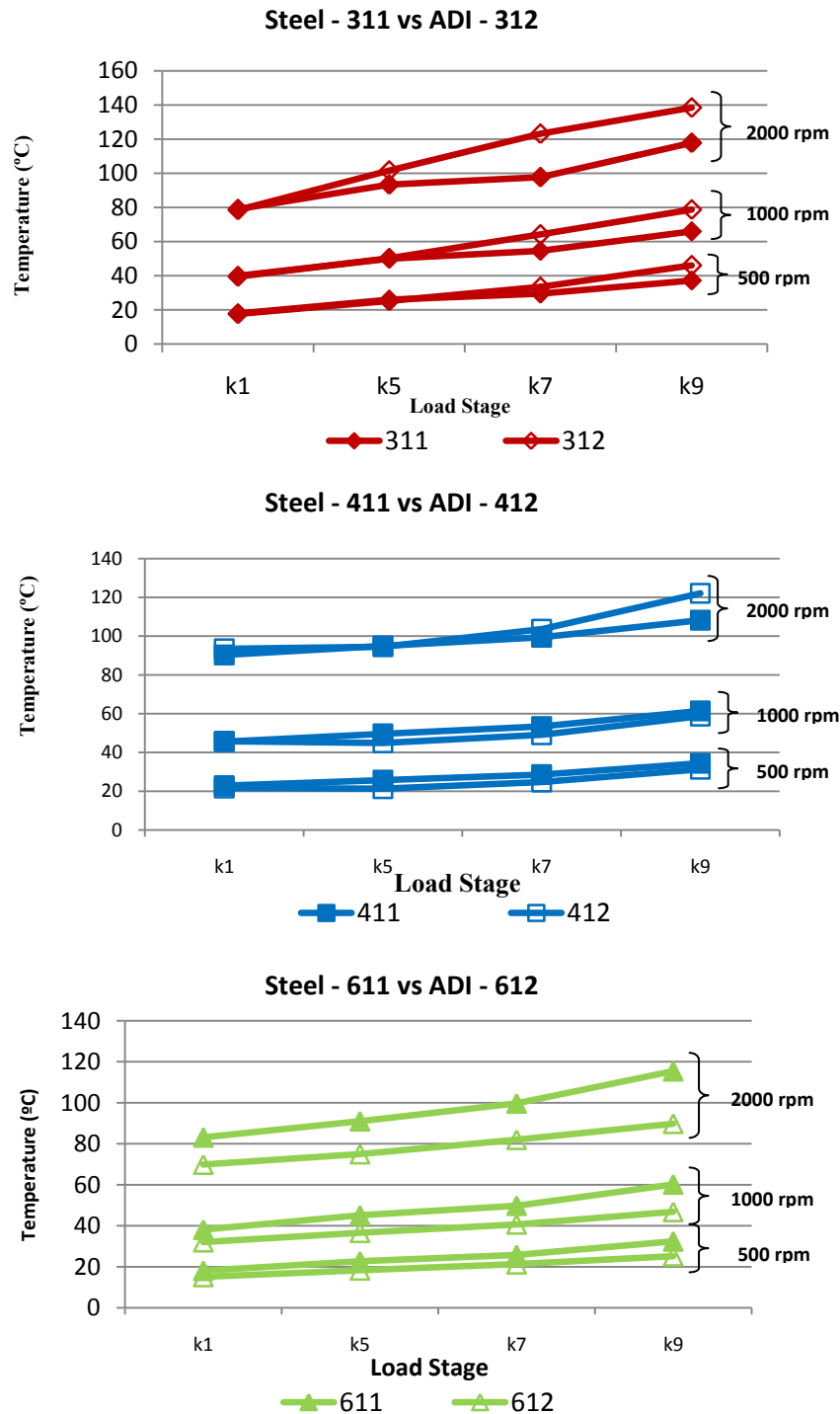


Figure 56 – Stabilization temperatures of 20MnCR5 steel vs. ADI gears: E2 gear oil and high oil level.

The analysis of Figure 56 clearly indicates that the ADI gears always generate lower operating temperatures than the steel gears, when lubricated with the ester based oil E2, whatever the operating conditions considered.

4.1.3. Oil analysis wear particles – Ester gear oil E2, high oil level, steel and ADI

A summary of the oil analysis results by Direct Reading Ferrography is presented in Figure 57 and Figure 58, for steel and ADI gears lubricated with ester based oil and high oil level.

In the case of the steel gears, geometries 411 and 611 show similar DL, CPUC and ISUC values, in general smaller than those of gear geometry 311. This means that gear geometries 411 and 611, not only generate lower stabilization temperatures (thus lower power loss) than gear 311, but also generate a significantly lower amount of wear particles, when lubricated with ester based oil E2.

In the case of the ADI gears (see Figure 58) it is clear that gear 412 generates less wear particles than gears 312 and 612, mainly in terms of large particles DL and CPUC.

Steel and ADI gears show different trends. Whatever the operating conditions ADI gears generate much more wear particles than the steel gears (e.g. 411 steel gear - CPUC = 60 and 412 ADI gear – CPUC = 300, 5 times more).

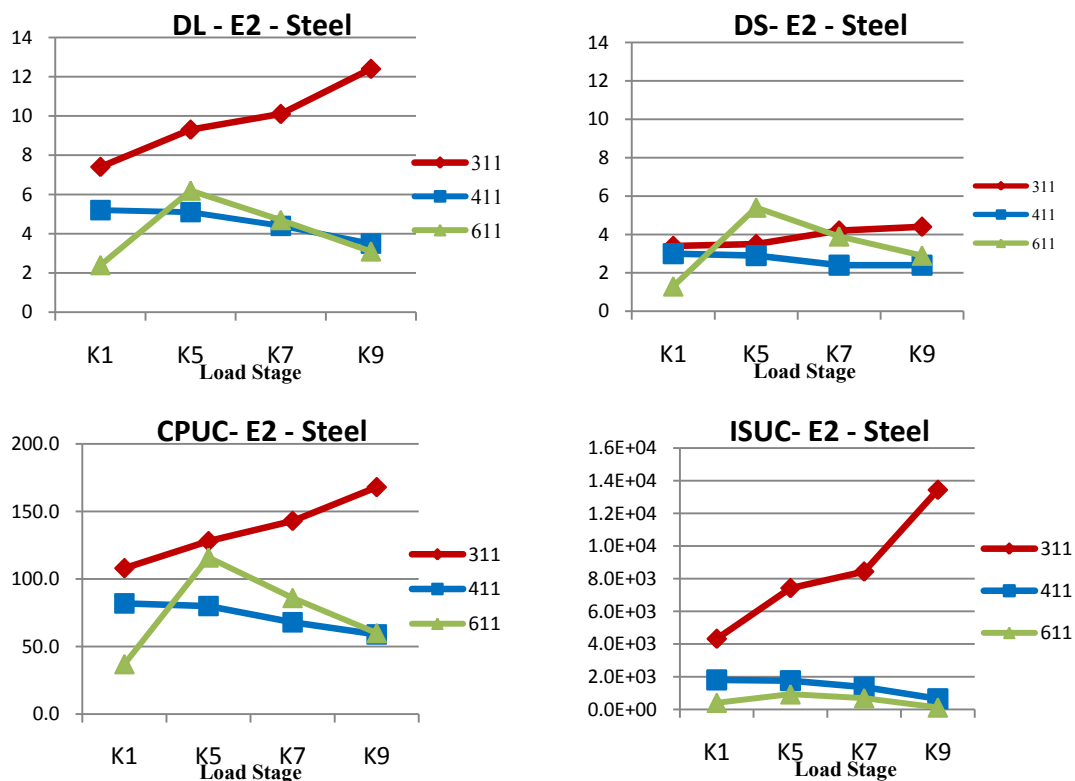


Figure 57 – Oil analysis wear particle indexes for 20MnCr5 steel gears: geometries 311, 411 and 611, E2 gear oil and high oil level.

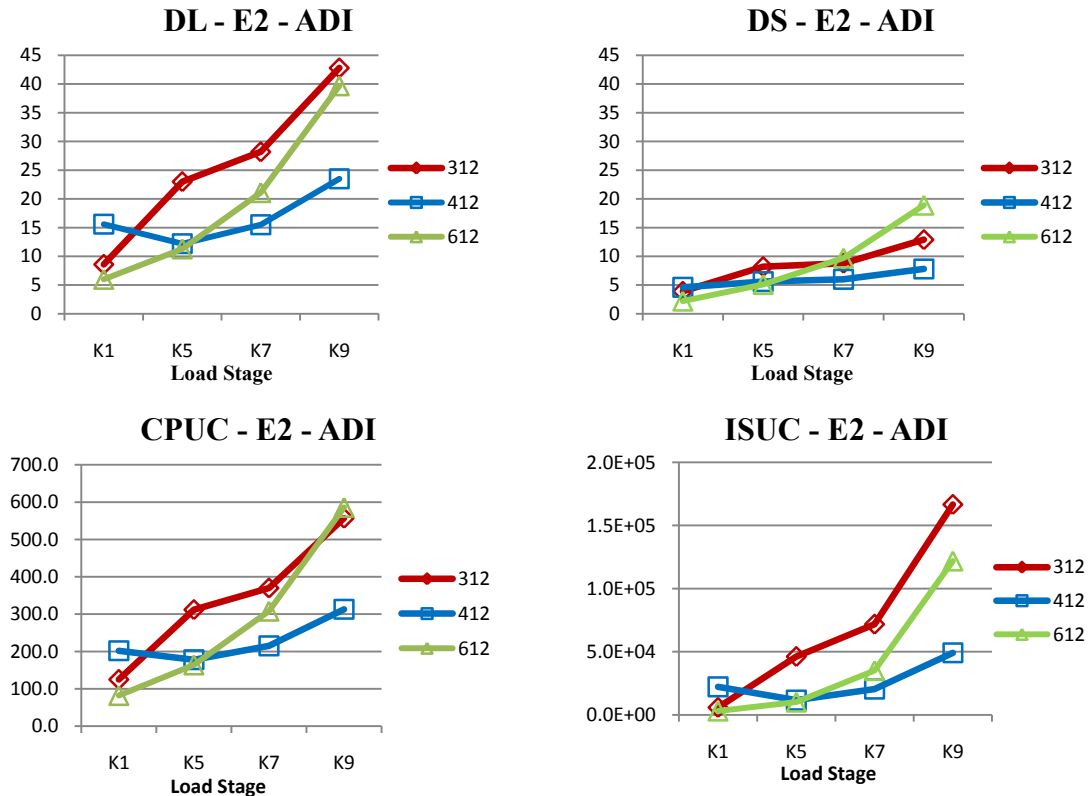


Figure 58 – Oil analysis wear particle indexes for ADI gears: geometries 311, 411 and 611, E2 gear oil and high oil level.

4.1.4. Surface roughness – Ester gear oil E2, high oil level, steel and ADI

Tooth flank surface roughness measurements were made on each pinion and wheel, along the radial direction, before and after the power loss tests. Table 19 and Table 20 show the values measured for steel gears 311 and 411, respectively, and Table 21 and Table 22 the values measured for ADI gears 312 and 412, respectively, all lubricated with E2 ester based oil and high oil level. In the case of gears 611 and 612, it was not possible to perform the roughness measurements.

The steel gears 311 and 411 show a very significant evolution of the tooth flank roughness: R_a , R_q , R_z , R_{max} and R_k decreased between 40% and 50% both for the pinions and the wheels.

Roughness parameter R_{pk} , representative of the roughness peaks, also decreased significantly, and R_{vk} , representative of the roughness valleys (and micropitting), also decreased significantly. At the end of the power loss tests all gears showed a very good surface finishing with a R_a of $0.14\ \mu\text{m}$ – $0.16\ \mu\text{m}$ for gear 311 and $0.12\ \mu\text{m}$ – $0.15\ \mu\text{m}$ for gear 411. In the case of the ADI gears 312 and 412 the initial roughness values were significantly higher than those of the steel gears. Gear 312 also showed a very significant evolution of the tooth flank roughness: R_a , R_q , R_z and R_k decreased between 20% and 50% both for the pinions and the wheels.

Rpk also decreased significantly, between 25% and 45%, but Rmax and Rvk increased significantly (15% and 37% respectively) in the case of 312 wheel. During operation ADI graphite nodules become empty, losing the graphite, and generating surface holes that contribute to the increase of roughness valleys.

Gear 412 had a completely different evolution, showing a very significant increase of the tooth flank roughness: Ra, Rq, Rz and Rk increased between 20% and 200% both for the pinions and the wheels. Both the 412 pinion and wheel presented a very high increase of the Rvk parameter, respectively 200% and 475%, meaning that a significant number of graphite nodules were emptied during the power loss test

**Table 19 – Tooth flank surface roughness of 20MnCr5 steel gear 311:
E2 gear oil and high oil level.**

			Pinion surface roughness [μm]									
	direction	position	Ra	Rq	Rz	Rmax	Rpk	Rk	Rvk	Mr1	Mr2	Vo
Initial	wheel	radial	0.29	0.38	1.77	2.76	0.4	0.83	0.60	9.23	84.9	12.5
	pinion	radial	0.28	0.34	1.62	1.96	0.2	0.88	0.47	7.33	85.8	10.8
Final	wheel	radial	0.14	0.18	0.78	0.97	0.1	0.38	0.34	5.73	80.4	6.3
	pinion	radial	0.16	0.21	0.86	1.16	0.1	0.47	0.30	8.70	82.9	6.3
Wheel Roughness evolution(%)			-50.57	-53.04	-55.66	-64.86	-81.42	-54.00	-43.33	-37.91	-5.30	-49.40
Pinion Roughness evolution(%)			-40.96	-39.81	-46.60	-40.92	-33.85	-46.42	-36.17	18.64	-3.38	-41.79

**Table 20 – Tooth flank surface roughness of 20MnCr5 steel gear 411:
E2 gear oil and high oil level.**

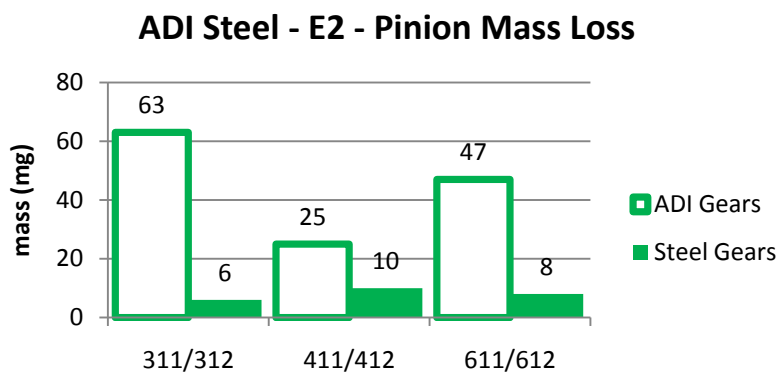
			Pinion surface roughness [μm]									
	direction	position	Ra	Rq	Rz	Rmax	Rpk	Rk	Rvk	Mr1	Mr2	Vo
Initial	wheel	radial	0.24	0.30	1.45	1.93	0.2	0.75	0.44	8.20	86.6	9.9
	pinion	radial	0.30	0.38	1.81	2.16	0.2	0.89	0.59	7.27	84.4	12.5
Final	wheel	radial	0.12	0.15	0.71	0.94	0.1	0.37	0.24	6.47	85.0	5.0
	pinion	radial	0.15	0.19	0.87	1.06	0.1	0.42	0.33	8.30	83.2	6.5
Wheel Roughness evolution(%)			-50.70	-50.00	-51.38	-51.21	-51.79	-50.88	-45.45	-21.14	-1.77	-49.56
Pinion Roughness evolution(%)			-50.56	-50.88	-52.02	-50.93	-55.56	-52.63	-43.75	14.22	-1.38	-47.72

**Table 21 – Tooth flank surface roughness of ADI gear312:
E2 gear oil and high oil level.**

			Pinion surface roughness [μm]									
	direction	position	Ra	Rq	Rz	Rmax	Rpk	Rk	Rvk	Mr1	Mr2	Vo
Initial	wheel	radial	0.76	0.96	4.29	5.07	0.7	2.47	1.06	9.22	88.0	26.6
	pinion	radial	0.81	1.01	4.59	5.60	0.7	2.57	1.31	6.83	87.0	29.9
Final	wheel	radial	0.54	0.79	3.19	5.85	0.5	1.37	1.46	8.70	82.2	26.6
	pinion	radial	0.43	0.59	2.97	4.03	0.4	1.21	1.17	8.10	85.3	22.3
Wheel Roughness evolution(%)			-29.26	-17.10	-25.56	15.53	-24.94	-44.53	37.74	-5.61	-6.67	0.11
Pinion Roughness evolution(%)			-47.11	-41.29	-35.40	-27.99	-45.85	-52.92	-10.09	18.54	-1.95	-25.38

**Table 22 – Tooth flank surface roughness of ADI gear412:
E2 gear oil and high oil level.**

			Pinion surface roughness [μm]									
	direction	position	Ra	Rq	Rz	Rmax	Rpk	Rk	Rvk	Mr1	Mr2	Vo
Initial	wheel	radial	0.33	0.43	2.42	3.98	0.5	1.08	0.53	9.63	88.5	12.9
	pinion	radial	0.52	0.62	3.07	4.08	0.6	1.63	0.78	10.15	87.6	18.3
Final	wheel	radial	0.73	1.28	6.57	11.08	0.6	1.50	3.07	8.23	83.5	51.4
	pinion	radial	0.60	1.05	5.17	10.65	0.5	1.28	2.33	9.28	84.3	40.3
Wheel Roughness evolution(%)			120.00	196.15	171.72	178.24	6.45	38.46	475.00	-14.53	-5.65	298.58
Pinion Roughness evolution(%)			16.13	70.27	68.48	160.82	-24.32	-21.43	197.87	-8.54	-3.84	119.95

**Figure 59 – Pinion mass loss of 20MnCr5 steel vs. ADI gears:
E2 gear oil and high oil level.**

4.1.5. Gear mass loss – Ester gear oil E2, high oil level, steel and ADI

During the gear power loss tests the pinion performs more cycles than the wheel (50% more, due to the transmission ratio $i = 1/1.5$), and thus the pinions normally had higher mass loss than the wheels. Figure 56 presents the mass loss of all gears (311/312, 411/412 and 611/612). The 20MnCr5 pinions (311, 411 and 611) had very similar mass losses, between 6 mg and 10 mg, which are very low values for a new gear not run-in.

ADI pinions (312, 412 and 612) had significantly higher mass losses, between 25 mg and 63 mg, which are typical values for the ADI material since it is significantly less hard than the carburized 20MnCr5 steel.

4.2. PAO base (P1) lubricant oil gear tests

4.2.1. Stabilization temperatures – PAO gear oil P1, high oil level and steel gears

Figure 60, Figure 61 and Figure 62 show the oil maximum temperatures as well as the stabilization temperatures of gears 311, 411 and 611, respectively, lubricated with the PAO based gear oil P1, for all the combinations of applied torque and operating speed, high oil level, and both gear materials.

A summary of the stabilization temperatures can be found in Figure 63 for each operating load stage and speed, comparing gear geometries 311, 411 and 611. Whatever the operating conditions, torque stage and speed, 611 gear always generates the lowest stabilization temperatures and gear 311 the highest stabilization temperatures, while gear 411 generated temperatures in between the other two. In load stage K9 the behavior of gear 411 and 311 was very similar.

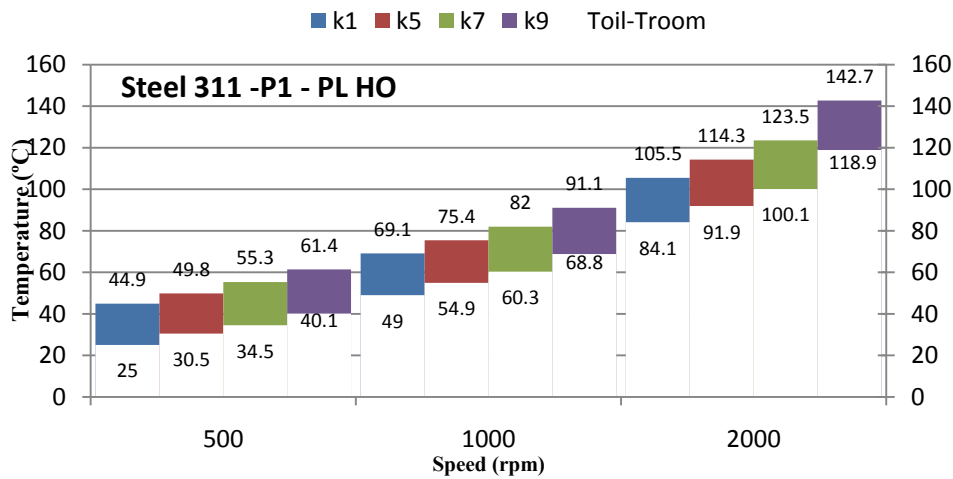


Figure 60 – Maximum oil temperature and stabilization temperature of gear 311: 20MnCr5 steel, E2 gear oil and high oil level.

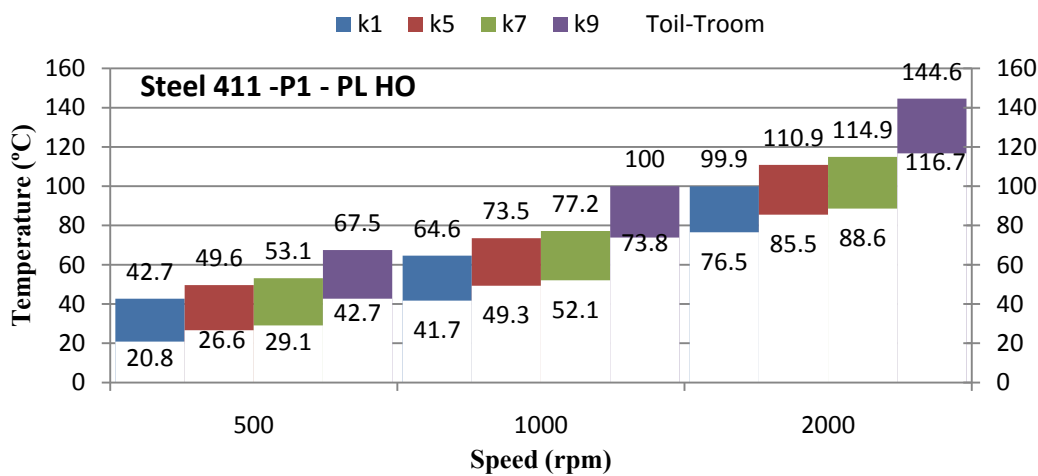


Figure 61 – Maximum oil temperature and stabilization temperature of gear 411: 20MnCr5 steel, E2 gear oil and high oil level.

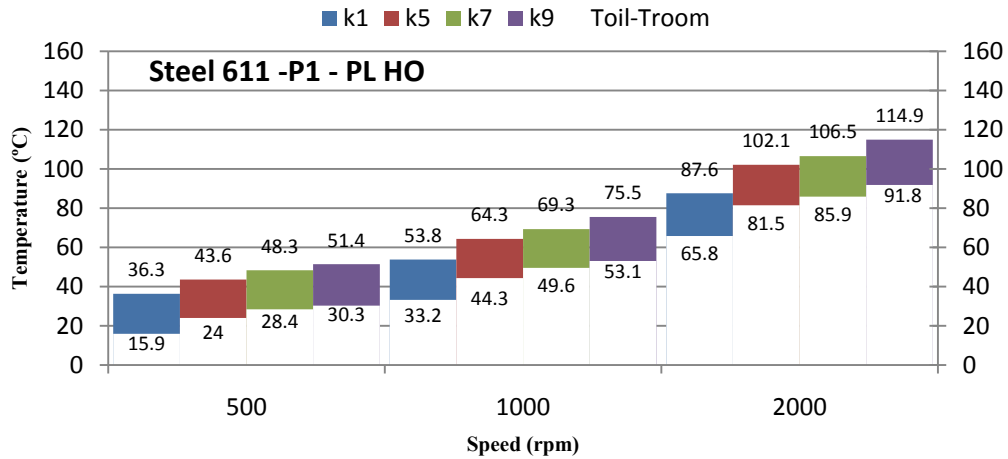


Figure 62 – Maximum oil temperature and stabilization temperature of gear 611: 20MnCr5 steel, E2 gear oil and high oil level.

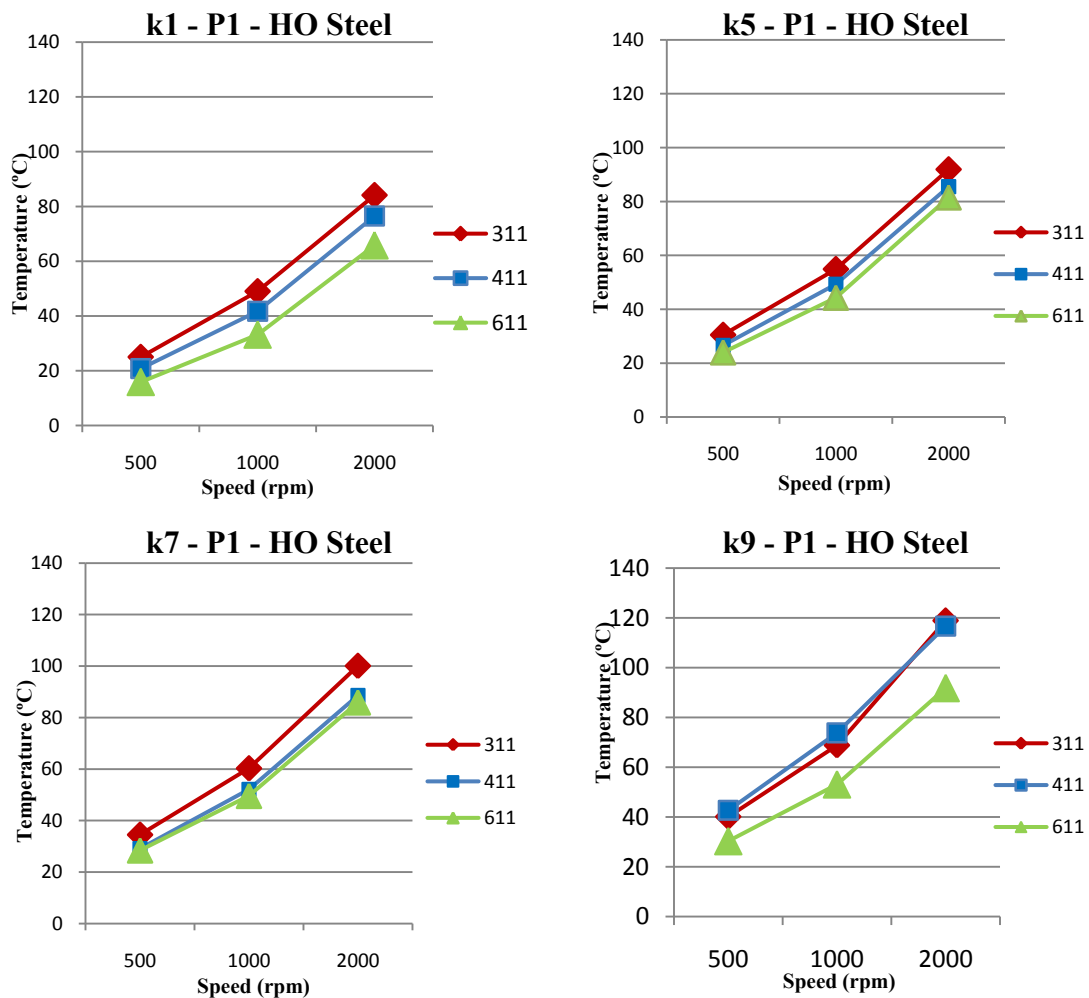


Figure 63 – Stabilization temperatures of 20MnCr5 steel gears: geometries 311, 411 and 611, P1 gear oil and high oil level.

4.2.2. Stabilization temperatures – PAO gear oil P1, high oil level and ADI gears

The stabilization temperatures charts for the ADI gears are identical to those of the steel gears (see Figure 60, Figure 61 and Figure 62). In Figure 64 a summary of the stabilization temperatures is provided. In the case of the ADI gears the results are very clear: whatever the operating torque and speed gear 612 always generates lower stabilization temperature than gear 412, and this on lower values than gear 312. In load stage K7 gears 312 and 412 generated very similar stabilization temperatures.

An assessment of the main differences between steel and ADI gears when submitted to the FZG gear power loss test, lubricated with gear oil P1 and high oil level is given in Figure 65. When lubricated with gear oil P1, steel and ADI gears generated similar stabilization temperatures mainly at low speed (500 rpm) when the churning losses are smaller. At 1000 rpm and 2000 rpm the steel gears (311, 411 and 611) generated slightly lower stabilization than the ADI gears (312, 412 and 612).

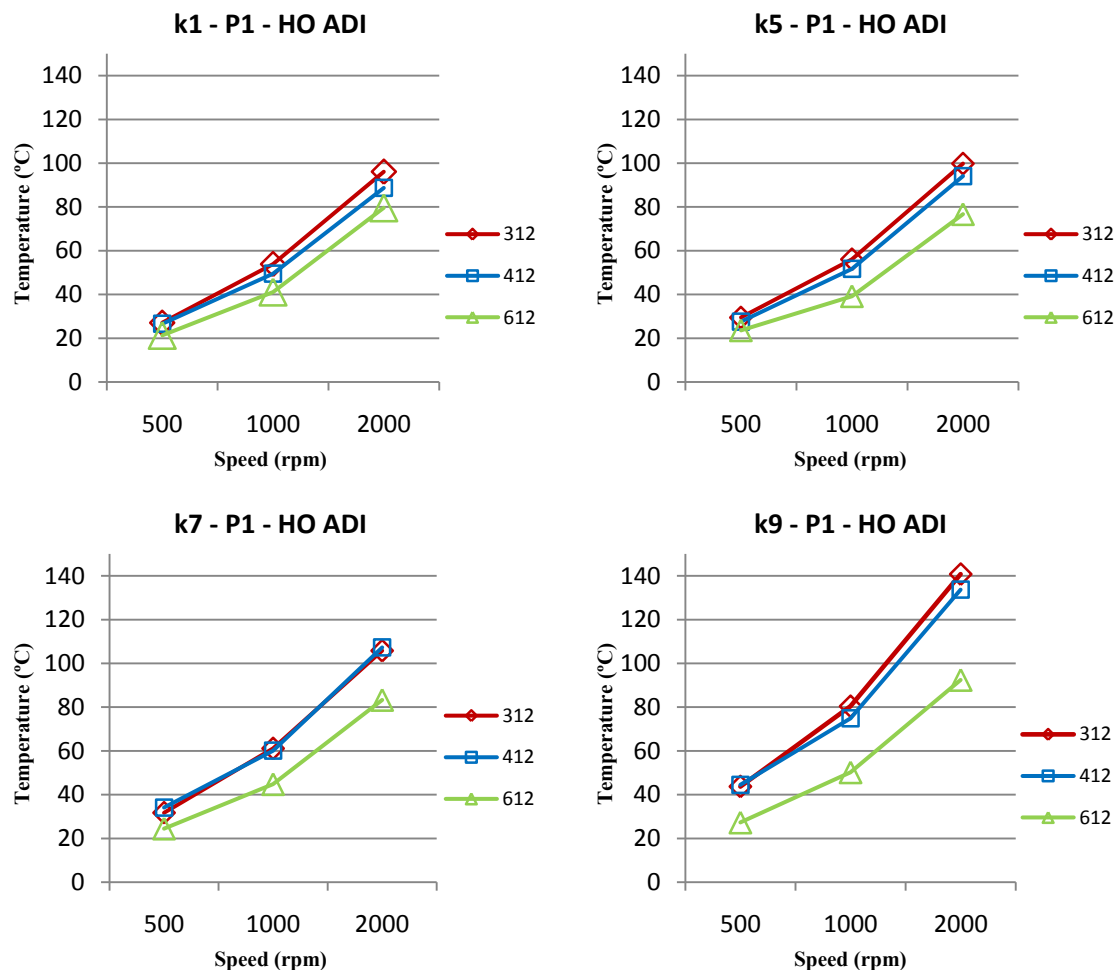


Figure 64 – Stabilization temperatures of ADI gears: geometries 312, 412 and 612, P1 gear oil and high oil level.

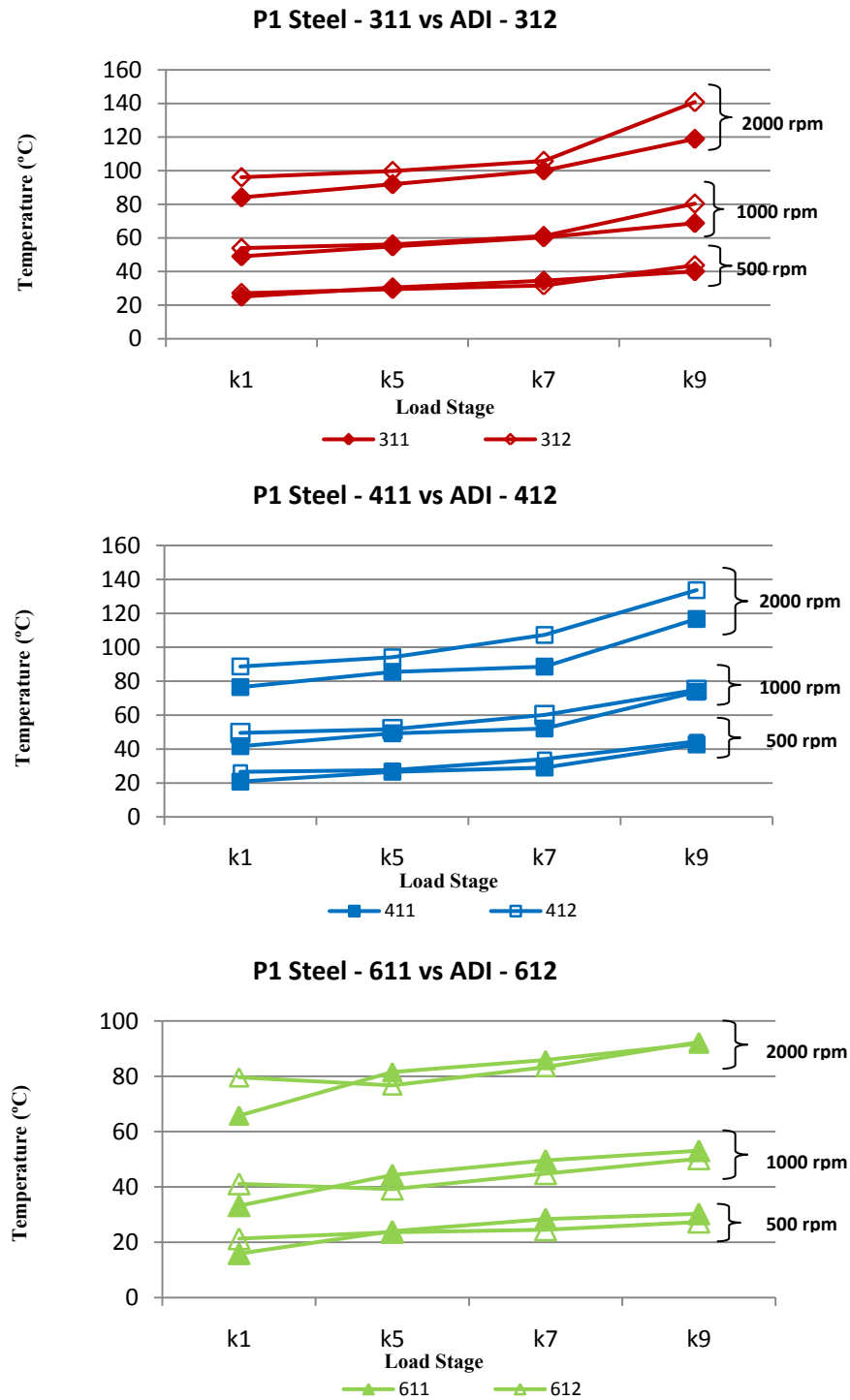


Figure 65 – Stabilization temperatures of 20MnCr5 steel vs. ADI gears: P1 gear oil and high oil level.

4.2.3. Oil analysis wear particles – PAO gear oil P1, high oil level, steel and ADI

A summary of the oil analysis results by Direct Reading Ferrography are presented in Figure 66 and Figure 67, for steel and ADI gears, respectively, lubricated with PAO based oil and a high oil level.

In the case of the steel gears, the oil analysis indicated that gear 611 generated lower ferrographic indexes (DL, DS, CPUC and ISUC) values than gear 411, and this one lower indexes than gear 311. This means that gear geometries 411 and 611, not only generate lower stabilization temperatures (thus lower power loss) than gear 311, but also generate a significantly lower amount of wear particles, when lubricated with PAO based oil P1. It's interesting to notice that, during the power loss test, the index for large particles, DL, decreased or remained almost constant till the end of load stage K7, and had a small increase during the last load stage K9.

In the case of the ADI gears (see Figure 67) it is clear that gear 612 generates less wear particles than gear 412 and this one less wear particles than gear 312, whatever the ferrographic wear indexes considered (DL, DS, CPUC and ISUC).

Steel and ADI gears show different trends. The amount of wear particles generated by the ADI gears increased continuously during the gear power loss test.

Whatever the operating conditions ADI gears generate much more wear particles than the steel gears (e.g. 411 steel gear - CPUC = 320 and 412 ADI gear – CPUC = 720, 2 times more).

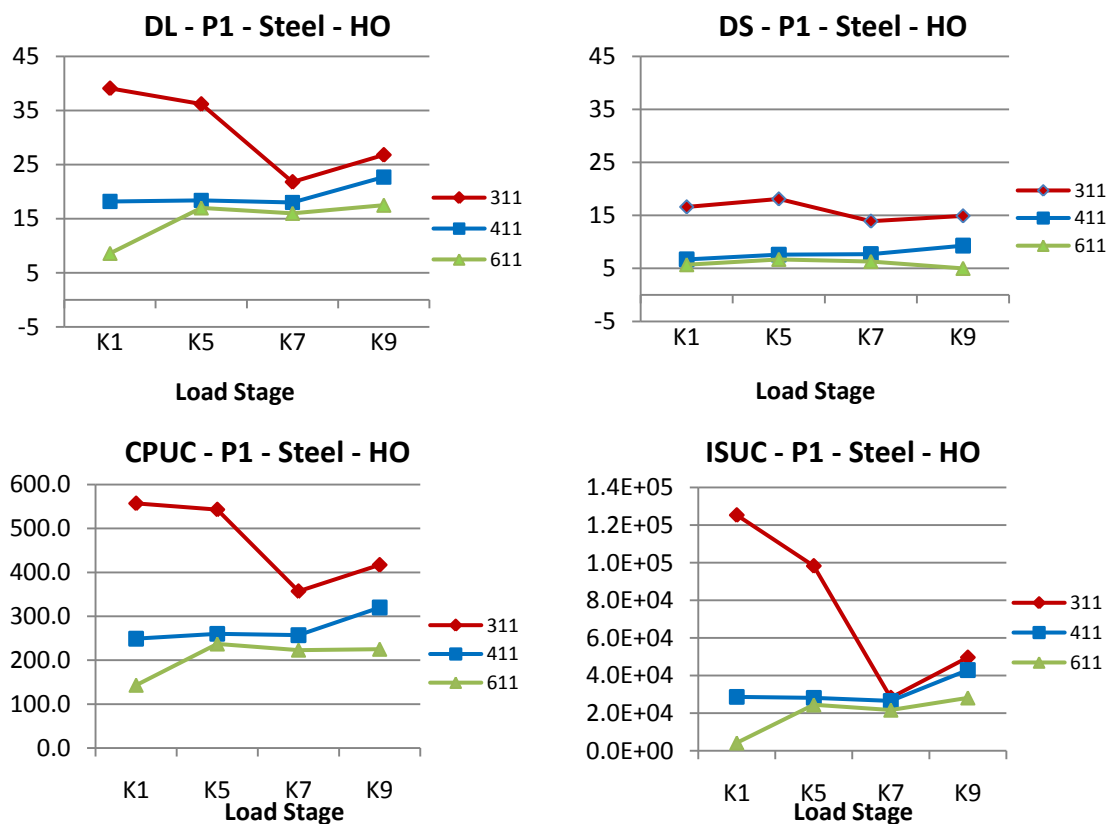


Figure 66 – Oil analysis wear particle indexes for 20MnCr5 steel gears: geometries 311, 411 and 611, P1 gear oil and high oil level.

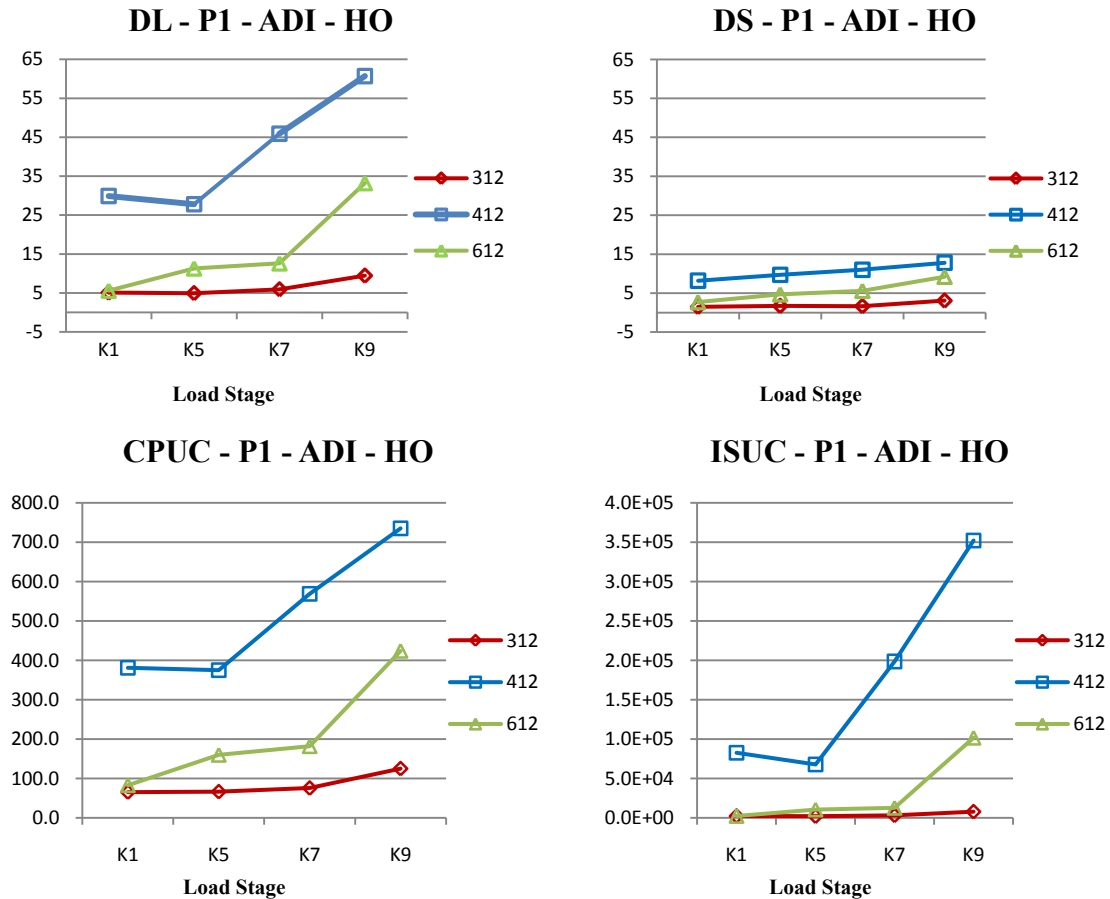


Figure 67 - Oil analysis wear particle indexes for ADI gears: geometries 312, 412 and 612, P1 gear oil and high oil level.

4.2.4. Surface roughness – PAO gear oil (P1), High oil level, steel and ADI

Tooth flank surface roughness measurements were made on each pinion and wheel, along the radial direction, before and after the power loss tests.

Table 23 and Table 24 show the values measured for steel gears 311 and 411, respectively, and Table 25 and the values measured for ADI gears 312 and 412, respectively, all lubricated with P1 PAO based oil and a high oil level. Due to some technical difficulties, related to the very small tooth height of gears 611 and 612, it was not possible to perform the roughness measurements on these gears.

The steel gears 311 and 411 show a significant evolution of the tooth flank roughness: R_a , R_q , R_z , R_{max} and R_k decreased between 1% and 27% in the case of the steel wheels and pinions. Roughness parameter R_{pk} , representative of the roughness peaks, also decreased significantly (between 30% and 40 %).

**Table 23 – Tooth flank surface roughness of steel gear 311:
P1 gear oil and high oil level.**

			Pinion surface roughness [μm]									
	direction	position	Ra	Rq	Rz	Rmax	Rpk	Rk	Rvk	Mr1	Mr2	Vo
Initial	wheel	radial	0.23	0.30	1.50	2.1	0.24	0.71	0.51	8.9	87.67	10.7
	pinion	radial	0.25	0.32	1.53	1.8	0.24	0.78	0.42	8.8	86.93	9.8
Final	wheel	radial	0.18	0.23	1.21	1.6	0.16	0.52	0.38	8.5	85.40	7.8
	pinion	radial	0.23	0.31	1.47	2.3	0.12	0.70	0.47	5.8	84.73	9.8
Wheel Roughness evolution(%)			-24.29	-23.08	-19.33	-22.37	-32.88	-26.76	-26.62	-4.49	-2.59	-27.41
Pinion Roughness evolution(%)			-6.67	-4.17	-3.71	26.88	-49.30	-10.68	10.24	-34.72	-2.53	0.24

**Table 24 – Tooth flank surface roughness of steel gear 411:
P1 gear oil and high oil level.**

			Pinion surface roughness [μm]									
	direction	position	Ra	Rq	Rz	Rmax	Rpk	Rk	Rvk	Mr1	Mr2	Vo
Initial	wheel	radial	0.20	0.26	1.27	1.6	0.20	0.66	0.31	6.7	87.80	7.6
	pinion	radial	0.21	0.26	1.30	1.8	0.20	0.66	0.37	8.1	88.40	8.4
Final	wheel	radial	0.18	0.23	1.12	1.3	0.12	0.58	0.34	7.2	87.00	7.6
	pinion	radial	0.19	0.24	1.28	1.6	0.12	0.56	0.38	6.8	85.23	8.0
Wheel Roughness evolution(%)			-11.48	-10.39	-11.84	-15.70	-41.67	-13.07	9.78	7.50	-0.91	-0.04
Pinion Roughness evolution(%)			-9.68	-8.86	-1.03	-8.17	-38.98	-15.58	3.64	-16.46	-3.58	-5.07

**Table 25 – Tooth flank surface roughness of steel gear 312:
P1 gear oil and high oil level.**

			Pinion surface roughness [μm]									
	direction	position	Ra	Rq	Rz	Rmax	Rpk	Rk	Rvk	Mr1	Mr2	Vo
Initial	wheel	radial	0.33	0.43	2.15	3.25	0.3	0.97	0.78	8.88	84.1	15.6
	pinion	radial	0.23	0.30	1.57	2.28	0.4	0.75	0.30	10.98	90.2	7.9
Final	wheel	radial	0.17	0.28	1.72	2.95	0.5	0.48	0.43	10.97	83.5	8.2
	pinion	radial	0.53	0.83	4.42	7.03	0.5	1.15	1.77	7.97	79.5	30.2
Wheel Roughness evolution(%)			-50.00	-34.62	-20.16	-9.23	45.00	-50.00	-44.68	23.45	-0.73	-47.49
Pinion Roughness evolution(%)			128.57	177.78	181.91	208.03	39.13	53.33	488.89	-27.47	-11.81	283.30

**Table 26 – Tooth flank surface roughness of steel gear 412:
P1 gear oil and high oil level.**

			Pinion surface roughness [μm]									
	direction	position	Ra	Rq	Rz	Rmax	Rpk	Rk	Rvk	Mr1	Mr2	Vo
Initial	wheel	radial	0.33	0.43	2.42	3.98	0.5	1.08	0.53	9.63	88.5	12.9
	pinion	radial	0.52	0.62	3.07	4.08	0.6	1.63	0.78	10.15	87.6	18.3
Final	wheel	radial	0.53	0.82	4.70	7.87	0.4	1.28	1.62	7.37	82.4	28.8
	pinion	radial	0.57	0.92	4.97	8.80	0.4	1.18	1.98	7.88	81.7	34.4
Wheel Roughness evolution(%)			60.00	88.46	94.48	97.49	-25.81	18.46	203.13	-23.53	-6.97	123.16
Pinion Roughness evolution(%)			9.68	48.65	61.96	115.51	-43.24	-27.55	153.19	-22.33	-6.75	88.07

Roughness parameter Rvk, representative of the roughness valleys (and micropitting), increased slightly (between 4% and 10 %). In the case of the 311 steel wheel, Rvk decreased 27%. At the end of the power loss tests all gears showed a very good surface finishing with a Ra of 0.18 μm – 0.23 μm for gear 311 and 0.18 μm – 0.19 μm for gear 411.

In the case of the ADI gears 312 and 412 the initial roughness values were slightly higher than those of the steel gears. Gear 312 also showed a very significant evolution of the tooth flank roughness: Ra, Rq, Rz and Rk decreased between 20% and 50% for the wheels and an increase between 40% and 180% for the 312 pinion. Gear 412 shows a even more pronounced evolution of the tooth flank roughness: Ra, Rq, Rz and Rk increase between 20% and 95% for the wheels and for the pinion an increase between 10% and 60% for the Ra, Rq and a decrease of around 30% for the Rk.

For 312 ADI gear wheel, a decrease of 45% was identified in the Rvk parameter, contrasting with the increase of near 490% occurred in the pinion. In the 412 the Rvk increase was slightly lower than in 312 being 150% and 200% for the pinion and wheel respectively.

4.2.5. Gear mass loss – PAO gear oil E2, high oil level, steel and ADI

During the gear power loss tests the pinion performs more cycles than the wheel (50% more, due to the transmission ratio $i = 1/1.5$), and thus the pinions normally had higher mass loss than the wheels. Figure 68 presents the mass loss of all gears (311/312, 411/412 and 611/612).

The 20MnCr5 steel pinions (311, 411 and 611) had very similar mass losses, between 5 mg and 11 mg, which are very low values for a new gear not run-in. ADI pinions (312 and 412) had significantly higher mass losses, between 29 mg and 40 mg, which are typical values for the ADI material since it is significantly less hard than the carburized 20MnCr5 steel. The result for ADI pinion 612 is not available.

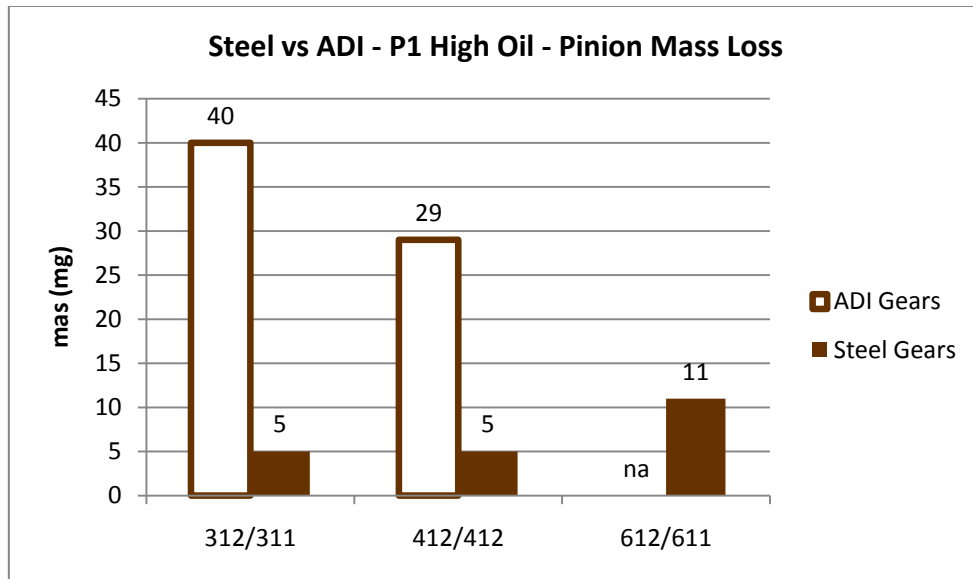


**Figure 68 – Pinion mass loss of 20MnCr5 steel vs. ADI gears:
PAO gear oil and high oil level.**

4.3. Steel vs. ADI gears and Ester vs. PAO gear oils

In Figure 69, Figure 70 and Figure 71 are represented the stabilization temperatures plotted against the input power, for the steel and ADI gears when submitted to power loss test with high level of P1 and E2 lubricant oils, for gears 311/312, 411/412 and 611/612, respectively.

Figure 69 shows three levels of temperatures that correspond to the three operational speeds of the FZG power loss test. The 311 steel gear with E2 oil has the lower stabilization temperature for nearly all values of speed and input power, and gear 312 lubricated with the same E2 oil had a very close behavior, but only at low input power and low speed, having the highest temperature at 2000 rpm for almost all values of input power.

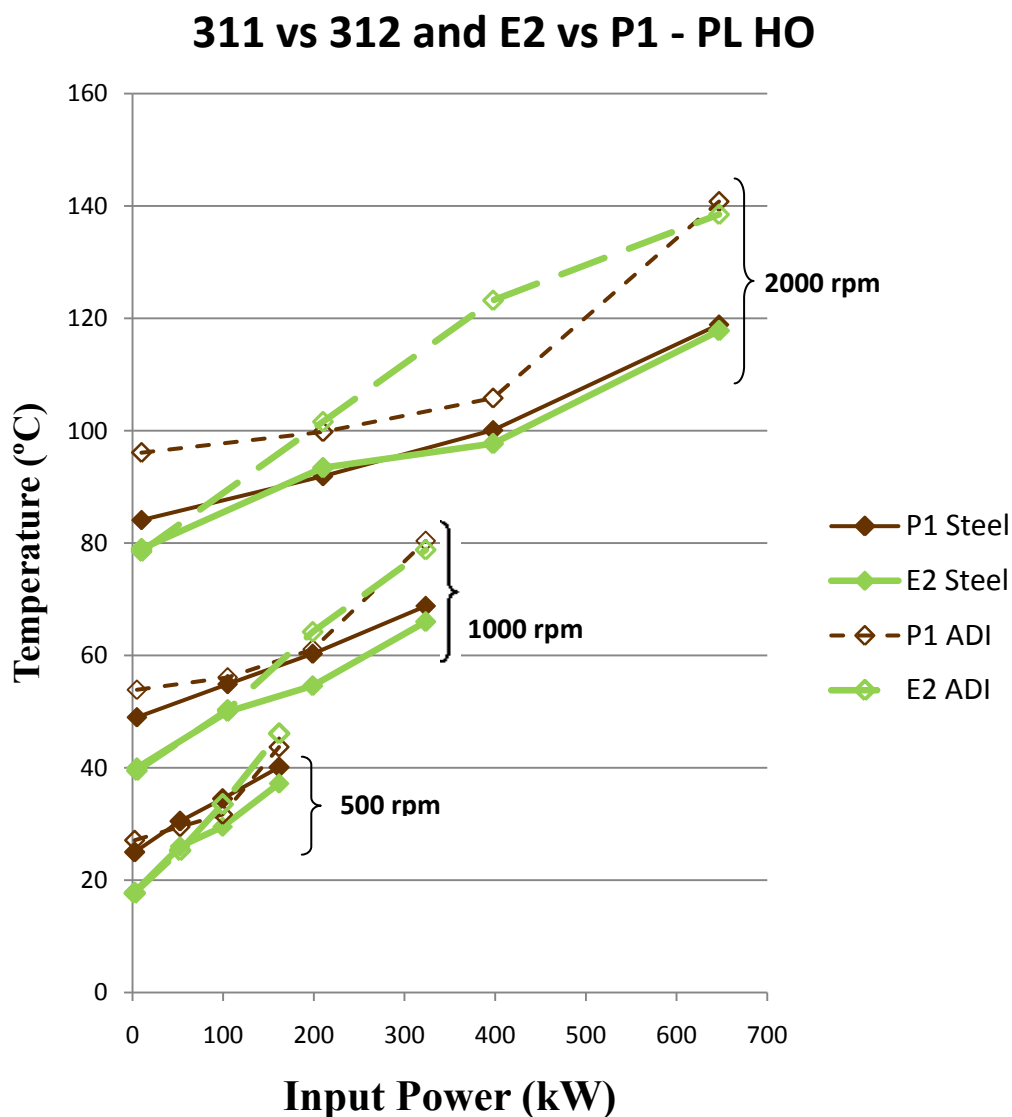


Figure 69 – Variation of stabilization temperatures with Input Power for 311 steel and 312 ADI gears with E2 and P1 high oil level.

The 311 steel gear has virtually the same behavior with P1 and E2 oil, for any input torque at 2000 rpm, but at 500rpm and 1000rpm oil E2 always generates lower temperatures for any input power. The 312 ADI gear with P1 and E2 oils has the highest temperatures at 2000rpm for any input power, but for 500rpm and 1000rpm oil E2 has lower temperatures for low input power and the P1 has lower temperatures for high input power. ADI gears with P1 and E2 oils have very similar temperatures to the steel gears with P1 oil for 500rpm and 1000rpm, being the steel gears for any oil better than the ADI ones for any oil at any input power and 2000rpm.

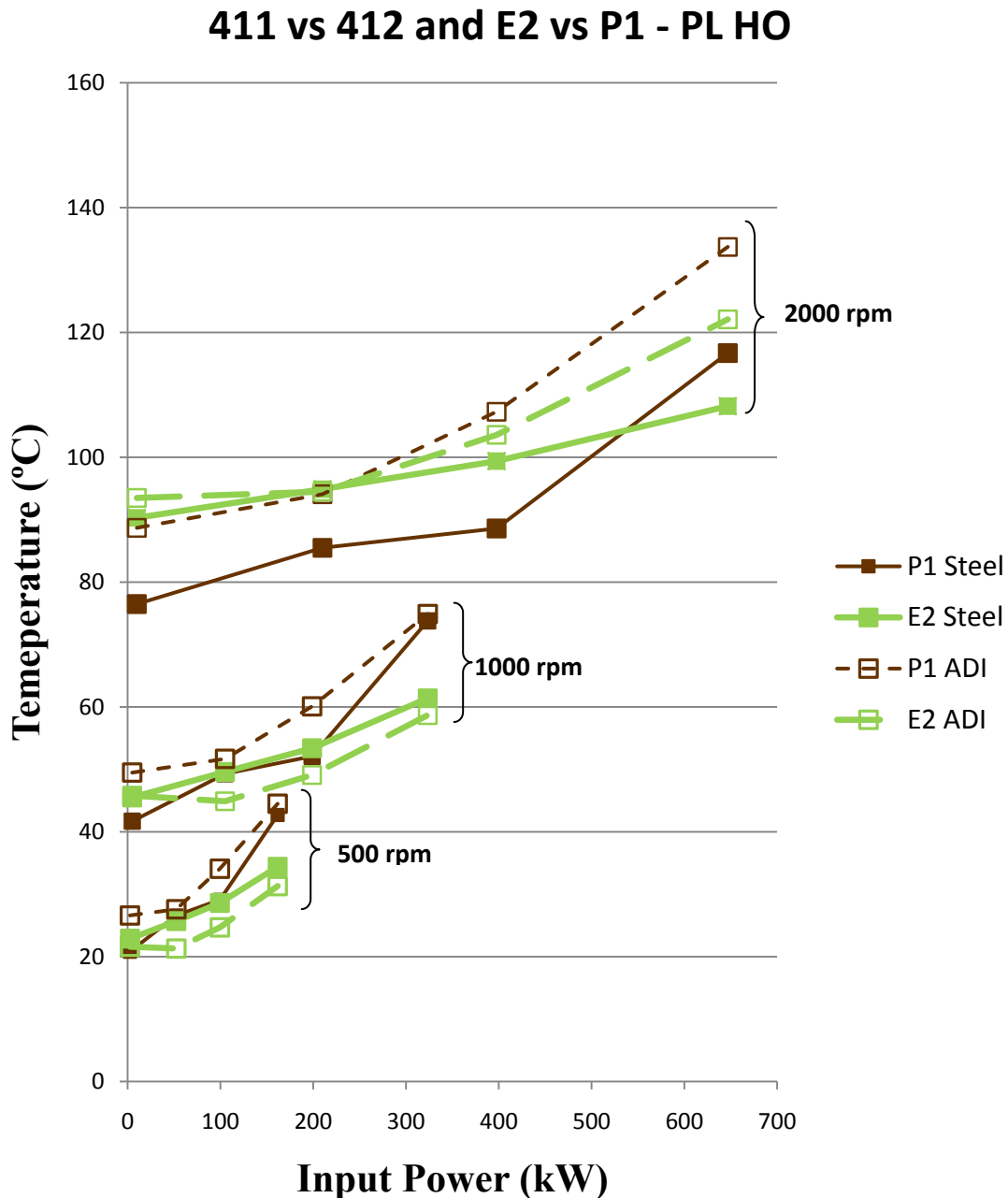


Figure 70 – Variation of stabilization temperatures with Input Power for 411 steel and 412 ADI gears with E2 and P1 high oil level.

Figure 70 shows the variation of stabilization temperatures function of input power, and after analyze it we see that 412 ADI gear with E2 oil has the lower stabilization temperature for all input power values at 500 rpm and 1000 rpm being only overcome by steel gears with E2 and P1 oils at 2000 rpm and higher input power. The 411 steel gears for both oils have intermediate stabilization temperatures being the worst case represented by the 412 ADI gear with P1 oil, by having the highest temperatures for all input torque values at all rotating speeds.

Figure 71 shows once again that the ADI (612) gear with E2 oil has the lower temperature for all input power values at all speeds, being the second best also the 612 gear but with P1 oil. 611 steel gear with E2 oil has almost the same stabilization temperatures as 612 ADI gears with P1 oil at 500rpm for all input power values but for 1000 rpm and 2000 rpm has the higher stabilization temperature.

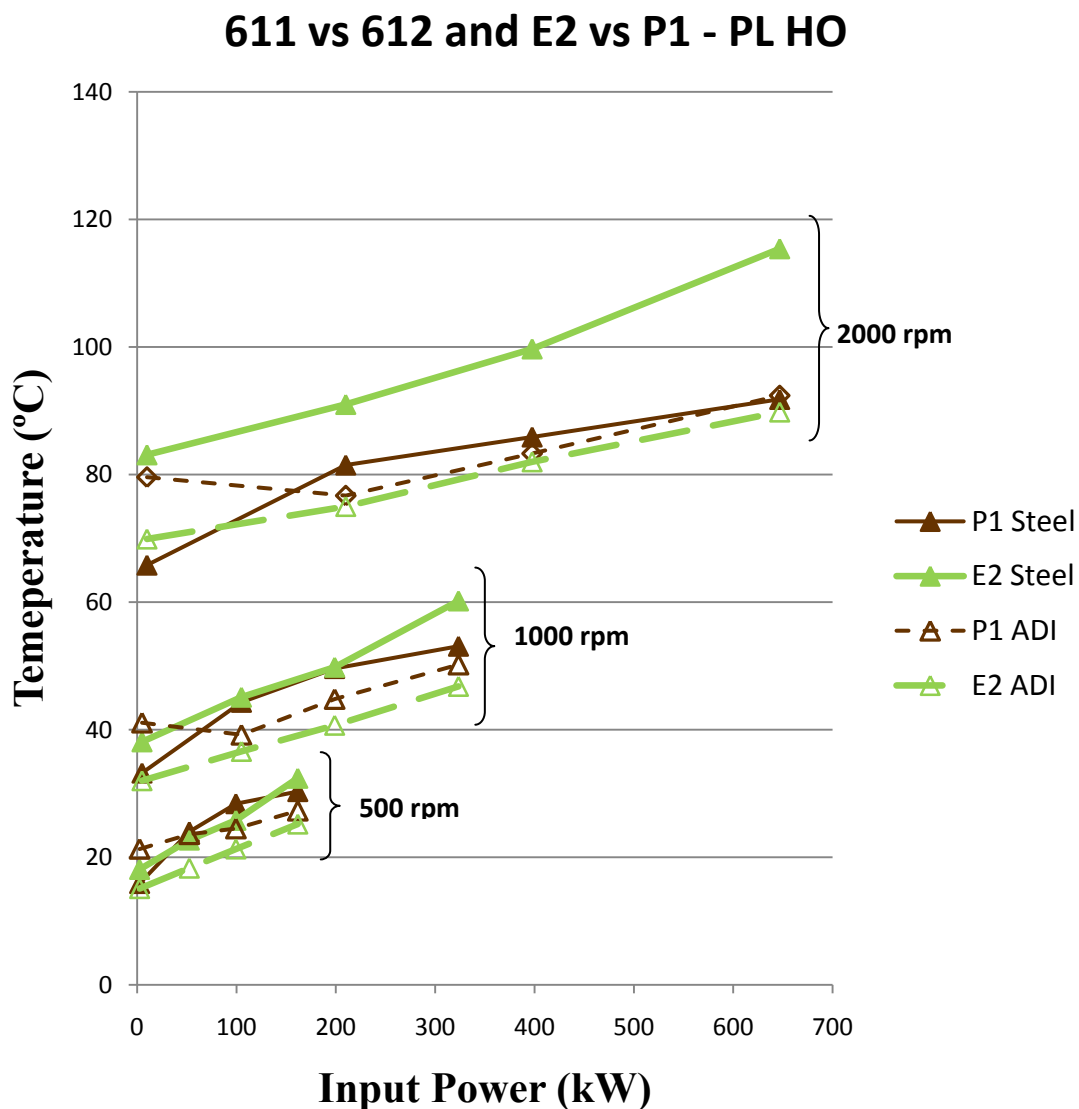


Figure 71 – Variation of stabilization temperatures with Input Power for 611 steel and 612 ADI gears with E2 and P1 high oil level.

611steel gear with P1 oil has the higher temperature for almost all input power at 500rpm having the second higher temperature for almost all input power values at 1000rpm and 2000rpm.

Figure 72 shows that in general, gears lubricated by oil E2 have larger amount of mass loss, 612 gear with P1 oil does not have a mass loss value due to reasons out of my responsibility.

Figure 73 shows the concentration of wear particles at the end of FZG load stage k9, being clear that, for steel gears, E2 oil promotes a lower amount of wear, while the opposite occurs ADI gears.

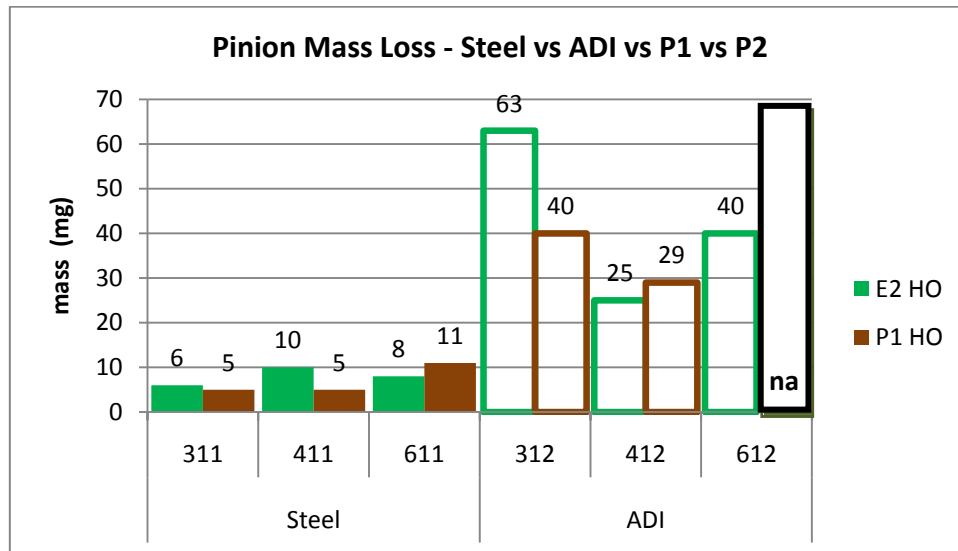


Figure 72 – Pinion mass loss of 20MnCr5 steel vs. ADI gears: PAO and Ester gear oil and high oil level.

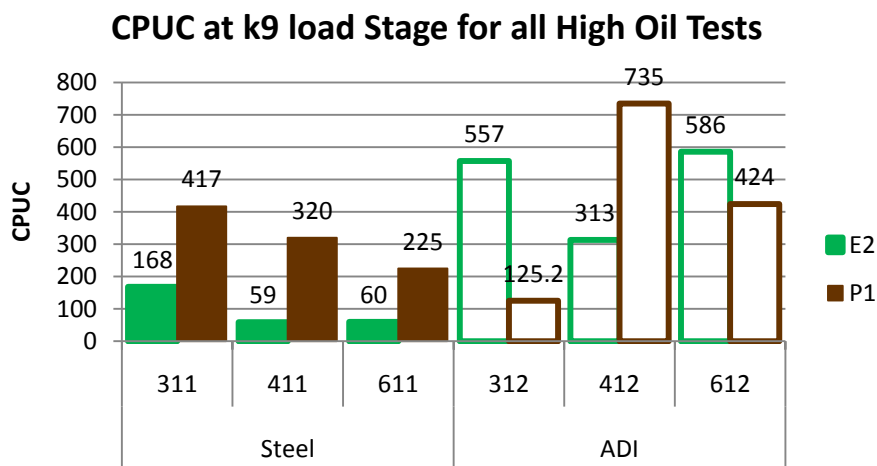


Figure 73 – CPUC Ferrometric Index values for all Steel and ADI gears in the end of k9 High oil Power loss test.

4.4. PAO based gear oil (P1) with low oil level

4.4.1. Stabilization temperatures – PAO (P1) gear oil, low oil level and steel gears

The maximum oil temperature reached during the gear power loss tests, performed with gear oils E2 and P1, showed that the churning losses were very high, although the maximum operating speed was only 2000 rpm.

The main reason for these high temperatures was the high oil shearing in the contact between the pressure pads and the gear wheels. The low loss gear concept implies the use of helical gears and these can only be tested in the standard FZG test gear box if pressure pads are used.

In order to decrease the influence of the pressure pads and generate lower churning power losses, the gear power loss test performed with PAO based gear oil (P1) was repeated using a lower oil level, corresponding to 1000 cm³, instead of 1500 cm³.

Figure 74 shows the stabilization temperatures measured during the gear power loss test performed with steel gears and PAO based oil P1, with a low oil level. Once more, gear 611 generated the lowest stabilization temperatures, followed by gear 411 and 311, whatever the operating conditions (torque stage and speed) considered.

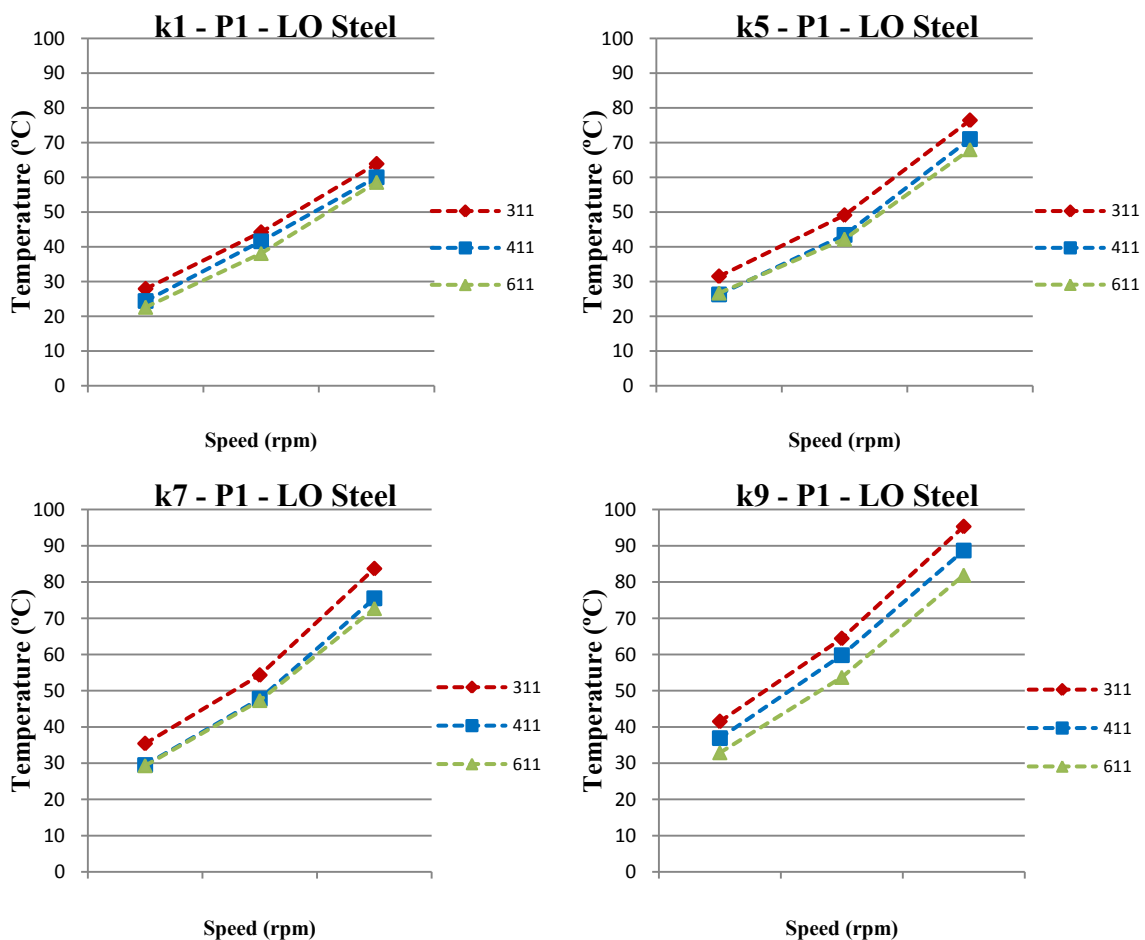


Figure 74 – Stabilization temperatures of steel gears: geometries 311, 411 and 611, P1 gear oil and low oil level.

In Figure 75 the stabilization temperatures obtained with high and low oil levels are compared, for steel gears lubricated with P1. As expected, a lower oil level generates lower stabilization temperatures, although such differences are smaller at low operating speed.

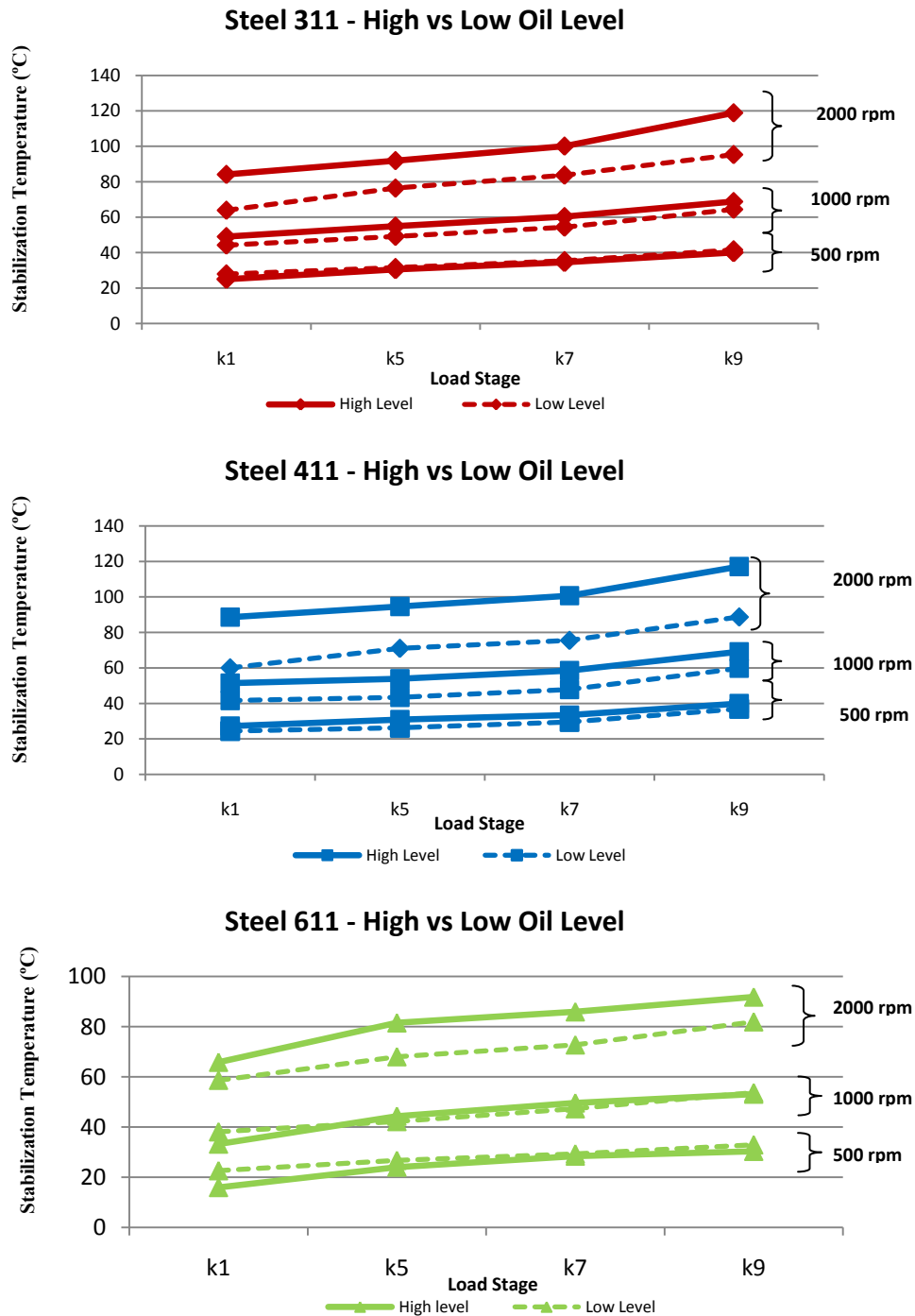


Figure 75 – Resume of stabilization temperature differences between the three gear geometries for high oil and low oil FZG Power Loss test, with P1 lubricant oil.

At 1000 rpm and 2000 rpm the differences in stabilization temperature might be significantly high: more than 20 °C at 2000 rpm with gear 311 and around 10 °C at 1000 rpm with gear 411. It's interesting to notice that gear 611 is less sensitive to the oil level, since the stabilization temperatures are very similar both at 500 rpm and 1000 rpm.

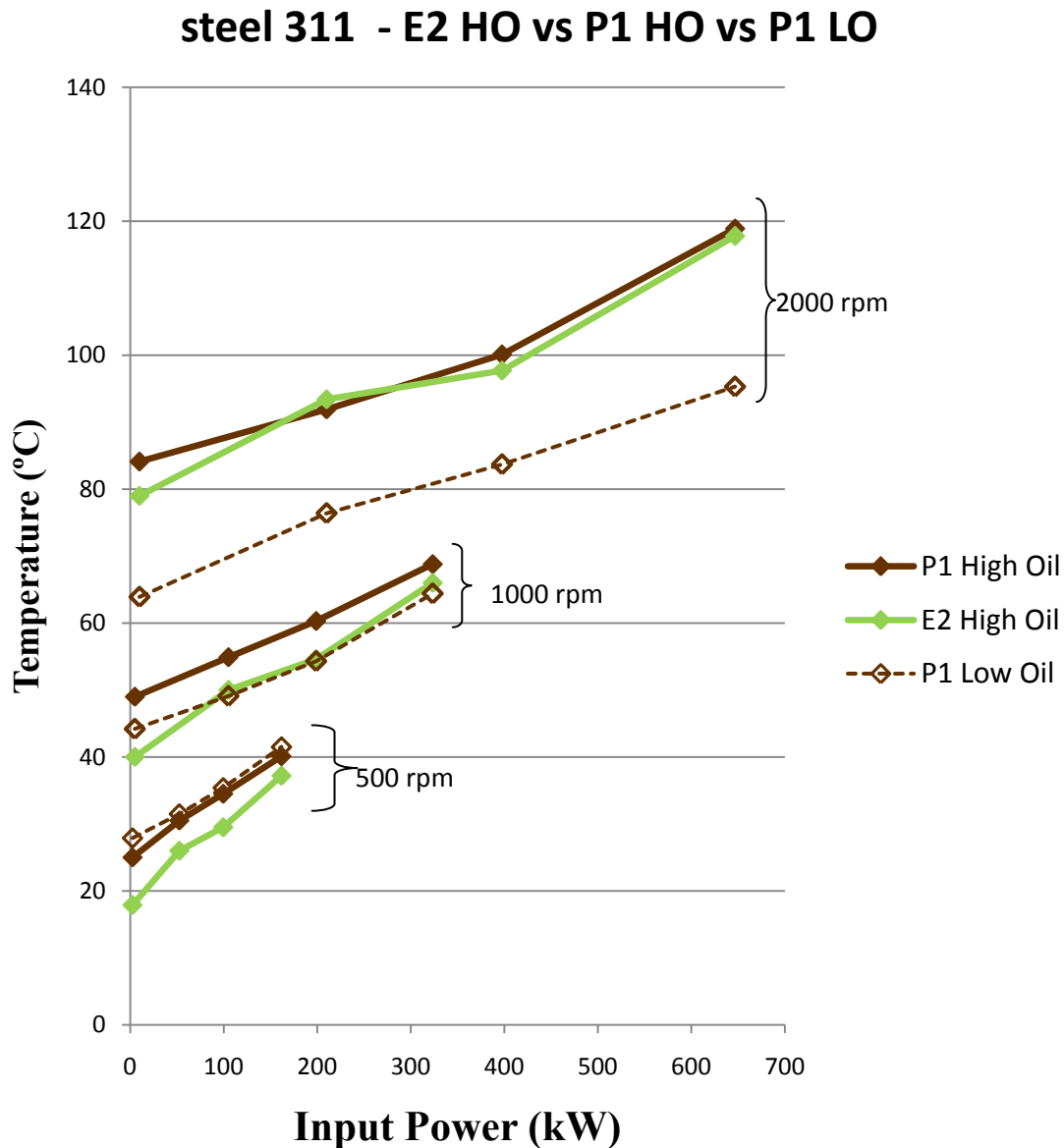


Figure 76 – Variation of stabilization temperatures with Input Power for 311 steel gear with E2 and P1 high oil level and P1 Low oil level.

Figure 76 shows that for 311 steel gears the P1 low oil level has the lower stabilization temperature for any input power value at 1000 rpm and 2000 rpm being the lower temperature for 500 rpm obtained by the 311 with E2 high oil level. The 311 gear with high level of P1 oil has the higher temperatures for all input power values at 1000rpm and 2000 rpm.

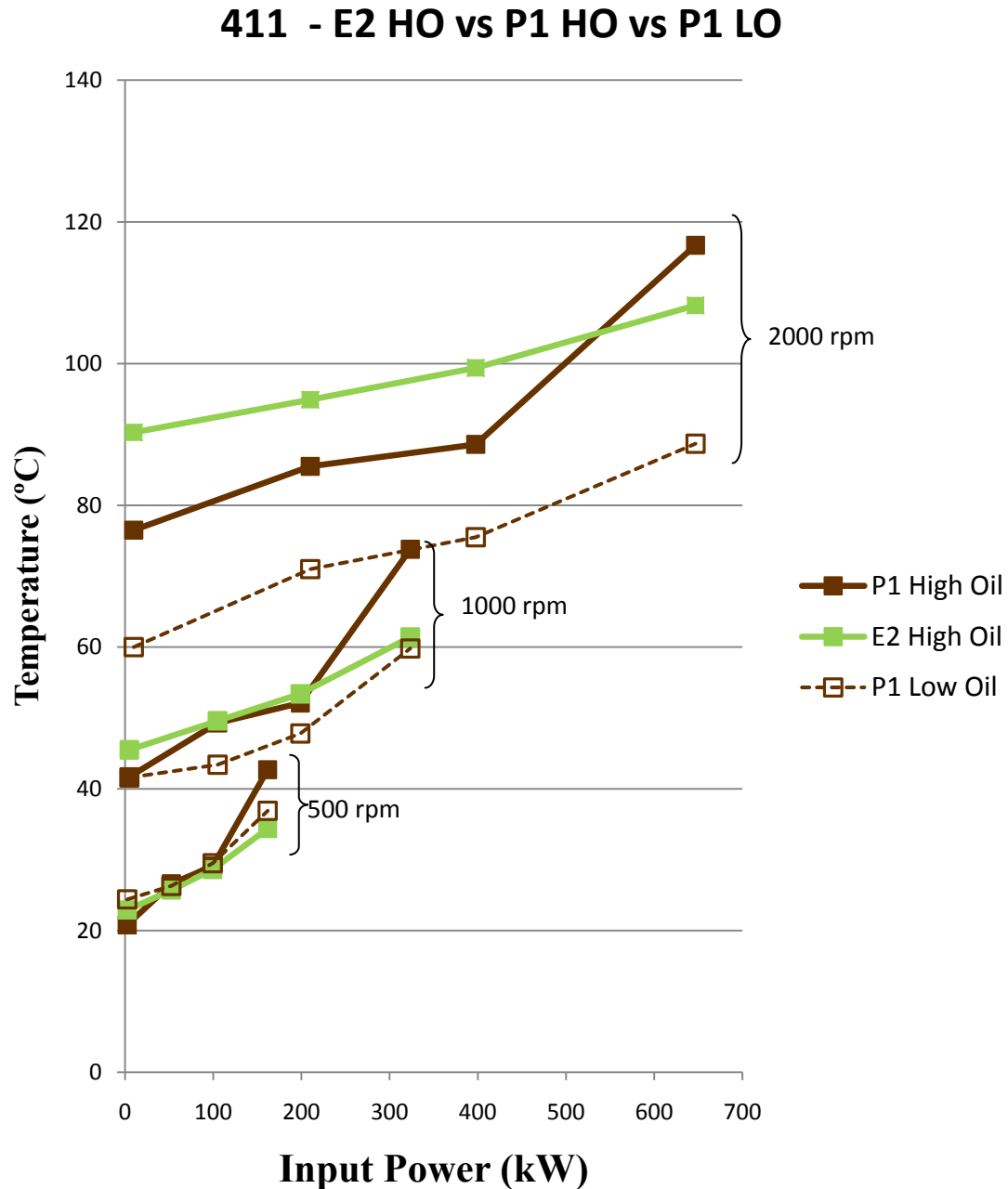


Figure 77 – Variation of stabilization temperatures with Input Power for 411 steel gear with E2 and P1 high oil level and P1 Low oil level.

Figure 77 shows at 411 gear with low P1 oil level has the lowest stabilization temperatures for all input power values at 1000 rpm and 2000 rpm having the same behavior as the 311 gear with the same oil and level. Once again the 411 steel gear with high E2 oil level has the lower stabilization temperature for all input power values at 500 rpm and the higher at 1000rpm and 2000rpm for all input power values. The 411 with high P1 oil level has an intermediate stabilization temperature for almost all input power values and rotational speeds.

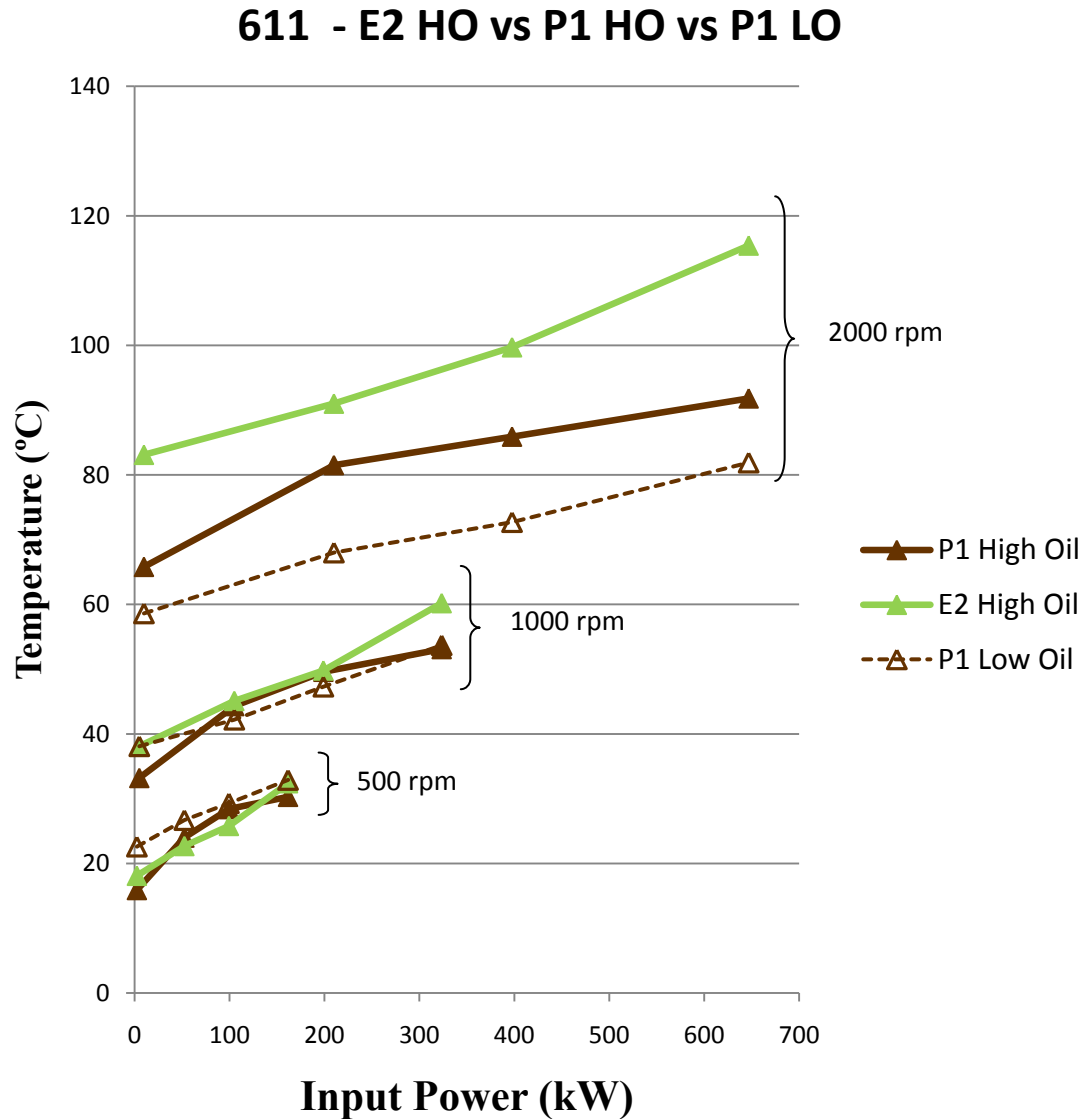


Figure 78 –Variation of stabilization temperatures with Input Power for 611 steel gear with E2 and P1 high oil level and P1 Low oil level.

Figure 78 shows almost exactly the same results for 611 steel gear in comparative terms to 411 and 311 gears, being the 611 steel gear with P1 low oil level the one with lower stabilization temperatures for all input power values at 1000rpm and 2000rpm, being the E2 with high oil level the one with the lower temperature at 500rpm.

4.4.2. Oil analysis wear particles – PAO (P1) gear oil, low oil level and steel gears

Figure 79 shows the wear particle indexes, measured by Direct Reading Ferrography, of the gear oil samples gathered during the gear power loss tests with low oil level.

Gears 311 and 411 generated very low and similar wear particles indexes, with an index for large particles (DL) between 30 and 35, at the end of the test. Gear 611 presented higher values (DL = 63 at the end of the test) but still a low value for gears.

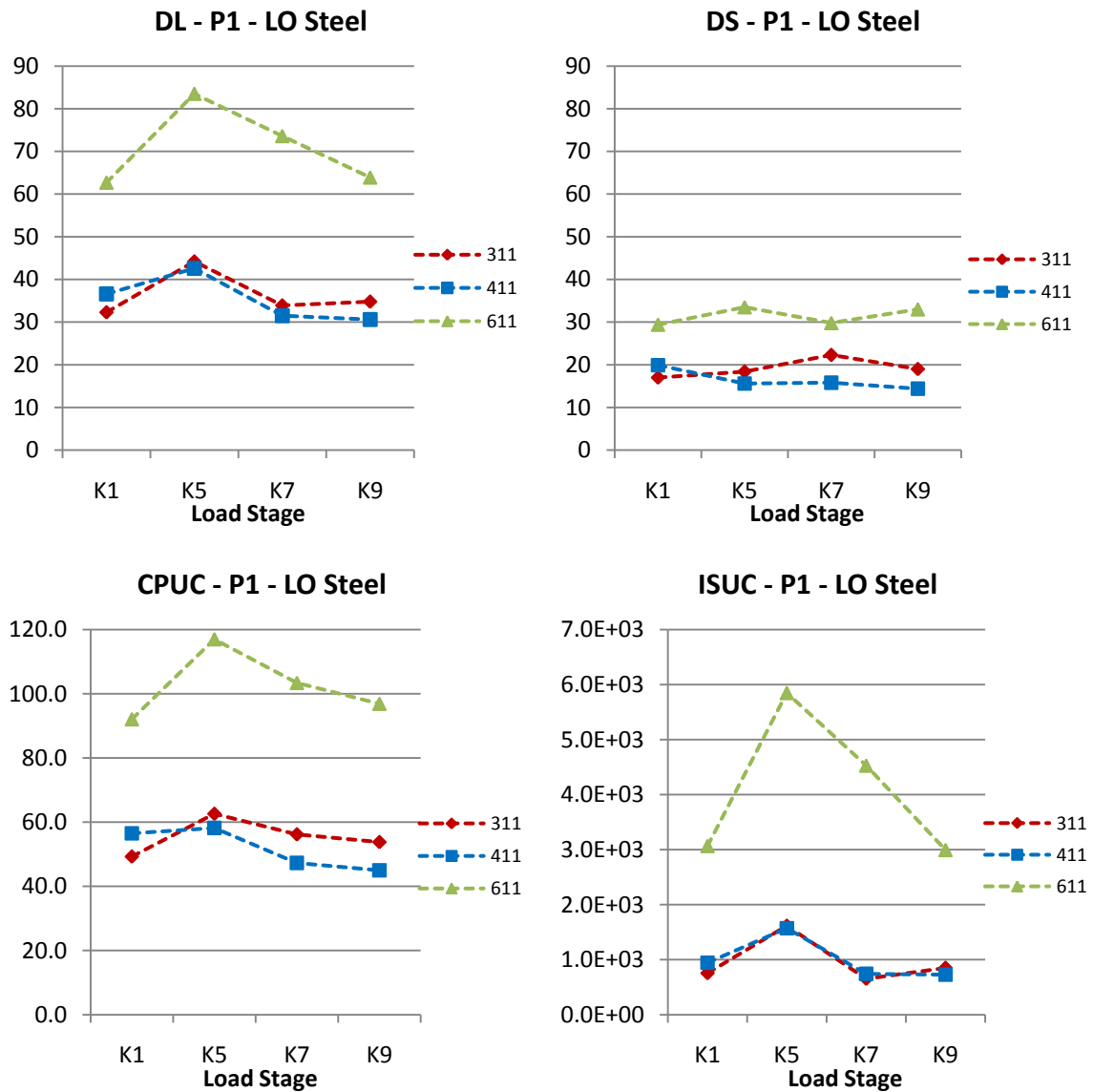


Figure 79 – Oil analysis wear particle indexes: steel gears lubricated with P1 gear oil and low oil level.

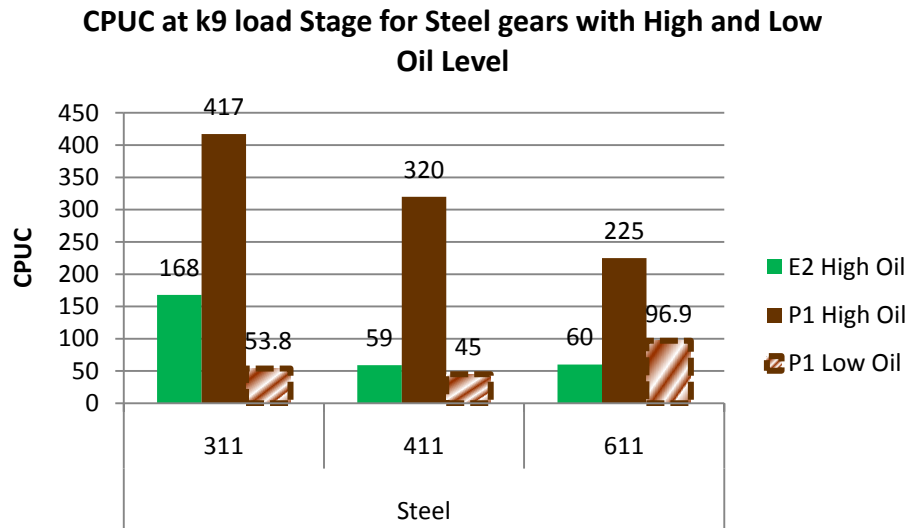


Figure 80 – CPUC Ferrometric Index values for Steel gears in the end of k9 High oil and Low oil Power loss tests.

Figure 80 shows that steel gear with a low level of P1 lubricant oil have a lower wear particle concentration being the same oil but with the high level the one promoting the higher amount of wear particles for all steel geometries. The high level of E2 oil prove to generate less than half the wear concentration particles of the high level of P1 oil being very close to the levels of the low level of P1 oil, indicating that a future low oil version of E2 oil would promote even lower wear particles than the low oil level of P1.

4.4.3. Surface roughness – PAO gear oil (P1), low oil level, steel

Table 27, Table 28 and Table 29, show the roughness parameters measured on each pinion and wheel along the radial direction, before and after the gear power loss test. In the case of gear 311, lubricated with low oil level, all the pinion and wheel roughness parameters increased very significantly (between 47% and 189%), although the final roughness parameters were small ($R_a = 0.18 \mu\text{m}$ for the pinion and $R_a = 0.20 \mu\text{m}$ for the wheel).

Table 27 – 311 Steel Gear Geometry roughness parameters for the wheel and pinion before and after the Standard FZG power loss test with low level of P1 lubricant oil.

			Pinion surface roughness [μm]									
	direction	position	Ra	Rq	Rz	Rmax	Rpk	Rk	Rvk	Mr1	Mr2	Vo
Initial	wheel	radial	0.12	0.13	0.65	1.0	0.10	0.35	0.20	7.1	82.35	4.3
	pinion	radial	0.10	0.10	0.53	0.9	0.10	0.20	0.15	9.9	87.92	2.8
Final	wheel	radial	0.20	0.23	1.10	1.4	0.12	0.58	0.40	4.9	82.65	8.4
	pinion	radial	0.18	0.23	1.07	1.4	0.12	0.55	0.43	6.7	84.28	8.7
Wheel Roughness evolution(%)			71.43	75.00	69.23	47.37	16.67	66.67	100.00	-31.13	0.36	96.47
Pinion Roughness evolution(%)			83.33	133.33	100.00	50.91	16.67	175.00	188.89	-32.21	-4.13	213.25

Table 28 – 411 Steel Gear Geometry roughness parameters for the wheel and pinion before and after the Standard FZG power loss test with low level of P1 lubricant oil.

			Pinion surface roughness [μm]									
	direction	position	Ra	Rq	Rz	Rmax	Rpk	Rk	Rvk	Mr1	Mr2	Vo
Initial	wheel	radial	0.22	0.28	1.37	1.8	0.17	0.67	0.48	8.1	85.53	9.7
	pinion	radial	0.10	0.15	0.70	1.1	0.15	0.32	0.17	10.0	86.18	4.1
Final	wheel	radial	0.17	0.23	1.10	1.5	0.13	0.47	0.45	6.5	83.23	8.5
	pinion	radial	0.18	0.23	1.10	1.4	0.13	0.55	0.35	8.5	83.33	7.1
Wheel Roughness evolution(%)			-23.08	-17.65	-19.51	-15.60	-20.00	-30.00	-6.90	-20.04	-2.69	-12.03
Pinion Roughness evolution(%)			83.33	55.56	57.14	28.13	-11.11	73.68	110.00	-15.19	-3.31	76.13

Table 29 – 611 Steel Gear Geometry roughness parameters for the wheel and pinion before and after the Standard FZG power loss test with low level of P1 lubricant oil.

			Pinion surface roughness [μm]									
	direction	position	Ra	Rq	Rz	Rmax	Rpk	Rk	Rvk	Mr1	Mr2	Vo
Initial	wheel	radial	0.18	0.22	1.05	1.3	0.12	0.53	0.33	6.7	83.78	6.9
	pinion	radial	0.28	0.37	1.70	2.2	0.27	0.85	0.52	6.8	82.33	10.4
Final	wheel	radial	0.22	0.27	1.40	1.8	0.20	0.73	0.37	7.1	88.00	8.6
	pinion	radial	0.28	0.30	1.68	1.9	0.20	0.73	0.53	6.3	82.60	10.2
Wheel Roughness evolution(%)			18.18	23.08	33.33	36.36	71.43	37.50	10.00	5.69	5.03	24.51
Pinion Roughness evolution(%)			0.00	-18.18	-0.98	-14.39	-25.00	-13.73	3.23	-7.56	0.32	-2.09

In the case of gear 411, the wheel roughness parameters decreased (Ra decreased from 0.22 μm to 0.17 μm), but the pinion roughness parameters increased significantly (between 28% and 83%). In the case of gear 611 the evolution of the pinion and wheel surface roughness was very small, with a slight increase on the wheel and decrease on the pinion.

4.4.4. Mass loss – PAO gear oil (P1), low oil level, steel

Figure 81 presents the mass loss of gears 311, 411 and 611 lubricated with low and high oil levels of gear oil P1 and also of gear oil E2 with high oil level. The steel pinions (311, 411 and 611) had very similar mass losses, between 2 mg and 11 mg, which are very low values for a new gear not run-in. In general, the gears lubricated with low oil level generated similar or lower mass loss then the gears with high oil level

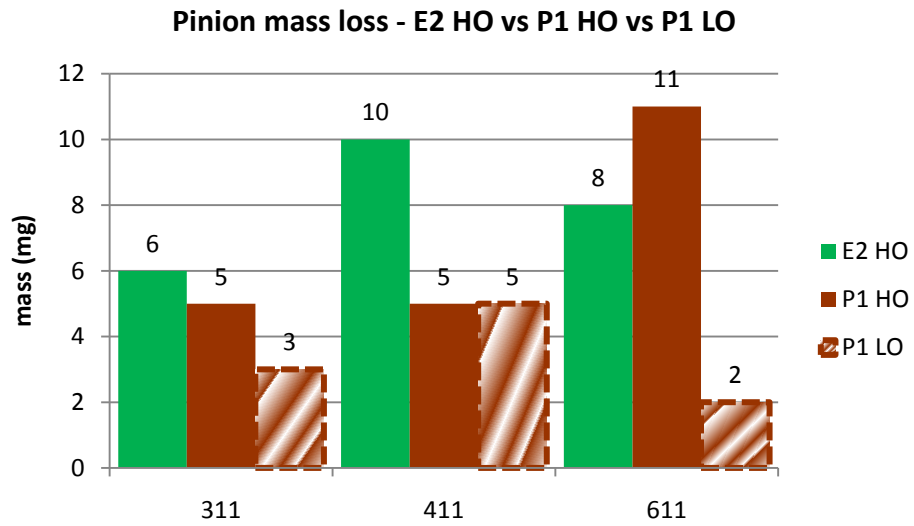


Figure 81 – Pinion mass loss in FZG power loss test for the Steel gear geometries with high and low P1 Lubricant oil level.

4.5. “No load” power loss tests with oil P1

4.5.1. Stabilization temperatures – PAO (P1) gear oil, low and high oil level and steel gears

As mentioned before, the “no load” or churning power losses were very important in these gear power loss tests performed with the pressure pads, necessary to support the axial loads introduced by the helical gears. In order to have a better assessment of these “no load” losses an extensive experimental study was performed, using steel gears 311, 411 and 611, oils E2 and P1, and two oil levels, 1000 and 1500 cm³. These “no load” gear power loss tests were all performed in load stage K1 (very low applied torque) and wheel speeds between 500 rpm and 2500 rpm. The test program with oil E2 is not yet completed.

Figure 82 presents the stabilization temperatures at the end of each stage, for all the conditions tested and shows, as expected, that a lower oil level generates lower stabilization temperatures. In the case of the high oil level, gear geometries 311 and 411 generate very similar stabilization temperatures, which are slightly smaller in the case of geometry 611. In the case of a low oil value gear 311 generates slightly lower stabilization temperatures than gears 411 and 611. However, the stabilization temperatures are only slightly dependent on the gear geometry, for each oil level.

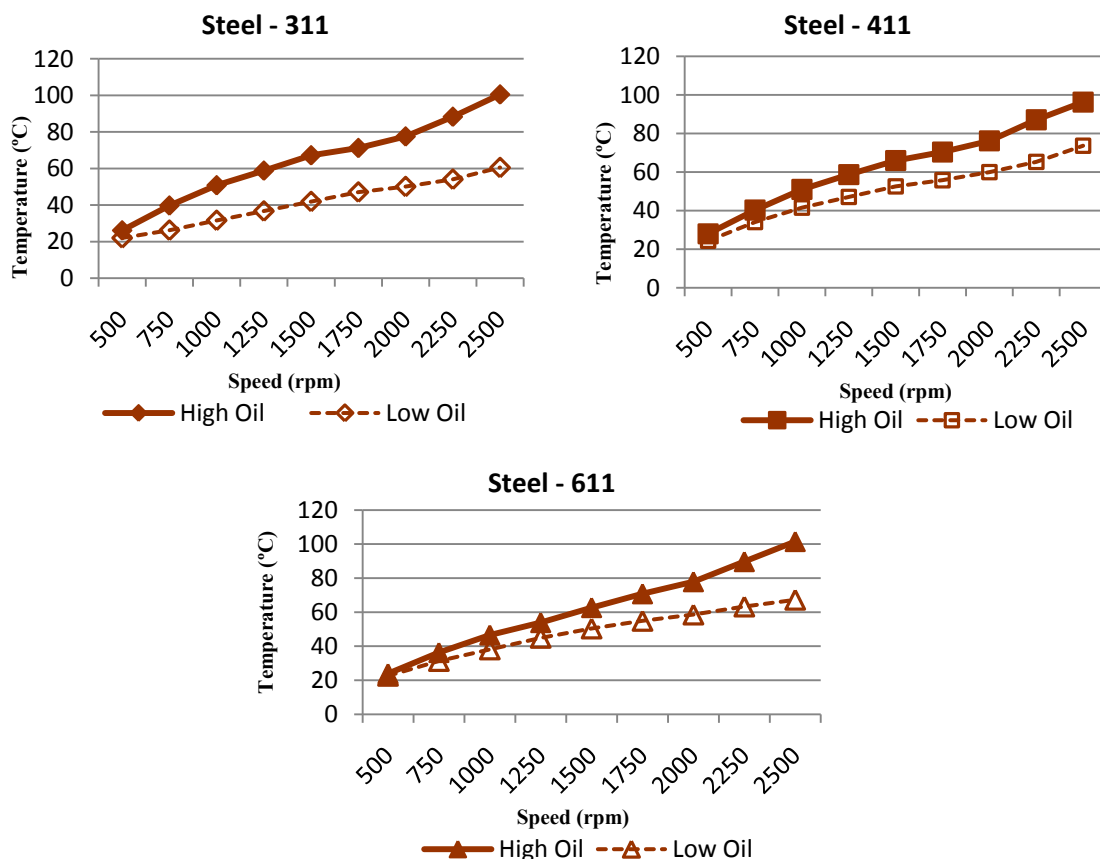


Figure 82 – Stabilization temperature for 311, 411 and 611 steel gears: gear oil P1, low and high oil levels.

4.5.2. Oil analysis wear particles – PAO (P1) gear oil, low and high oil level and steel gears

Figure 83 shows the Direct Reading Ferrography wear indexes (DL, DS, CPUC and ISUC), at the end of the “no load” gear power loss tests, performed with steel gears and lubricated with P1 gear oil and two different oil levels.

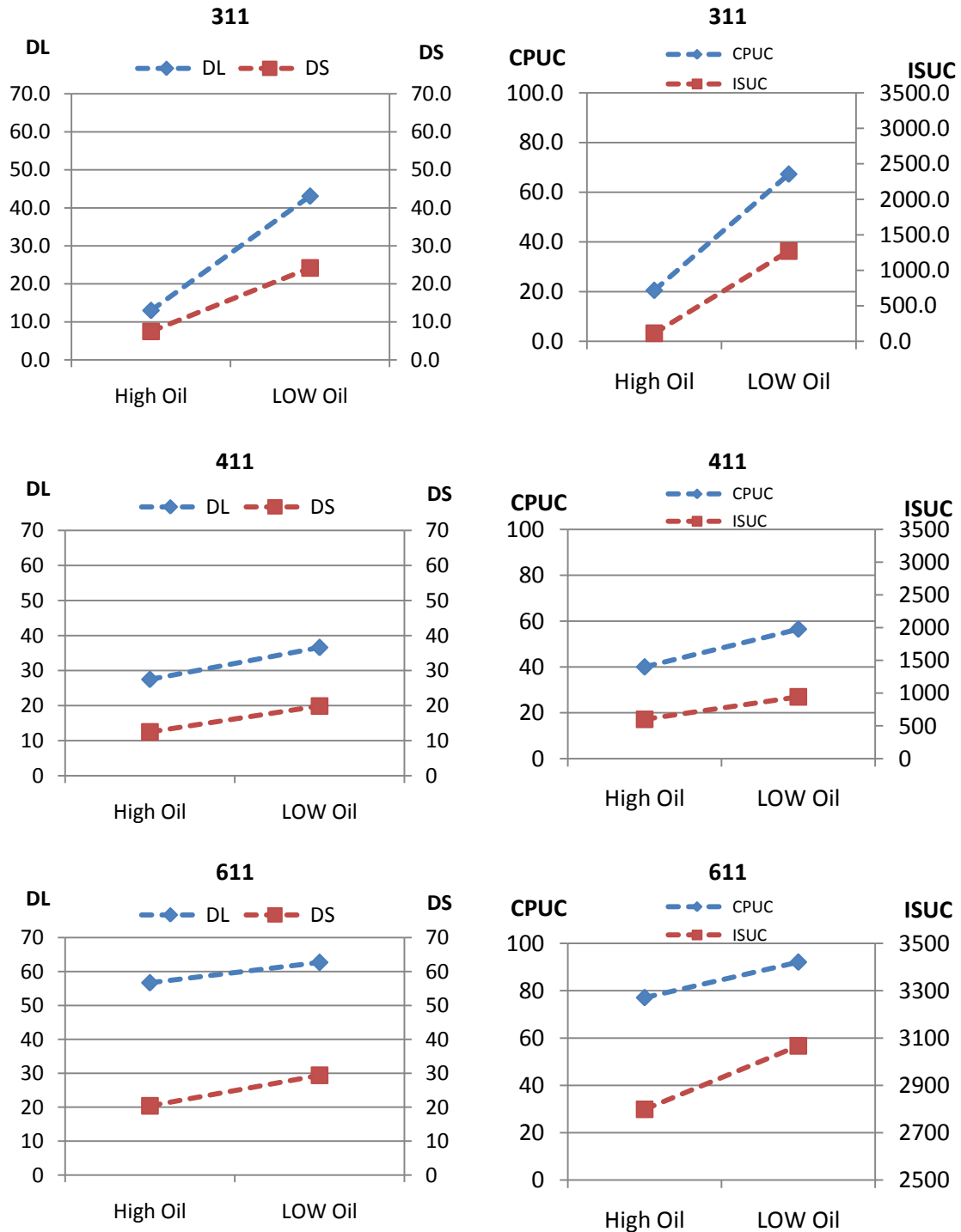


Figure 83 - Oil analysis wear particle indexes at high and low oil levels: “no load” power loss tests and steel gears lubricated with P1 gear oil.

Figure 83 indicates that the wear indexes (DL, DS, CPUC and ISUC) are always higher in the case of the low oil level (1000 cm^3), whatever the geometry considered (311, 411 or 611). Gear 411 had the lowest wear indexes, whatever the oil level, followed by gear 311 and finally gear 611 with the highest values. This means that gear geometry has some influence on gear wear.

5 – Conclusion

5. Conclusion

The analysis of the experimental results allow several statements about the general ADI and steel performance when tested with the Ester oil E2 and Polyalphaolefine oil P1.

5.1. Gear geometries

5.1.1. Stabilization temperatures

The different gear geometries have in most cases, a very distinct behavior. The 311/312 gears have in general the highest stabilization temperatures, 411/412 gears have lower stabilization temperatures than 311/312 gears, and finally the 611/612 gears have lower stabilization temperatures than both preceding gear geometries as shown in Figure 54, Figure 55, Figure 63 and Figure 64. In the case of steel gears lubricated with ester E2, the difference between the different gear geometries is very small.

5.1.2. Mass loss

In general, gears 311/312 generate higher CPUC indexes than 411/412, and this one higher values than 611, whatever the lubricant considered (see Figure 73). Gear 612 doesn't follow this trend. However, the mass loss results are less conclusive. All steel gears (311, 411 and 611) have very low mass loss, between 5 mg and 11 mg, and ADI gears between 25 mg and 63 mg (see Figure 72).

5.2. 20MnCr5 carburized steel vs ADI (Austempered Ductile Iron)

5.2.1. Stabilization temperatures

412 and 612 ADI gears have lower stabilization temperatures than the 411 and 611 steel ones when lubricated with ester oil E2 (see Figure 56). However, 311 steel gear has lower stabilization temperature than the 312 ADI one for all speeds and load stages.

311 and 411 steel gears have lower stabilization temperatures than the 312 and 412 ADI ones, when lubricated with P1 oil (see Figure 65), for all load stages and speeds. 611 steel gear generates slightly higher operating temperatures than gear 612.

5.2.2. Mass Loss

As shown in Figure 72, ADI gears have a mass loss significantly higher than steel gears, whatever the lubricant considered.

The same trend is observed when the CPUC results are compared (see Figure 73).

5.3. Ester base oil E2 vs PAO base oil P1

5.3.1. Stabilization temperatures

The influence of the oil formulation on the stabilization temperature is complex, because it depends both on gear geometry and material, as shown in Figure 69, Figure 70 and Figure 71. Besides this, the operating temperature depends both on the lubricant viscosity and operating speed, which have a strong influence in the churning power losses.

However, in the case of ADI, the Ester oil always generates lower stabilization temperatures than PAO.

5.3.2. Mass Loss

As shown in Figure 72, the influence of the oil formulation in mass loss is very small, whatever the gear material. In what concerns to CPUC index, Figure 73, clearly shows that in the case of steel gears, P1 generates more wear particles than E1

5.4. Oil level

5.4.1. Temperatures

Comparing the P1 and E2 high oil level with P1 low oil level for steel gears, 311, 411 and 611 gear geometries with a low P1 oil level have lower stabilization temperatures at 1000rpm and 2000rpm for all input power values. Nevertheless, high E2 oil level is the one with lower stabilization temperature for 500rpm in steel gears, because of its lower viscosity than P1.

5.4.2. Mass loss

As shown in Figure 80, gears 311, 411 and 611 generate less wear particles if the oil level is lower. The main reason for such behavior is that low oil level generates lower operating temperatures, higher film thickness, and, thus, lower wear. However, similar results were obtained with the high level of oil E2. This behavior is observed in Figure 81, where gears lubricated with low oil level generate lower mass loss.

5.5. Churning Losses

The churning loss test, showed that a decrease in the gearbox oil level of 1/3 of the oil volume is enough to decrease the stabilization temperatures up to near 40% in the case of 311 gear geometry. Such decrease in the stabilization temperature s observed for all speeds and gear geometries. As a consequence of this temperature decrease and corresponding augmentation of film thickness, the corresponding ferrometric indexes decreased as well.

5.6. General conclusion

The E2 lubricant oil with 611 steel gears has proven to be the most efficient among the steel geometries, and the 612 ADI gears are also the better among ADI geometries with the same lubricant.

ADI gears have the better behavior in almost all geometries regardless oil formulation, being a valid, cheap and easy to manufacture option when compared with the standard carburized steel.

E2 ester oil prove to be a good choice, joining great performance in power loss tests for both materials and the three geometries when compared with the high performance industrial oil P1, being better in most material and geometry combinations, having also the advantages of the biodegradable and low toxicity properties.

6 – Future Work Perspectives

6. Future Work Perspectives

The work presented in this thesis is not yet completed, a wide group of tests are still to be done using these gear profiles, and a large amount of post test analysis that can and will be done. A great breakthrough step is a computerized energetic model that will allow us to simulate and modulate the different components of heat dissipation of the FZG test box, which unfortunately, was not ready in time to make part of this thesis. Several analyses of the teeth surfaces are still yet to be done among other procedures, the work that will be performed hopefully soon is described in the topics below:

- Analyze the oil samples in the Reometer to obtain the reologic properties of the lubricant after the power loss tests;
- Perform the power loss test with a low oil level of E2 lubricant oil;
- Perform churning loss test to the different gear geometries with E2 lubricant oil with high oil level and low oil level;
- Perform a low oil version of the FZG power loss test to the ADI gears;
- Perform churning loss tests to the ADI gears with high and low oil levels;
- Proceed to the substitution of the current FZG spur gear test gearbox that obligate the use of pressure pads by a helical gear FZG test gearbox and repeat if not all the test performed before at least the more important, in order to remove from results the losses introduced by the pressure pads.

7 - References and Attachments

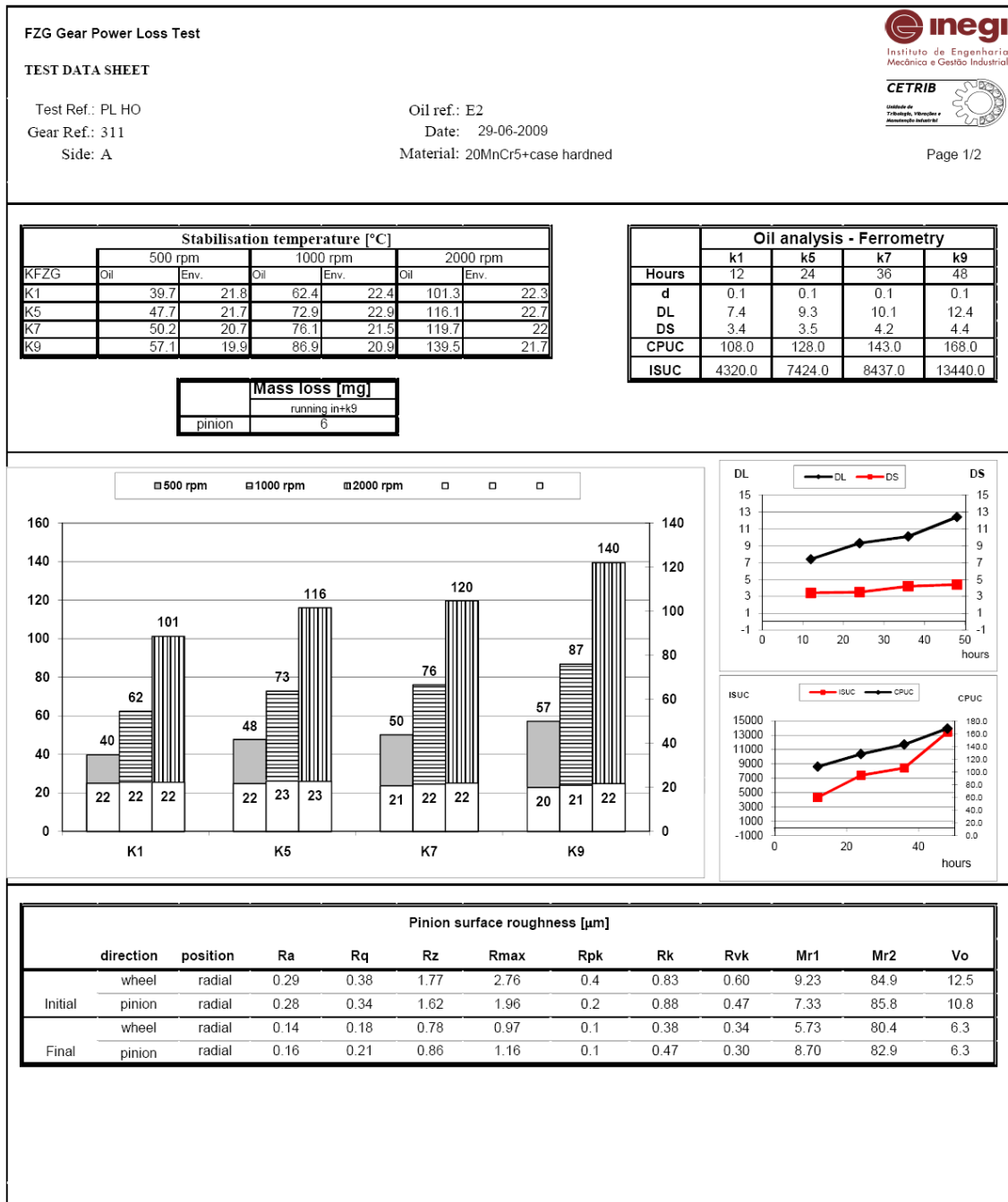
References

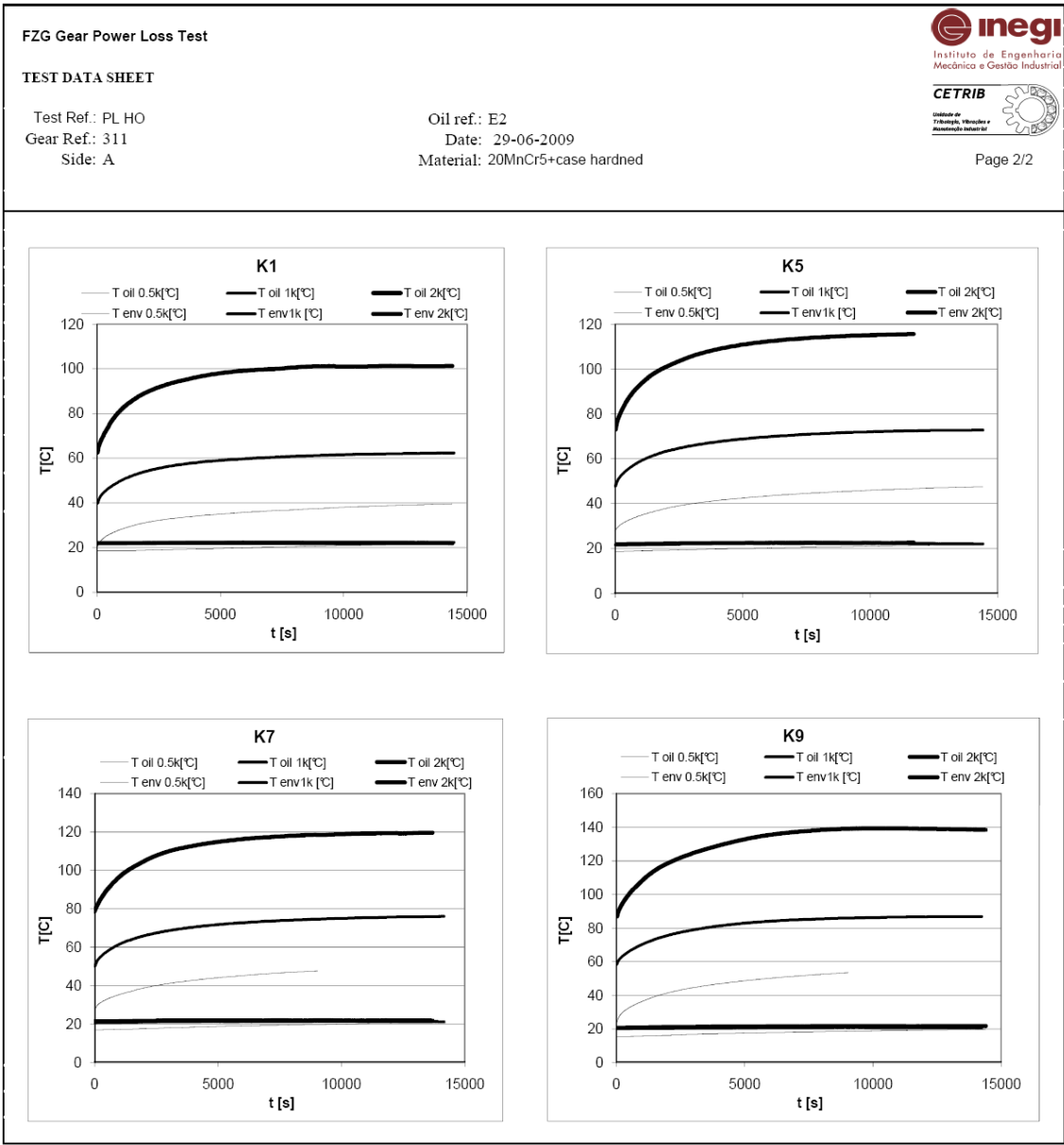
1. Hohn, B.R., K. Michaelis, and A. Wimmer, *Gearboxes with minimised power loss*. VDI Berichte, 2005(1904 II): p. 1451-1465.
2. Magalhães, L., et al., *Influence of tooth profile and oil formulation on gear power loss*. Tribology International. In Press, Accepted Manuscript.
3. Magalhães, L.a.M., Ramiro and Locateli, Cristiano and Seabra, Jorge. *Influence of tooth profile on gear power loss*. in *IRF'2009 – Integrity Reliability Failure - Challenges and Opportunities, Third International Conference*. 2009. Faculty of Engineering, University of Porto, Porto, Portugal: INEGI.
4. Martins, R., N. Cardoso, and J. Seabra, *Gear power loss performance of biodegradable low-toxicity ester-based oils*. Proceedings of the Institution of Mechanical Engineers Part J-Journal of Engineering Tribology, 2008. 222(J3): p. 431-440.
5. Höhn, B.R., K. Michaelis, and A. Wimmer, *Low loss gears*. Gear Technology, 2007. 24(4): p. 28-35.
6. Martins, R., et al., *Friction coefficient in FZG gears lubricated with industrial gear oils: Biodegradable ester vs. mineral oil*. Tribology International, 2006. 39(6): p. 512-521.
7. Magalhães, L., et al., *LOW TORQUE LOSS GEARS: AUSTEMPERED DUCTILE IRON vs CARBURIZED STEEL*, in *NORDTRIB 2010*. 2010: Sweden.
8. Cardoso, N., *Mechanical performance of biodegradable, low toxicity ester based industrial gear oils*. 2007, Faculdade de Engenharia, Universidade do Porto.
9. *Modern Tribology handbook*. <<The>> mechanics and materials science series. 2001, Boca Raton: CRC Press. 2 vol.
10. Ferreira, L.A.d.A., *Tribologianotas de curso*. Vol. 2ª ed 0009. 2000, Porto: Publindústria.
11. Seabra, J., *Engrenagens - Lubrificação, Rendimento e Avarias*. FEUP ed. 2005, Porto: DEMEGI SMAP.
12. Seabra, J., *Mecânica do Contacto Hertziano*. 2ª ed, ed. FEUP. 2003, Porto: DEMEGI SMAP.
13. Pirro, D.M. and A.A. Wessol, *Lubrication fundamentals*. 2nd , rev. and expanded ed. Mechanical Engineering 137. 2001, New York: Marcel Dekker. VIII, 523.
14. Dowson, D. and G. R. Higginson, *Elastohydrodynamic lubrication*. S. I. Editon. 1977: Pergamon Press Ltd.
15. *Friction, lubrication and wear technology*. ASM Handbook 18. 1992, [S. I.]: ASM International. XIII, 942.
16. G, H., *La Lubrification Industrielle, Tome 1 - La Lubrification des Engrenages*: Publications de L+.
17. Winter, H. and K. Michaelis. *Investigations on the thermal balance of gear drives*. in *Fifth World Congress on Theory of Machines and Mechanisms*. 1979: American Society of Mechanical Engineers.
18. Carreteiro, R.P. and P.N.A. Belmiro, *Lubrificantes & lubrificação industrial*. 2006, Rio de Janeiro: Interciência. XXVIII, 504.
19. Castro, M.J.D.d., *Gripagem de engrenagens FZG lubrificadas com óleos base Novos critérios de gripagem globais e locais*. 2004, Porto: FEUP. VI, 323.
20. Hohn, B.R. and K. Michaelis, *Influence of oil temperature on gear failures*. Tribology International, 2004. 37(2): p. 103-109.
21. Höhn, B.-R., K. Michaelis, and T. Vollmer, *Thermal Rating of Gear Drives: Balance Between Power Loss and Heat Dissipation*. AGMA Technical Paper, 1996.
22. Changenet, C. and M. Pasquier, *Power losses and heat exchange in reduction gears: Numerical and experimental results*. VDI Berichte, 2002. 2(1665): p. 603-613.
23. Hohn, B.R., P. Oster, and U. Schrade, *Studies on the micropitting resistance of case-carburised gears - Industrial application of the new calculation method*. VDI Berichte, 2005. Vol. II(Nr. 1904): p. 1287-1307.
24. Martins, R., J. Seabra, and L. Magalhaes, *Austempered ductile iron (ADI) gears: Power loss, pitting and micropitting*. Wear, 2008. 264(9-10): p. 838-849.
25. Harding, R., *The use of austempered ductile iron for gears*, in *2ª World Congress of Gears*. 1986: Paris.
26. Magalhães, L., *Caracterização Tribológica de um Ferro Nodular Austemperado em Ensaio Disco-Disco e de Engrenagens FZG*. 2003, Faculdade de Engenharia, Universidade do Porto.

27. Magalhães, L. and J. Seabra. *Contact properties of Cu-Mn austempered ductile iron gears. Experimental evaluation using the FZG test rig.* in *Proceedings of the International Conference on Gears*. 2005. Garching, Germany: VDI - Berichte 1904.
28. Magalhães, L. and J. Seabra, *Artificial indentations for the study of contact fatigue of austempered ductile iron (ADI) discs.* WEAR, 2005. 258(11-12): p. 1755-1763.
29. Magalhães, L. and J. Seabra, *Wear and scuffing of austempered ductile iron gears.* Wear, 1998. 215(1-2): p. 237-246.
30. Rolf Luther, et al., *Emission Reduction from engines and transmissions substituting harmful additives in biolubricants by triboreactive materials (EREBIO).* 2006.
31. Winter, H. and K. Michaelis, *FZG gear test rig - Description and possibilities.* In: Coordinate European Council Second International Symposium on The performance Evaluation of Automotive Fuels and Lubricants, 1985.
32. Mummery, L., *Surface Texture Analysis: The Handbook.* 1992: Hommelwerke GmbH.
33. Cousseau, T., *Análise comparativa do comportamento de massas lubrificantes num rolamento axial de esferas.* 2009, Porto: [s. n.]. XXX, 155, [1].
34. Jorge Seabra, Armando Campos, and A. Sottomayor, *Lubrificação ElastoHidrodinâmica*, DEMec and SMAP, Editors. 2002, FEUP: Porto.

Appendix A: Power Loss Data Sheets

311 Gear Power Loss High Oil – E2





411 Gear Power Loss High Oil – E2

FZG Gear Power Loss Test

TEST DATA SHEET

Test Ref.: PL HL

Oil ref.: E2

Gear Ref.: 411

Date: 29-06-2009

Side: A

Material: 20MnCr5+case hardened

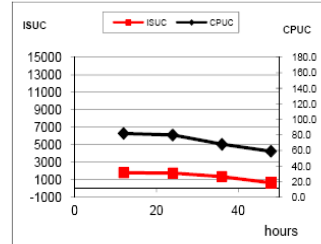
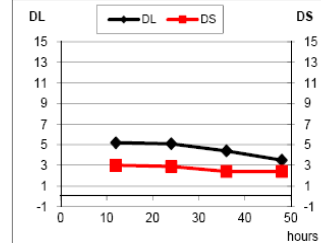
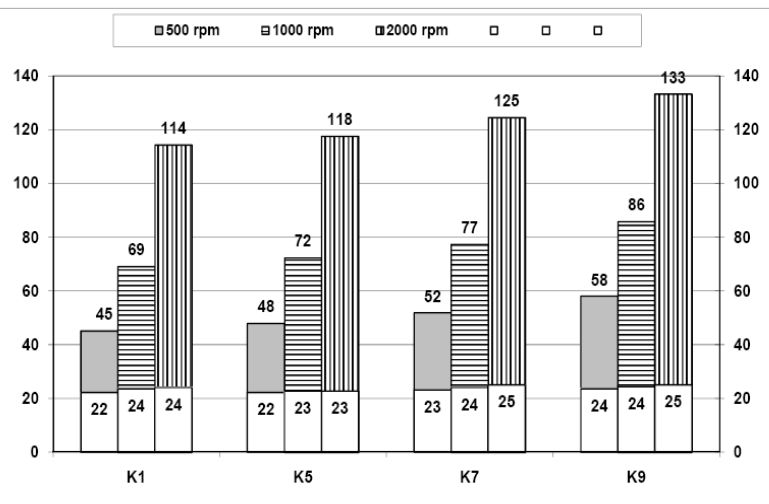


Page 1/2

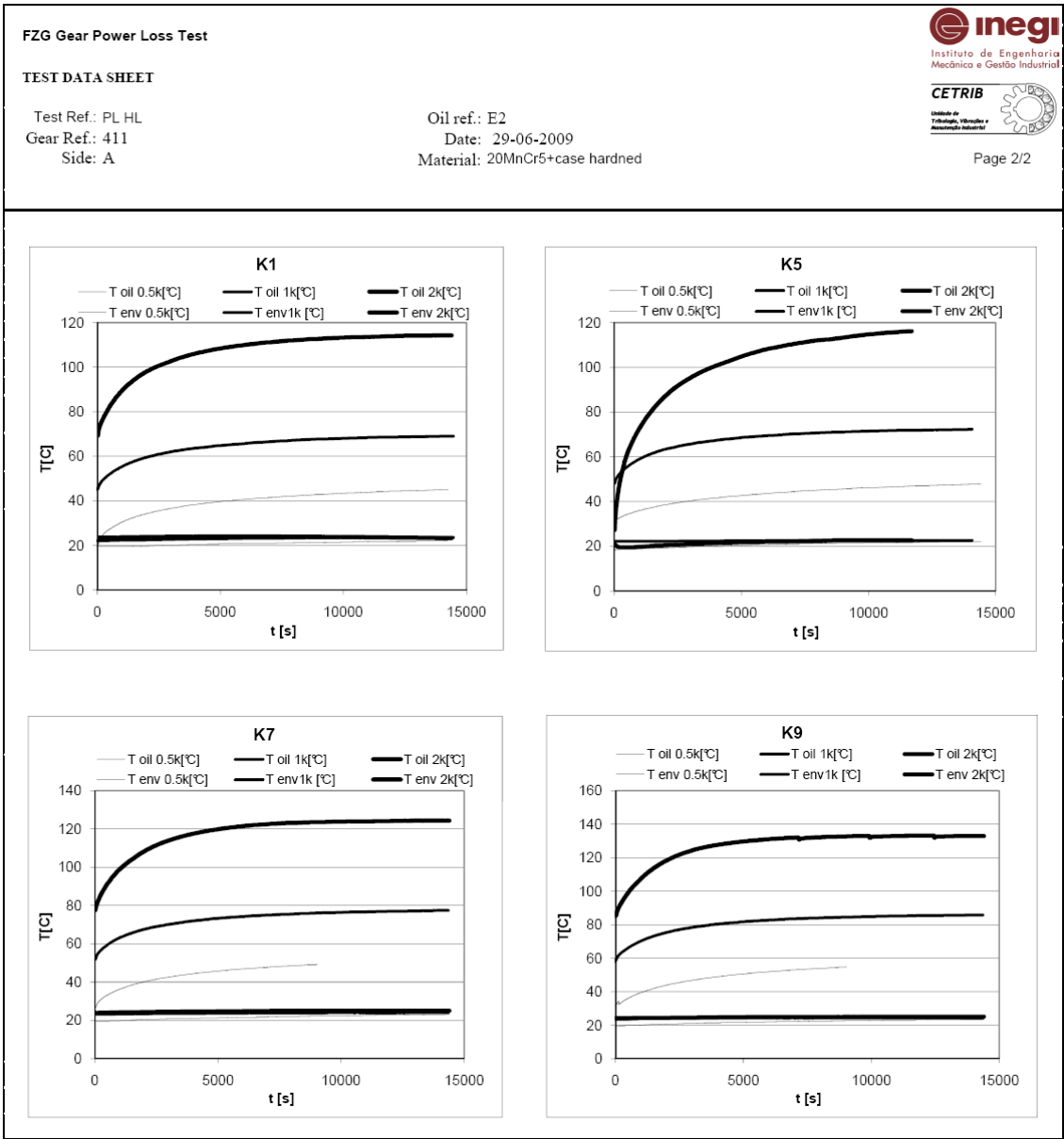
KFZG	Stabilisation temperature [°C]					
	500 rpm		1000 rpm		2000 rpm	
	Oil	Env.	Oil	Env.	Oil	Env.
K1	45.1	22.2	69.1	23.6	114.3	24
K5	47.9	22.2	72.3	22.7	117.6	22.7
K7	51.8	23.2	77.4	24	124.5	25.1
K9	58	23.6	85.8	24.4	133.3	25.1

	Oil analysis - Ferrometry			
	k1	k5	k7	k9
Hours	12	24	36	48
d	0.1	0.1	0.1	0.1
DL	5.2	5.1	4.4	3.5
DS	3	2.9	2.4	2.4
CPUC	82.0	80.0	68.0	59.0
ISUC	1804.0	1760.0	1360.0	649.0

Mass loss [mg]	
running in+k9	
pinion	10



Pinion surface roughness [µm]												
	direction	position	Ra	Rq	Rz	Rmax	Rpk	Rk	Rvk	Mr1	Mr2	Vo
Initial	wheel	radial	0.24	0.30	1.45	1.93	0.2	0.75	0.44	8.20	86.6	9.9
	pinion	radial	0.30	0.38	1.81	2.16	0.2	0.89	0.59	7.27	84.4	12.5
Final	wheel	radial	0.12	0.15	0.71	0.94	0.1	0.37	0.24	6.47	85.0	5.0
	pinion	radial	0.15	0.19	0.87	1.06	0.1	0.42	0.33	8.30	83.2	6.5



611 Gear Power Loss High Oil – E2

FZG Gear Power Loss Test

TEST DATA SHEET

Test Ref.: PL HL

Gear Ref.: 611

Side: A

Oil ref.: E2

Date: 14-04-2009

Material: 20MnCr5+case hardened

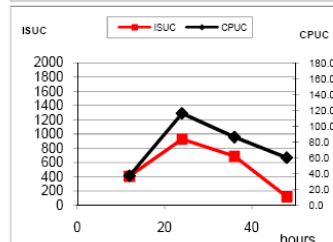
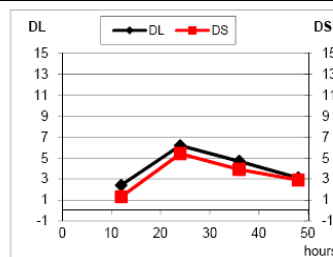
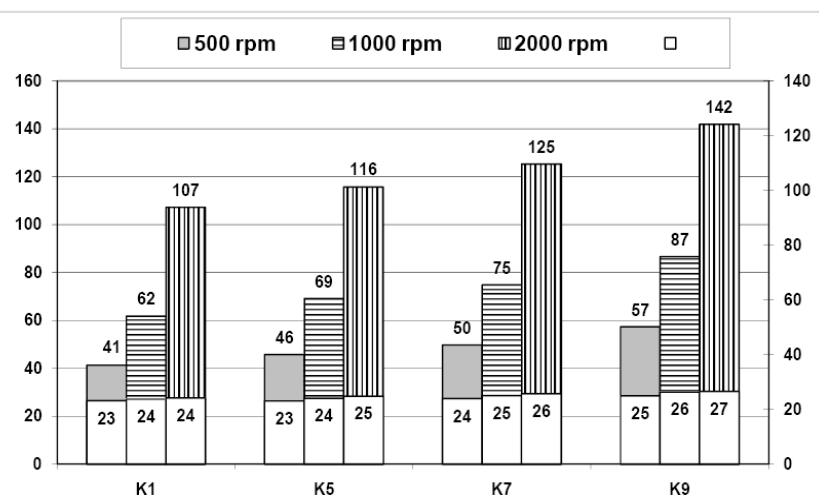


Page 1/2

KFZG	Stabilisation temperature [°C]					
	500 rpm		1000 rpm		2000 rpm	
	Oil	Env.	Oil	Env.	Oil	Env.
K1	41.3	23.2	61.8	23.7	107.3	24.2
K5	45.7	23	69.2	24.1	115.8	24.8
K7	49.7	23.9	74.9	25.1	125.4	25.7
K9	57.3	24.9	86.6	26.4	142	26.6

	Mass loss [mg]
	running in+K9
pinion	8

Hours	Oil analysis - Ferrometry			
	k1	k5	k7	k9
12	12	24	36	48
d	0.1	0.1	0.1	0.1
DL	2.4	6.2	4.7	3.1
DS	1.3	5.4	3.9	2.9
CPUC	37.0	116.0	86.0	60.0
ISUC	407.0	928.0	688.0	120.0



Pinion surface roughness [μm]												
	direction	position	Ra	Rq	Rz	Rmax	Rpk	Rk	Rvk	Mr1	Mr2	Vo
Initial	wheel	radial	Not done									
	pinion	radial	Not done									
Final	wheel	radial	Not done									
	pinion	radial	Not done									

FZG Gear Power Loss Test

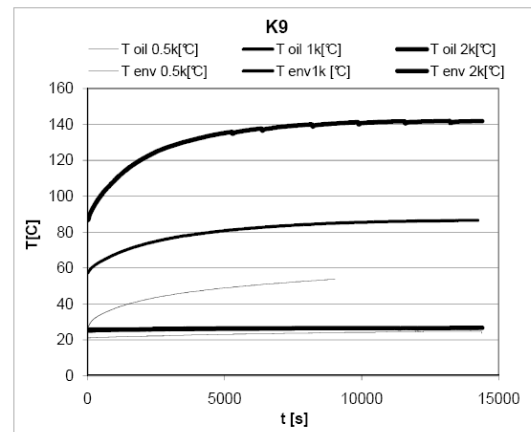
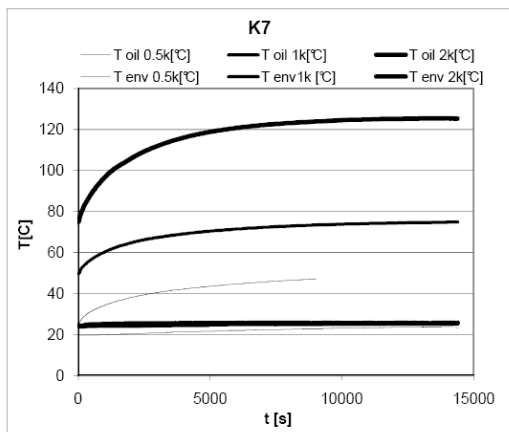
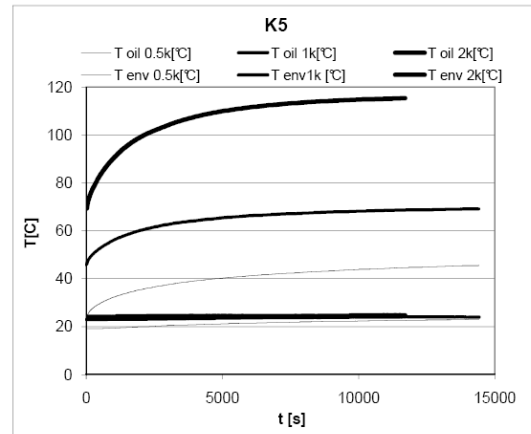
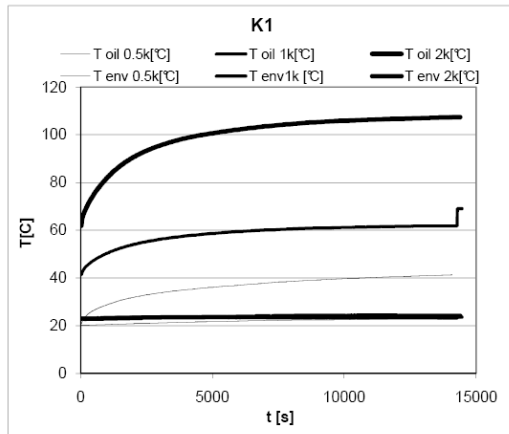
TEST DATA SHEET

Test Ref.: PL HL
Gear Ref.: 611
Side: A

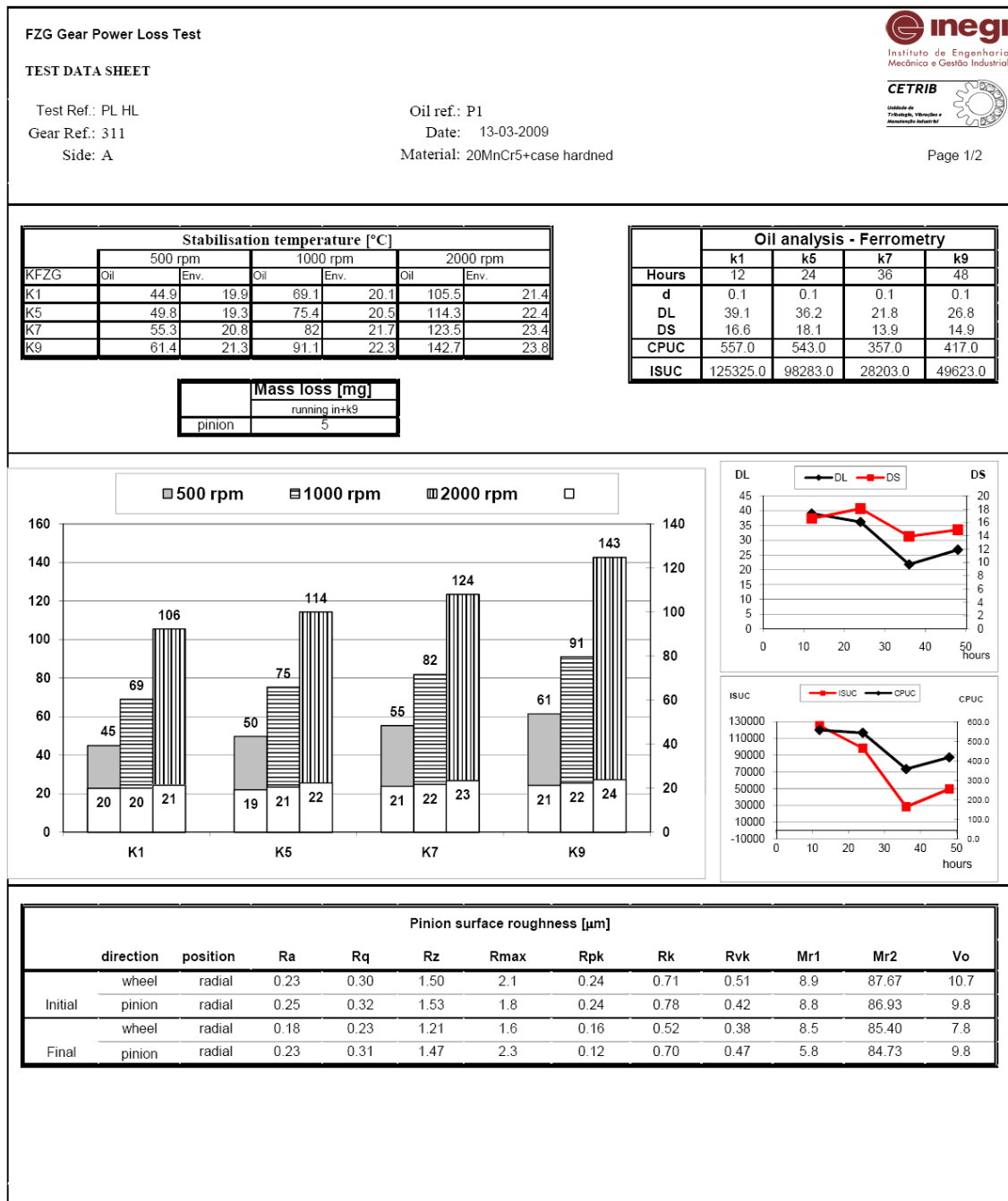
Oil ref.: E2
Date: 14-04-2009
Material: 20MnCr5+case hardened

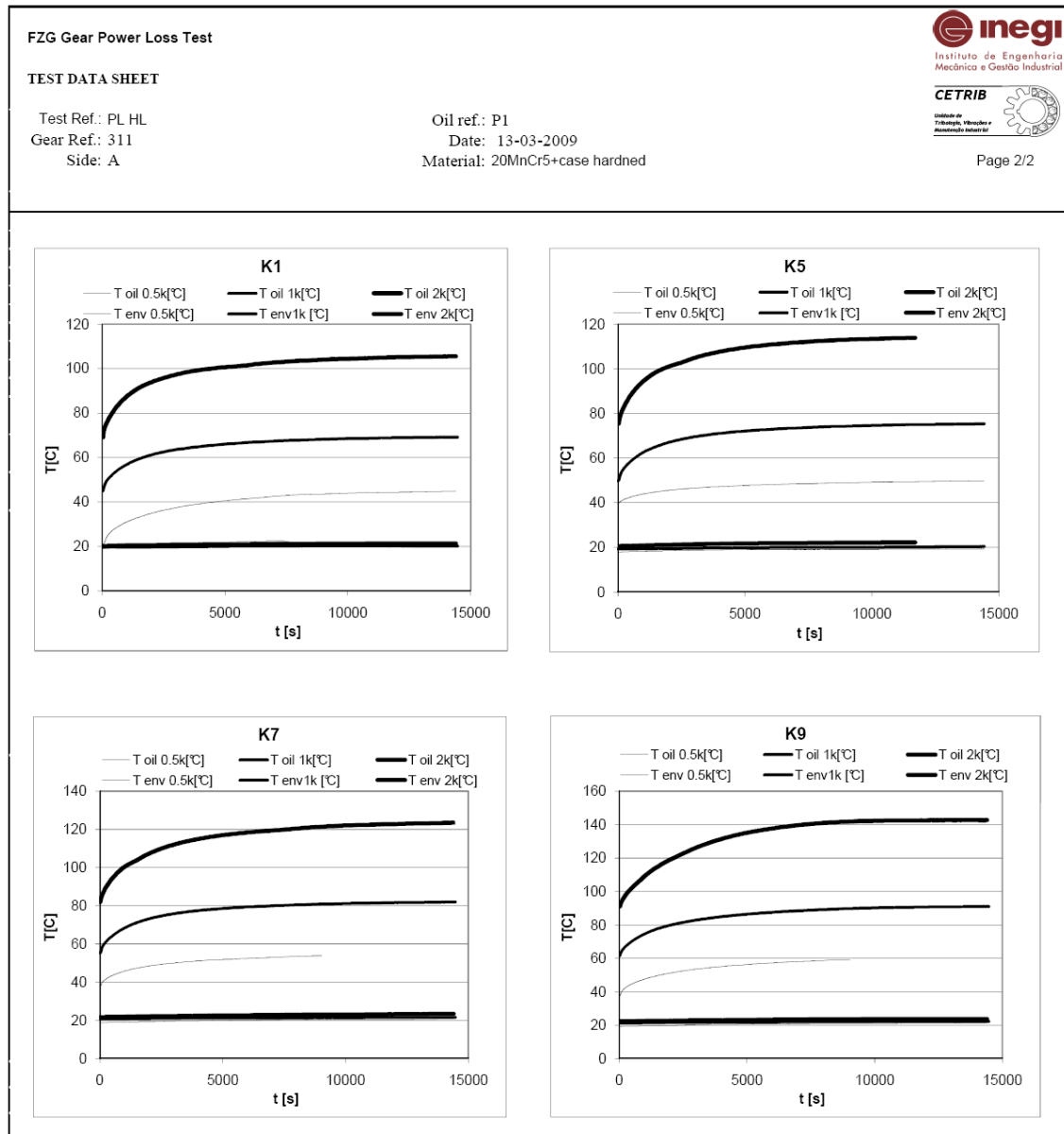


Page 2/2

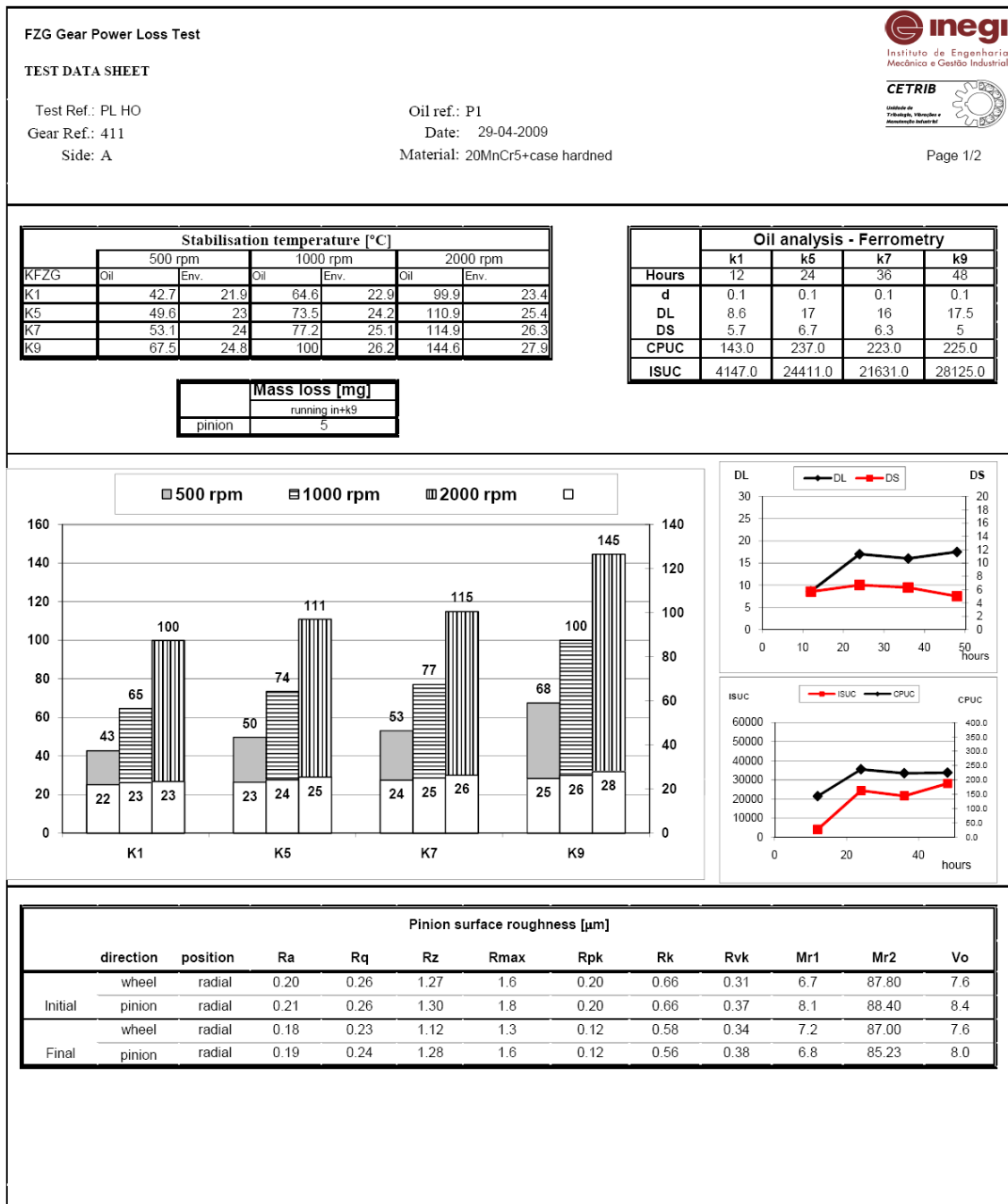


311 Gear Power Loss High Oil – P1





411 Gear Power Loss High Oil – P1



FZG Gear Power Loss Test

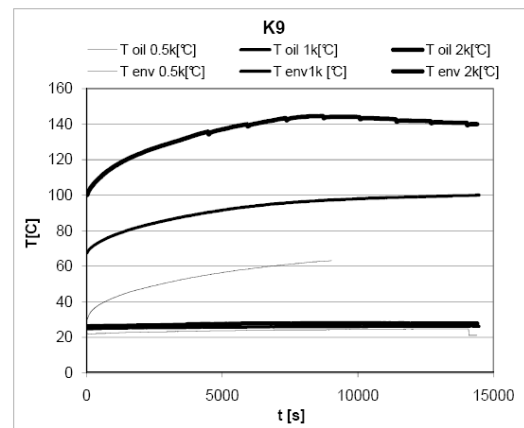
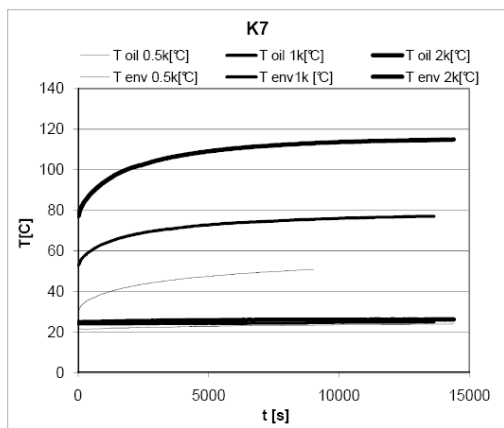
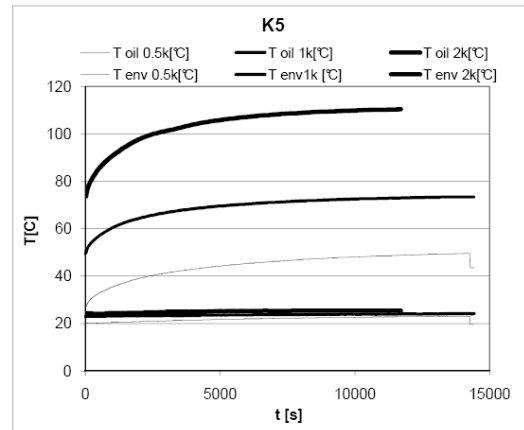
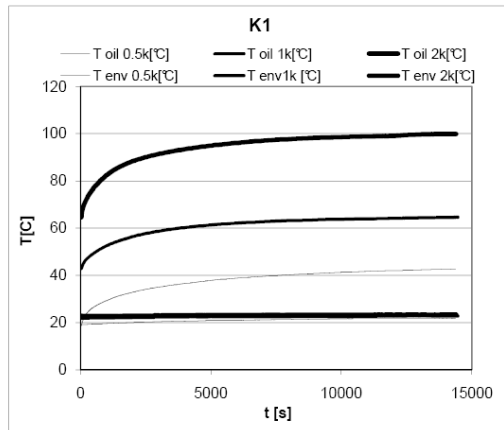
TEST DATA SHEET

Test Ref.: PL HO
Gear Ref.: 411
Side: A

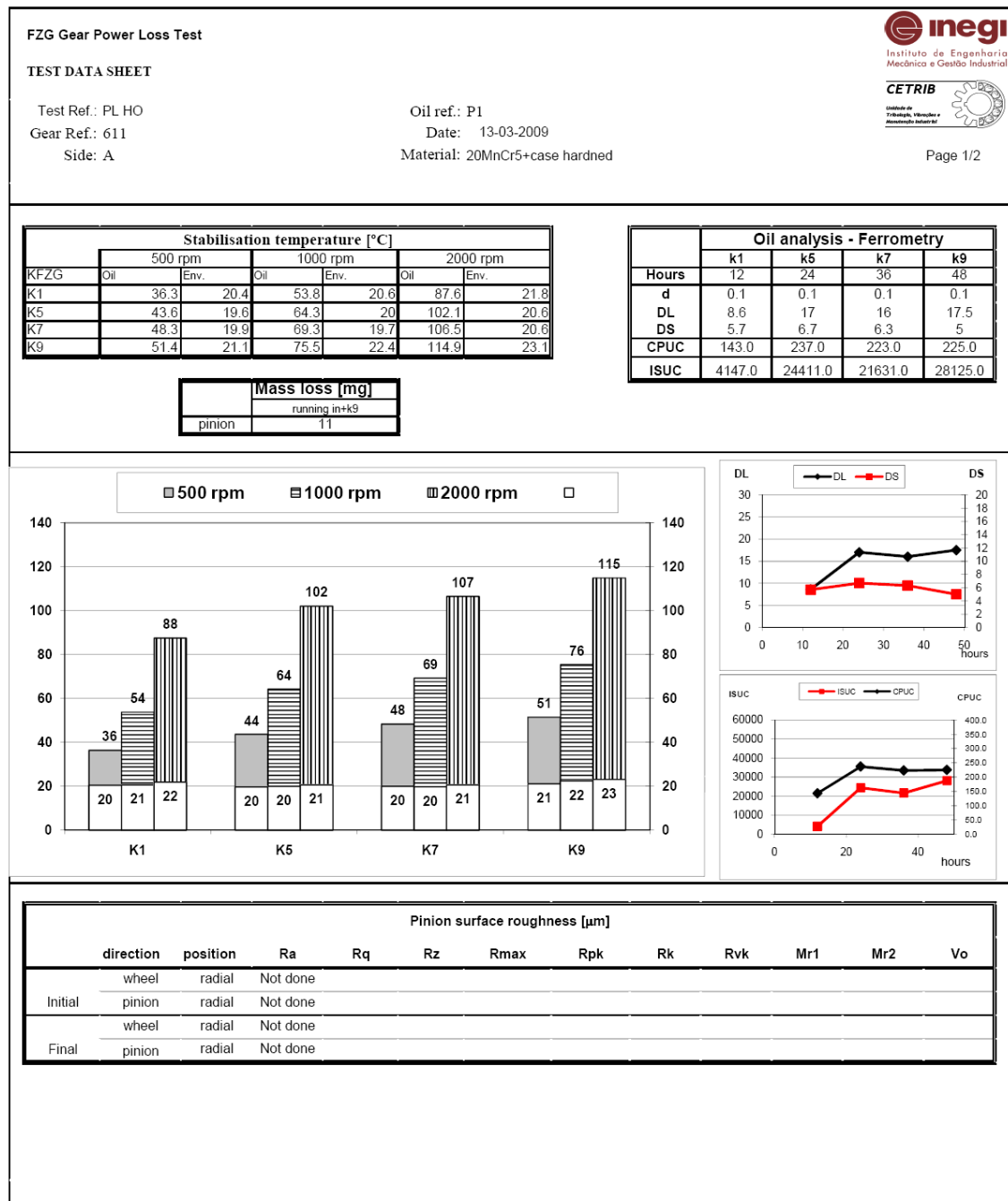
Oil ref.: P1
Date: 29-04-2009
Material: 20MnCr5+case hardened

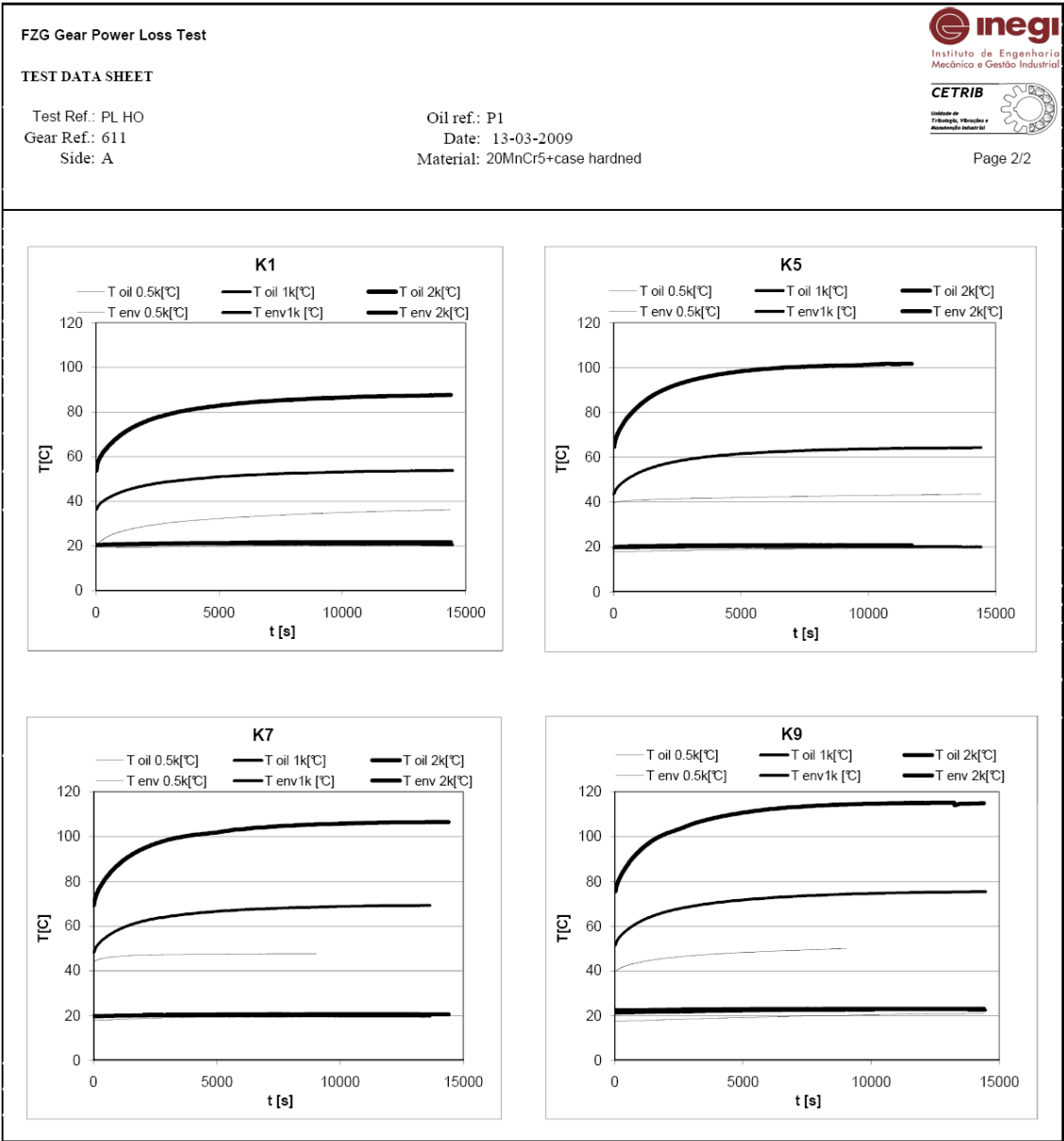


Page 2/2



611 Gear Power Loss High Oil – P1





312 Power Loss High Oil – E2

FZG Gear Power Loss Test

TEST DATA SHEET

Test Ref.: PL-C14

Oil ref.: E2

Gear Ref.: 312

Date: 20-11-2009

Side: A

Material: ADI

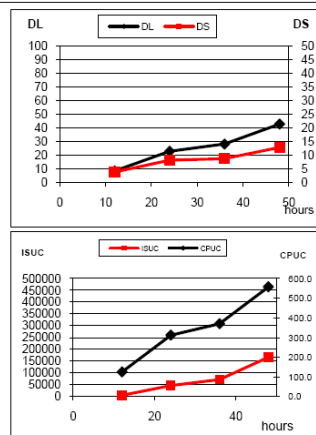
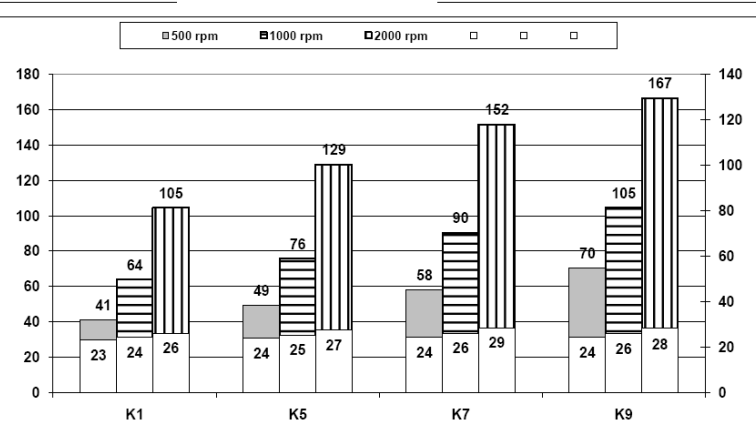


Page 1/2

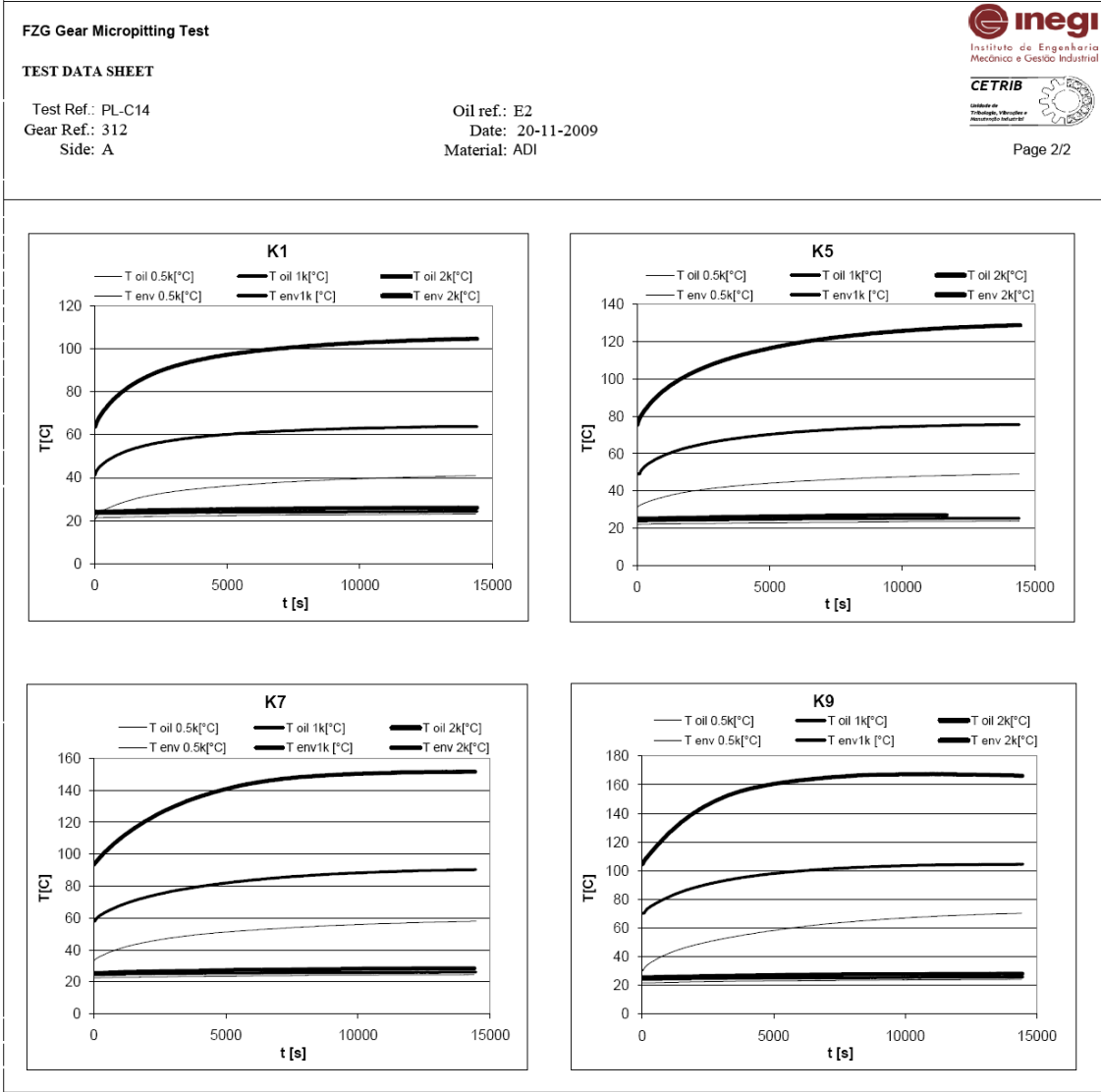
KFZG	Stabilisation temperature [°C]					
	500 rpm		1000 rpm		2000 rpm	
	Oil	Env.	Oil	Env.	Oil	Env.
K1	40.9	23.2	63.8	24.3	104.6	26.1
K5	49.1	23.8	75.6	25.3	128.9	27.3
K7	57.9	24.4	90.3	26.1	151.7	28.5
K9	70.3	24.2	104.5	25.7	166.6	28.1

Mass loss [mg]	
	running in+K6
pinion	63

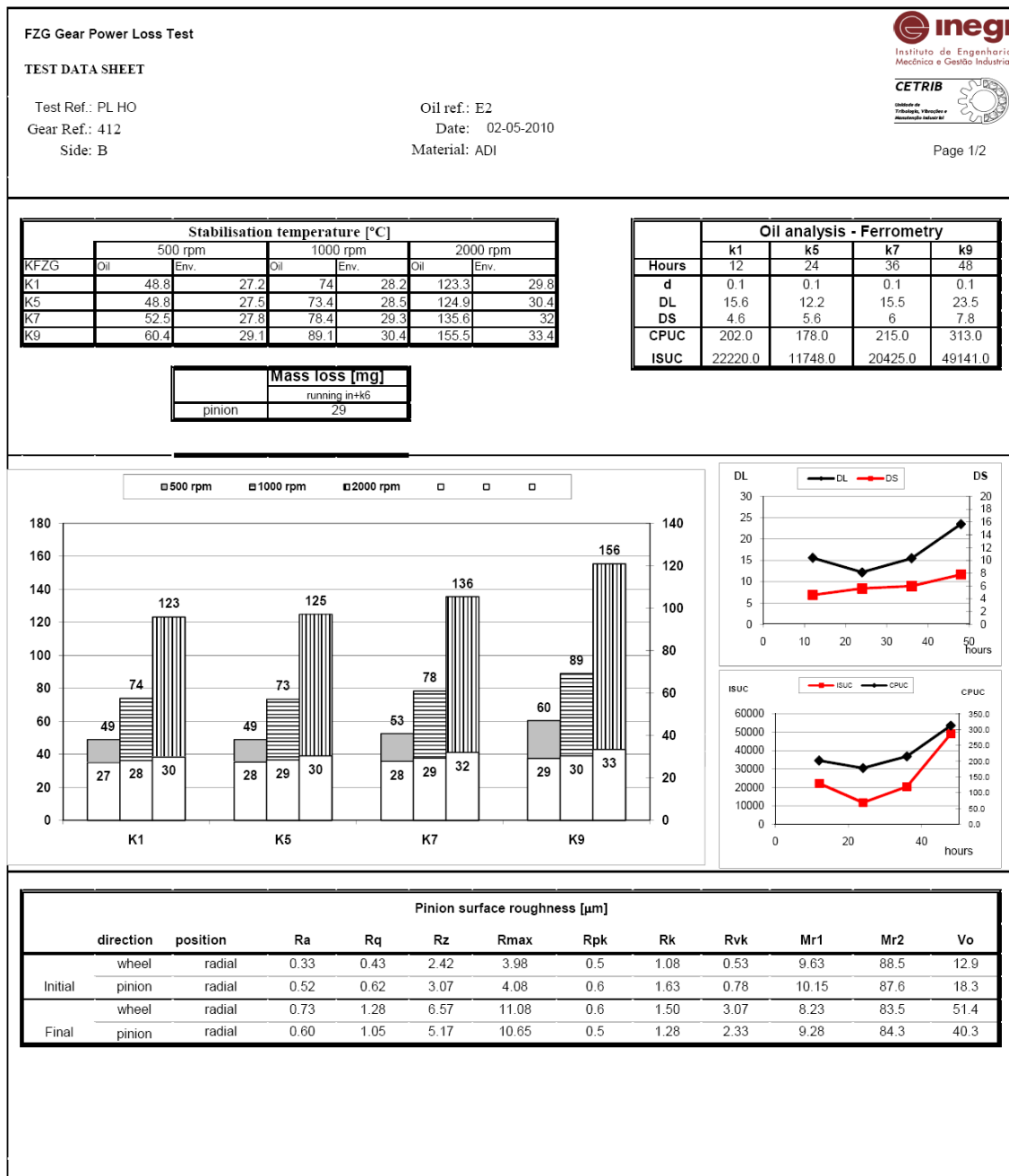
Hours	Oil analysis - Ferrometry			
	k1	k5	k7	k9
d	0.1	0.1	0.1	0.1
DL	8.6	23	28.2	42.8
DS	3.9	8.2	8.8	12.9
CPUC	125.0	312.0	370.0	557.0
ISUC	5875.0	46176.0	71780.0	166543.0
PLP [%]	3.8	4.7	5.2	5.4

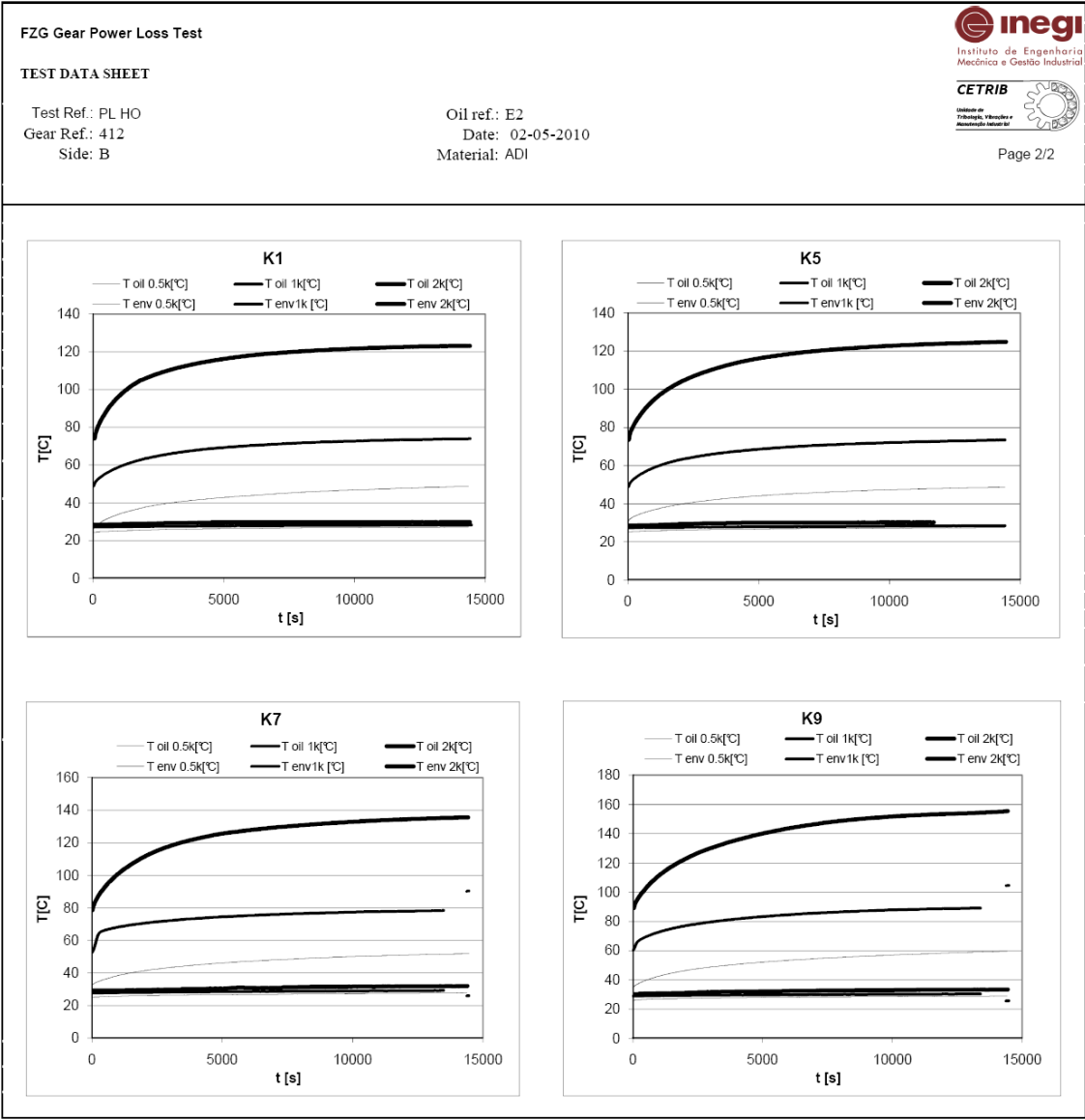


Pinion surface roughness [μm]												
	direction	position	Ra	Rq	Rz	Rmax	Rpk	Rk	Rvk	Mr1	Mr2	Vo
Initial	wheel	radial	0.76	0.96	4.29	5.07	0.7	2.47	1.06	9.22	88.0	26.6
	pinion	radial	0.81	1.01	4.59	5.60	0.7	2.57	1.31	6.83	87.0	29.9
Final	wheel	radial	0.54	0.79	3.19	5.85	0.5	1.37	1.46	8.70	82.2	26.6
	pinion	radial	0.43	0.59	2.97	4.03	0.4	1.21	1.17	8.10	85.3	22.3

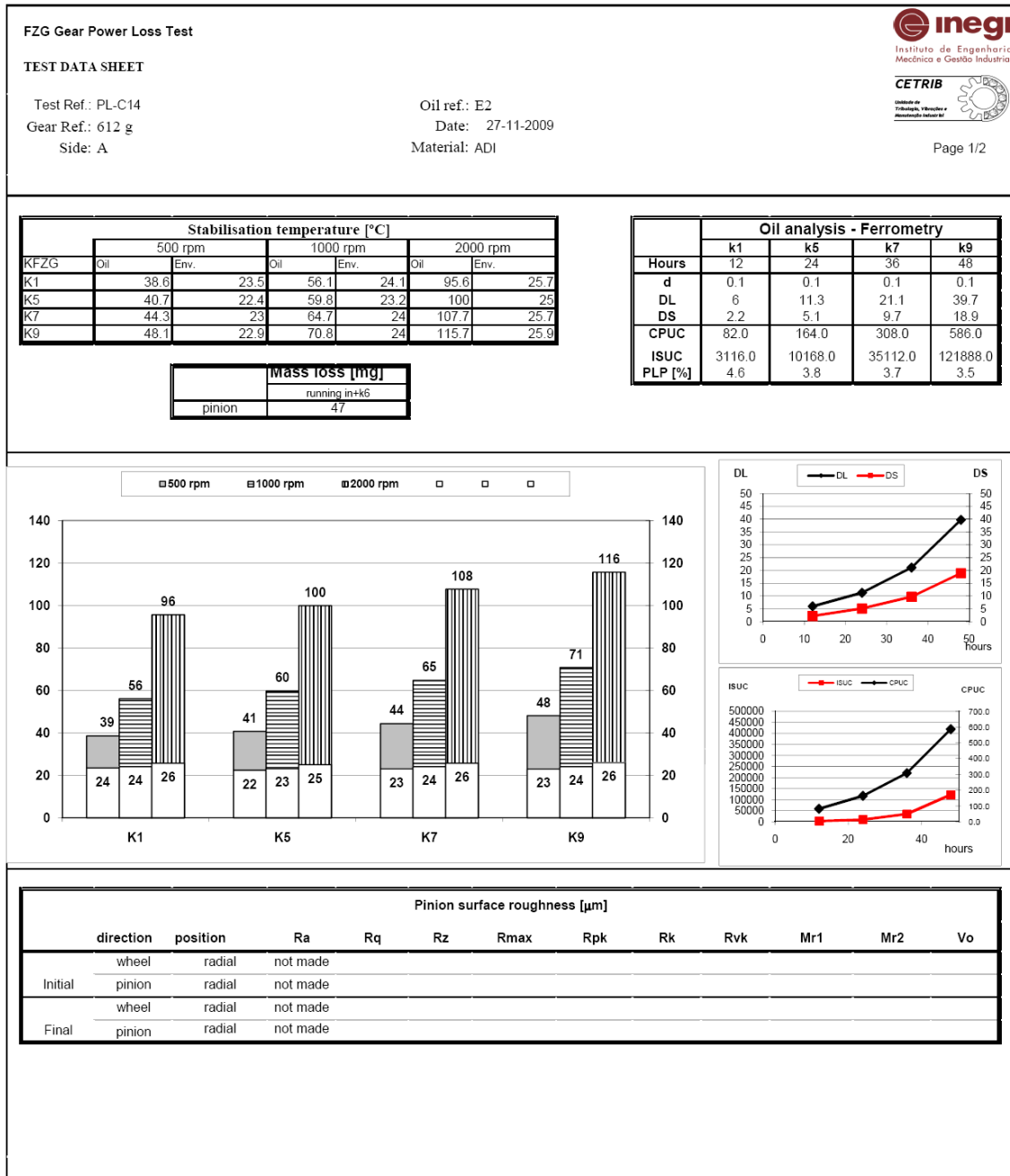


412 Power Loss High Oil – E2





612 Power Loss High Oil – E2



FZG Gear Power Loss Test

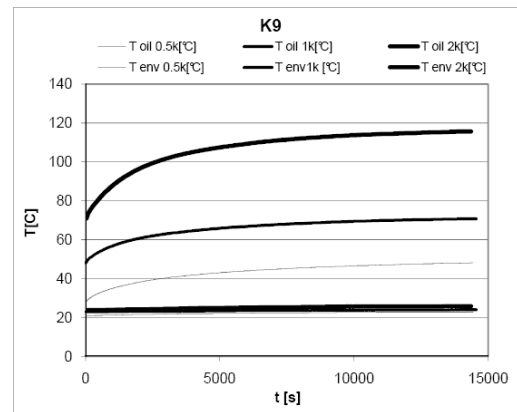
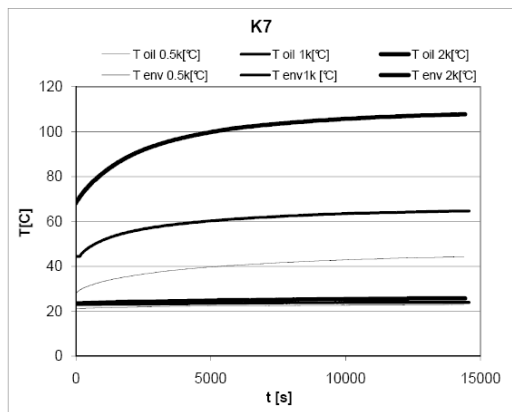
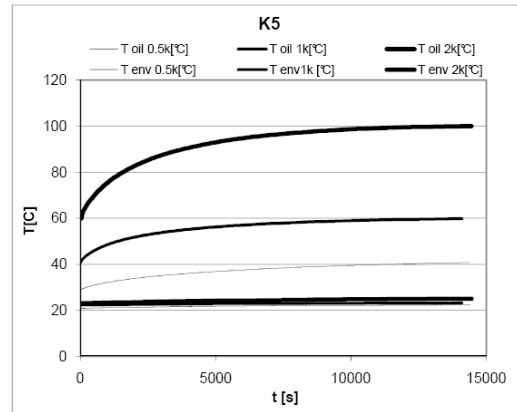
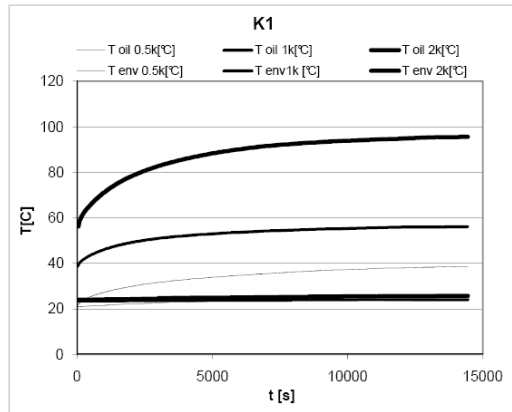
TEST DATA SHEET

Test Ref.: PL-C14
Gear Ref.: 612 g
Side: A

Oil ref.: E2
Date: 27-11-2009
Material: ADI

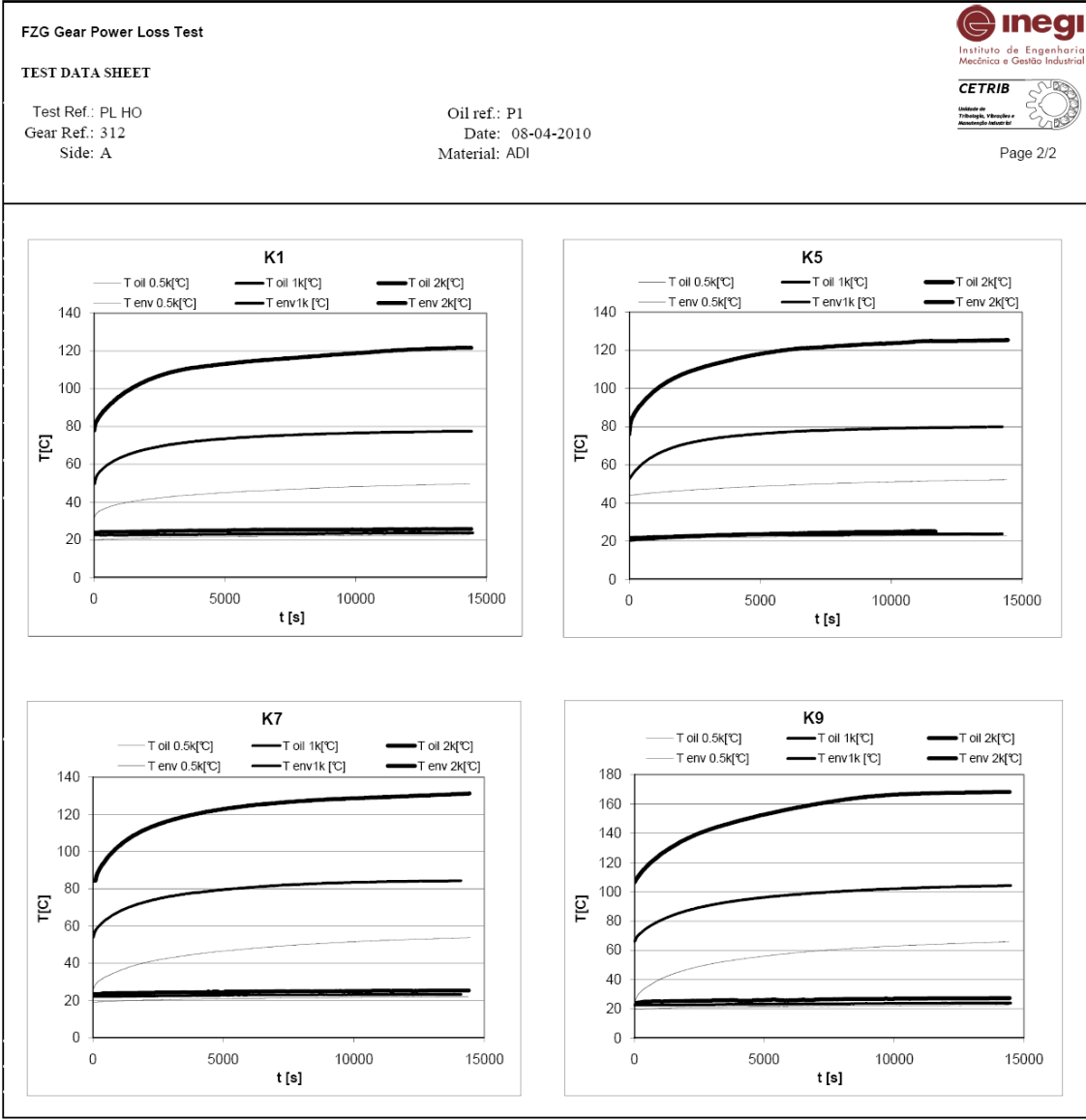


Page 2/2

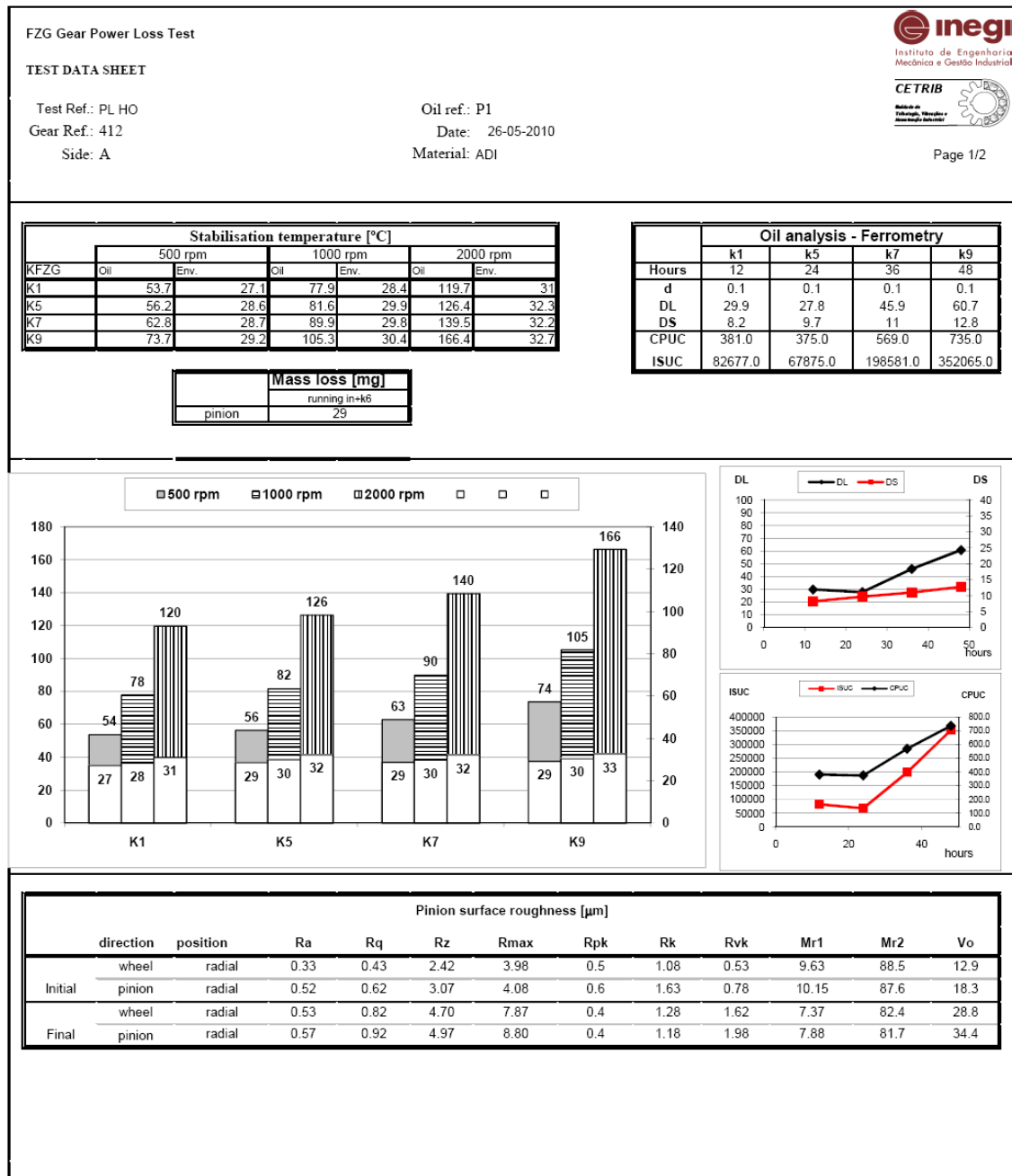


312 Power Loss High Oil – P1

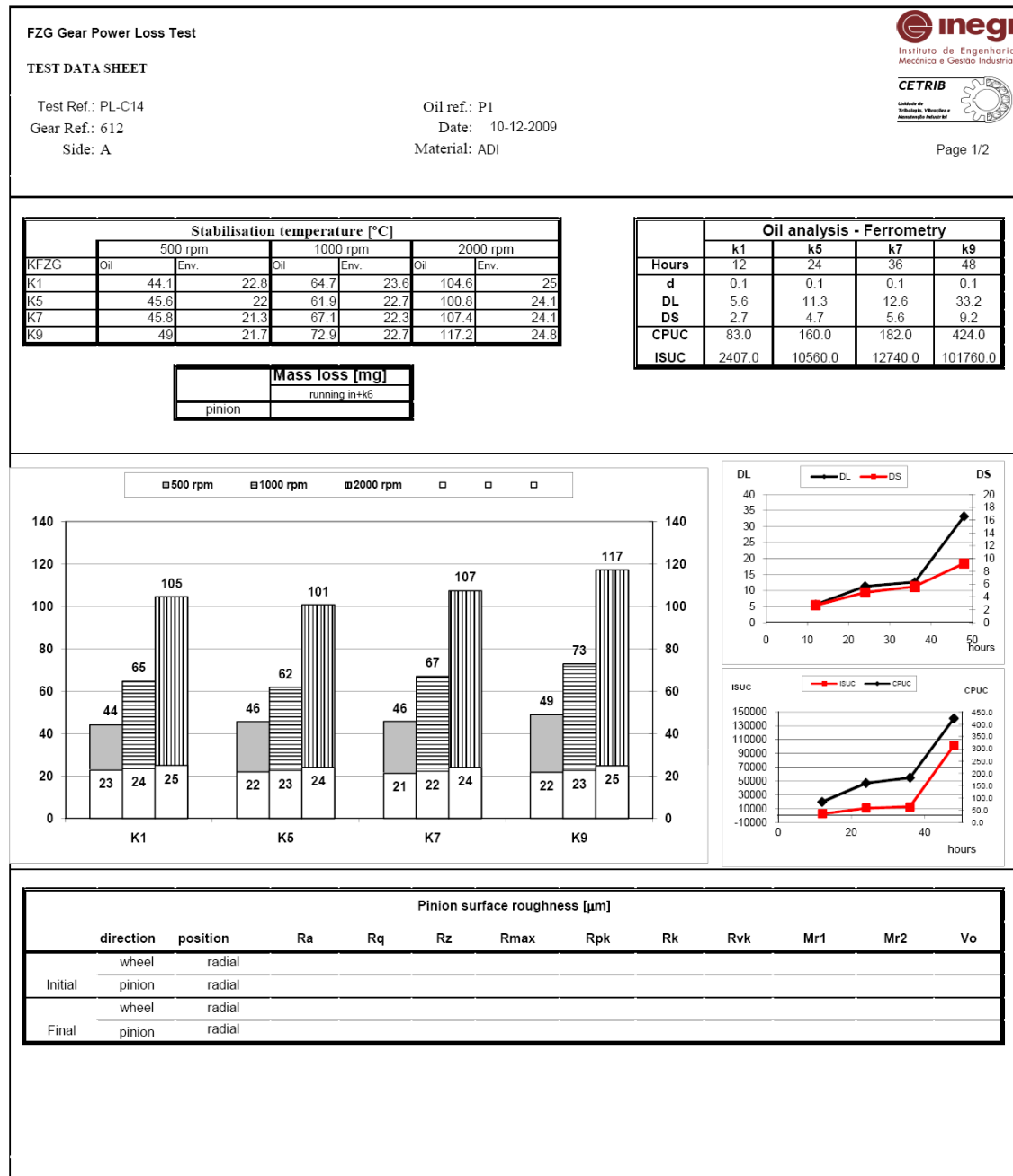




412 Power Loss High Oil – P1



612 Power Loss High Oil – P1



FZG Gear Micropitting Test

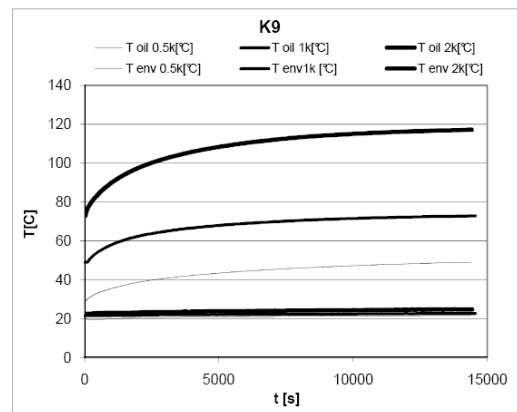
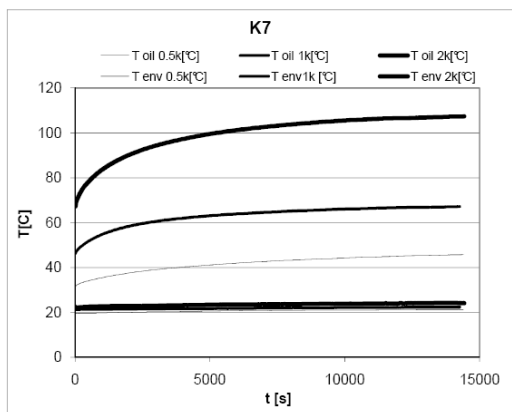
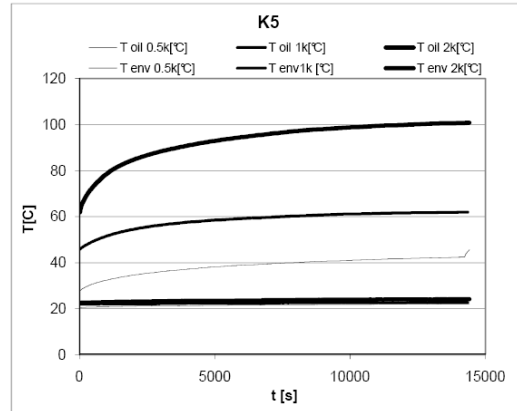
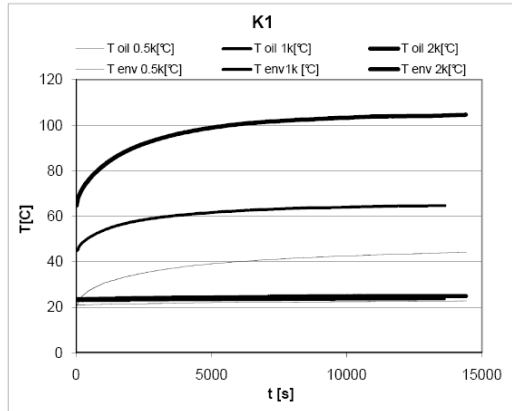
TEST DATA SHEET

Test Ref.: PL-C14
Gear Ref.: 612
Side: A

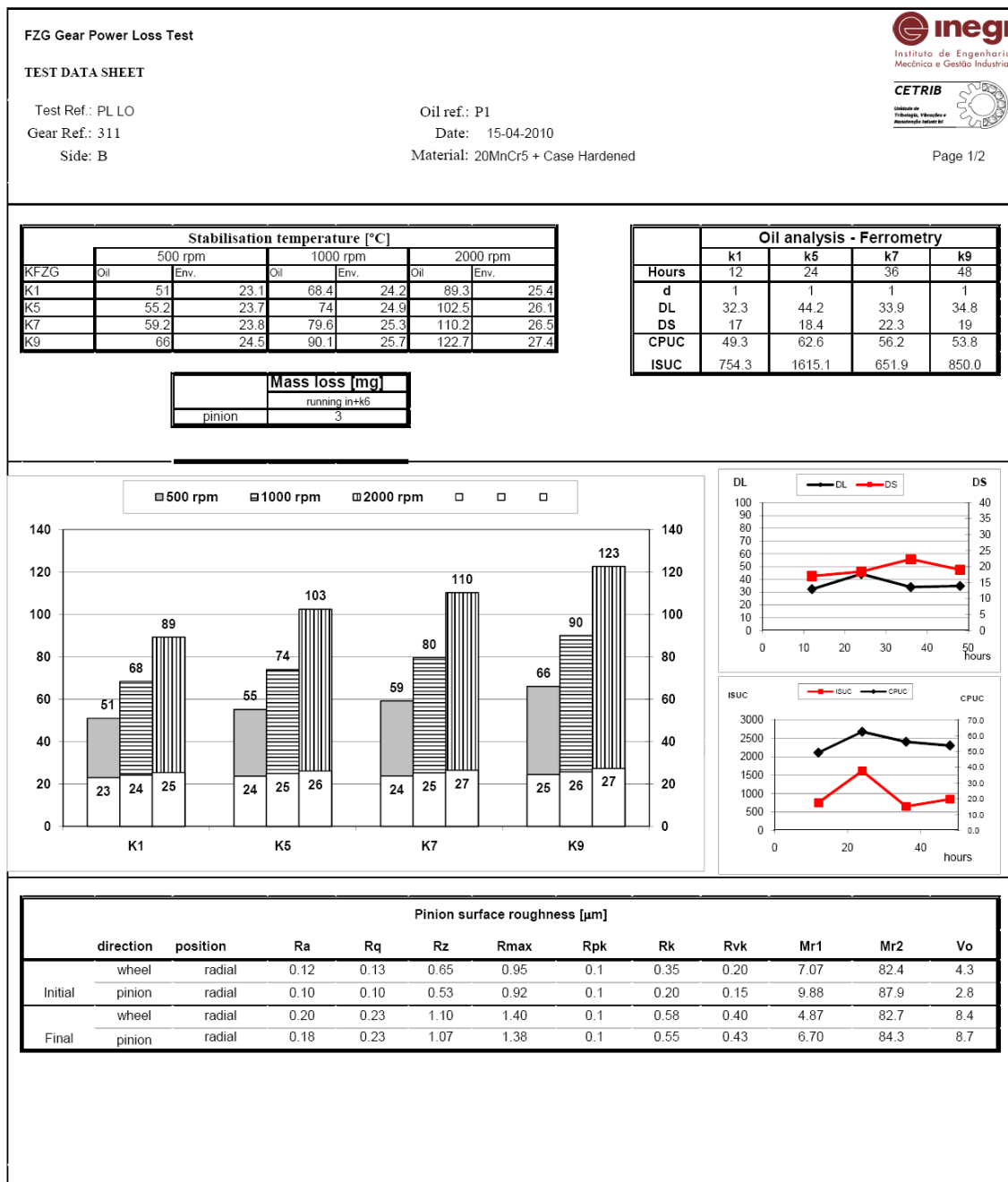
Oil ref.: P1
Date: 10-12-2009
Material: ADI

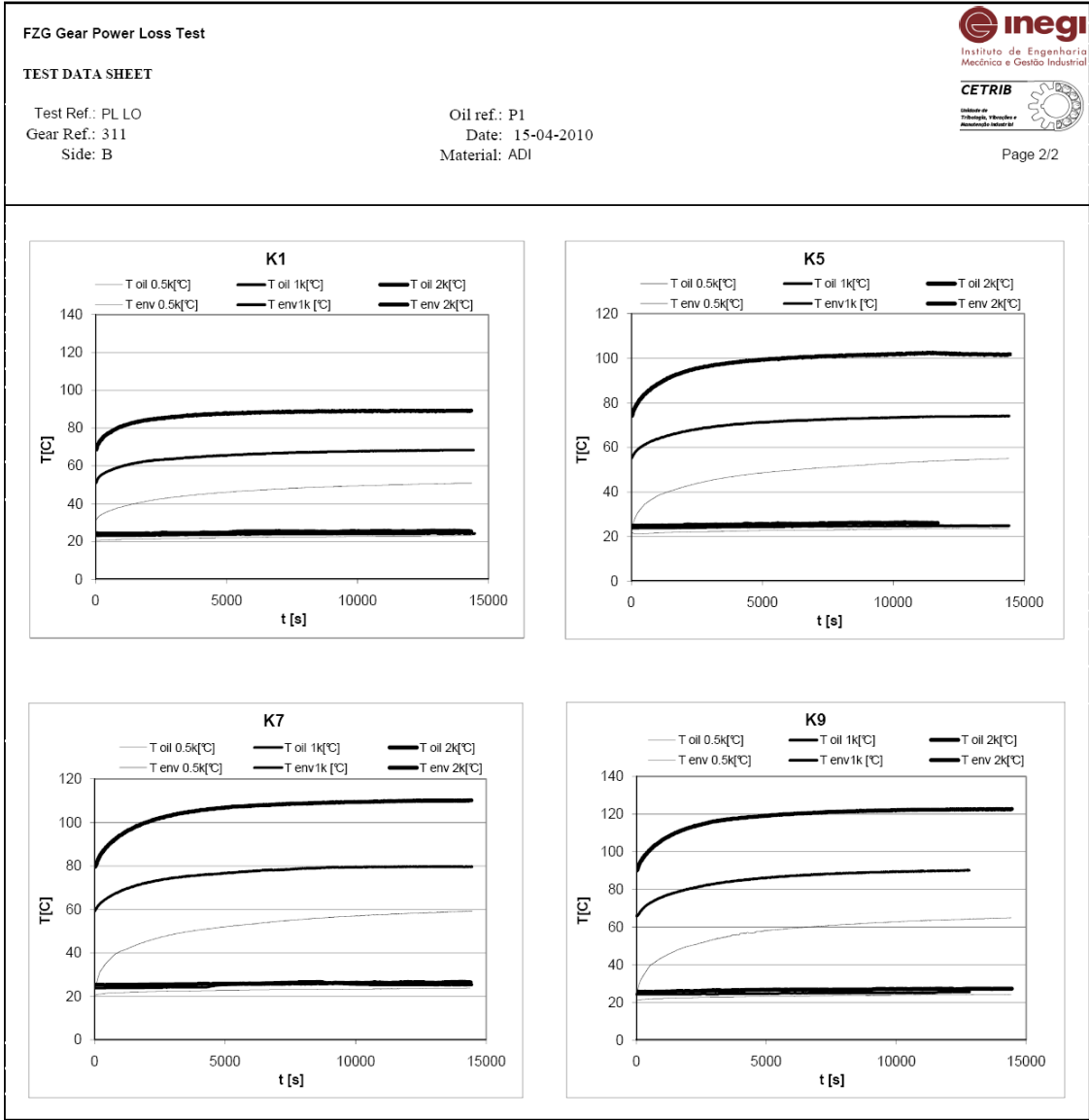


Page 2/2

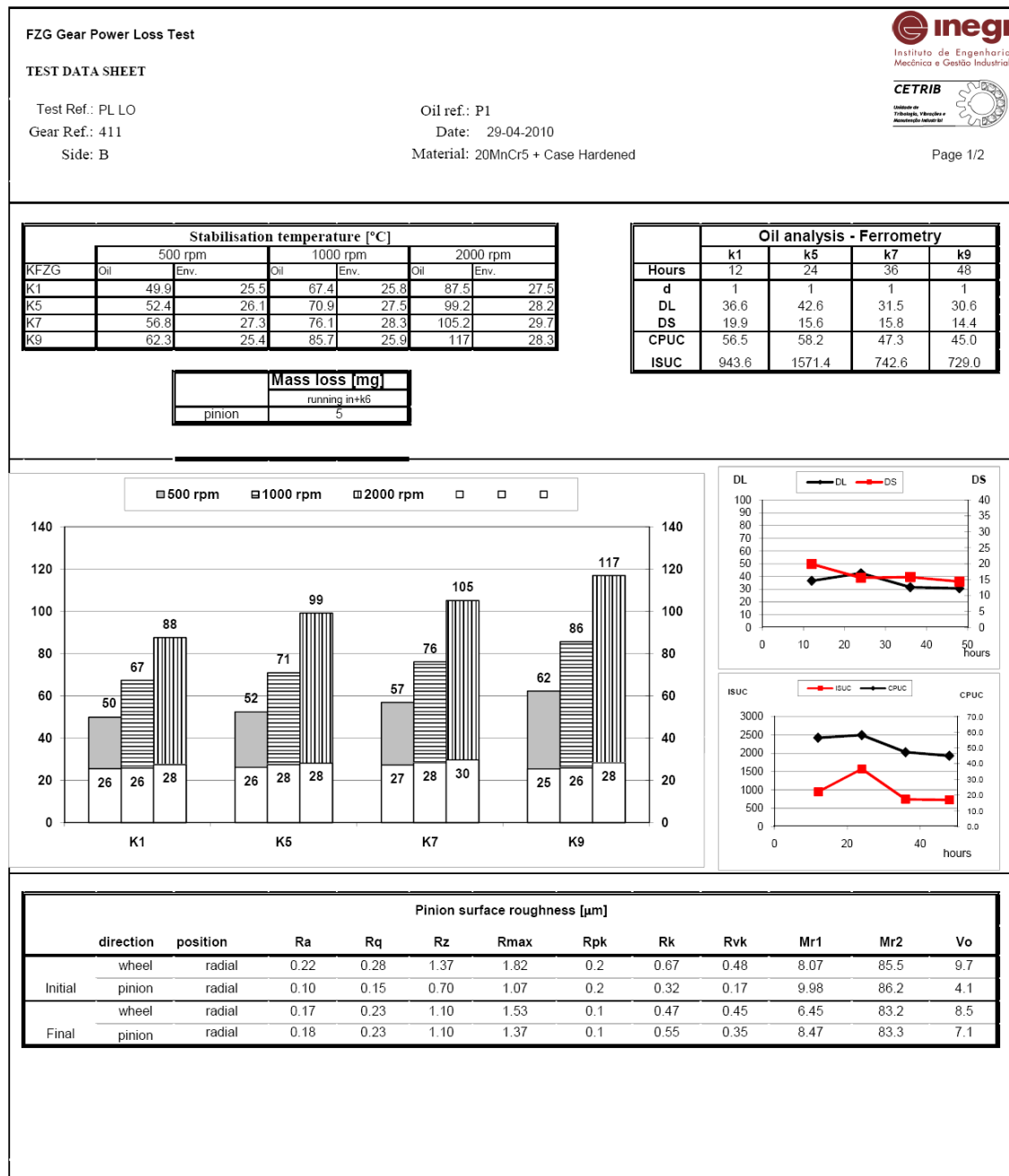


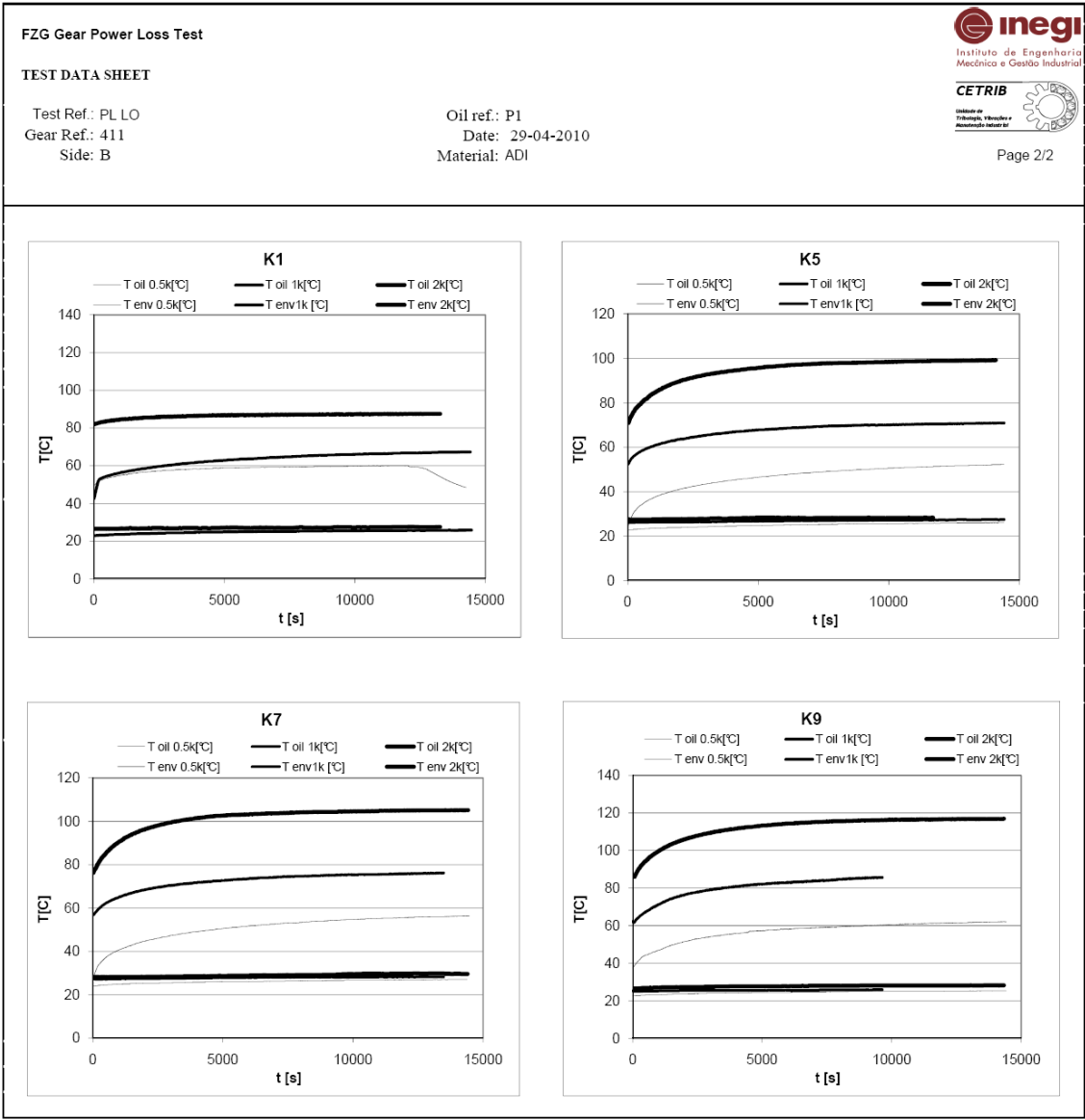
311 Power Loss Low Oil – P1



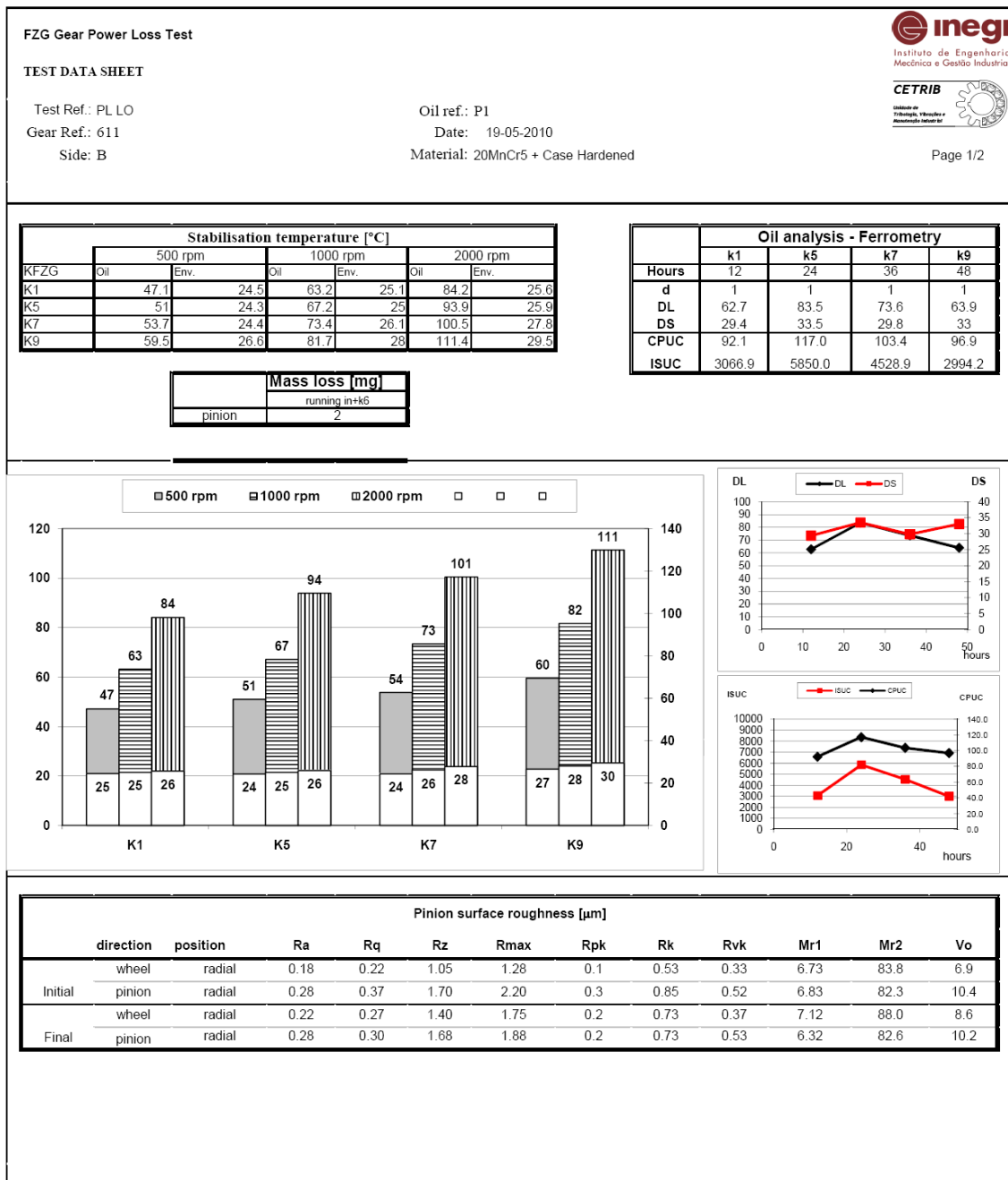


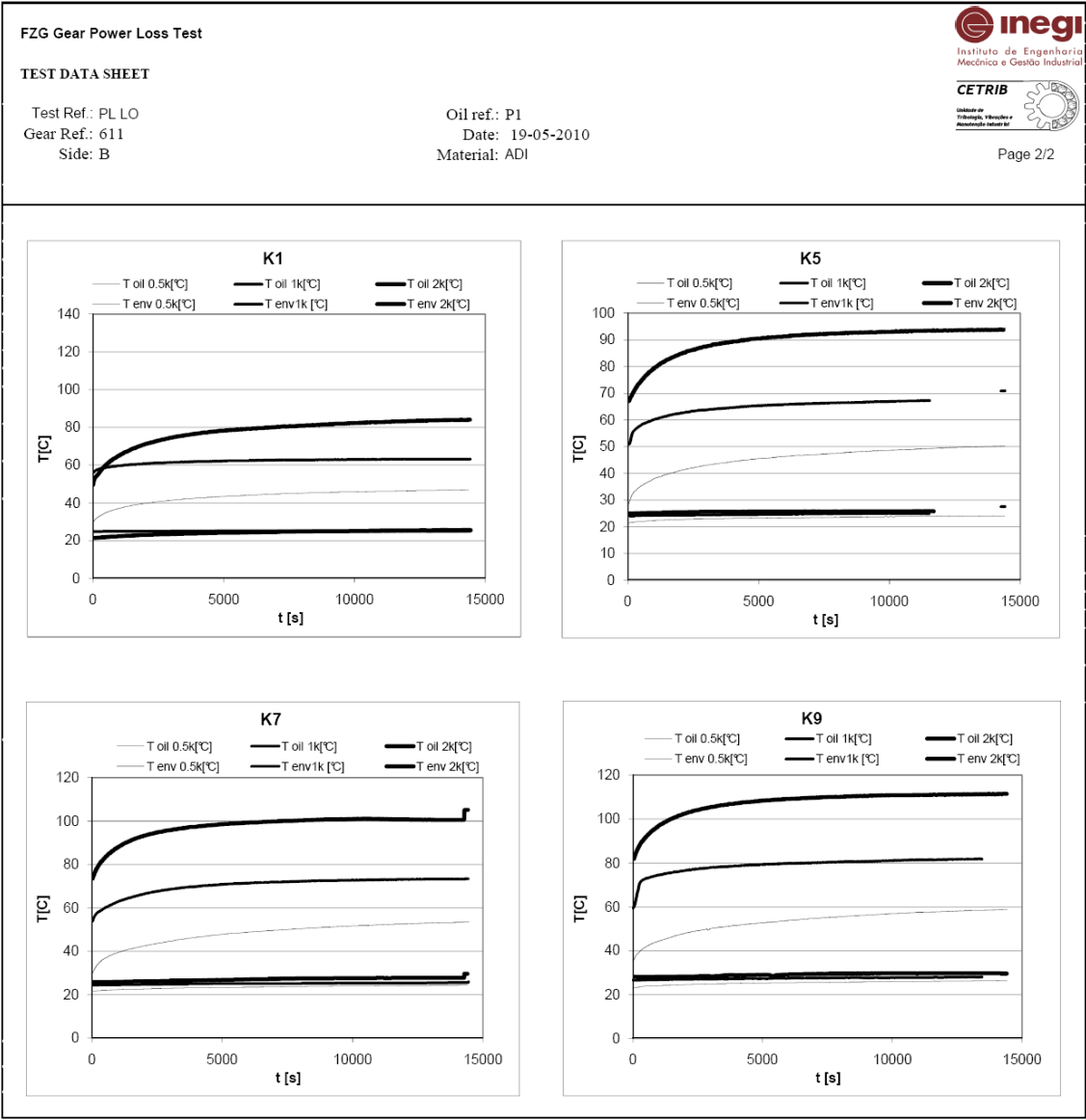
411 Power Loss Low Oil – P1



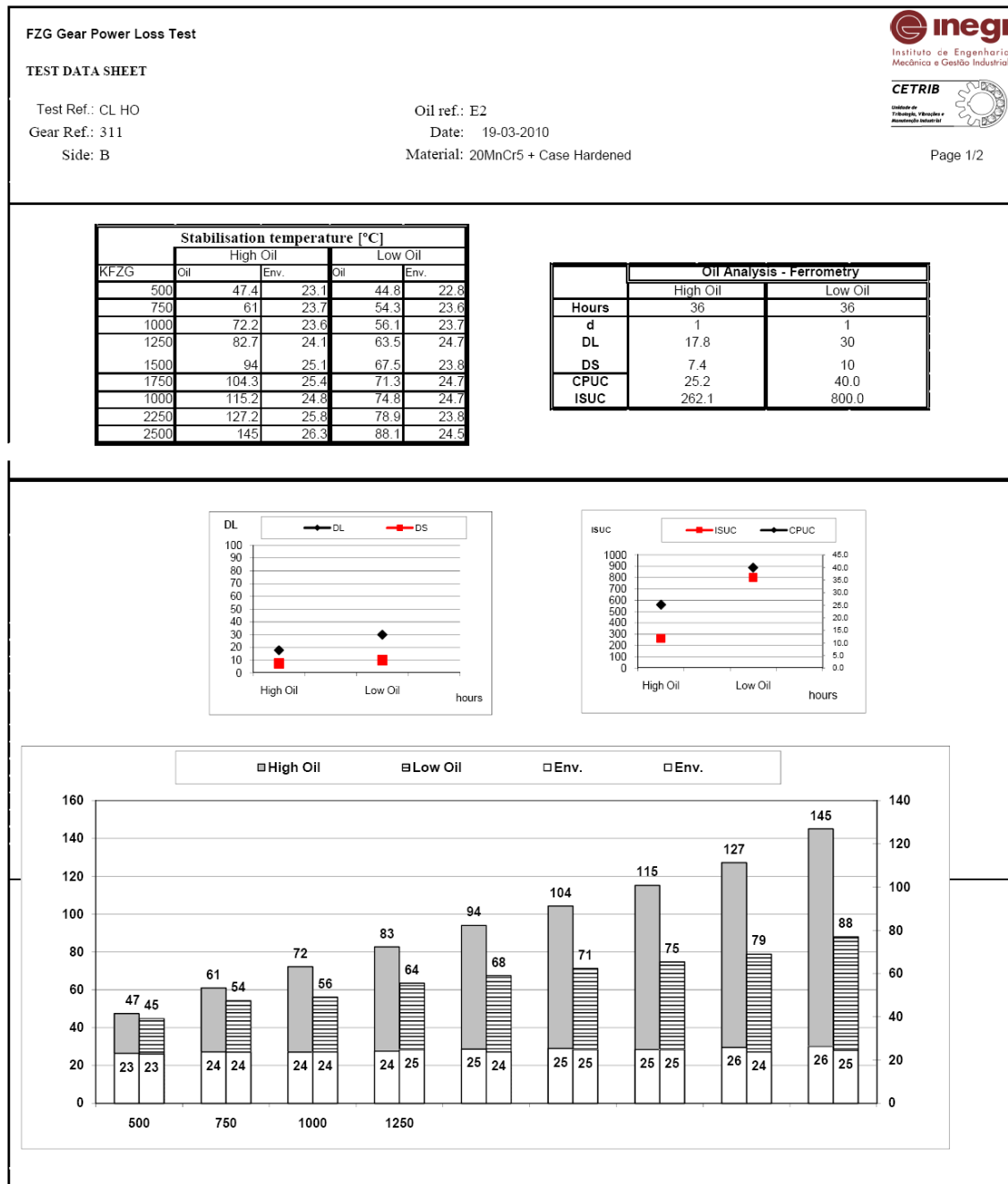


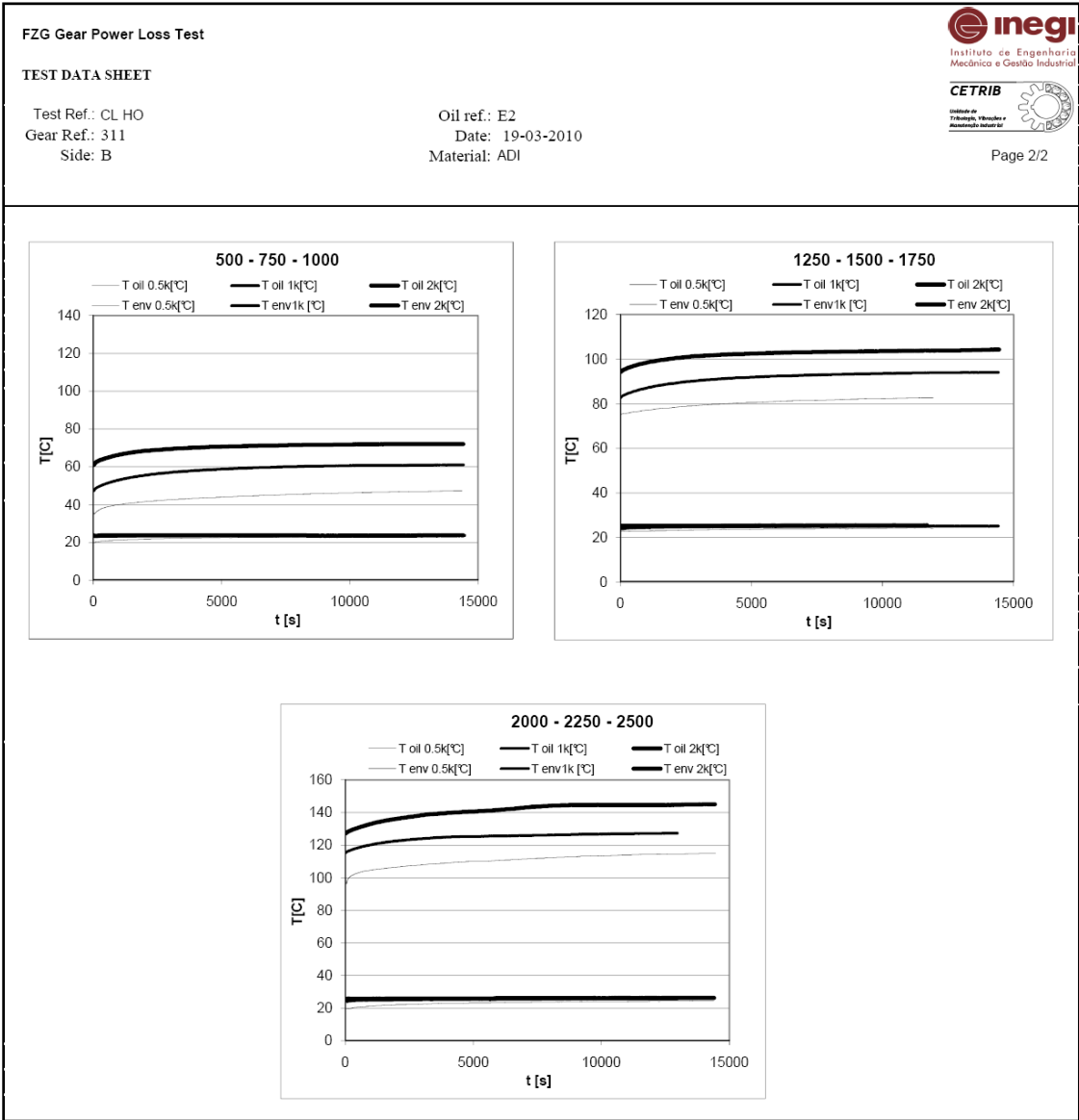
611 Power Loss Low Oil – P1



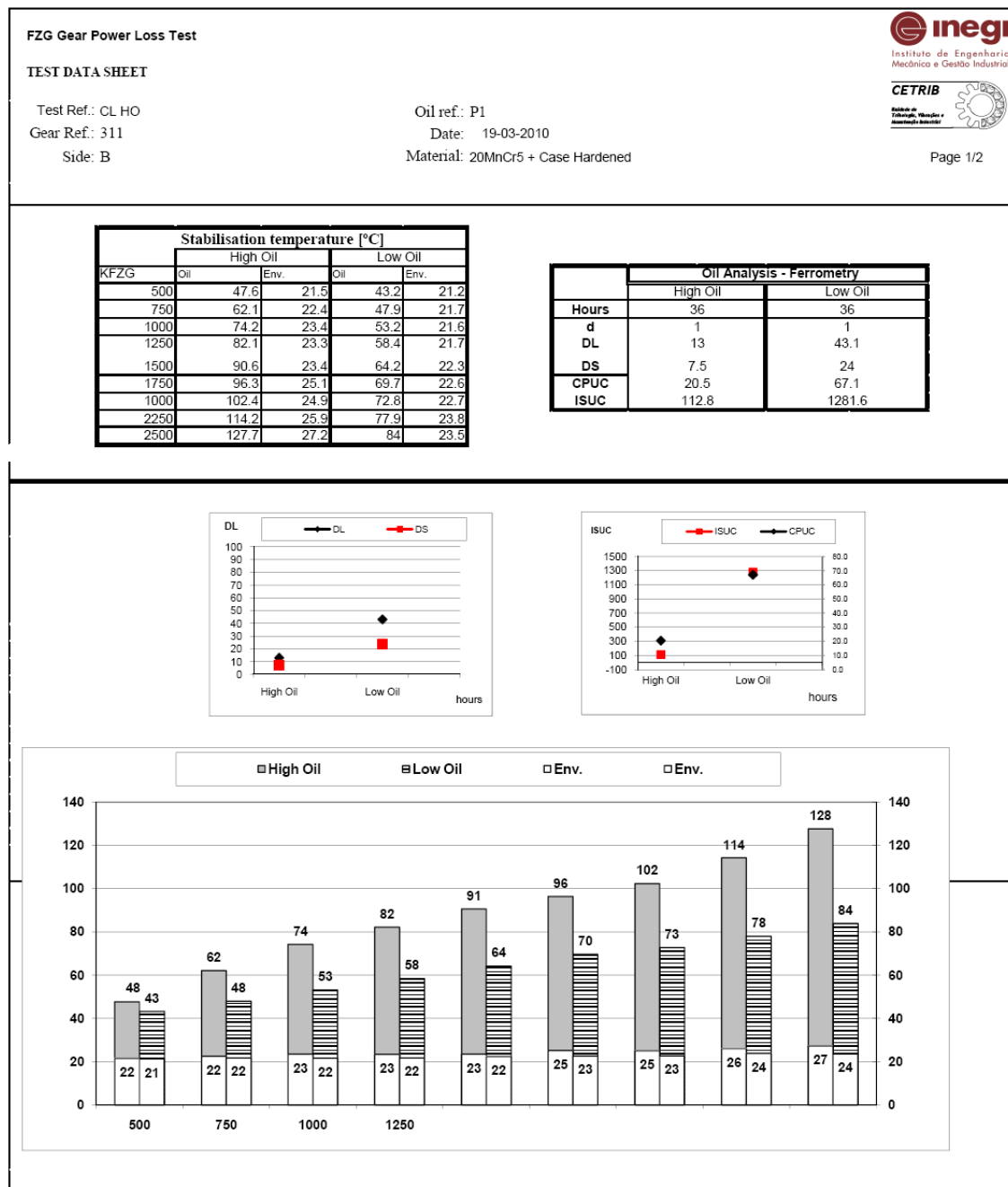


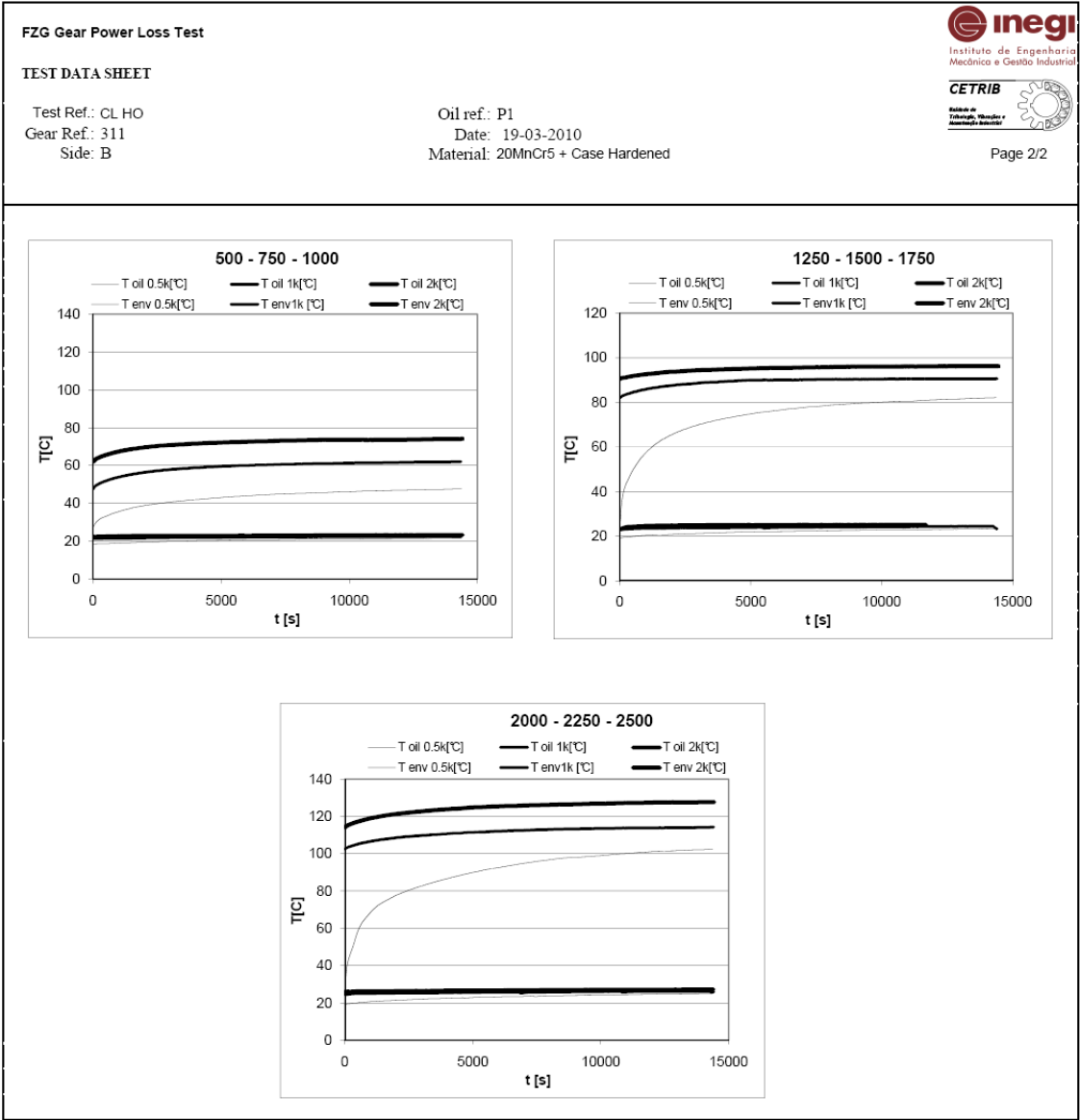
311 Churning Loss high and Low Oil – E2



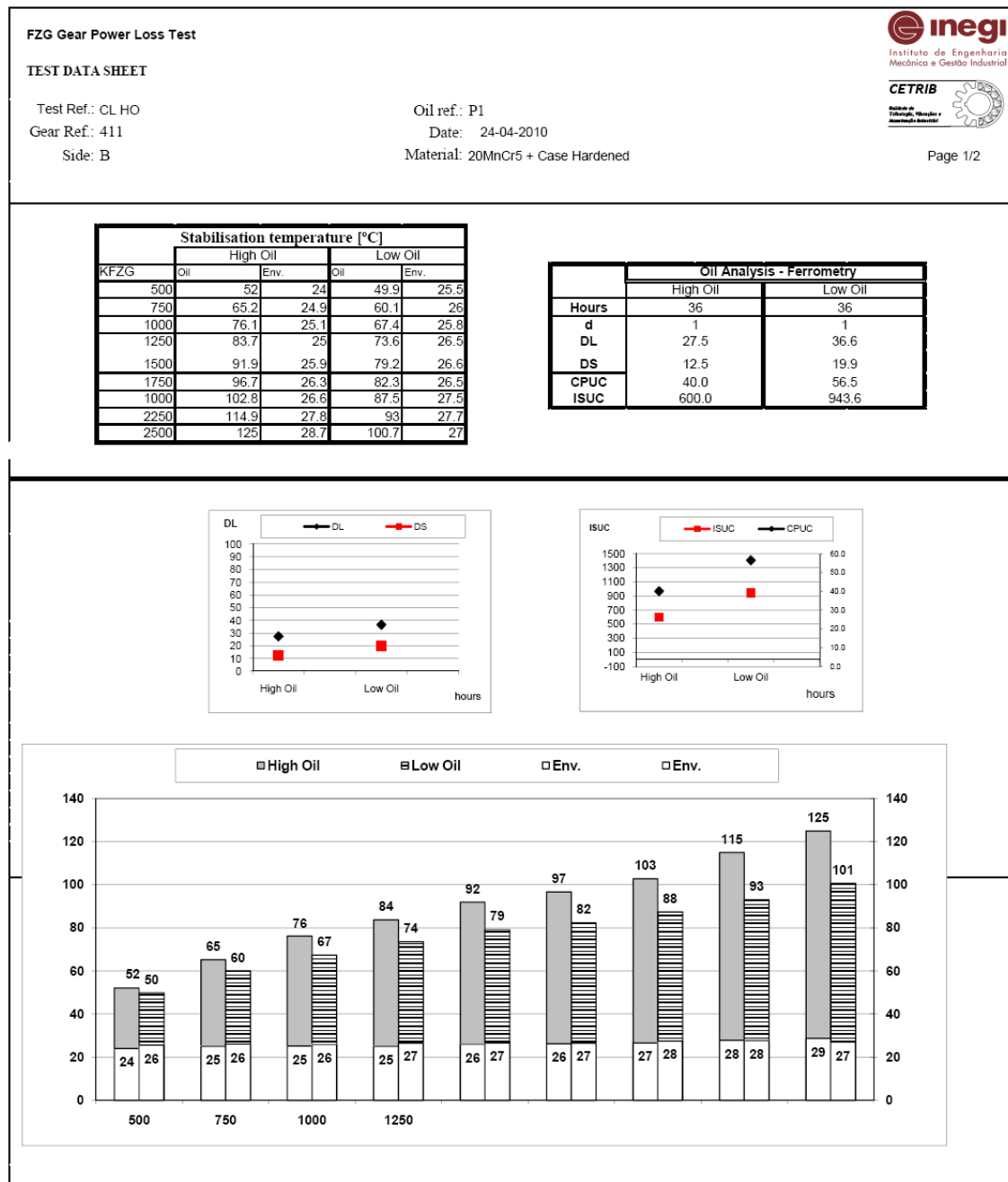


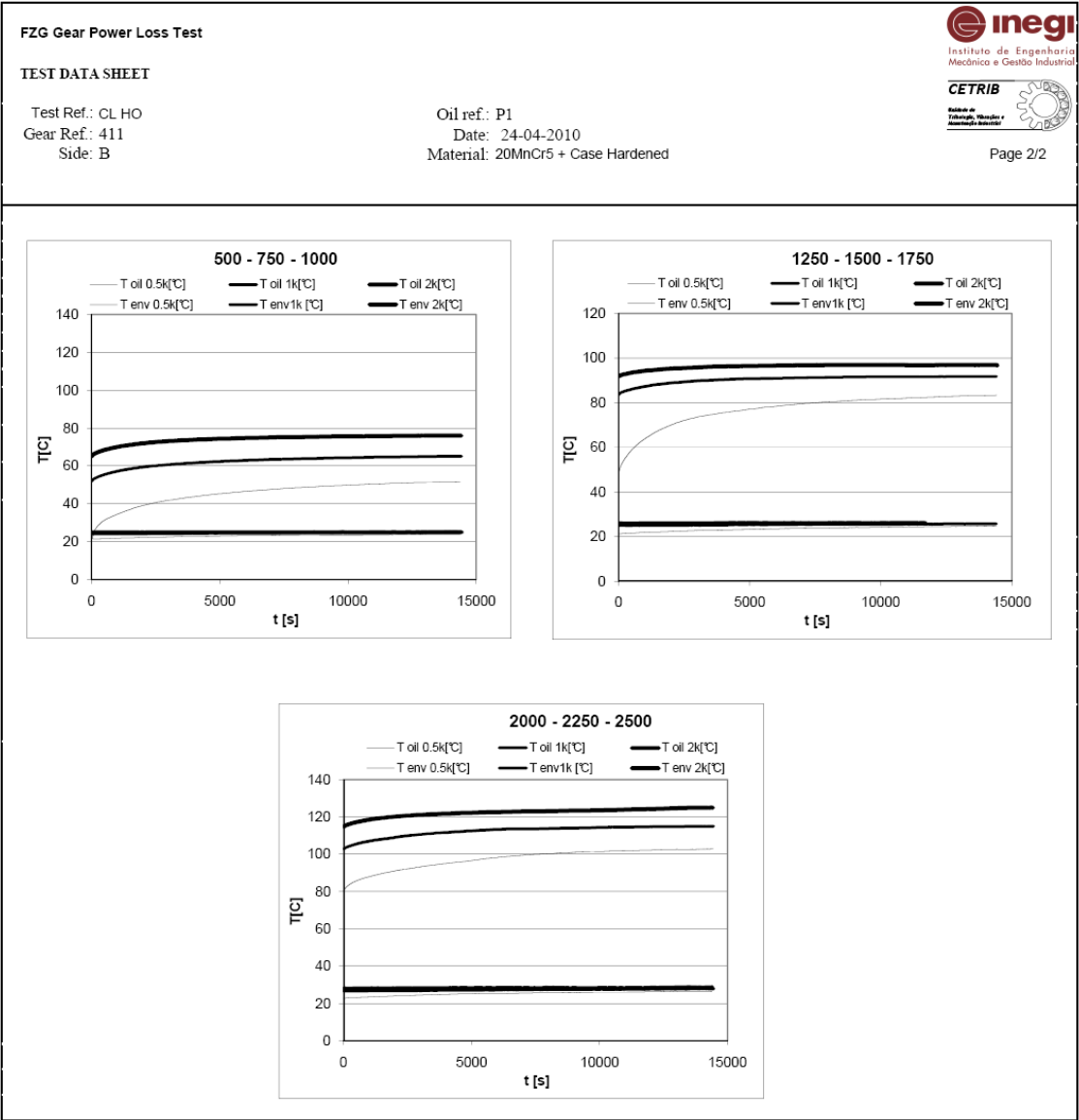
311 Churning Loss high and Low Oil – P1





411 Churning Loss high and Low Oil – P1





611 Churning Loss high and Low Oil – P1

FZG Gear Power Loss Test

TEST DATA SHEET

Test Ref.: CL HO

Oil ref.: P1

Gear Ref.: 611

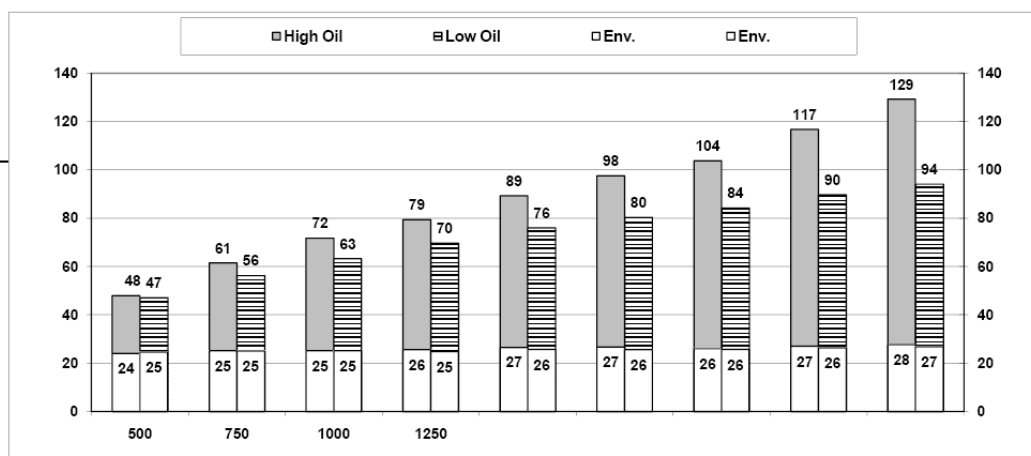
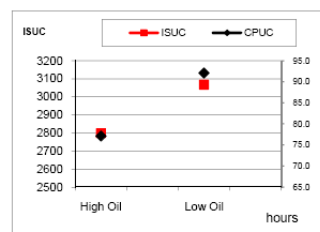
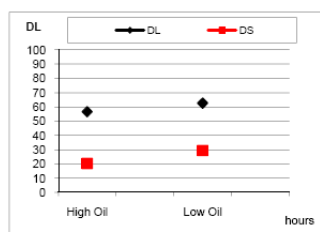
Date: 13-05-2010

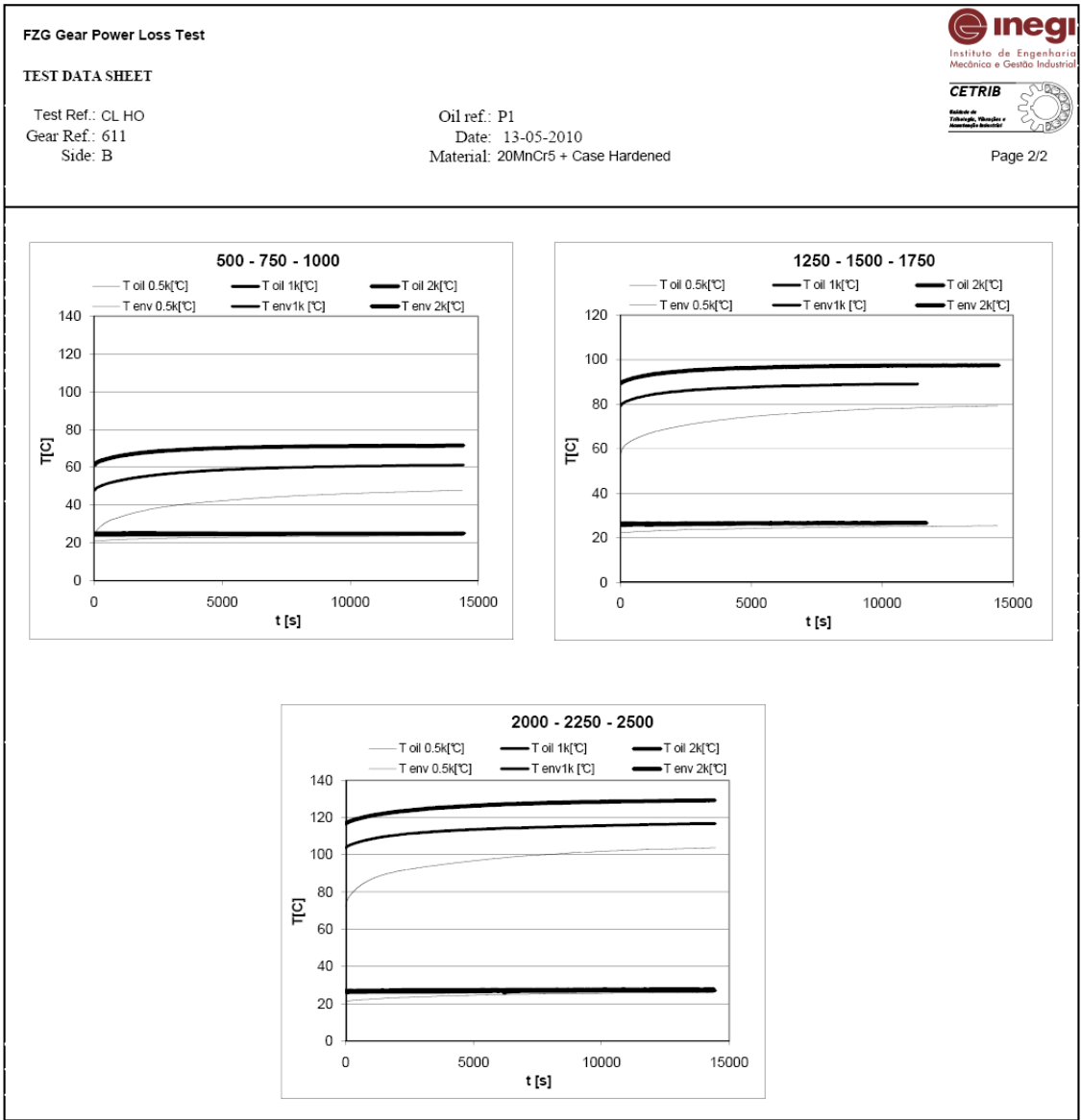
Side: B

Material: 20MnCr5 + Case Hardened

KFZG	Stabilisation temperature [°C]			
	High Oil		Low Oil	
	Oil	Env.	Oil	Env.
500	47.9	24	47.1	24.5
750	61.4	25.1	56.2	24.9
1000	71.7	25.1	63.2	25.1
1250	79.4	25.5	69.6	24.7
1500	89.2	26.5	76	25.6
1750	97.5	26.7	80.4	25.5
2000	103.8	25.9	84.2	25.6
2250	116.7	27	89.7	26.4
2500	129.2	27.7	94.1	26.8

	Oil Analysis - Ferrometry	
	High Oil	Low Oil
	Hours	Hours
d	1	1
DL	56.7	62.7
DS	20.4	29.4
CPUC	77.1	92.1
ISUC	2798.7	3066.9





Appendix B: Stribeck curve with Portuguese nomenclature.

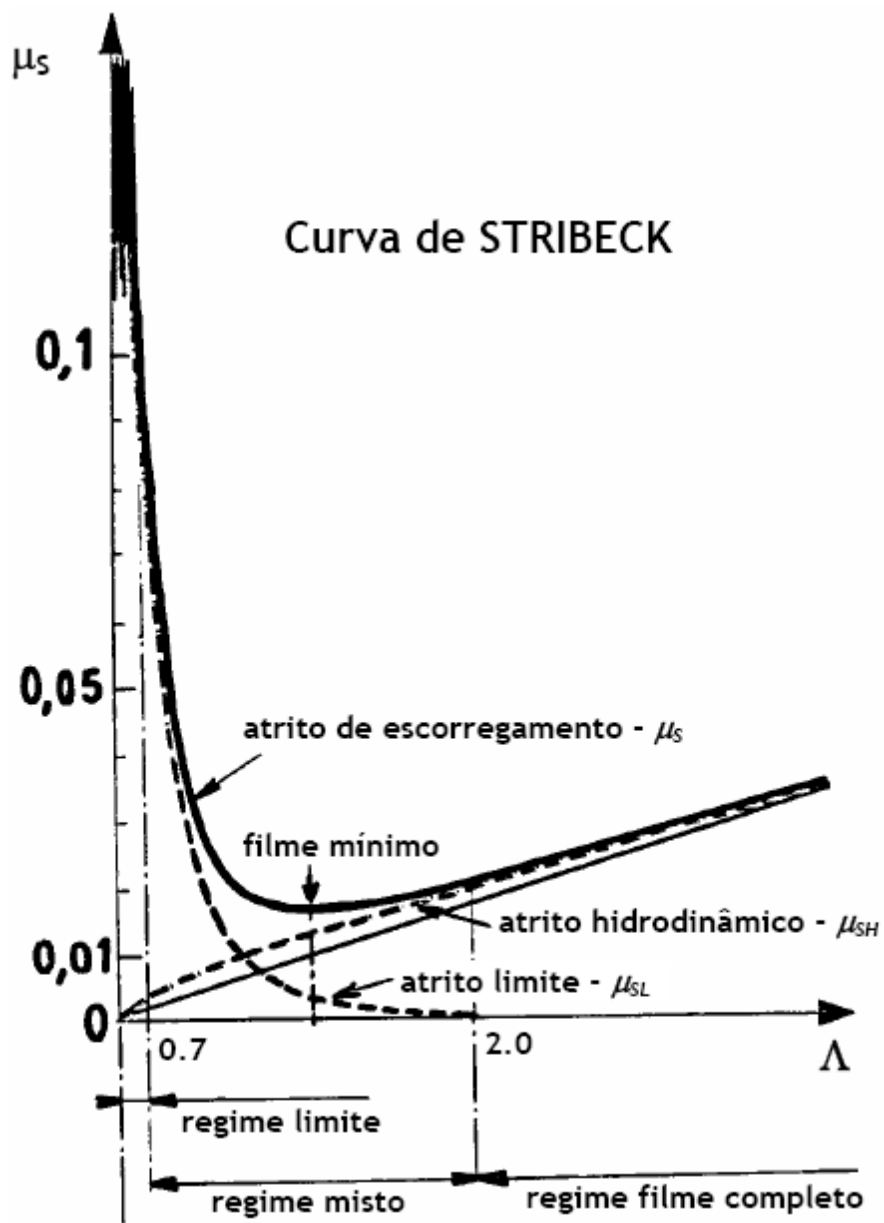


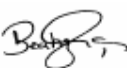

Figure 84 – Stribeck Curve with Portuguese nomenclature[11].

Appendix C: Oil Reports

311 – P1 Churning Loss: High Oil and Low Oil



Relatório de Análise de Lubrificantes

Análise n°:	09-10 / 10
Tipo de análise:	Ferrometria e Ferrografia Analítica
Confidencialidade:	1
Cliente:	INEGI - Cetrib
Morada:	Porto
Telefone / Fax:	
Equipamento:	FZG (20MnCr5 – 311)
Lubrificante:	P1
Dossier:	/
N° de páginas:	5
Data:	15/03/2010
Responsável:	Beatriz Graça – Jorge Seabra
Rúbrica:	 

Os resultados apresentados referem-se exclusivamente às amostras ensaiadas.
Este documento não pode ser reproduzido, total ou parcialmente, sem a autorização por escrito do INEGI.

Pág. 1 / 5
Relatório N° 10/10
MOD LAL-REL01



CETRIB - Laboratório
de Análise de Lubrificantes

OBJECTIVO

Análise de duas amostras de óleos lubrificantes – P1, resultantes de ensaios na Máquina FZG com engrenagens de aço (20MnCr5), para avaliação do desgaste presente.

As amostras analisadas foram as seguintes:

Amostra Nº	Ciclos	Análises efectuadas	
		Ferrometria	Ferrografia Analítica
Low Loss	-	X	X
Low Oil	-	X	X

RESULTADOS DAS ANÁLISES

Nas páginas seguintes são apresentados os resultados referentes às análises de Ferrometria (DR III) e Ferrografia Analítica (FM III).

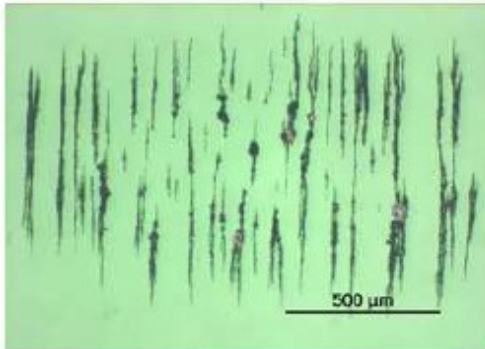
Os resultados apresentados referem-se exclusivamente às amostras ensaiadas.
Este documento não pode ser reproduzido, total ou parcialmente, sem a autorização por escrito do INEGI.

Pág. 2 / 5
Relatório Nº 10/10
MOD LAL-REL01

CLIENTE: **INEGI**
MORADA: Porto
DATA: 15/03/10

MÁQUINA: Máquina de Ensaios FZG
Ref. ÓLEO: PI LOW LOSS
ENSAIOS FZG - 20MnCr5 Gears 311 - K1

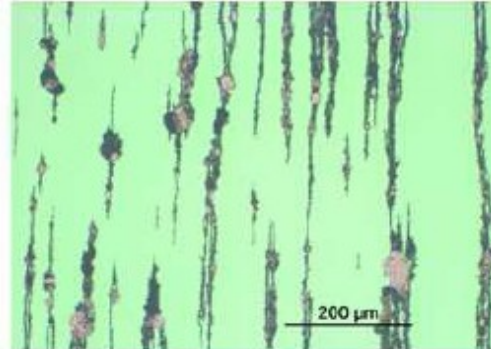
Fotografia 1



Ampliação: x 100 Diluição: 1
Localização: Núcleo Luz: Branca / Verde

Observações: Presença de partículas ferrosas de pequenas dimensões e algumas de grandes dimensões.

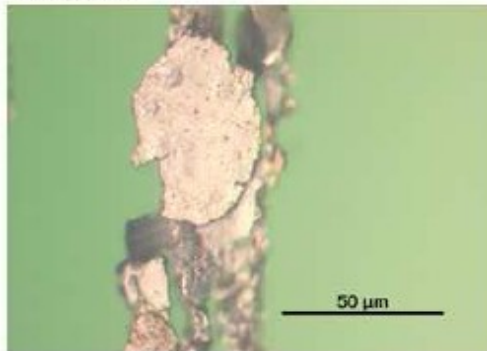
Fotografia 2



Ampliação: x 200 Diluição: 1
Localização: Núcleo Luz: Branca / Verde

Observações: Ampliação da Fotografia 1. Presença de algumas partículas ferrosas de grandes dimensões.

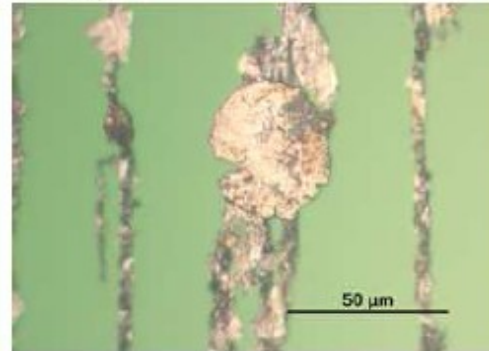
Fotografia 3



Ampliação: x 1000 Diluição: 1
Localização: Núcleo Luz: Branca / Verde

Observações: Ampliação da Fotografia 2. Partícula ferrosa laminar de forma arredondada, típica de fadiga e de grandes dimensões.

Fotografia 4



Ampliação: x 1000 Diluição: 1
Localização: Núcleo Luz: Branca / Verde

Observações: Ampliação da Fotografia 2. Partícula ferrosa laminar de forma arredondada, típica de fadiga e de grandes dimensões.

Os resultados apresentados referem-se exclusivamente às amostras ensaladas.
Este documento não pode ser reproduzido, total ou parcialmente, sem a autorização por escrito do INEGI.

Pág. 4 / 5
Relatório Nº 10/10
MOD LAL-REL01

CLIENTE: **INEGI**

MORADA: Porto

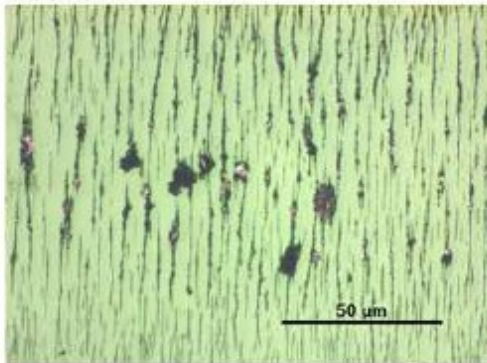
DATA: 15/03/10

MÁQUINA: Máquina de Ensaios FZG

Ref. ÓLEO: P1 LOW OIL

ENSAIOS FZG - 20MnCr5 Gears 311 - K1

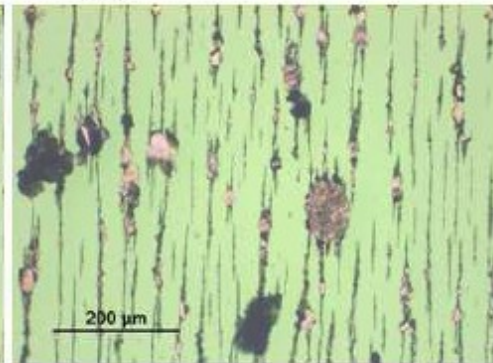
Fotografia 5



Ampliação: x 100 Diluição: 1
Localização: Núcleo Luz Branca / Verde

Observações: Presença significativa de partículas ferrosas de pequenas e grandes dimensões.

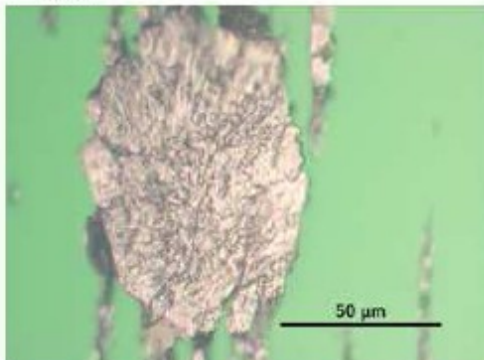
Fotografia 6



Ampliação: x 200 Diluição: 1
Localização: Núcleo Luz Branca / Verde

Observações: Ampliação da Fotografia 5.
Presença significativa de partículas ferrosas de pequenas e grandes dimensões.

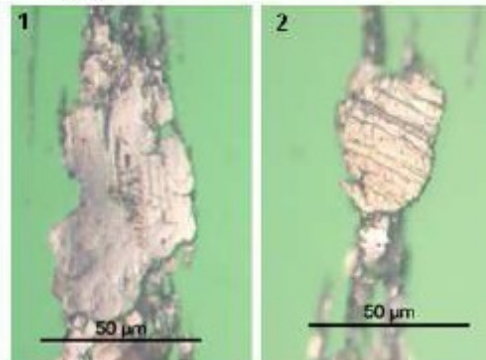
Fotografia 7



Ampliação: x 1000 Diluição: 1
Localização: Núcleo Luz Branca / Verde

Observações: Ampliação da Fotografia 6.
Partícula ferrosa de desgaste de fadiga com grandes dimensões.

Fotografia 8





Ampliação: x 1000 Diluição: 1
Localização: Núcleo Luz Branca / Verde

Observações: Ampliação da Fotografia 6.
1 - Partícula ferrosa de desgaste de fadiga;
2 - Partícula ferrosa de desgaste combinado.

311 – E2 Churning Loss: High Oil and Low Oil



Relatório de Análise de Lubrificantes

Análise nº:	13 -14 / 10
Tipo de análise:	Ferrometria e Ferrografia Analítica
Confidencialidade:	1
Cliente:	INEGI - Cetrib
Morada:	Porto
Telefone / Fax:	
Equipamento:	FZG (20MnCr5 – 311)
Lubrificante:	EIGO 2
Dossier:	/
Nº de páginas:	5
Data:	23/03/10
Responsável:	Beatriz Graça – Jorge Seabra
Rúbrica:	 

Os resultados apresentados referem-se exclusivamente às amostras ensaiadas.
Este documento não pode ser reproduzido, total ou parcialmente, sem a autorização por escrito do INEGI.

Pág. 1 / 5
Relatório Nº 14/10
MOD LAL-REL01



OBJECTIVO

Análise de duas amostras de óleo lubrificante EIGO 2 resultantes de ensaios na Máquina FZG com engrenagens de aço (20MnCr5), para avaliação do desgaste presente.

As amostras analisadas foram as seguintes:

Amostra Nº	Ciclos	Análises efectuadas	
		Ferrometria	Ferrografia Analítica
Low Loss	-	X	X
Low Oil	-	X	X

RESULTADOS DAS ANÁLISES

Nas páginas seguintes são apresentados os resultados referentes às análises de Ferrometria (DR III) e Ferrografia Analítica (FM III).

Os resultados apresentados referem-se exclusivamente às amostras ensaladas.

Este documento não pode ser reproduzido, total ou parcialmente, sem a autorização por escrito do INEGI.

Pág. 2 / 5

Relatório Nº 14/10

MOD LAL-REL01



CETRIB - Laboratório
de Análise de Lubrificantes

CLIENTE: INEGI		MÁQUINA: Máquina de Ensaios FZG					
MORADA: Porto		Ref. ÓLEO: EIGO 2					
DATA: 23/03/10		ENSAIOS FZG - 20MnCr5 Gears 311 - K1					
IDENTIFICAÇÃO							
Amostra nº:	Low Loss	Low Oil					
Data amostra:	Mar-10	Mar-10					
Análise nº:	13/10	14/10					
Ciclos/Máquina:	-	-					
Ciclos/Óleo:	-	-					
FERROMETRIA							
d:	1	1					
DL:	3,2	7,6					
DS:	1,2	6,1					
CPUC:	9,4	13,7					
ISUC:	65,8	20,6					
FERROGRAFIA							
Desgaste normal							
Desgaste severo							
Desgaste abrasão							
Desgaste combinado							
Desgaste fadiga							
Esferas Metálicas							
Ligas não ferrosas							
Óxidos de ferro							
Minerais/Orgânicos							
OIL VIEW							
Índice OilLife:							
Índice Oxidação:							
Índice Contaminação:							
Índice Ferromagnético:							
Grandes Contaminantes:							
Constante Dielétrica:							
FILTRAGEM							
(Nº Partículas/10 ml)							
5 - 15 µm							
15 - 25 µm							
25 - 50 µm							
50 - 100 µm							
> 100 µm							
VISCOSIDADE							
(cSt a 40°C):							
ACIDEZ (TAN)							
(mg KOH)							
P. INFLAMAÇÃO							
(°C)							
DIAGNOSTICO:							
LEGENDA							
DL - Índice de partículas grandes							Não existe
DS - Índice de partículas pequenas							Fraco
CPUC - Concentração part. de desgaste							Médio
ISUC - Índice Severidade de Desgaste							Forte

Os resultados apresentados referem-se exclusivamente às amostras ensaiadas.

Este documento não pode ser reproduzido, total ou parcialmente, sem a autorização por escrito do INEGI.

Pág. 3 / 5

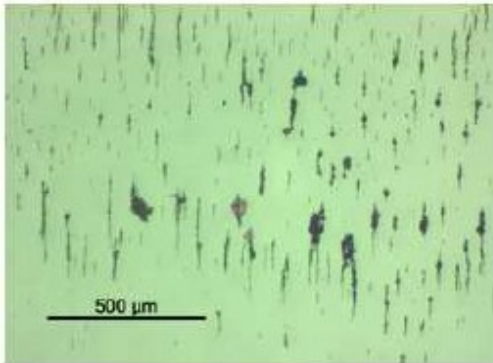
Relatório Nº 14/10

MOD LAL-REL01

CLIENTE: **INEGI**
MORADA: Porto
DATA: 23/03/10

MÁQUINA: Máquina de Ensaios FZG
Ref. ÓLEO: EIGO 2 LOW LOSS
ENSAIOS FZG - 20MrCr5 Gears 311 - K1

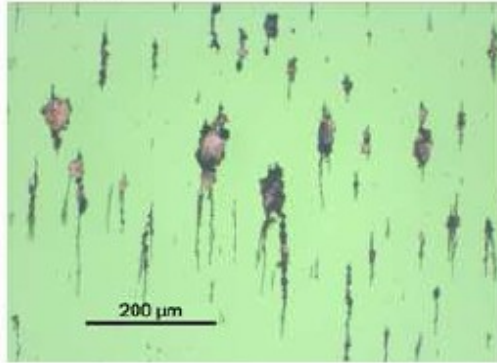
Fotografia 1



Ampliação: x 100 Diluição: 1
Localização: Núcleo Luz: Branca / Verde

Observações: Presença de partículas ferrosas de pequenas dimensões e algumas de grandes dimensões.

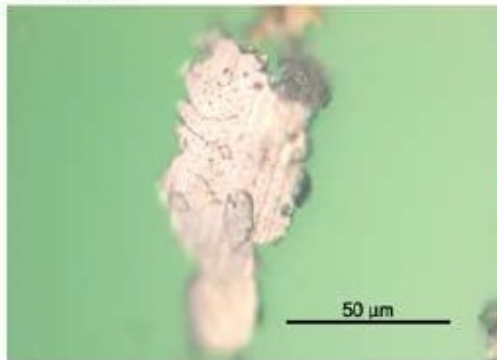
Fotografia 2



Ampliação: x 200 Diluição: 1
Localização: Núcleo Luz: Branca / Verde

Observações: Ampliação da Fotografia 1. Presença de algumas partículas ferrosas de grandes dimensões.

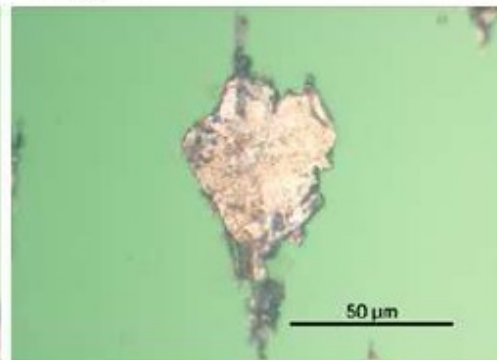
Fotografia 3



Ampliação: x 1000 Diluição: 1
Localização: Núcleo Luz: Branca / Verde

Observações: Ampliação da Fotografia 2. Partícula ferrosa laminar de forma arredondada, típica de fadiga e de grandes dimensões.

Fotografia 4



Ampliação: x 1000 Diluição: 1
Localização: Núcleo Luz: Branca / Verde

Observações: Ampliação da Fotografia 2. Partícula ferrosa laminar, típica de fadiga e de grandes dimensões.

CLIENTE: **INEGI**

MORADA: Porto

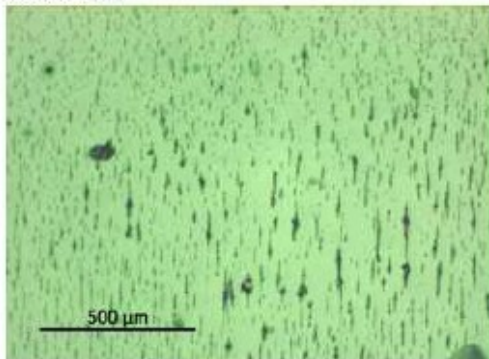
DATA: 23/03/10

MÁQUINA: Máquina de Ensaios FZG

Ref ÓLEO: EIGO 2 LOW OIL

ENSAIOS FZG - 20MnCr5 Gears 311 - K1

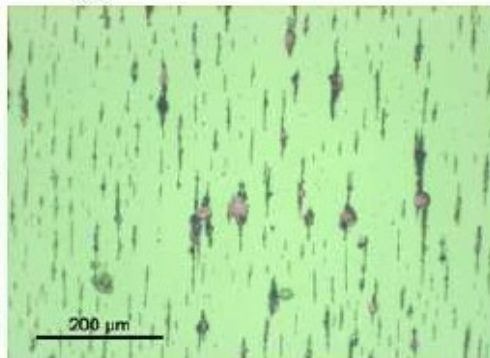
Fotografia 5



Ampliação: x 100 Diluição: 1
Localização: Núcleo Luz: Branca / Verde

Observações: Presença de partículas ferrosas de pequenas dimensões.

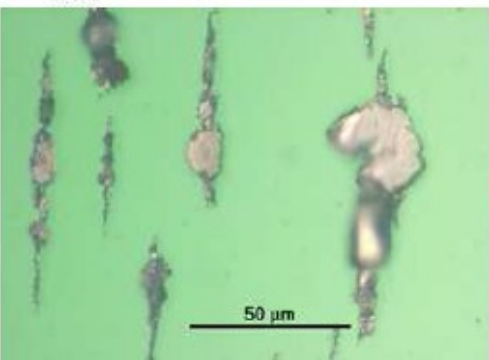
Fotografia 6



Ampliação: x 200 Diluição: 1
Localização: Núcleo Luz: Branca / Verde

Observações: Ampliação da Fotografia 5. Presença de partículas ferrosas de pequenas dimensões e algumas de média dimensão.

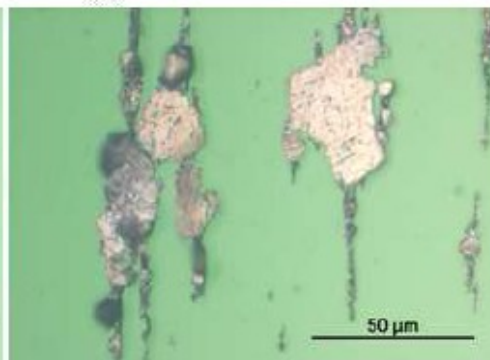
Fotografia 7



Ampliação: x 1000 Diluição: 1
Localização: Núcleo Luz: Branca / Verde

Observações: Ampliação da Fotografia 6. Partículas ferrosas de desgaste de fadiga com dimensões médias.

Fotografia 8



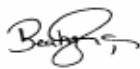

Ampliação: x 1000 Diluição: 1
Localização: Núcleo Luz: Branca / Verde

Observações: Ampliação da Fotografia 6. Partículas ferrosas de desgaste de fadiga com dimensões médias, algumas oxidadas.

412 – E2 Power Loss: High Oil



Relatório de Análise de Lubrificantes

Análise nº:	43 - 46 / 10
Tipo de análise:	Ferrometria e Ferrografia Analítica
Confidencialidade:	1
Cliente:	INEGI - Cetrib
Morada:	Porto
Telefone / Fax:	
Equipamento:	FZG (ADI – 412)
Lubrificante:	EIGO 2 (E2) – HIGH OIL
Dossier:	/
Nº de páginas:	5
Data:	14/06/10
Responsável:	Beatriz Graça – Jorge Seabra
Rúbrica:	 

Os resultados apresentados referem-se exclusivamente às amostras ensaiadas.
Este documento não pode ser reproduzido, total ou parcialmente, sem a autorização por escrito do INEGI.

Pág. 1 / 7
Relatório Nº 46/10
MOD LAL-REL01



OBJECTIVO

Análise de quatro amostras de óleo lubrificante EIGO 2 (High Oil) resultantes de ensaios na Máquina FZG com engrenagens de ADI 412, para avaliação do desgaste presente.

As amostras analisadas foram as seguintes:

Amostra Nº	Ciclos	Análises efectuadas	
		Ferrometria	Ferrografia Analítica
K1	-	X	X
K5	-	X	X
K7	-	X	X
K9	-	X	X

RESULTADOS DAS ANÁLISES

Nas páginas seguintes são apresentados os resultados referentes às análises de Ferrometria (DR III) e Ferrografia Analítica (FM III).

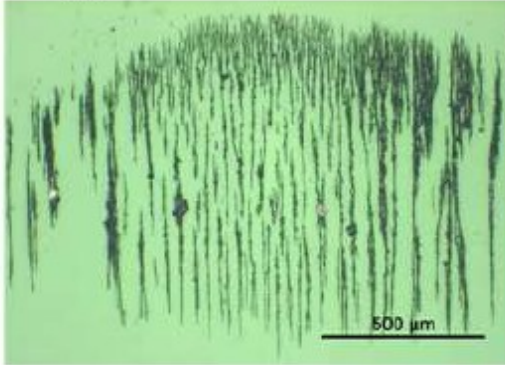
Os resultados apresentados referem-se exclusivamente às amostras ensaiadas.
Este documento não pode ser reproduzido, total ou parcialmente, sem a autorização por escrito do INEGI.

Pág. 2 / 7
Relatório Nº 46/10
MOD LAL-REL01

CLIENTE: INEGI
MORADA: Porto
DATA: 14/06/10

MÁQUINA: Máquina de Ensaios FZG
Ref. ÓLEO: EIDO 2 - HIGH OIL
ENSAIOS FZG - ADI Gears 412

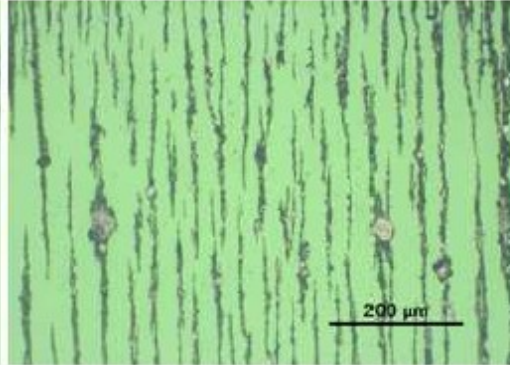
Fotografia 1



Ampliação: x 100 Diluição: 0,1
Localização: Núcleo Luz: Branca / Verde

Observações: Presença de partículas ferrosas de pequenas dimensões.

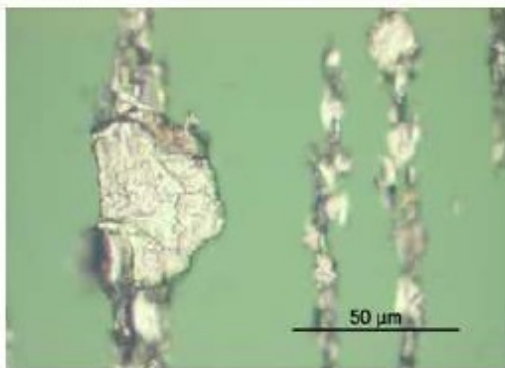
Fotografia 2



Ampliação: x 200 Diluição: 0,1
Localização: Núcleo Luz: Branca / Verde

Observações: Ampliação da Fotografia 1. Presença praticamente de partículas ferrosas de pequenas dimensões e poucas de grandes dimensões.

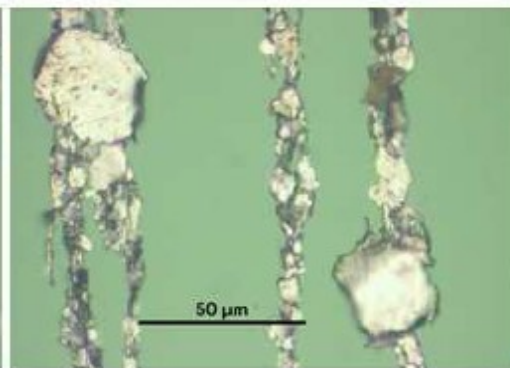
Fotografia 3



Ampliação: x 1000 Diluição: 0,1
Localização: Núcleo Luz: Branca / Verde

Observações: Ampliação da Fotografia 2. Partícula ferrosa de desgaste com grandes dimensões.

Fotografia 4



Ampliação: x 1000 Diluição: 0,1
Localização: Núcleo Luz: Branca / Verde

Observações: Partículas ferrosas laminares de médias dimensões.

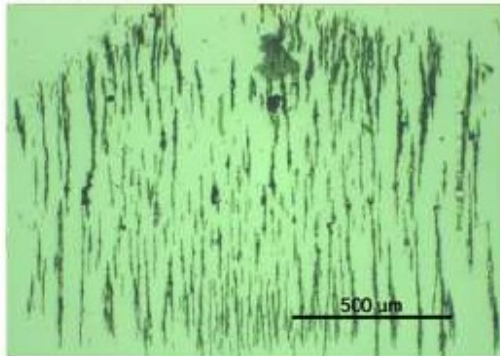
Os resultados apresentados referem-se exclusivamente às amostras ensaiadas.
Este documento não pode ser reproduzido, total ou parcialmente, sem a autorização por escrito do INEGI.

Pág. 4 / 7
Relatório Nº 46/10
MOD LAL-REL01

CLIENTE: **INEGI**
MORADA: Porto
DATA: 14/06/10

MÁQUINA: Máquina de Ensaios FZG
Ref. ÓLEO: EIGO 2 - HIGH OIL
ENSAIOS FZG - ADI Gears 412

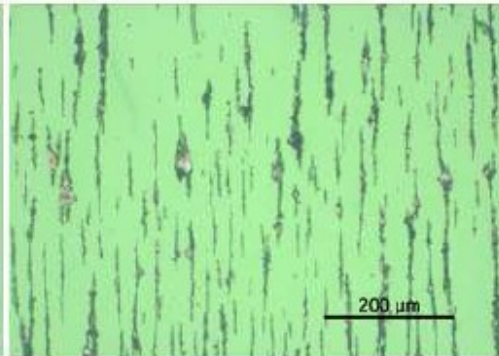
Fotografia 5



Ampliação: x 100 Diluição: 0,1
Localização: Núcleo Luz: Branca / Verde

Observações: Presença de partículas ferrosas de pequenas dimensões.

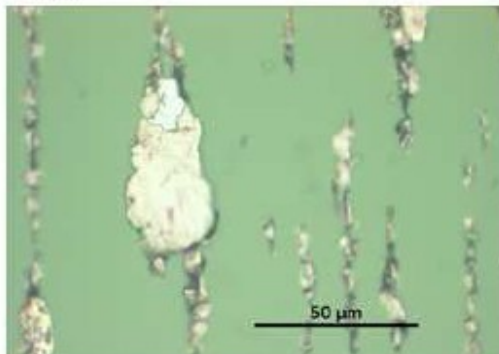
Fotografia 6



Ampliação: x 200 Diluição: 0,1
Localização: Núcleo Luz: Branca / Verde

Observações: Ampliação da Fotografia 1.
Presença praticamente de partículas ferrosas de pequenas dimensões e poucas de grandes dimensões.

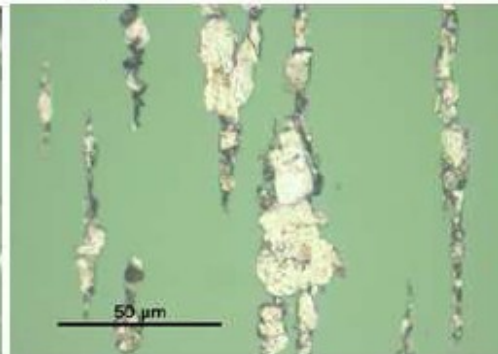
Fotografia 7



Ampliação: x 1000 Diluição: 0,1
Localização: Núcleo Luz: Branca / Verde

Observações: Ampliação da Fotografia 6.
Partícula ferrosa de desgaste com grandes dimensões.

Fotografia 8



Ampliação: x 1000 Diluição: 0,1
Localização: Núcleo Luz: Branca / Verde

Observações: Ampliação da Fotografia 6.
Partículas ferrosas laminares de médias dimensões.

Os resultados apresentados referem-se exclusivamente às amostras ensaiadas.
Este documento não pode ser reproduzido, total ou parcialmente, sem a autorização por escrito do INEGI.

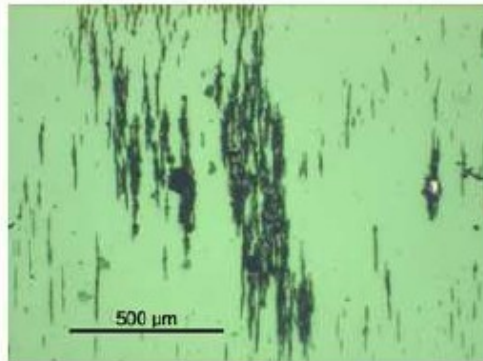
Pág. 5 / 7
Relatório Nº 45/10
MOD LAL-RELD1



CLIENTE: **INEGI**
MORADA: Porto
DATA: 14/06/10

MÁQUINA: Máquina de Ensaios FZG
Ref. ÓLEO: EIGO 2 - HIGH OIL
ENSAIOS FZG - ADI Gears 412

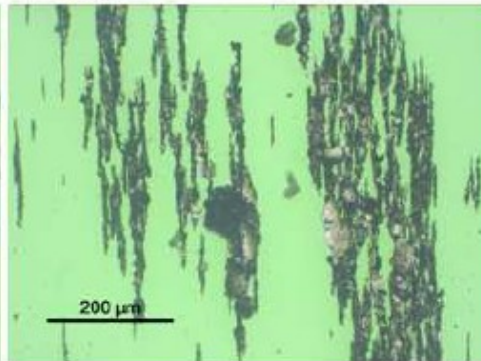
Fotografia 9



Ampliação: x 100 Diluição: 0,1
Localização: Núcleo Luz: Branca / Verde

Observações: Presença de partículas ferrosas de pequenas dimensões e algumas de grandes dimensões.

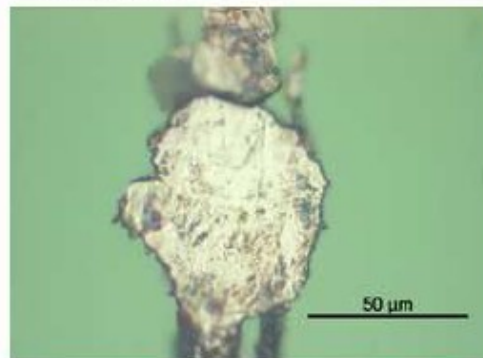
Fotografia 10



Ampliação: x 200 Diluição: 0,1
Localização: Núcleo Luz: Branca / Verde

Observações: Ampliação da Fotografia 9.
Presença de partículas ferrosas de pequenas e grandes dimensões.

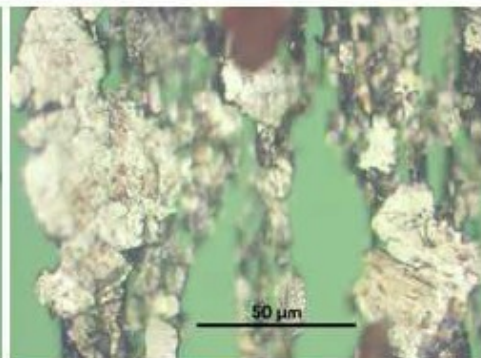
Fotografia 11



Ampliação: x 1000 Diluição: 0,1
Localização: Núcleo Luz: Branca / Verde

Observações: Ampliação da Fotografia 10.
Partícula ferrosa de grandes dimensões.

Fotografia 12



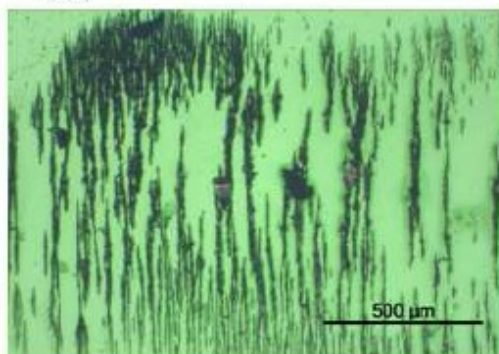
Ampliação: x 1000 Diluição: 0,1
Localização: Núcleo Luz: Branca / Verde

Observações: Ampliação da Fotografia 10.
Partículas ferrosas de pequenas e grandes dimensões.

CLIENTE: **INEGI**
MORADA: Porto
DATA: 14/06/10

MÁQUINA: Máquina de Ensaios FZG
Ref. ÓLEO: EIGO 2 - HIGH OIL
ENSAIOS FZG - ADI Gears 412

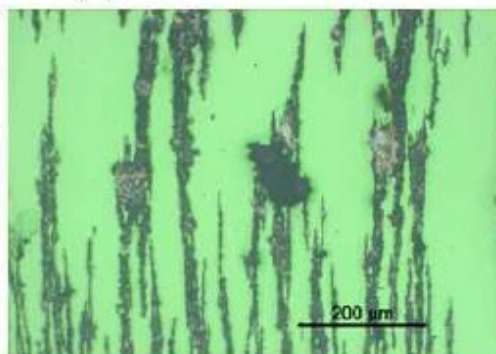
Fotografia 13



Ampliação: x 100 Diluição: 0,1
Localização: Núcleo Luz Branca / Verde

Observações: Presença de partículas ferrosas de pequenas dimensões e algumas de grandes dimensões.

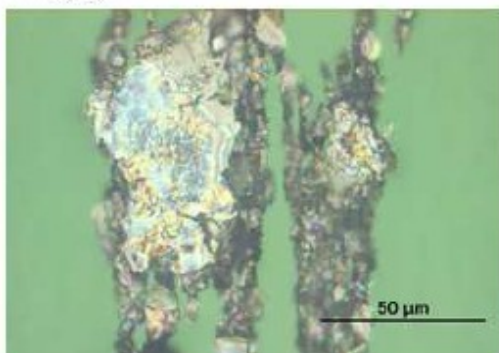
Fotografia 14



Ampliação: x 200 Diluição: 0,1
Localização: Núcleo Luz: Branca / Verde

Observações: Ampliação da Fotografia 13.
Presença de partículas ferrosas de pequenas e grandes dimensões.

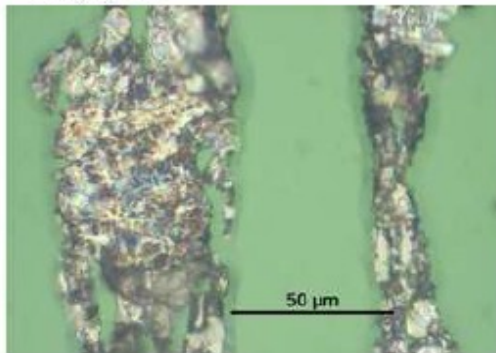
Fotografia 15



Ampliação: x 1000 Diluição: 0,1
Localização: Núcleo Luz Branca / Verde

Observações: Ampliação da Fotografia 14.
Partículas ferrosas de grandes dimensões revestidas por uma película transparente.
Presença significativa de óxidos térmicos.

Fotografia 16





Ampliação: x 1000 Diluição: 0,1
Localização: Núcleo Luz: Branca / Verde

Observações: Ampliação da Fotografia 14.
Partículas ferrosas de grandes dimensões revestidas por uma película transparente.
Presença significativa de óxidos térmicos.

412 – P1 Power Loss: High Oil



Relatório de Análise de Lubrificantes

Análise nº:	39-42 / 10
Tipo de análise:	Ferrometria e Ferrografia Analítica
Confidencialidade:	1
Cliente:	INEGI - Cetrib
Morada:	Porto
Telefone / Fax:	
Equipamento:	FZG (ADI – 412F – Lado A)
Lubrificante:	P1
Dossier:	/
Nº de páginas:	7
Data:	02/06/10
Responsável:	Beatriz Graça – Jorge Seabra
Rúbrica:	 

Os resultados apresentados referem-se exclusivamente às amostras ensaiadas.
Este documento não pode ser reproduzido, total ou parcialmente, sem a autorização por escrito do INEGI.

Pág. 1 / 7
Relatório Nº 42/10
MOD LAL-REL01



OBJECTIVO

Análise de quatro amostras de óleo lubrificante P1 resultantes de ensaios na Máquina FZG com engrenagens de ADI (412F – Lado A), para avaliação do desgaste presente.

As amostras analisadas foram as seguintes:

Amostra Nº	Ciclos	Análises efectuadas	
		Ferrometria	Ferrografia Analítica
K1	840 000	X	X
K5	1 680 000	X	X
K7	2 520 000	X	X
K9	3 369 000	X	X

RESULTADOS DAS ANÁLISES

Nas páginas seguintes são apresentados os resultados referentes às análises de Ferrometria (DR III) e Ferrografia Analítica (FM III).



CETRIB - Laboratório
de Análise de Lubrificantes

CLIENTE: INEGI		MÁQUINA: Máquina de Ensaios FZG					
MORADA: Porto		Ref. ÓLEO: P1 - 411F - Lado A					
DATA: 01/06/10		ENSAIOS FZG - ADI Gears					
IDENTIFICAÇÃO							
Amostra n°:	K1	K5	K7	K9			
Data amostra:	Mai-10	Mai-10	Mai-10	Mai-10			
Análise n°:	39/10	40/10	41/10	42/10			
Ciclos/Máquina:	-	-	-	-			
Ciclos/Óleo:	-	-	-	-			
FERROMETRIA							
d:	0,1	0,1	0,1	0,1			
DL:	29,9	27,8	43,9	60,7			
DS:	8,2	9,7	11,0	12,8			
CPUC:	381,0	375,0	569,0	735,0			
ISUC:	8,3E+04	6,8E+04	2,0E+05	3,5E+05			
FERROGRAFIA:							
Desgaste normal							
Desgaste severo							
Desgaste abrasão							
Desgaste combinado							
Desgaste fadiga							
Esferas Metálicas							
Ligas não ferrosas							
Óxidos de ferro							
Minerais/Orgânicos							
OILVIEW:							
Índice OilLife:							
Índice Oxidação:							
Índice Contaminação:							
Índice Ferromagnético:							
Grandes Contaminantes:							
Constante Dielétrica:							
FILTRAGEM							
(N° Partículas/10 ml)							
5 - 15 µm							
15 - 25 µm							
25 - 50 µm							
50 - 100 µm							
> 100 µm							
VISCOSIDADE							
(cSt a 40° C):							
ACIDEZ (TAN)							
(mg KOH)							
P. INFLAMAÇÃO							
(° C)							
DIAGNOSTICO:							
LEGENDA							
DL - Índice de partículas grandes					Não existe		
DS - Índice de partículas pequenas				f	Fraco		
CPUC - Concentração part. de desgaste				M	Médio		
ISUC - Índice Severidade de Desgaste				F	Forte		

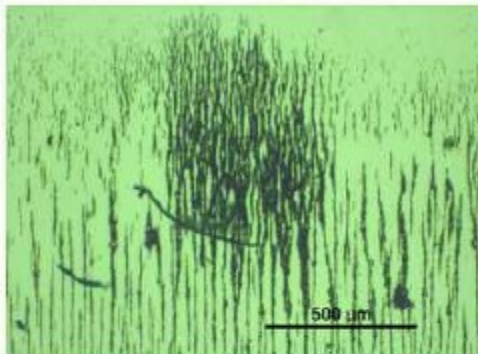
Os resultados apresentados referem-se exclusivamente às amostras ensaiadas.
Este documento não pode ser reproduzido, total ou parcialmente, sem a autorização por escrito do INEGI.

Pág. 3 / 7
Relatório Nº 42/10
MOD LAL-REL01

CLIENTE: **INEGI**
MORADA: Porto
DATA: 01/06/10

MÁQUINA: Máquina de Ensaio FZG
Ref. ÓLEO: P1 - 412F - Lado A
ENSAIOS FZG - ADI Gears K1

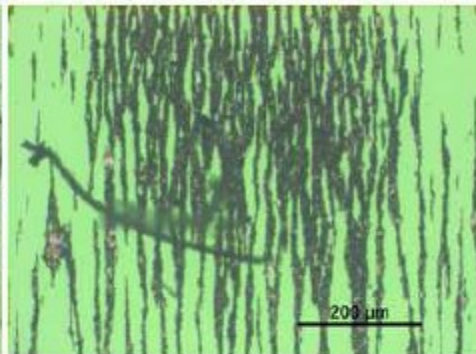
Fotografia 1



Ampliação: x 100 Diluição: 0,1
Localização: Núcleo Luz: Branca / Verde

Observações: Presença de partículas ferrosas de pequenas e algumas de grandes dimensões.

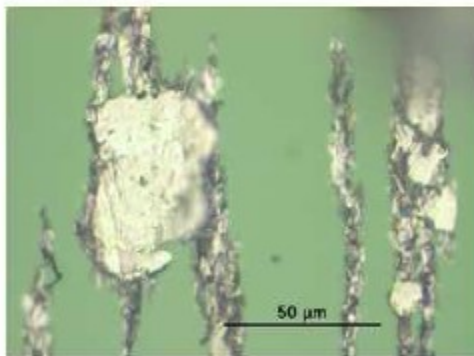
Fotografia 2



Ampliação: x 200 Diluição: 0,1
Localização: Núcleo Luz: Branca / Verde

Observações: Ampliação da Fotografia 1.
Presença de partículas ferrosas de pequenas e de algumas de grandes dimensões.

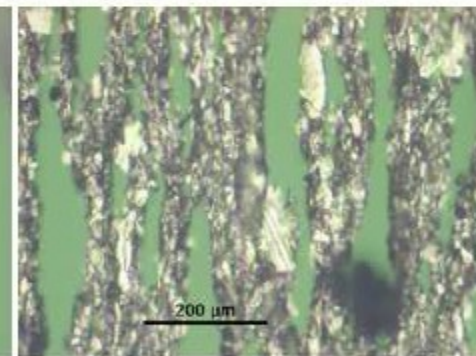
Fotografia 3



Ampliação: x 1000 Diluição: 0,1
Localização: Núcleo Luz: Branca / Verde

Observações: Ampliação da Fotografia 2.
Presença de algumas partículas ferrosas laminares de grandes dimensões.

Fotografia 4



Ampliação: x 1000 Diluição: 0,1
Localização: Núcleo Luz: Branca / Verde

Observações: Ampliação da Fotografia 2.
Partículas ferrosas de desgaste de médias dimensões, algumas onçadas termicamente.

Os resultados apresentados referem-se exclusivamente às amostras ensaiadas.
Este documento não pode ser reproduzido, total ou parcialmente, sem a autorização por escrito do INEGI.

Pág. 4 / 7

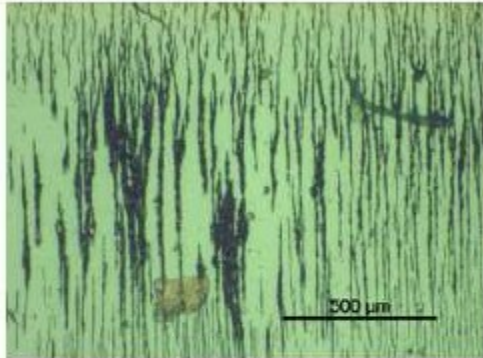
Relatório Nº 42/10

MOD LAL-REL01

CLIENTE: **INEGI**
MORADA: Porto
DATA: 01/06/10

MÁQUINA: Máquina de Ensaios FZG
Ref. ÓLEO: P1 - 412F - Lado A
ENSAIOS FZG - ADI Gear K5

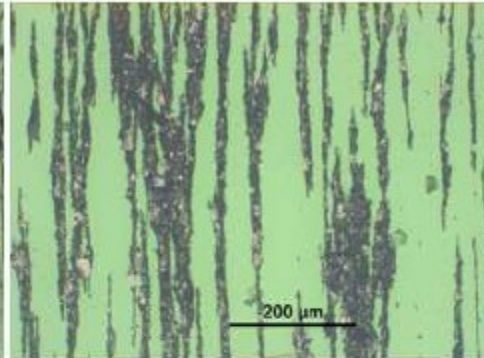
Fotografia 5



Ampliação: x 100 Diluição: 0,1
Localização: Núcleo Luz: Branca / Verde

Observações: Presença significativa de partículas ferrosas de pequenas dimensões.

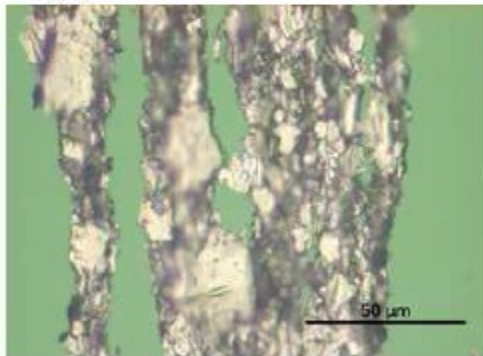
Fotografia 6



Ampliação: x 200 Diluição: 0,1
Localização: Núcleo Luz: Branca / Verde

Observações: Ampliação da Fotografia 5.
Presença de partículas ferrosas de pequenas e de médias dimensões.

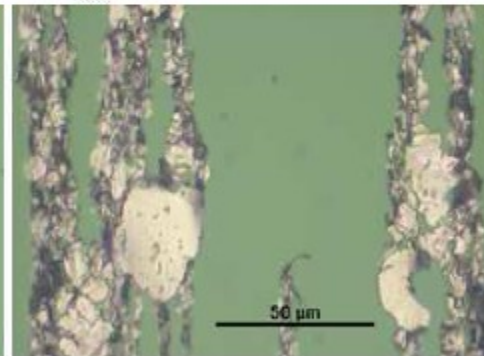
Fotografia 7



Ampliação: x 1000 Diluição: 0,1
Localização: Núcleo Luz: Branca / Verde

Observações: Ampliação da Fotografia 6.
Partículas ferrosas de desgaste de médias dimensões.

Fotografia 8



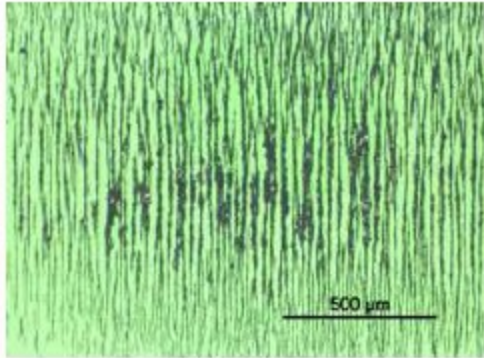
Ampliação: x 1000 Diluição: 0,1
Localização: Núcleo Luz: Branca / Verde

Observações: Ampliação da Fotografia 6.
Partículas ferrosas de desgaste de médias dimensões.

CLIENTE: **INEGI**
MORADA: Porto
DATA: 01/06/10

MÁQUINA: Máquina de Ensaio FZG
Ref. ÓLEO: P1 - 412F - Lado A
ENSAIOS FZG - ADI Gears K7

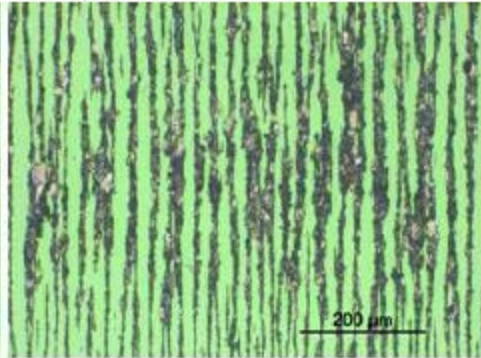
Fotografia 9



Ampliação: x 100 Diluição: 0,1
Localização: Núcleo Luz: Branca / Verde

Observações: Presença significativa de partículas ferrosas de pequenas dimensões.

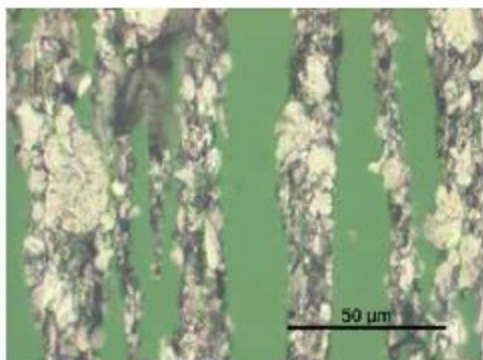
Fotografia 10



Ampliação: x 200 Diluição: 0,1
Localização: Núcleo Luz: Branca / Verde

Observações: Ampliação da Fotografia 9. Presença significativa de partículas ferrosas de pequenas e de médias dimensões.

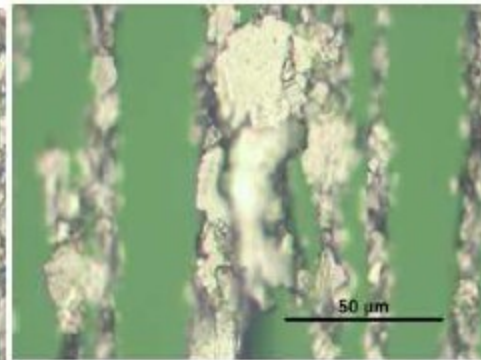
Fotografia 11



Ampliação: x 1000 Diluição: 0,1
Localização: Núcleo Luz: Branca / Verde

Observações: Ampliação da Fotografia 10. Partículas ferrosas de desgaste de médias dimensões.

Fotografia 12



Ampliação: x 1000 Diluição: 0,1
Localização: Núcleo Luz: Branca / Verde

Observações: Ampliação da Fotografia 10. Partículas ferrosas de desgaste de médias dimensões e algumas de grandes dimensões.

Os resultados apresentados referem-se exclusivamente às amostras ensaiadas.
Este documento não pode ser reproduzido, total ou parcialmente, sem a autorização por escrito do INEGI.

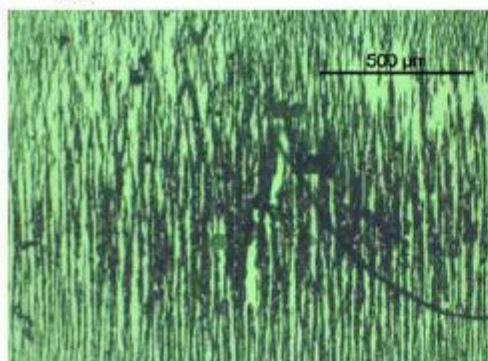
Pág. 6 / 7
Relatório Nº 42/10
MOD LAL-REL01



CLIENTE: **INEGI**
MORADA: Porto
DATA: 01/06/10

MÁQUINA: Máquina de Ensaios FZG
Ref. ÓLEO: Pl - 412F - Lado A
ENSAIOS FZG - ADI Gears KP

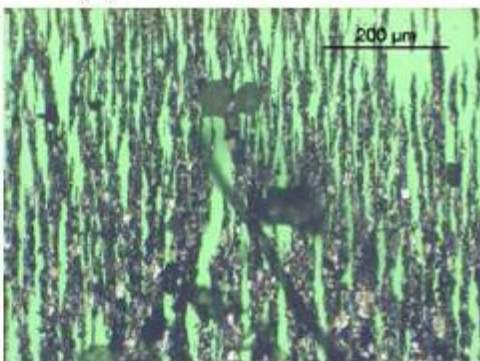
Fotografia 13



Ampliação: x 100 Diluição: 0,1
Localização: Núcleo Luz: Branca / Verde

Observações: Presença significativa de partículas ferrosas de pequenas dimensões.

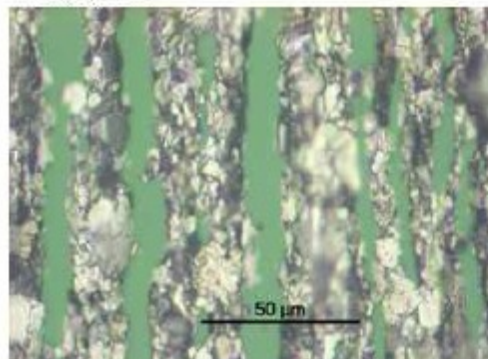
Fotografia 14



Ampliação: x 200 Diluição: 0,1
Localização: Núcleo Luz: Branca / Verde

Observações: Ampliação da Fotografia 13.
Presença significativa de partículas ferrosas de pequenas e de médias dimensões.

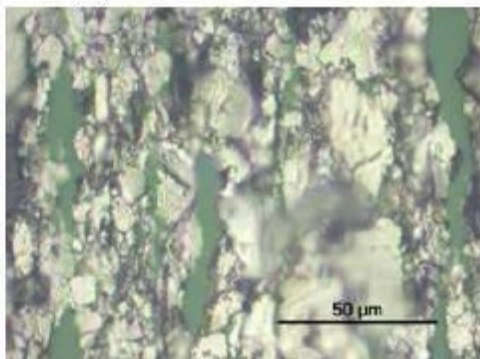
Fotografia 15



Ampliação: x 1000 Diluição: 0,1
Localização: Núcleo Luz: Branca / Verde

Observações: Ampliação da Fotografia 14.
Partículas ferrosas de desgaste de médias dimensões.

Fotografia 16



Ampliação: x 200 / x 1000 Diluição: 0,1
Localização: Núcleo Luz: Branca / Verde

Observações: Ampliação da Fotografia 14.
Partículas ferrosas de desgaste de médias dimensões.

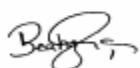

Os resultados apresentados referem-se exclusivamente às amostras ensaiadas.
Este documento não pode ser reproduzido, total ou parcialmente, sem a autorização por escrito do INEGI.

Pág. 7 / 7
Relatório Nº 42/10
MOD LAL-REL01

312 – P1 Power Loss: High Oil



Relatório de Análise de Lubrificantes

Análise nº:	16-19 / 10
Tipo de análise:	Ferrometria e Ferrografia Analítica
Confidencialidade:	1
Cliente:	INEGI - Cetrib
Morada:	Porto
Telefone / Fax:	
Equipamento:	FZG (ADI – 312C – Lado A)
Lubrificante:	P1
Dossier:	/
Nº de páginas:	7
Data:	09/04/10
Responsável:	Beatriz Graça – Jorge Seabra
Rúbrica:	 

Os resultados apresentados referem-se exclusivamente às amostras ensaiadas.
Este documento não pode ser reproduzido, total ou parcialmente, sem a autorização por escrito do INEGI.

Pág. 1 / 7
Relatório Nº 19/10
MOD LAL-REL01



OBJECTIVO

Análise de quatro amostras de óleo lubrificante P1 resultantes de ensaios na Máquina FZG com engrenagens de ADI (312C – Lado A), para avaliação do desgaste presente.

As amostras analisadas foram as seguintes:

Amostra Nº	Ciclos	Análises efectuadas	
		Ferrometria	Ferrografia Analítica
K1	840 000	X	X
K5	1 680 000	X	X
K7	2 520 000	X	X
K9	3 369 000	X	X

RESULTADOS DAS ANÁLISES

Nas páginas seguintes são apresentados os resultados referentes às análises de Ferrometria (DR III) e Ferrografia Analítica (FM III).

[illegible]

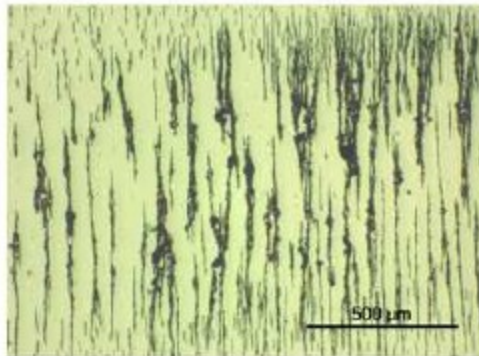
Os resultados apresentados referem-se exclusivamente às amostras ensaiadas.
Este documento não pode ser reproduzido, total ou parcialmente, sem a autorização por escrito do INEGI.

Pág. 3 / 7
Relatório Nº 19/10
MOD LAL-REL01

CLIENTE: **INEGI**
MORADA: Porto
DATA: 09/04/10

MÁQUINA: Máquina de Ensaios FZG
Ref. ÓLEO: P1 - 312C - Lado A
ENSAIOS FZG - ADI Gears K1

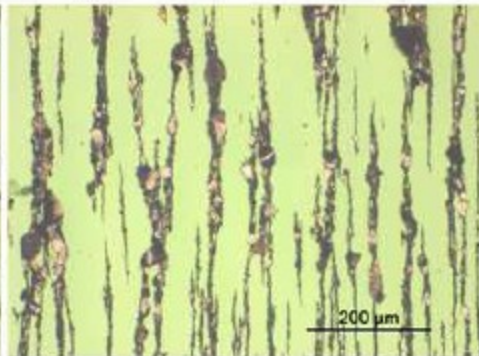
Fotografia 1



Ampliação: x 100 Dilução: 1
Localização: Núcleo Luz: Branca / Verde

Observações: Presença de partículas ferrosas de pequenas e algumas de grandes dimensões.

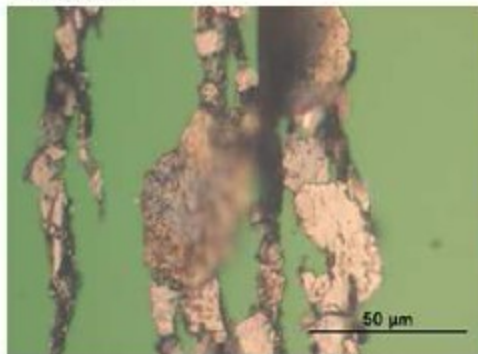
Fotografia 2



Ampliação: x 200 Dilução: 1
Localização: Núcleo Luz: Branca / Verde

Observações: Ampliação da Fotografia 1.
Presença de partículas ferrosas de pequenas e de algumas de grandes dimensões.

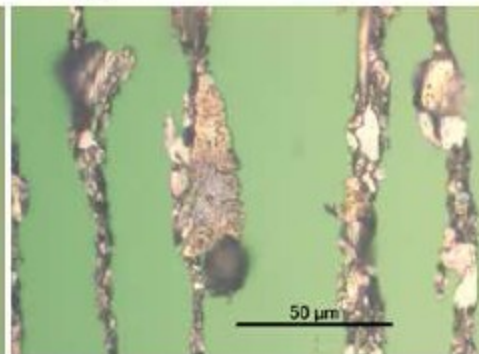
Fotografia 3



Ampliação: x 1000 Dilução: 1
Localização: Núcleo Luz: Branca / Verde

Observações: Ampliação da Fotografia 2.
Partículas ferrosas laminares de grandes dimensões e oxidadas termicamente.

Fotografia 4



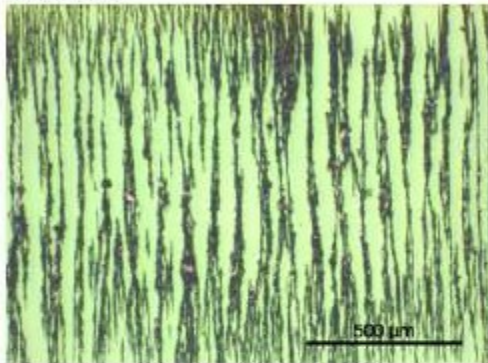
Ampliação: x 1000 Dilução: 1
Localização: Núcleo Luz: Branca / Verde

Observações: Ampliação da Fotografia 2.
Partículas ferrosas laminares de médias dimensões e oxidadas termicamente.

CLIENTE: **INEGI**
MORADA: Porto
DATA: 09/04/10

MÁQUINA: Máquina de Ensaios FZG
Ref. ÓLEO: P1 - 312C - Lado A
ENSAIOS FZG - ADI Gears K5

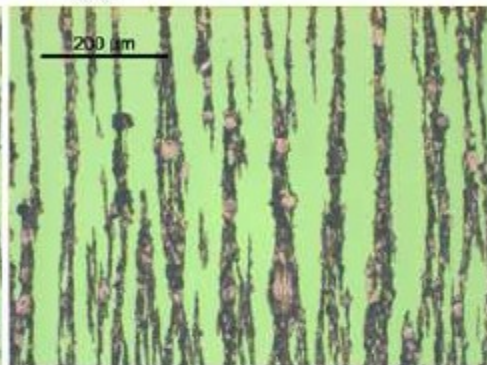
Fotografia 5



Ampliação: x 100 Diluição: 1
Localização: Núcleo Luz Branca / Verde

Observações: Presença significativa de partículas ferrosas de pequenas e algumas de grandes dimensões.

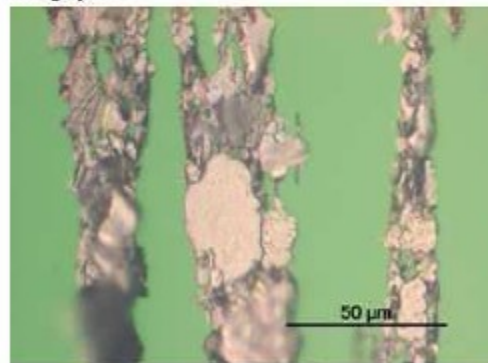
Fotografia 6



Ampliação: x 200 Diluição: 1
Localização: Núcleo Luz Branca / Verde

Observações: Ampliação da Fotografia 5.
Presença de partículas ferrosas de pequenas e de algumas de grandes dimensões.

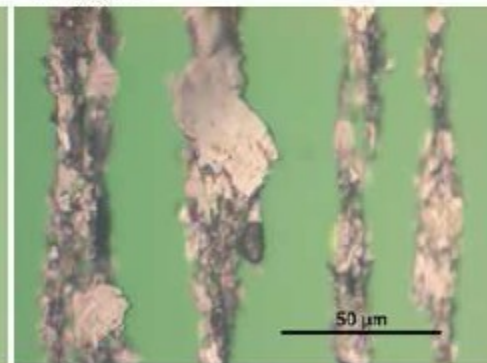
Fotografia 7



Ampliação: x 1000 Diluição: 1
Localização: Núcleo Luz: Branca / Verde

Observações: Ampliação da Fotografia 6.
Partículas ferrosas de desgaste de fadiga, algumas oxidadas termicamente.

Fotografia 8



Ampliação: x 1000 Diluição: 1
Localização: Núcleo Luz: Branca / Verde

Observações: Ampliação da Fotografia 6.
Partículas ferrosas de desgaste de fadiga, algumas oxidadas termicamente.

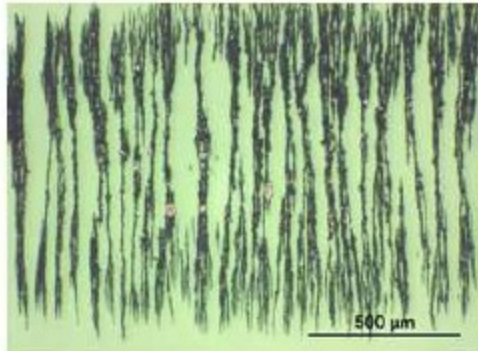
Os resultados apresentados referem-se exclusivamente às amostras ensaiadas.
Este documento não pode ser reproduzido, total ou parcialmente, sem a autorização por escrito do INEGI.

Pág. 5 / 7
Relatório Nº 19/10
MOD LAL-REL01

CLIENTE: **INEGI**
MORADA: Porto
DATA: 09/04/10

MÁQUINA: Máquina de Ensaio FZG
Ref. ÓLEO: P1 - 312C - Lado A
ENSAIOS FZG - AD1 Gear: K7

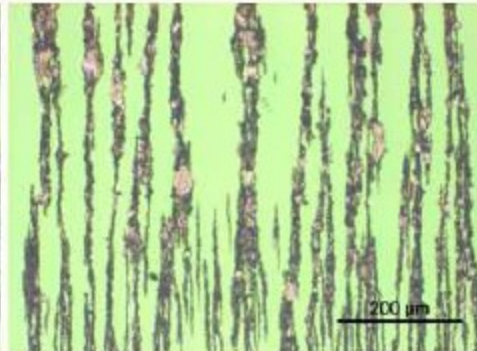
Fotografia 9



Ampliação: x 100 Dilução: 1
Localização: Núcleo Luz: Branca / Verde

Observações: Presença significativa de partículas ferrosas de pequenas e grandes dimensões.

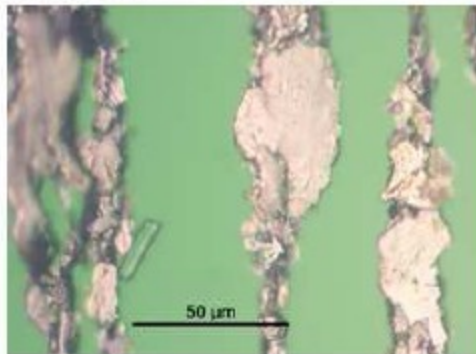
Fotografia 10



Ampliação: x 200 Dilução: 1
Localização: Núcleo Luz: Branca / Verde

Observações: Ampliação da Fotografia 9. Presença de algumas partículas ferrosas de grandes dimensões.

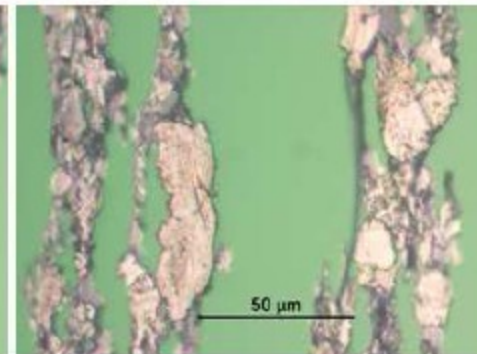
Fotografia 11



Ampliação: x 1000 Dilução: 1
Localização: Núcleo Luz: Branca / Verde

Observações: Ampliação da Fotografia 10. Partículas ferrosas laminares de desgaste e de grandes dimensões.

Fotografia 12



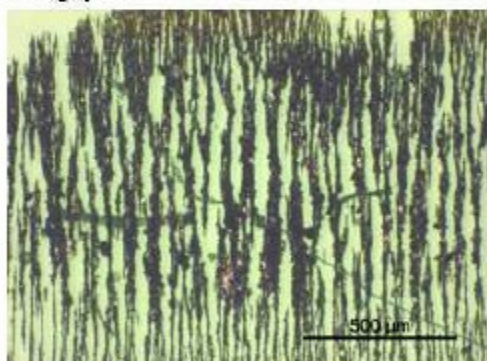
Ampliação: x 1000 Dilução: 1
Localização: Núcleo Luz: Branca / Verde

Observações: Ampliação da Fotografia 10. Partículas ferrosas de desgaste de média e grande dimensão.

CLIENTE: **INEGI**
MORADA: Porto
DATA: 09/04/10

MÁQUINA: Máquina de Ensaios FZG
Ref. ÓLEO: PL - 312C - Lado A
ENSAIOS FZG - ADIGears K9

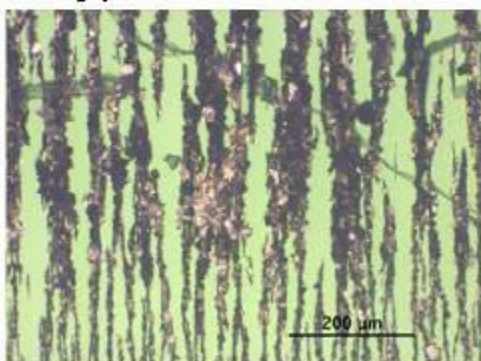
Fotografia 13



Ampliação: x 100 Diluição: 1
Localização: Núcleo Luz: Branca / Verde

Observações: Presença significativa de partículas ferrosas de pequenas e grandes dimensões.

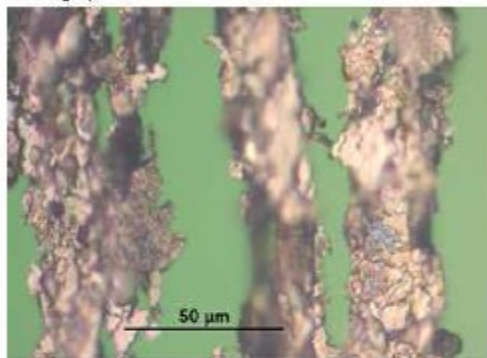
Fotografia 14



Ampliação: x 200 Diluição: 1
Localização: Núcleo Luz: Branca / Verde

Observações: Ampliação da Fotografia 13. Presença significativa de partículas ferrosas de pequenas e grandes dimensões. Presença abundante de óxidos térmicos.

Fotografia 15



Ampliação: x 1000 Diluição: 1
Localização: Núcleo Luz: Branca / Verde

Observações: Ampliação da Fotografia 14. Partículas ferrosas de grandes dimensões oxidadas termicamente.

Fotografia 16



Ampliação: x 200 / x 1000 Diluição: 1
Localização: Saída Luz: Branca / Verde

Observações: Presença de várias partículas de óxidos de ferro negros (1). Estes óxidos surgem frequentemente em condições de lubrificação limite.

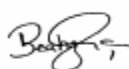

Os resultados apresentados referem-se exclusivamente às amostras ensaiadas.
Este documento não pode ser reproduzido, total ou parcialmente, sem a autorização por escrito do INEGI.

Pag. 7 / 7
Relatório Nº 19/10
MOD LAL-REL01

311 – P1 Power Loss: Low Oil



Relatório de Análise de Lubrificantes

Análise nº:	20-23 / 10
Tipo de análise:	Ferrometria e Ferrografia Analítica
Confidencialidade:	1
Cliente:	INEGI - Cetrib
Morada:	Porto
Telefone / Fax:	
Equipamento:	FZG (20MnCr5 – 311) Lado B
Lubrificante:	P1 (Power Loss – Low Oil)
Dossier:	/
Nº de páginas:	7
Data:	20/10/2010
Responsável:	Beatriz Graça – Jorge Seabra
Rúbrica:	 

Os resultados apresentados referem-se exclusivamente às amostras ensaiadas.
Este documento não pode ser reproduzido, total ou parcialmente, sem a autorização por escrito do INEGI.

Pág. 1 / 7
Relatório Nº 23/10
MOD LAL-REL01



OBJECTIVO

Análise de quatro amostras de óleos lubrificantes – P1, resultantes de ensaios de Power Loss – Low Oil na Máquina FZG com engrenagens de aço (20MnCr5, Lado B), para avaliação do desgaste presente.

As amostras analisadas foram as seguintes:

Amostra Nº	Ciclos	Análises efectuadas	
		Ferrometria	Ferrografia Analítica
K1	-	X	X
K5	-	X	X
K7	-	X	X
K9	-	X	X

RESULTADOS DAS ANÁLISES

Nas páginas seguintes são apresentados os resultados referentes às análises de Ferrometria (DR III) e Ferrografia Analítica (FM III).



CETRIB - Laboratório
de Análise de Lubrificantes

CLIENTE: INEGI		MÁQUINA: Máquina de Ensaios FZG					
MORADA: Porto		Ref. ÓLEO: F1 (Power Loss - Low Oil)					
DATA: 20/04/10		ENSAIOS FZG - 20MnCr5 Gears 311 - K1					
IDENTIFICAÇÃO							
Amostragem:	K1	K5	K7	K9			
Data amostra:	Abr-10	Abr-10	Abr-10	Abr-10			
Análise nº:	20/10	21/10	22/10	23/10			
Ciclos/Máquina:	-	-	-	-			
Ciclos/Óleo:	-	-	-	-			
FERROMETRIA							
d:	1	1	1	1			
DL:	32,3	44,2	33,9	34,8			
DS:	17,0	18,4	22,3	19,0			
CPUC:	49,3	62,6	56,2	53,8			
ISUC:	754,3	1615,1	651,9	850,0			
FERROGRAFIA:							
Desgaste normal							
Desgaste severo							
Desgaste abrasão							
Desgaste combinado							
Desgaste fadiga							
Esferas Metálicas							
Ligas não ferrosas							
Oxidos de ferro							
Minerais/Orgânicos							
OE VIEW:							
Índice OilLife:							
Índice Oxidação:							
Índice Contaminação:							
Índice Ferromagnético:							
Grandes Contaminantes:							
Constante Dielétrica:							
FILTRAGEM							
(Nº Partículas/10 ml)							
5 - 15 µm							
15 - 25 µm							
25 - 50 µm							
50 - 100 µm							
> 100 µm							
VISCOSIDADE							
(cSt a 40° C):							
ACIDEZ (TAN)							
(mg KOH)							
P. INFLAMAÇÃO							
(° C)							
DIAGNOSTICO:							
LEGENDA							
DL - Índice de partículas grandes							Não existe
DS - Índice de partículas pequenas							Fraco
CPUC - Concentração part. de desgaste							Médio
ISUC - Índice Severidade de Desgaste							Forte

Os resultados apresentados referem-se exclusivamente às amostras ensaiadas.

Este documento não pode ser reproduzido, total ou parcialmente, sem a autorização por escrito do INEGI.

Pág. 3 / 7

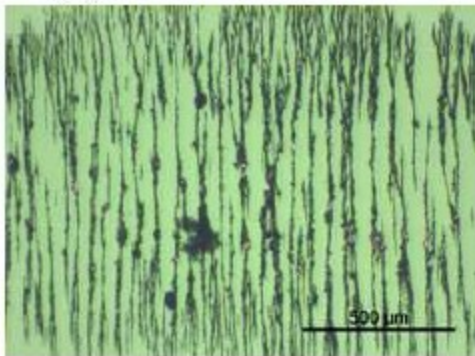
Relatório Nº 23/10

MOD LAL-REL01

CLIENTE: **INEGI**
MORADA: Porto
DATA: 20/04/10

MÁQUINA: Máquina de Ensaio FZG
Ref. ÓLEO: P1 (Power Loss - Low Oil)
ENSAIOS FZG - 20MnCr5 Gears 311 - K1

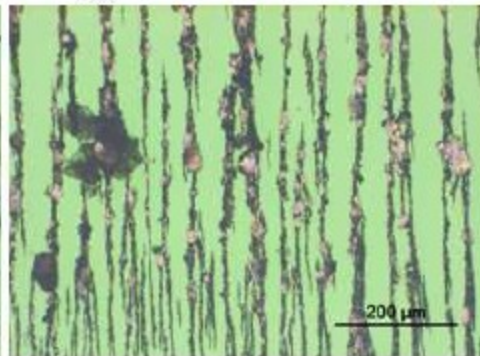
Fotografia 1



Ampliação: x 100 Diluição: 1
Localização: Núcleo Luz: Branca / Verde

Observações: Presença de partículas ferrosas de pequenas dimensões e algumas de grandes dimensões.

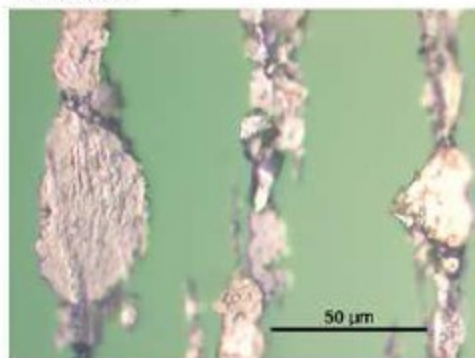
Fotografia 2



Ampliação: x 200 Diluição: 1
Localização: Núcleo Luz: Branca / Verde

Observações: Ampliação da Fotografia 1. Presença de algumas partículas ferrosas de grandes dimensões.

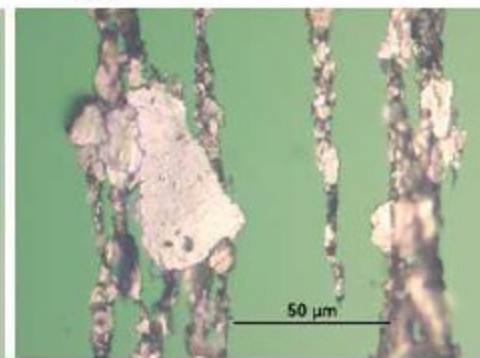
Fotografia 3



Ampliação: x 1000 Diluição: 1
Localização: Núcleo Luz: Branca / Verde

Observações: Ampliação da Fotografia 2. Partículas ferrosas de desgaste, típicas de fadiga e de grandes dimensões.

Fotografia 4



Ampliação: x 1000 Diluição: 1
Localização: Núcleo Luz: Branca / Verde

Observações: Ampliação da Fotografia 2. Partícula ferrosa laminar típica de fadiga e de grandes dimensões.

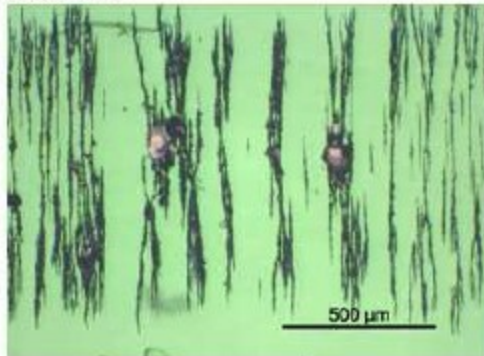
Os resultados apresentados referem-se exclusivamente às amostras ensaiadas.
Este documento não pode ser reproduzido, total ou parcialmente, sem a autorização por escrito do INEGI.

Pág. 4 / 7
Relatório Nº 23/10
MOD LAL-REL01

CLIENTE: **INEGI**
MORADA: Porto
DATA: 20/04/10

MÁQUINA: Máquina de Ensaio FZG
Ref. ÓLEO: P1 (Power Loss - Low Oil)
ENSAIOS FZG - 20MnCr5 Gears 311 - K5

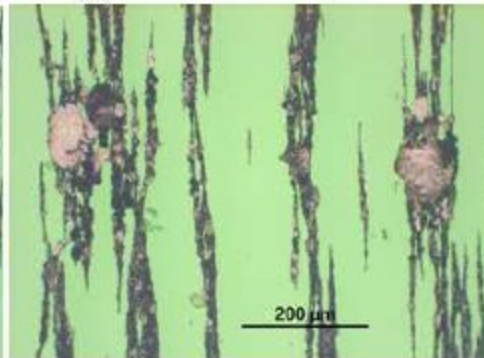
Fotografia 5



Ampliação: x 100 Diluição: 1
Localização: Núcleo Luz: Branca / Verde

Observações: Presença de partículas ferrosas de pequenas dimensões e algumas de grandes dimensões.

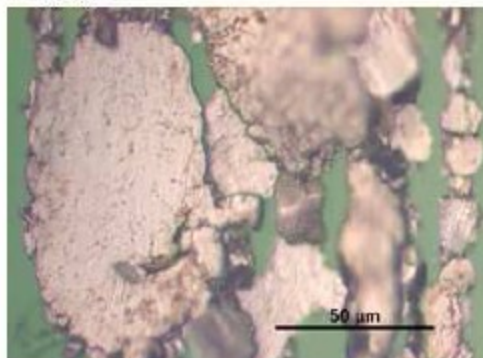
Fotografia 6



Ampliação: x 200 Diluição: 1
Localização: Núcleo Luz: Branca / Verde

Observações: Ampliação da Fotografia 5. Presença de algumas partículas ferrosas de muito grandes dimensões.

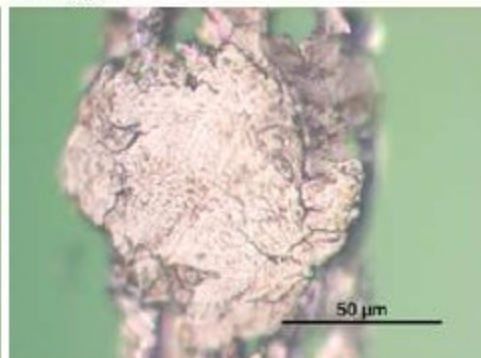
Fotografia 7



Ampliação: x 1000 Diluição: 1
Localização: Núcleo Luz: Branca / Verde

Observações: Ampliação da Fotografia 6. Partículas ferrosas de desgaste de fadiga com grandes dimensões.

Fotografia 8



Ampliação: x 1000 Diluição: 1
Localização: Núcleo Luz: Branca / Verde

Observações: Ampliação da Fotografia 6. Partícula ferrosa de desgaste de fadiga com grandes dimensões.

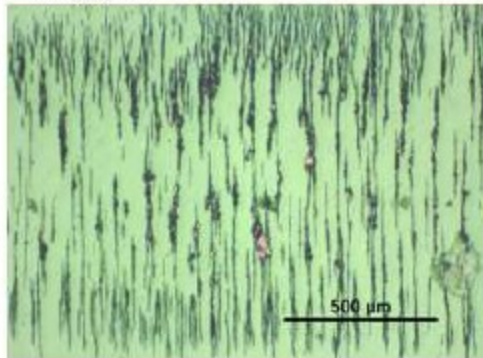
Os resultados apresentados referem-se exclusivamente às amostras ensaiadas.
Este documento não pode ser reproduzido, total ou parcialmente, sem a autorização por escrito do INEGI.

Pág. 5 / 7
Relatório Nº 23/10
MOD LAL-REL01

CLIENTE: **INEGI**
MORADA: Porto
DATA: 20/04/10

MÁQUINA: Máquina de Ensaio FZG
Ref. ÓLEO: P1 (Power Loss - Low Oil)
ENSAIOS FZG - 20MnCr1 Gears 311 - K7

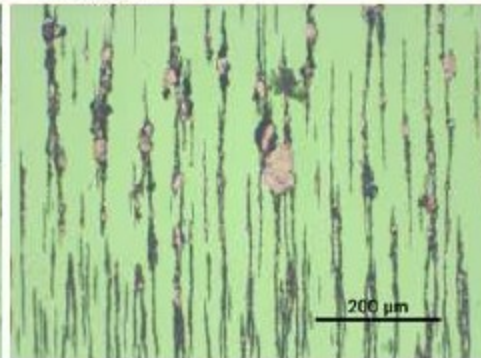
Fotografia 9



Ampliação: x 100 Dilução: 1
Localização: Núcleo Luz: Branca / Verde

Observações: Presença de partículas ferrosas de pequenas dimensões e algumas de grandes dimensões.

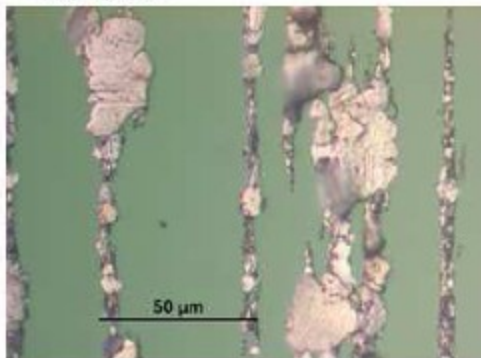
Fotografia 10



Ampliação: x 200 Dilução: 1
Localização: Núcleo Luz: Branca / Verde

Observações: Ampliação da Fotografia 9. Presença de algumas partículas ferrosas de grandes dimensões.

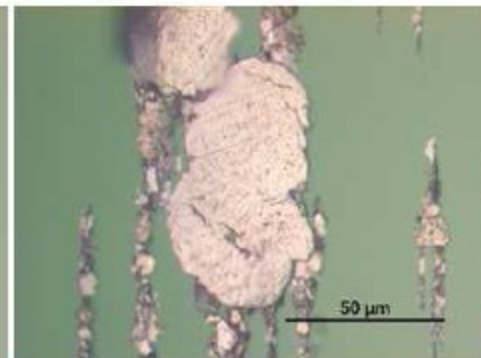
Fotografia 11



Ampliação: x 1000 Dilução: 1
Localização: Núcleo Luz: Branca / Verde

Observações: Ampliação da Fotografia 10. Partícula ferrosa de desgaste de fadiga com grandes dimensões.

Fotografia 12



Ampliação: x 1000 Dilução: 1
Localização: Núcleo Luz: Branca / Verde

Observações: Ampliação da Fotografia 10. Partícula ferrosa de desgaste de fadiga com grandes dimensões.

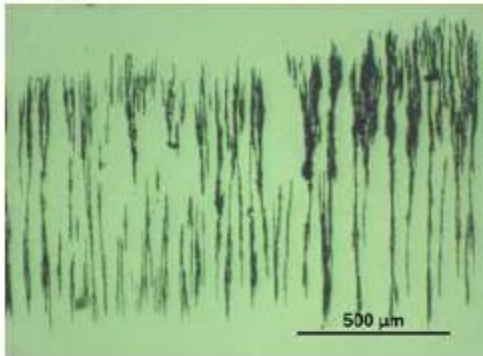
Os resultados apresentados referem-se exclusivamente às amostras ensaiadas.
Este documento não pode ser reproduzido, total ou parcialmente, sem a autorização por escrito do INEGI.

Pág. 6 / 7
Relatório Nº 23/10
MOD LAL-REL01

CLIENTE: **INEGI**
MORADA: Porto
DATA: 20/04/10

MÁQUINA: Máquina de Ensaios FZG
Ref. ÓLEO: PL (Power Loss - Low Oil)
ENSAIOS FZG - 20MnCr5 Gears 311 - K9

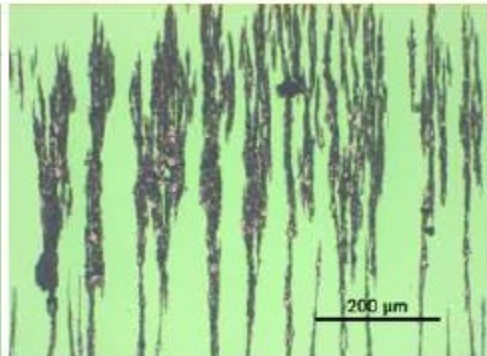
Fotografia 13



Ampliação: x 100 Diluição: 1
Localização: Núcleo Luz: Branca / Verde

Observações: Presença de partículas ferrosas de pequenas dimensões e algumas de grandes dimensões.

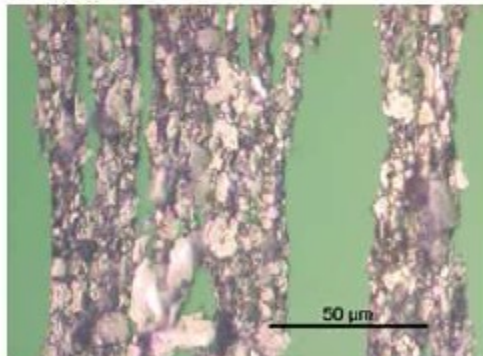
Fotografia 14



Ampliação: x 200 Diluição: 1
Localização: Núcleo Luz: Branca / Verde

Observações: Ampliação da Fotografia 13.
Presença de muito poucas partículas ferrosas de grandes dimensões.

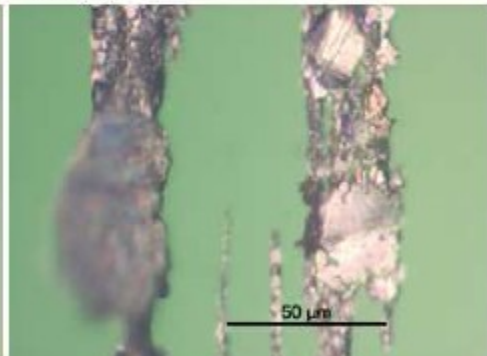
Fotografia 15



Ampliação: x 1000 Diluição: 1
Localização: Núcleo Luz: Branca / Verde

Observações: Ampliação da Fotografia 14.
Partículas ferrosas de pequenas e médias dimensões.

Fotografia 16



Ampliação: x 1000 Diluição: 1
Localização: Núcleo Luz: Branca / Verde

Observações: Ampliação da Fotografia 14.
Partículas ferrosas de grandes dimensões, algumas severamente oxidadas.

411 – P1 Churning Loss HO & LO + Power Loss: Low Oil



Relatório de Análise de Lubrificantes

Análise nº:	24-28 / 10
Tipo de análise:	Ferrometria e Ferrografia Analítica
Confidencialidade:	1
Cliente:	INEGI - Cetrib
Morada:	Porto
Telefone / Fax:	
Equipamento:	FZG (20MnCr5 – 411) Lado B
Lubrificante:	P1 (Power Loss – High Oil / Low Oil)
Dossier:	/
Nº de páginas:	8
Data:	12/05/2010
Responsável:	Beatriz Graça – Jorge Seabra
Rúbrica:	 

Os resultados apresentados referem-se exclusivamente às amostras ensaiadas.
Este documento não pode ser reproduzido, total ou parcialmente, sem a autorização por escrito do INEGI.

Pág. 1 / 8
Relatório Nº 28/10
MOD LAL-REL01



OBJECTIVO

Análise de quatro amostras de óleos lubrificantes – P1, resultantes de ensaios de Power Loss – High Oil (HO) / Low Oil (LO) na Máquina FZG com engrenagens de aço (20MnCr5, 411 - Lado B), para avaliação do desgaste presente.

As amostras analisadas foram as seguintes:

Amostra Nº	Ciclos	Análises efectuadas	
		Ferrometria	Ferrografia Analítica
K1 -HO	-	X	X
K1 - LO	-	X	X
K5 - LO	-	X	X
K7 - LO	-	X	X
K9 - LO	-	X	X

RESULTADOS DAS ANÁLISES

Nas páginas seguintes são apresentados os resultados referentes às análises de Ferrometria (DR III) e Ferrografia Analítica (FM III).

Os resultados apresentados referem-se exclusivamente às amostras ensaiadas.
Este documento não pode ser reproduzido, total ou parcialmente, sem a autorização por escrito do INEGI.

Pág. 2 / 8
Relatório Nº 28/10
MOD LAL-REL01



CLIENTE: <i>INEGI</i>		MÁQUINA: Máquina de Ensaios FZG					
MORADA: Porto		Ref. ÓLEO: F1					
DATA: 10/05/10		ENSAIOS FZG - 20MnCr5 Gears 411 - Lado B					
IDENTIFICAÇÃO							
Amostram ^o :	K1 - HO	K1 - LO	K5 - LO	K7 - LO	K9 - LO		
Data amostra:	Abr-10	Abr-10	Abr-10	Abr-10	Abr-10		
Análise n ^o :	24/10	25/10	26/10	27/10	28/10		
Ciclos/Máquina:	-	-	-	-	-		
Ciclos/Óleo:	-	-	-	-	-		
FERROMETRIA							
d:	1	1	1	1	1		
DL:	27,5	36,6	42,6	31,5	30,6		
DS:	12,5	19,9	15,6	15,8	14,4		
CPUC:	40,0	56,5	58,2	47,3	45,0		
ISUC:	600,0	943,6	1571,4	742,6	729,0		
FERROGRAFIA							
<input type="checkbox"/> Desgaste normal							
<input type="checkbox"/> Desgaste severo							
<input type="checkbox"/> Desgaste abrasão							
<input type="checkbox"/> Desgaste combinado							
<input type="checkbox"/> Desgaste fadiga							
<input type="checkbox"/> Esferas Metálicas							
<input type="checkbox"/> Ligas não ferrosas							
<input type="checkbox"/> Óxidos de ferro							
<input type="checkbox"/> Minerais/Orgânicos							
OIL VIEW							
Índice OilLife:							
Índice Oxidação:							
Índice Contaminação:							
Índice Ferromagnético:							
Grandes Contaminantes:							
Constante Dielétrica:							
FILTRAGEM							
(N ^o Partículas/10 ml)							
5 - 15 µm							
15 - 25 µm							
25 - 50 µm							
50 - 100 µm							
> 100 µm							
VISCOSIDADE							
(cSt a 40° C):							
ACIDEZ (TAN)							
(mg KOH)							
P. INFLAMAÇÃO							
(° C)							
DIAGNOSTICO:							
LEGENDA							
DL - Índice de partículas grandes							Não existe
DS - Índice de partículas pequenas							Fraco
CPUC - Concentração part. de desgaste							Médio
ISUC - Índice Severidade de Desgaste							Forte

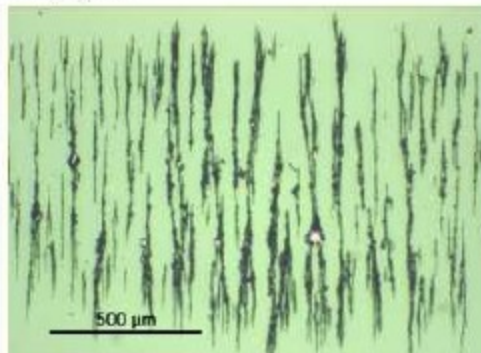
Os resultados apresentados referem-se exclusivamente às amostras ensaiadas.
 Este documento não pode ser reproduzido, total ou parcialmente, sem a autorização por escrito do INEGI.

Pág. 3 / 8
 Relatório Nº 28/10
 MOD LAL-REL01

CLIENTE: **INEGI**
MORADA: Porto
DATA: 10/05/10

MÁQUINA: Máquina de Ensaio FZG
Ref. ÓLEO: **P1 HIGH OIL - KI**
ENSAIOS FZG - 20MnCr5 Gears 411

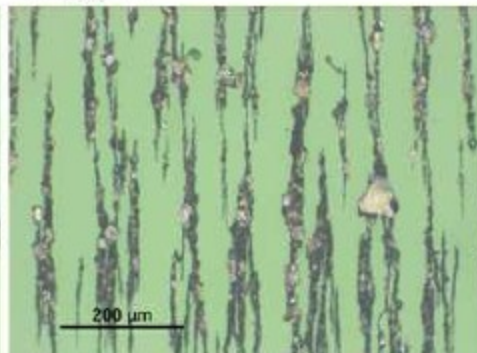
Fotografia 1



Ampliação: x 100 Dilução: 1
Localização: Núcleo Luz: Branca / Verde

Observações: Presença de partículas ferrosas de pequenas dimensões e algumas de grandes dimensões.

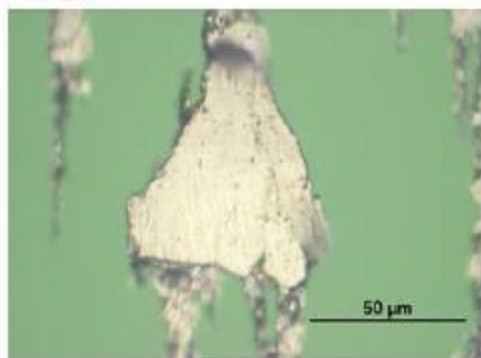
Fotografia 2



Ampliação: x 200 Dilução: 1
Localização: Núcleo Luz: Branca / Verde

Observações: Ampliação da Fotografia 1. Presença de algumas partículas ferrosas de grandes dimensões.

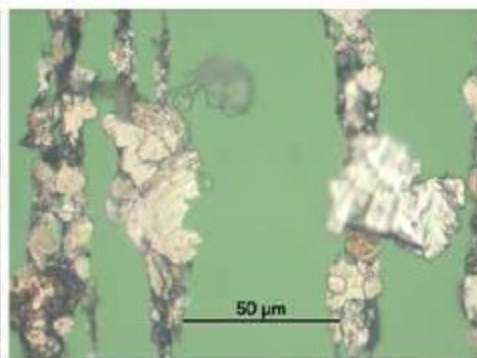
Fotografia 3



Ampliação: x 1000 Dilução: 1
Localização: Núcleo Luz: Branca / Verde

Observações: Ampliação da Fotografia 2. Partícula ferrosa laminar de grandes dimensões.

Fotografia 4



Ampliação: x 1000 Dilução: 1
Localização: Núcleo Luz: Branca / Verde

Observações: Ampliação da Fotografia 2. Partículas ferrosas de médias e grandes dimensões, algumas onduladas tenuemente.

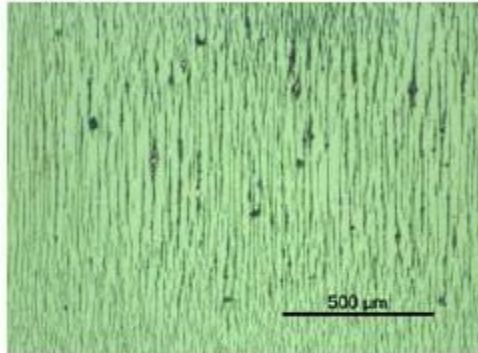
Os resultados apresentados referem-se exclusivamente às amostras ensaiadas.
Este documento não pode ser reproduzido, total ou parcialmente, sem a autorização por escrito do INEGI.

Pág. 4 / 8
Relatório Nº 28/10
MOD LAL-REL01

CLIENTE: **INEGI**
MORADA: Porto
DATA: 10/05/10

MÁQUINA: Máquina de Ensaios FZG
Ref. ÓLEO: P1 LOW OIL - KI
ENSAIOS FZG - 20MnCr5 Gears 411

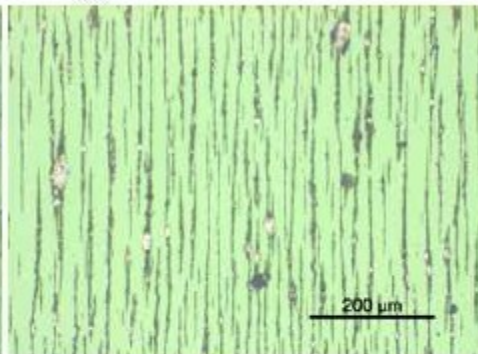
Fotografia 5



Ampliação: x 100 Diluição: 1
Localização: Núcleo Luz: Branca / Verde

Observações: Presença de partículas ferrosas de pequenas dimensões e algumas de grandes dimensões.

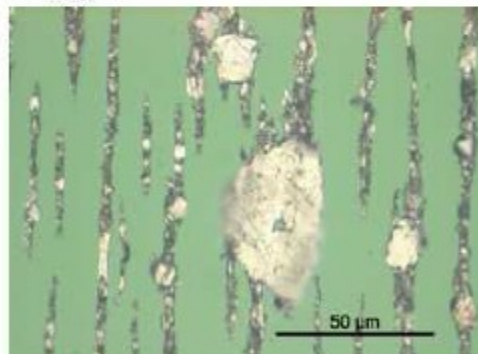
Fotografia 6



Ampliação: x 200 Diluição: 1
Localização: Núcleo Luz: Branca / Verde

Observações: Ampliação da Fotografia 5.
Presença de algumas partículas ferrosas de grandes dimensões.

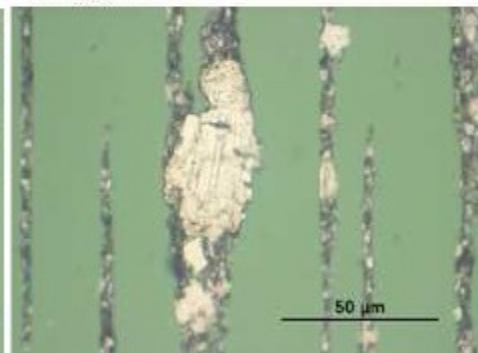
Fotografia 7



Ampliação: x 1000 Diluição: 1
Localização: Núcleo Luz: Branca / Verde

Observações: Ampliação da Fotografia 6.
Partícula ferrosa de desgaste de fadiga com grandes dimensões.

Fotografia 8



Ampliação: x 1000 Diluição: 1
Localização: Núcleo Luz: Branca / Verde

Observações: Ampliação da Fotografia 6.
Partícula ferrosa de desgaste de fadiga com grandes dimensões.

CLIENTE: **INEGI**

MORADA: Porto

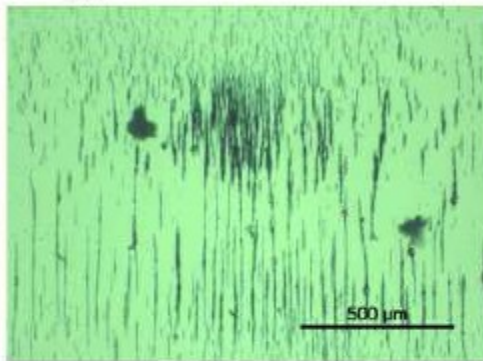
DATA: 10/05/10

MÁQUINA: Máquina de Ensaio FZG

Ref. ÓLEO: **P1 LOW OIL - K5**

ENSAIOS FZG - 20MnCr5 Gears 4L1

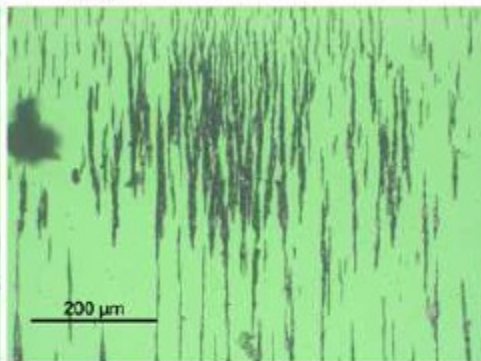
Fotografia 9



Ampliação: x 100 Diluição: 1
Localização: Núcleo Luz: Branca / Verde

Observações: Presença de partículas ferrosas de pequenas dimensões.

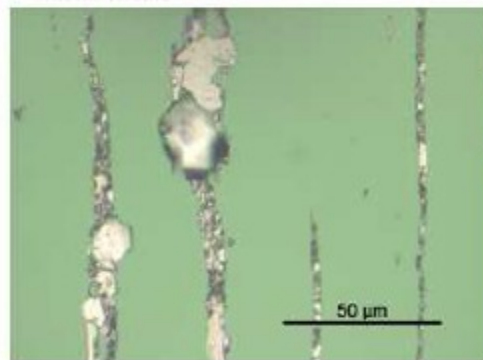
Fotografia 10



Ampliação: x 200 Diluição: 1
Localização: Núcleo Luz: Branca / Verde

Observações: Ampliação da Fotografia 9. Presença de poucas partículas ferrosas de grandes dimensões.

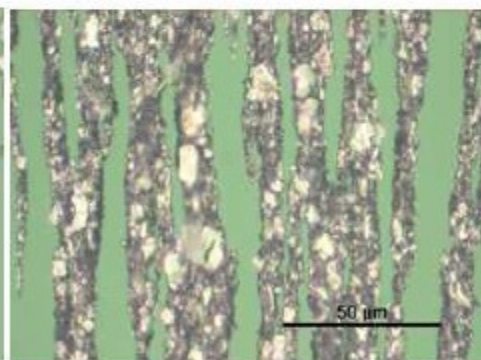
Fotografia 11



Ampliação: x 1000 Diluição: 1
Localização: Núcleo Luz: Branca / Verde

Observações: Ampliação da Fotografia 10. Partículas ferrosas de desgaste com médias dimensões.

Fotografia 12



Ampliação: x 1000 Diluição: 1
Localização: Núcleo Luz: Branca / Verde

Observações: Ampliação da Fotografia 10. Partículas ferrosas de desgaste de médias e pequenas dimensões.

Os resultados apresentados referem-se exclusivamente às amostras ensaiadas.
Este documento não pode ser reproduzido, total ou parcialmente, sem a autorização por escrito do INEGI.

Pág. 6 / 8

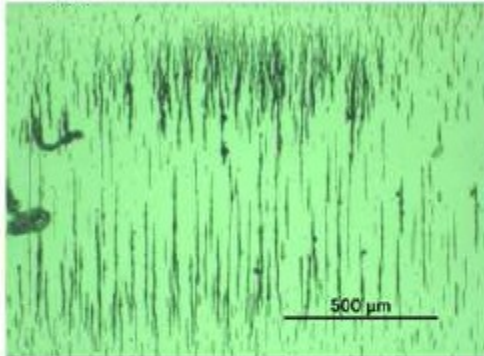
Relatório Nº 28/10

MOD LAL-REL01

CLIENTE: **INEGI**
MORADA: Porto
DATA: 10/05/10

MÁQUINA: Máquina de Ensaios FZG
Ref. ÓLEO: **P1 LOW OIL - K7**
ENSAIOS FZG - 20MrCr5 Gears 411

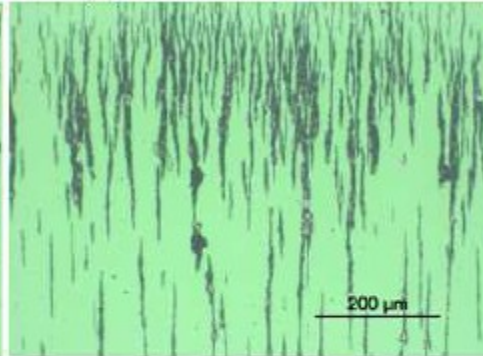
Fotografia 13



Ampliação: x 100 Diluição: 1
Localização: Núcleo Luz: Branca / Verde

Observações: Presença de partículas ferrosas de pequenas dimensões.

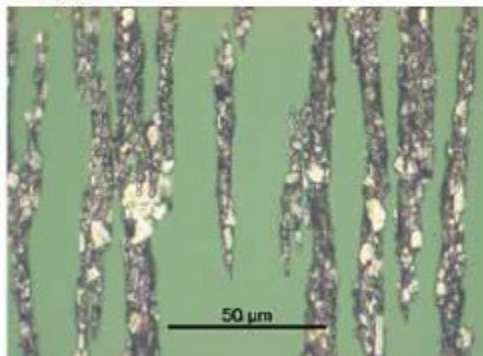
Fotografia 14



Ampliação: x 200 Diluição: 1
Localização: Núcleo Luz: Branca / Verde

Observações: Ampliação da Fotografia 13.
Presença de poucas partículas ferrosas de grandes dimensões.

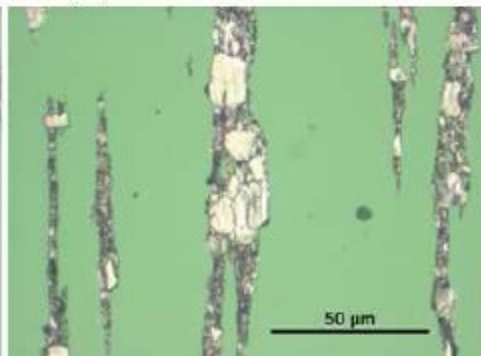
Fotografia 15



Ampliação: x 1000 Diluição: 1
Localização: Núcleo Luz: Branca / Verde

Observações: Ampliação da Fotografia 14.
Partículas ferrosas de desgaste de médias e pequenas dimensões.

Fotografia 16



Ampliação: x 1000 Diluição: 1
Localização: Núcleo Luz: Branca / Verde

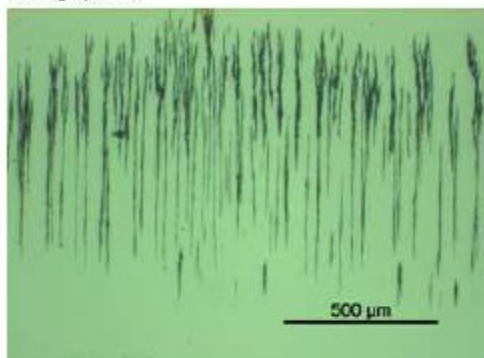
Observações: Ampliação da Fotografia 14.
Partículas ferrosas de desgaste de médias e pequenas dimensões.



CLIENTE: **INEGI**
MORADA: Porto
DATA: 10/05/10

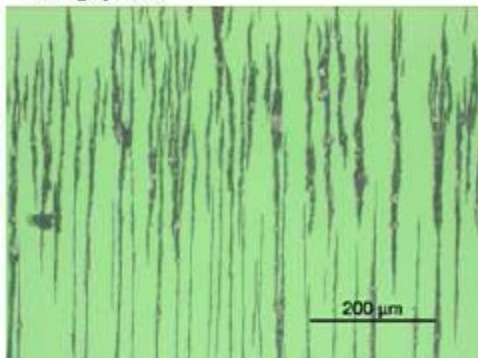
MÁQUINA: Máquina de Ensaio FZG
Ref. ÓLEO: **P1 LOW OIL - K9**
ENSAIOS FZG - 20MnCr5 Gears 411

Fotografia 17



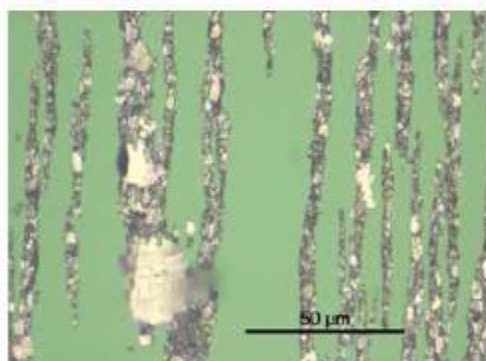
Ampliação: x 100 Dilução: 1
Localização: Núcleo Luz: Branca / Verde
Observações: Presença de partículas ferrosas de pequenas dimensões.

Fotografia 18



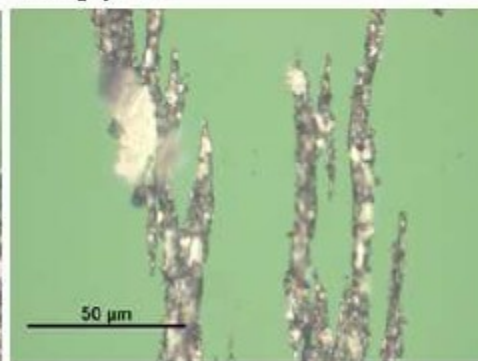
Ampliação: x 200 Dilução: 1
Localização: Núcleo Luz: Branca / Verde
Observações: Ampliação da Fotografia 17. Presença de poucas partículas ferrosas de grandes dimensões.

Fotografia 19



Ampliação: x 1000 Dilução: 1
Localização: Núcleo Luz: Branca / Verde
Observações: Ampliação da Fotografia 18. Partículas ferrosas de desgaste de médias e pequenas dimensões.

Fotografia 20



Ampliação: x 1000 Dilução: 1
Localização: Núcleo Luz: Branca / Verde
Observações: Ampliação da Fotografia 18. Partículas ferrosas de desgaste de médias e pequenas dimensões.



Os resultados apresentados referem-se exclusivamente às amostras ensaiadas.
Este documento não pode ser reproduzido, total ou parcialmente, sem a autorização por escrito do INEGI.

Pág. 8 / 8
Relatório Nº 28/10
MOD LAL-REL01

611 – P1 Churning Loss HO & LO + Power Loss: Low Oil



Relatório de Análise de Lubrificantes

Análise nº:	29-33 / 10
Tipo de análise:	Ferrometria e Ferrografia Analítica
Confidencialidade:	1
Cliente:	INEGI - Cetrib
Morada:	Porto
Telefone / Fax:	
Equipamento:	FZG (20MnCr5 – 611) Lado B
Lubrificante:	P1 (Power Loss – High Oil / Low Oil)
Dossier:	/
Nº de páginas:	8
Data:	21/05/2010
Responsável:	Beatriz Graça – Jorge Seabra
Rúbrica:	 

Os resultados apresentados referem-se exclusivamente às amostras ensaiadas.
Este documento não pode ser reproduzido, total ou parcialmente, sem a autorização por escrito do INEGI.

Pág. 1 / 8
Relatório Nº 33/10
MOD LAL-REL01



OBJECTIVO

Análise de cinco amostras de óleos lubrificantes – P1, resultantes de ensaios de Power Loss – High Oil (HO) / Low Oil (LO) na Máquina FZG com engrenagens de aço (20MnCr5, 411 - Lado B), para avaliação do desgaste presente.

As amostras analisadas foram as seguintes:

Amostra Nº	Ciclos	Análises efectuadas	
		Ferrometria	Ferrografia Analítica
K1 -HO	-	X	X
K1 - LO	-	X	X
K5 - LO	-	X	X
K7 - LO	-	X	X
K9 - LO	-	X	X

RESULTADOS DAS ANÁLISES

Nas páginas seguintes são apresentados os resultados referentes às análises de Ferrometria (DR III) e Ferrografia Analítica (FM III).



CLIENTE: INEGI		MÁQUINA: Máquina de Ensaios FZG					
MORADA: Porto		Ref. ÓLEO: P1					
DATA: 21/03/10		ENSAIOS FZG - 20MnCr5 Gears 611 - Lado B					
IDENTIFICAÇÃO							
Amostragem n°:	K1 - HO	K1 - LO	K5 - LO	K7 - LO	K9 - LO		
Data amostra:	Mai-10	Mai-10	Mai-10	Mai-10	Mai-10		
Análise n°:	29/10	30/10	31/10	32/10	33/10		
Ciclos/Máquina:	-	-	-	-	-		
Ciclos/Óleo:	-	-	-	-	-		
FERROMETRIA							
dk:	1	1	1	1	1		
DL:	56,7	62,7	83,5	73,6	63,9		
DS:	20,4	29,4	33,5	29,8	33,0		
CPUC:	77,1	92,1	117,0	103,4	96,9		
ISUC:	2798,7	3066,9	5850,0	4528,9	2994,2		
FERROGRAFIA:							
Desgaste normal							
Desgaste severo							
Desgaste abrasão							
Desgaste combinado							
Desgaste fadiga							
Esferas Metálicas							
Ligas não ferrosas							
Óxidos de ferro							
Minerais/Orgânicos							
OIL VIEW:							
Índice OilLife:							
Índice Oxidação:							
Índice Contaminação:							
Índice Ferromagnético:							
Grandes Contaminantes:							
Constante Dielétrica:							
FILTRAGEM							
(N° Partículas/10 ml)							
5 - 15 µm							
15 - 25 µm							
25 - 50 µm							
50 - 100 µm							
> 100 µm							
VISCOSIDADE							
(cSt a 40° C):							
ACIDEZ (TAN)							
(mg KOH)							
P. INFLAMAÇÃO							
(° C)							
DIAGNÓSTICO:							
LEGENDA:		DL - Índice de partículas grandes				Não existe	
		DS - Índice de partículas pequenas			I	Fraco	
		CPUC - Concentração part. de desgaste			M	Médio	
		ISUC - Índice Severidade de Desgaste			F	Forte	

Os resultados apresentados referem-se exclusivamente às amostras ensaiadas.

Este documento não pode ser reproduzido, total ou parcialmente, sem a autorização por escrito do INEGI.

Pag. 3 / 8

Relatório Nº 33/10

MOD LAL-REL01

CLIENTE: **INEGI**

MORADA: Porto

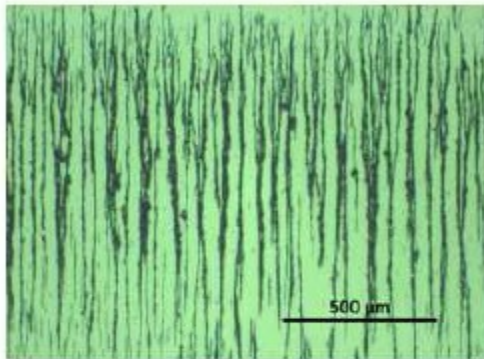
DATA: 21/05/10

MÁQUINA: Máquina de Ensaios FZG

Ref. ÓLEO: **P1 HIGH OIL - K1**

ENSAIOS FZG - 20MnCr5 Gears 611 - Lado B

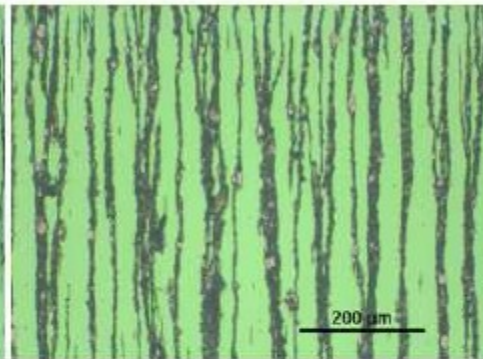
Fotografia 1



Ampliação: x 100 Diluição: 1
Localização: Núcleo Luz: Branca / Verde

Observações: Presença de partículas ferrosas de pequenas dimensões e algumas de grandes dimensões.

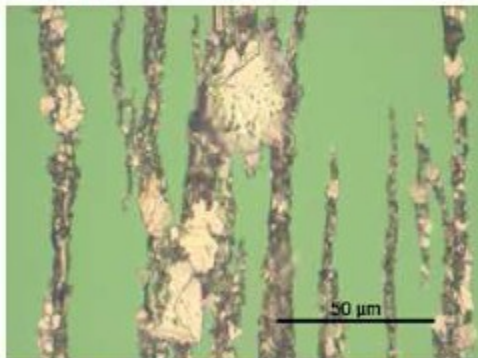
Fotografia 2



Ampliação: x 200 Diluição: 1
Localização: Núcleo Luz: Branca / Verde

Observações: Ampliação da Fotografia 1. Presença de algumas partículas ferrosas de grandes dimensões.

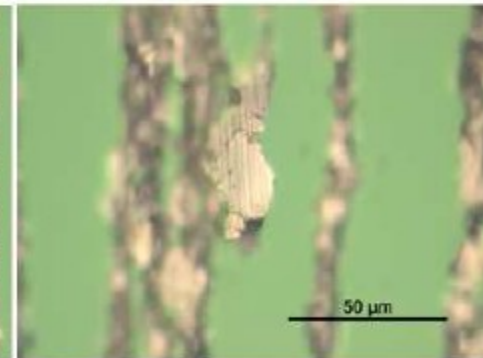
Fotografia 3



Ampliação: x 1000 Diluição: 1
Localização: Núcleo Luz: Branca / Verde

Observações: Ampliação da Fotografia 2. Partículas ferrosas de grandes dimensões.

Fotografia 4



Ampliação: x 1000 Diluição: 1
Localização: Núcleo Luz: Branca / Verde

Observações: Ampliação da Fotografia 2. Partícula ferrosa de desgaste combinado (fadiga + escorregamento).

Os resultados apresentados referem-se exclusivamente às amostras ensaiadas.
Este documento não pode ser reproduzido, total ou parcialmente, sem a autorização por escrito do INEGI.

Pág. 4 / 8
Relatório Nº 33/10
MOD LAL-REL01

CLIENTE: **INEGI**

MORADA: Porto

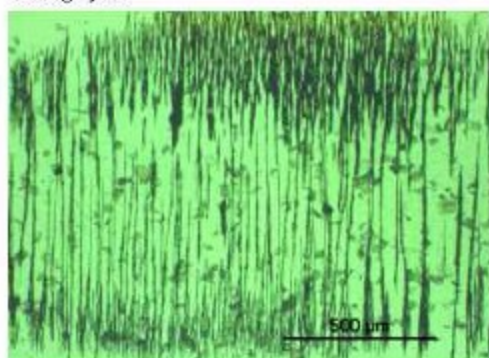
DATA: 21/05/10

MÁQUINA: Máquinas de Ensaio FZG

Ref ÓLEO: **P1 LOW OIL - K1**

ENSAIOS FZG - 20MnCr5 Gears 611 - Lado B

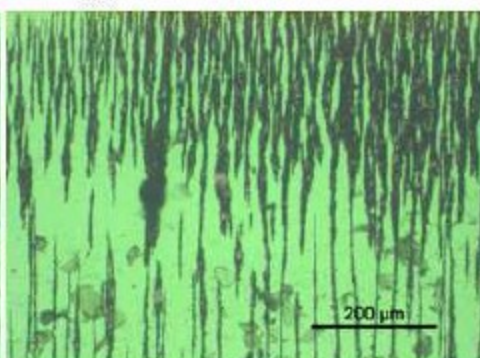
Fotografia 5



Ampliação: x 100 Diluição: 1
Localização: Núcleo Luz: Branca / Verde

Observações: Presença de partículas ferrosas de pequenas dimensões e algumas de grandes dimensões. Presença significativa de contaminantes externos.

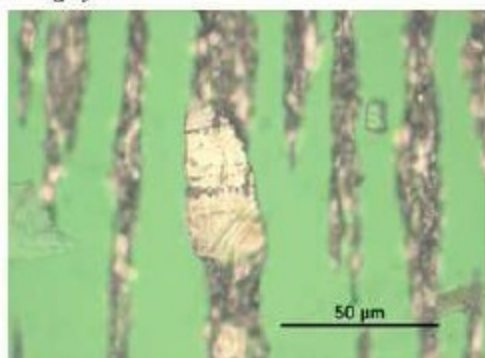
Fotografia 6



Ampliação: x 200 Diluição: 1
Localização: Núcleo Luz: Branca / Verde

Observações: Ampliação da Fotografia 5. Presença de algumas partículas ferrosas de grandes dimensões. Presença significativa de contaminantes externos.

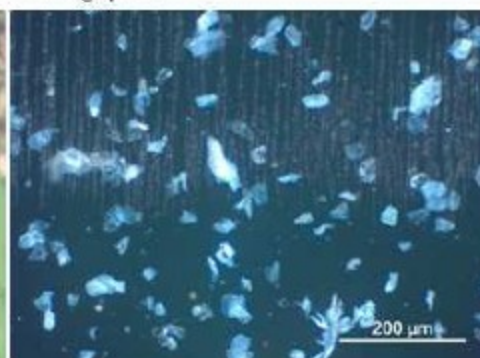
Fotografia 7



Ampliação: x 1000 Diluição: 1
Localização: Núcleo Luz: Branca / Verde

Observações: Ampliação da Fotografia 6. Partícula ferrosa de desgaste de fadiga com grandes dimensões.

Fotografia 8



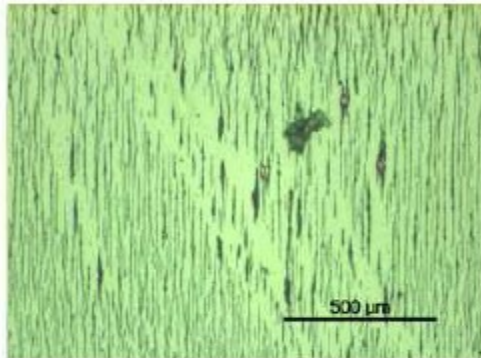
Ampliação: x 200 Diluição: 1
Localização: Núcleo Luz: Polarizada

Observações: Partículas contaminantes observadas com luz polarizada. O brilho emitido confirma a sua natureza não metálica.

CLIENTE: **INEGI**
MORADA: Porto
DATA: 21/05/10

MÁQUINA: Máquina de Ensaio FZG
Ref. ÓLEO: **P1 LOW OIL - K5**
ENSAIOS FZG - 20MnCr1 Gears 611 - Lado B

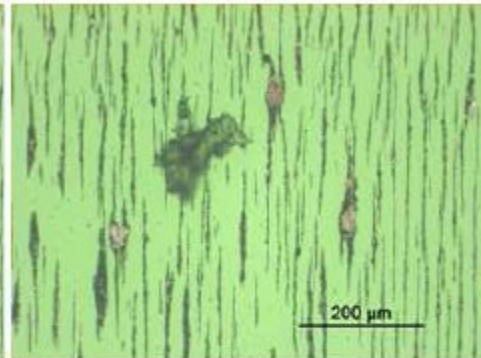
Fotografia 9



Ampliação: x 100 Dilução: 1
Localização: Núcleo Luz: Branca / Verde

Observações: Presença de partículas ferrosas de pequenas dimensões.

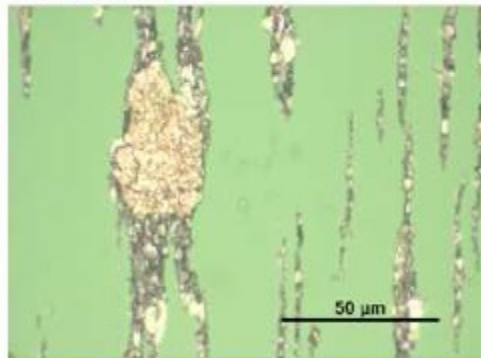
Fotografia 10



Ampliação: x 200 Dilução: 1
Localização: Núcleo Luz: Branca / Verde

Observações: Ampliação da Fotografia 9.
Presença de poucas partículas ferrosas de grandes dimensões.

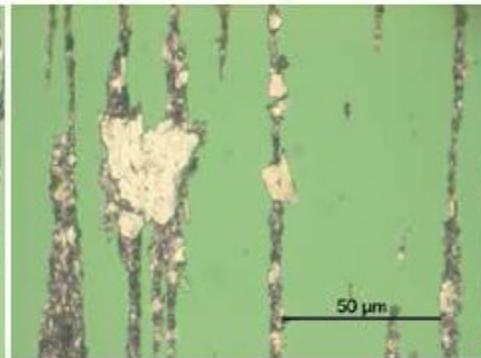
Fotografia 11



Ampliação: x 1000 Dilução: 1
Localização: Núcleo Luz: Branca / Verde

Observações: Ampliação da Fotografia 10.
Partícula ferrosa de desgaste com grandes dimensões.

Fotografia 12



Ampliação: x 1000 Dilução: 1
Localização: Núcleo Luz: Branca / Verde

Observações: Ampliação da Fotografia 10.
Partícula ferrosa de desgaste de grandes dimensões.

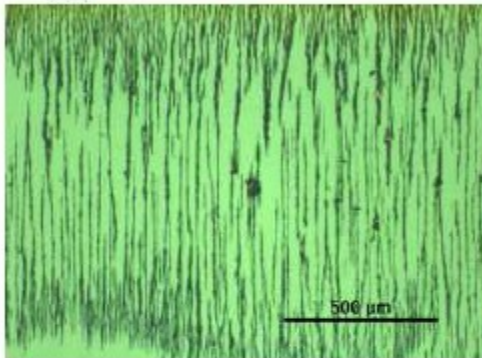
Os resultados apresentados referem-se exclusivamente às amostras ensaiadas.
Este documento não pode ser reproduzido, total ou parcialmente, sem a autorização por escrito do INEGI.

Pág. 6 / 8
Relatório Nº 33/10
MOD LAL-REL01

CLIENTE: **INEGI**
MORADA: Porto
DATA: 21/05/10

MÁQUINA: Máquina de Ensaios FZG
Ref. ÓLEO **PI LOW OIL - K7**
ENSAIOS FZG - 20MrCt5 Gears 611 - Lado B

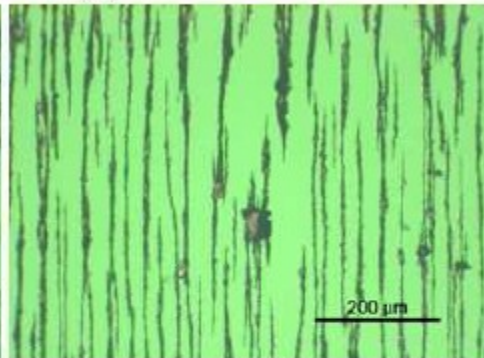
Fotografia 13



Ampliação: x 100 Diluição: 1
Localização: Núcleo Luz: Branca / Verde

Observações: Presença de partículas ferrosas de pequenas dimensões.

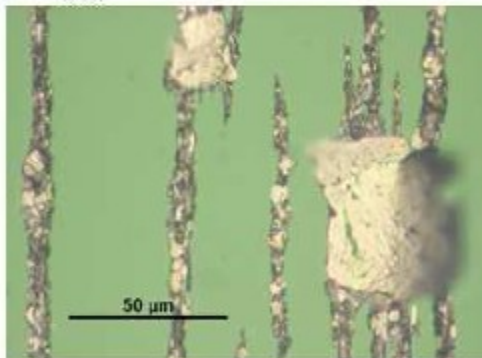
Fotografia 14



Ampliação: x 200 Diluição: 1
Localização: Núcleo Luz: Branca / Verde

Observações: Ampliação da Fotografia 13. Presença de poucas partículas ferrosas de grandes dimensões.

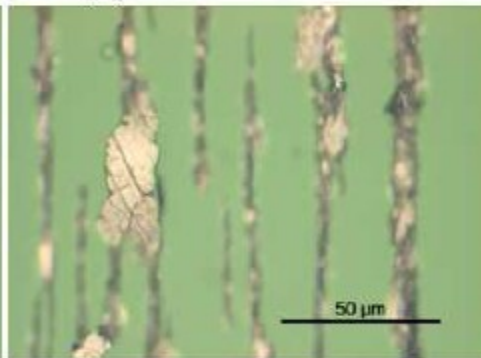
Fotografia 15



Ampliação: x 1000 Diluição: 1
Localização: Núcleo Luz: Branca / Verde

Observações: Ampliação da Fotografia 14. Partículas ferrosas de desgaste de médias e grandes dimensões típicas de desgaste de fadiga.

Fotografia 16



Ampliação: x 1000 Diluição: 1
Localização: Núcleo Luz: Branca / Verde

Observações: Ampliação da Fotografia 14. Partícula ferrosa de desgaste combinado (fadiga + escorregamento).

Os resultados apresentados referem-se exclusivamente às amostras ensaiadas.
Este documento não pode ser reproduzido, total ou parcialmente, sem a autorização por escrito do INEGI.

Pag. 7 / 8
Relatório Nº 33/10
MOD LAL-REL01

CLIENTE: **INEGI**

MORADA: Porto

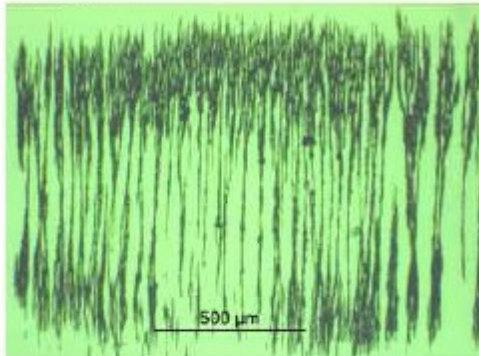
DATA: 21/05/10

MÁQUINA: Máquina de Ensaio FZG

Ref. ÓLEO: **P1 LOW OIL - K9**

ENSAIOS FZG - 20MnCr5 Gears 611 - Lado B

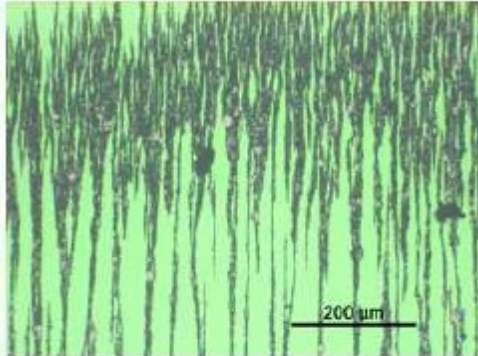
Fotografia 17



Ampliação: x 100 Diluição: 1
Localização: Núcleo Luz: Branca / Verde

Observações: Presença de partículas ferrosas de pequenas dimensões.

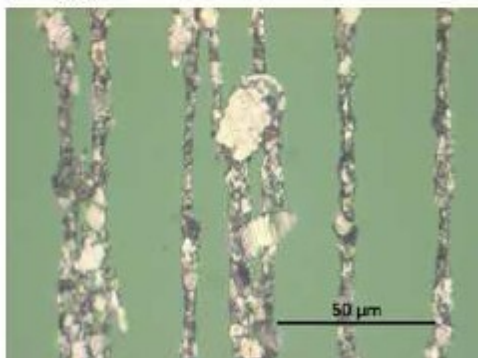
Fotografia 18



Ampliação: x 200 Diluição: 1
Localização: Núcleo Luz: Branca / Verde

Observações: Ampliação da Fotografia 17. Presença de poucas partículas ferrosas de grandes dimensões.

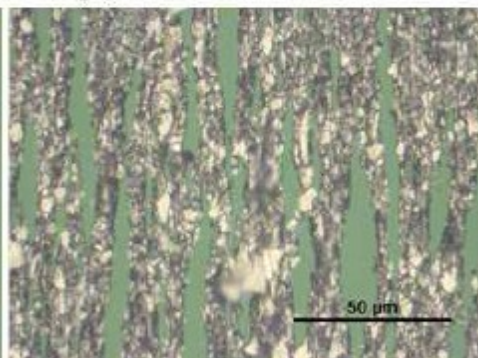
Fotografia 19



Ampliação: x 1000 Diluição: 1
Localização: Núcleo Luz: Branca / Verde

Observações: Ampliação da Fotografia 18. Partículas ferrosas de desgaste de médias e pequenas dimensões.

Fotografia 20



Ampliação: x 1000 Diluição: 1
Localização: Núcleo Luz: Branca / Verde

Observações: Ampliação da Fotografia 18. Partículas ferrosas de desgaste de médias e pequenas dimensões.

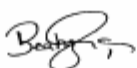

Os resultados apresentados referem-se exclusivamente às amostras ensaiadas.
Este documento não pode ser reproduzido, total ou parcialmente, sem a autorização por escrito do INEGI.

Pág. 8 / 8
Relatório Nº 33/10
MOD LAL-REL01

612 – P1 Power Loss: High Oil



Relatório de Análise de Lubrificantes

Análise nº:	05-08 / 10
Tipo de análise:	Ferrometria e Ferrografia Analítica
Confidencialidade:	1
Cliente:	INEGI - Cetrib
Morada:	Porto
Telefone / Fax:	
Equipamento:	FZG (ADI – 612)
Lubrificante:	P1
Dossier:	/
Nº de páginas:	7
Data:	19/02/10
Responsável:	Beatriz Graça – Jorge Seabra
Rúbrica:	 

Os resultados apresentados referem-se exclusivamente às amostras ensaiadas.
Este documento não pode ser reproduzido, total ou parcialmente, sem a autorização por escrito do INEGI.

Pág. 1 / 7
Relatório Nº 06/10
MOD LAL-REL01



OBJECTIVO

Análise de quatro amostras de óleo lubrificante P1 resultantes de ensaios na Máquina FZG com engrenagens de ADI, para avaliação do desgaste presente.

As amostras analisadas foram as seguintes:

Amostra Nº	Ciclos	Análises efectuadas	
		Ferrometria	Ferrografia Analítica
K1	840 000	X	X
K5	1 680 000	X	X
K7	2 520 000	X	X
K9	3 369 000	X	X

RESULTADOS DAS ANÁLISES

Nas páginas seguintes são apresentados os resultados referentes às análises de Ferrometria (DR III) e Ferrografia Analítica (FM III).



CLIENTE: INEGI		MÁQUINA: Máquina de Ensaios FZG					
MORADA: Porto		Ref. ÓLEO: P1 - 612					
DATA: 19/02/10		ENSAIOS FZG - ADI Gears					
IDENTIFICAÇÃO							
Amostragem:	K1	K3	K7	K9			
Data amostra:	Jan-10	Jan-10	Jan-10	Jan-10			
Análise nº:	05/10	06/10	07/10	08/10			
Ciclos/Máquina:	-	-	-	-			
Ciclos/Óleo:	-	-	-	-			
FERROMETRIA							
d:	0,1	0,1	0,1	0,1			
DL:	5,6	11,8	12,6	33,2			
DS:	2,7	4,7	5,6	9,2			
CPUC:	83,0	165,0	182,0	424,0			
ISUC:	2,4E+03	1,2E+04	1,3E+04	1,0E+05			
FERROGRAFIA							
Desgaste normal							
Desgaste severo							
Desgaste abrasão							
Desgaste combinado							
Desgaste fadiga							
Esferas Metálicas							
Ligas não ferrosas							
Óxidos de ferro							
Minerais/Orgânicos							
OIL VIEW							
Índice OilLife:							
Índice Oxidação:							
Índice Contaminação:							
Índice Ferromagnético:							
Grandes Contaminantes:							
Constante Dielétrica:							
FILTRAGEM							
(Nº Partículas/10 ml)							
5 - 15 µm							
15 - 25 µm							
25 - 50 µm							
50 - 100 µm							
> 100 µm							
VISCOSIDADE							
(cSt a 40° C):							
ACIDEZ (TAN)							
(mg KOH)							
P. ENFLAMAÇÃO							
(° C)							
DIAGNÓSTICO:							
LEGENDA							
DL - Índice de partículas grandes							Não existe
DS - Índice de partículas pequenas						F	Fraco
CPUC - Concentração part. de desgaste						M	Médio
ISUC - Índice Severidade de Desgaste						F	Forte

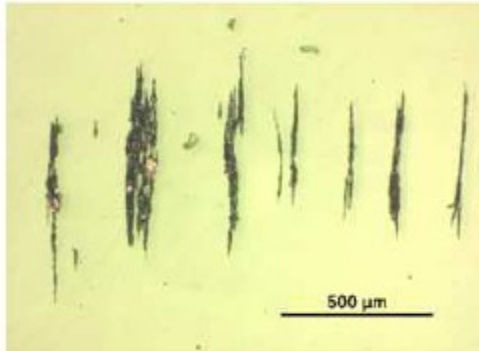
Os resultados apresentados referem-se exclusivamente às amostras ensaiadas.
 Este documento não pode ser reproduzido, total ou parcialmente, sem a autorização por escrito do INEGI.

Pág. 3 / 7
Relatório Nº 08/10
MOD LAL-REL01

CLIENTE: **INEGI**
MORADA: Porto
DATA: 19/02/10

MÁQUINA: Máquina de Ensaios FZG
Ref. ÓLEO: P1 - 612
ENSAIOS FZG - ADI Gears KI

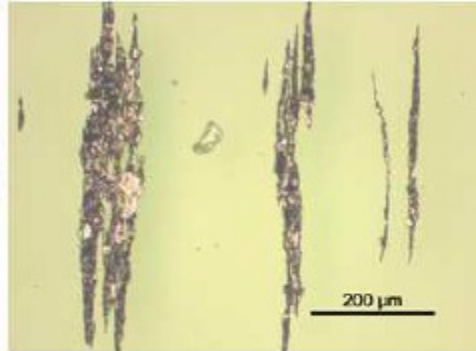
Fotografia 1



Ampliação: x 100 Dilução: 0,1
Localização: Núcleo Luz: Branca / Verde

Observações: Presença de partículas ferrosas de pequenas e algumas de grandes dimensões.

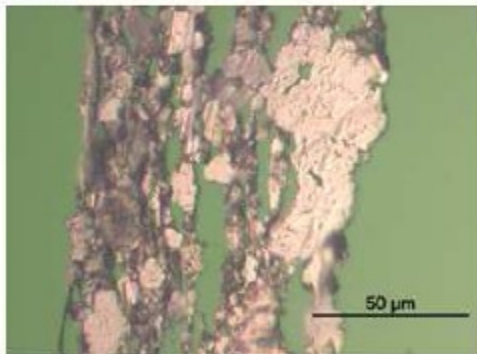
Fotografia 2



Ampliação: x 200 Dilução: 0,1
Localização: Núcleo Luz: Branca / Verde

Observações: Ampliação da Fotografia 1.
Presença de partículas ferrosas de pequenas e de poucas de grandes dimensões.

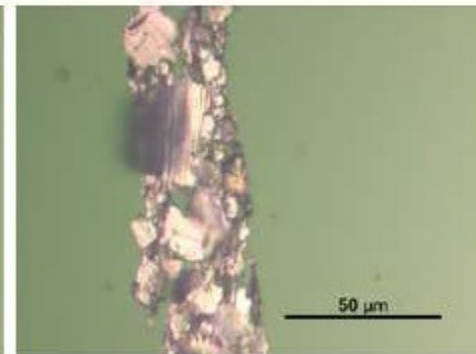
Fotografia 3



Ampliação: x 1000 Dilução: 0,1
Localização: Núcleo Luz: Branca / Verde

Observações: Ampliação da Fotografia 2.
Partícula ferrosa laminar, típica de fadiga e de grandes dimensões.

Fotografia 4



Ampliação: x 1000 Dilução: 0,1
Localização: Núcleo Luz: Branca / Verde

Observações: Partículas ferrosas laminares de média dimensão.

Os resultados apresentados referem-se exclusivamente às amostras ensaiadas.
Este documento não pode ser reproduzido, total ou parcialmente, sem a autorização por escrito do INEGI.

Pág. 4 / 7

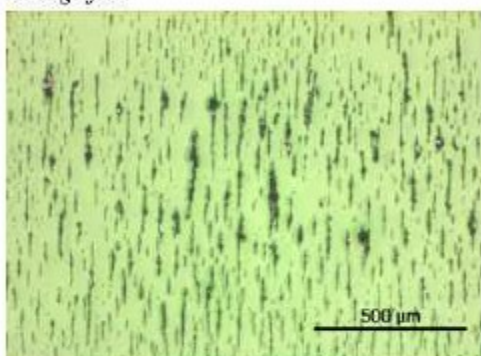
Relatório Nº 08/10

MOD LAL-REL01

CLIENTE: **INEGI**
MORADA: Porto
DATA: 19/02/10

MÁQUINA: Máquina de Ensaio FZG
Ref. ÓLEO: P1 - 612
ENSAIOS FZG - ADI Gears K5

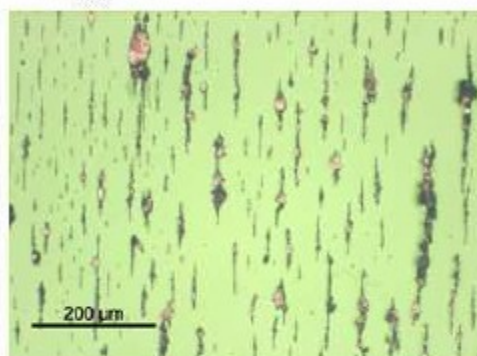
Fotografia 5



Ampliação: x 100 Diluição: 0,1
Localização: Núcleo Luz: Branca / Verde

Observações: Presença significativa de partículas ferrosas de pequenas e algumas de grandes dimensões.

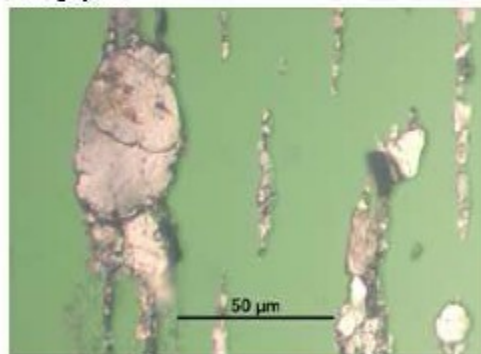
Fotografia 6



Ampliação: x 200 Diluição: 0,1
Localização: Núcleo Luz: Branca / Verde

Observações: Ampliação da Fotografia 5. Presença significativa de partículas ferrosas de pequenas e algumas de grandes dimensões.

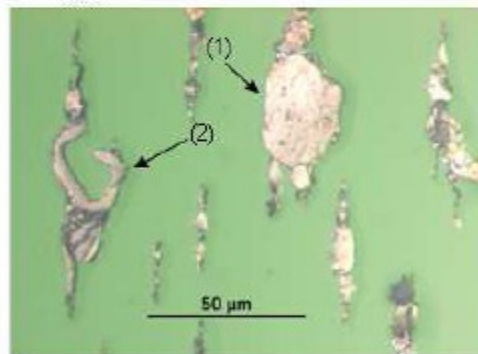
Fotografia 7



Ampliação: x 1000 Diluição: 0,1
Localização: Núcleo Luz: Branca / Verde

Observações: Ampliação da Fotografia 6. Partícula ferrosa de desgaste de fadiga com grandes dimensões e de forma arredondada.

Fotografia 8



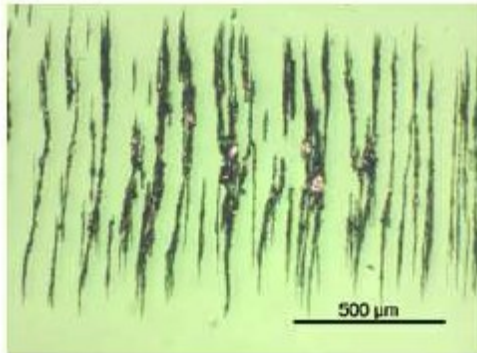
Ampliação: x 1000 Diluição: 0,1
Localização: Núcleo Luz: Branca / Verde

Observações: Ampliação da Fotografia 6.
(1) - Partícula ferrosa de desgaste de fadiga com grandes dimensões;
(2) - Partícula ferrosa de desgaste de corte.

CLIENTE: **INEGI**
MORADA: Porto
DATA: 19/02/10

MÁQUINA: Máquina de Ensaios FZG
Ref. ÓLEO: P1 - 612
ENSAIOS FZG - AD1 Gears K7

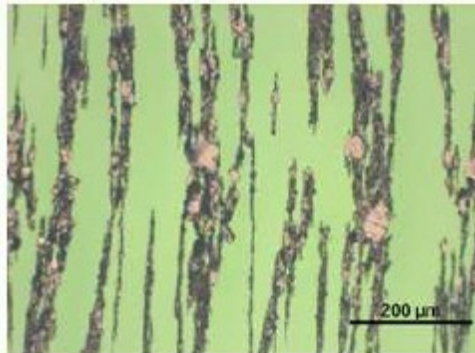
Fotografia 9



Ampliação: x 100 Dilução: 0,1
Localização: Núcleo Luz: Branca / Verde

Observações: Presença significativa de partículas ferrosas de pequenas e grandes dimensões.

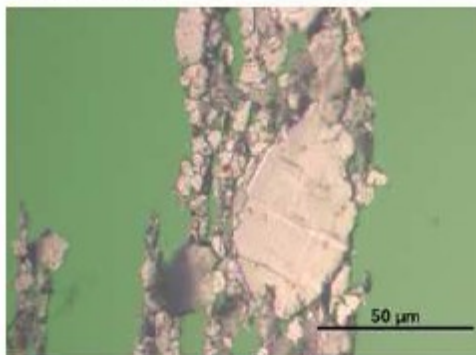
Fotografia 10



Ampliação: x 200 Dilução: 0,1
Localização: Núcleo Luz: Branca / Verde

Observações: Ampliação da Fotografia 9.
Presença de algumas partículas ferrosas de grandes dimensões.

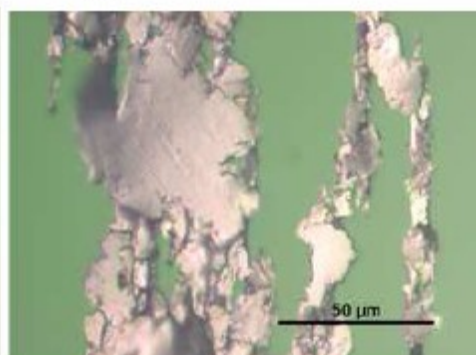
Fotografia 11



Ampliação: x 1000 Dilução: 0,1
Localização: Núcleo Luz: Branca / Verde

Observações: Ampliação da Fotografia 10.
Partícula ferrosa laminar de desgaste combinado e de grandes dimensões.

Fotografia 12



Ampliação: x 1000 Dilução: 0,1
Localização: Núcleo Luz: Branca / Verde

Observações: Ampliação da Fotografia 10.
Partículas ferrosas de desgaste de média e grande dimensão.

Os resultados apresentados referem-se exclusivamente às amostras ensaiadas.
Este documento não pode ser reproduzido, total ou parcialmente, sem a autorização por escrito do INEGI.

Pág. 6 / 7
Relatório Nº 08/10
MOD LAL-REL01

CLIENTE: **INEGI**

MORADA: Porto

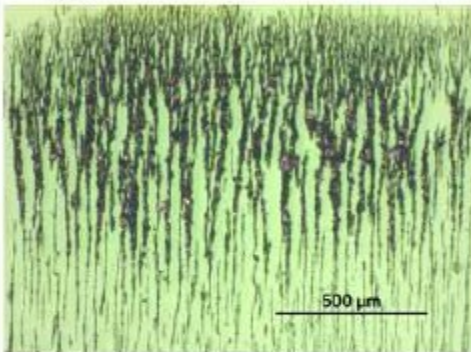
DATA: 19/02/10

MÁQUINA: Máquina de Ensaio FZG

Ref. ÓLEO: P1 - 612

ENSAIOS FZG - ADI Gears K9

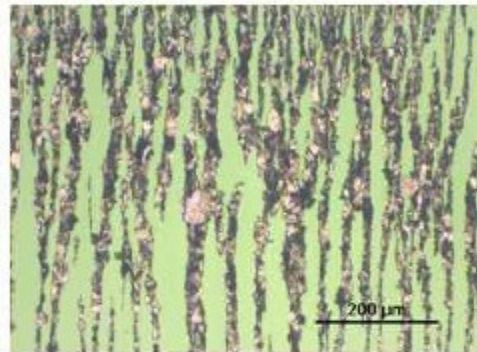
Fotografia 13



Ampliação: x 100 Diluição: 0,1
Localização: Núcleo Luz: Branca / Verde

Observações: Presença significativa de partículas ferrosas de pequenas dimensões e grandes dimensões.

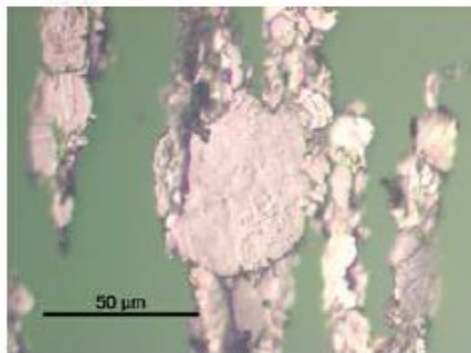
Fotografia 14



Ampliação: x 200 Diluição: 0,1
Localização: Núcleo Luz: Branca / Verde

Observações: Ampliação da Fotografia 13. Presença significativa de partículas ferrosas de pequenas dimensões e algumas de grandes dimensões.

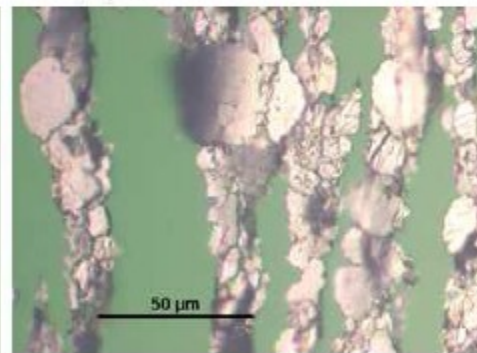
Fotografia 15



Ampliação: x 1000 Diluição: 0,1
Localização: Núcleo Luz: Branca / Verde

Observações: Ampliação da Fotografia 14. Partícula ferrosa de grandes dimensões e forma arredondada.

Fotografia 16



Ampliação: x 1000 Diluição: 0,1
Localização: Núcleo Luz: Branca / Verde

Observações: Ampliação da Fotografia 14. Presença significativa de partículas de médias dimensões e formas arredondadas.

Appendix D: Hydrostatic and Hydrodynamic Lubrication

A. Lubrication: Introduction and Basic Theory

i. Introduction.

Lubrication is one branch of tribology which pay special attention to contacts were a viscous fluid film separates two contacting surfaces. This fluid film can be a nearly compressible liquid like oils, water, etc; can also be a compressible gas which in most cases is air whose density varies widely with pressure[10].

The fluid film should separate completely the contacting surfaces, supposing that roughness and eventual superficial defects are smaller than oil the film thickness otherwise there will be contacting points between the surfaces being in presence of mix lubrication or in more extreme cases in presence of limit lubrication.

Lubricants capacity evolved along the years driven by the evolution of the mechanical components and it's demanding for more and better lubricants that could deal better with friction, minimization of superficial wear, evacuate a greater amount of heat from the contact area, ability to stop corrosion and be able to mix with chemical substances that improve their performance [34].

Besides all the concerns referred previously we need to add a couple more that have been growing along the years, and those concerns are the environmental awareness and the need for minimization of lubricant impact into nature, leading the search for low toxicity and biodegradable lubricants [6, 34].

Progress and the technological evolution lead to an increase of equipments with more and higher solicitations leading to an increase of the mechanical components temperature raising the need for a better and larger amount of lubricant[34].

Oils are one of the most common lubricants and they are mainly composed by a base fluid called "base lubricant", this base can have a mineral or synthetic origin, being added on top a package of additives which nature depends of the application it is being prepared to. The most common are the mineral based oils due to their low price and abundance in nature, but the synthetic oils are starting to appear more often from these last years, due to the need to solve specially hard lubrication problems.

In order for lubrication to be effective the lubricant need the have the correct viscosity in order to maintain a steady fluid film under operative conditions and on the other hand allow the fluid to flow in order to remove the heat and neutralize the power loss due to viscous drag.

To guarantee the correct formation and preservation of the fluid film is necessary the existence of a pressure applied to the film to balance the loads applied between the surfaces of the mechanism [10]. To the case were the pressure is generated by a system exterior to the contact, like the case of some bearings, it's called *hydrostatic* lubrication. When the pressure is generated by the relative movement of the surfaces, like the case of axial bearings, we call it *Hydrodynamic* lubrication [10]. This last type of lubrication is characterized by the lubricant being dragged to the contact due to the surface geometry and cinematic, being the oil so highly compressed between the surfaces of the contact that generates elastic deformation of the surfaces, being therefore called *ElastoHydrodynamic* lubrication.

These types of lubrication are described more accurately in the following chapters being special attention paid to the ElastoHydrodynamic lubrication because is the lubrication regime present in gears.

ii. Basic film Theory.

Lubrication and film formation was and still is studied intensively and film behavior can be described by mathematical and mechanical laws that allow us to calculate the film velocity field, pressure and shear stress. The most common laws that describe the fluids and the fluid mechanics are the Navier-Stokes and Reynolds equations but before presenting those principles, are pertinent to present some basic laws first. Those are the continuous mechanics laws, being in the origin of the Slim Newtonian film general equations. The continuum Mechanics laws are:

- Mass Conservation law:

$$\frac{\partial \rho}{\partial t} + \frac{\partial}{\partial x_1} (\rho u_1) = 0 \quad (\text{Eq. 19})$$

- Dynamics fundamental law:

$$\rho \left(\frac{\partial u_i}{\partial t} + u_j \frac{\partial u_i}{\partial x_j} \right) = \rho f_i + \frac{\partial \sigma_{ij}}{\partial x_j} \quad (\text{Eq. 20})$$

- Reologic behavior law for a Newtonian fluid:

$$\sigma_{ij} = (-p + \lambda \theta) \delta_{ij} + 2\mu \dot{\epsilon}_{ij} \quad (\text{Eq. 21})$$

- Energy conservation law for a Newtonian fluid:

$$\begin{aligned} \rho C_p \frac{dT}{dt} = \alpha T \frac{dP}{dt} + \frac{\partial}{\partial x_i} \left(k \frac{\partial T}{\partial x_i} \right) + \lambda \left(\frac{\partial u_i^2}{\partial x_i} \right) \\ + \mu \frac{\partial u_i}{\partial x_j} \left(\frac{\partial u_i}{\partial x_j} + \frac{\partial u_j}{\partial x_i} \right) \end{aligned} \quad (\text{Eq. 22})$$

The general equations of the thin viscous film mechanics are used to determine the characteristics of a thin film specially the sustentation force, being obtained from the continuous mechanics equations applied to a Newtonian fluid.

Not being the objective of this work the deduction of these equations there will be presented just the initial assumptions and the final equation for exemplification purposes.

Assuming then that when in a laminar flow, mass exterior forces are neglected, the Navier equations are written this way:

$$\begin{aligned} & \rho \left(\frac{\partial u_i}{\partial t} + u_j \frac{\partial u_i}{\partial x_j} \right) \\ &= -\frac{\partial P}{\partial x_i} + \lambda \frac{\partial^2 u_j}{\partial x_i \partial x_j} + \mu \left(\frac{\partial^2 u_i}{\partial x_j^2} + \frac{\partial^2 u_j}{\partial x_i \partial x_j} \right) \\ &+ \frac{\partial u_j}{\partial x_j} \frac{\partial \lambda}{\partial x_i} + \left(\frac{\partial u_i}{\partial x_i} + \frac{\partial u_j}{\partial x_i} \right) \frac{\partial \mu}{\partial x_j} \end{aligned} \quad (\text{Eq. 23})$$

Knowing the border conditions and using the equations mentioned before we are able to reach to the film velocity field, pressure and shears stress.

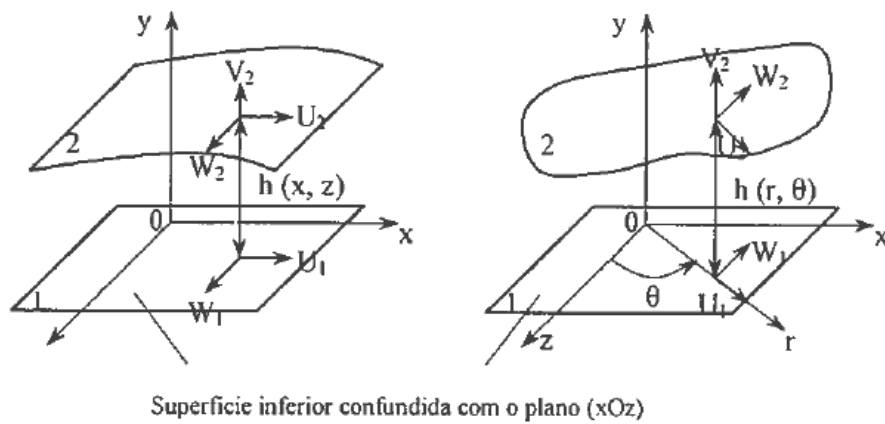


Figure 85 – Axis system[10].

After several calculation steps we finally get the thin viscous film mechanics generalized equation:

$$\begin{aligned}
& \frac{\partial}{\partial x_1} \left(G \frac{\partial P}{\partial x_1} \right) + \frac{\partial}{\partial x_3} \left(G \frac{\partial}{\partial x_3} \right) \\
&= \frac{\partial}{\partial x_1} [U_{21}(R_2 - F) + U_{11}F] - \rho_2 U_{21} \frac{\partial H_2}{\partial x_1} \\
&+ \rho_1 U_{11} \frac{\partial H_1}{\partial x_1} + \frac{\partial}{\partial x_1} [U_{23}(R_2 - F) + U_{13}F] \quad (\text{Eq. 24}) \\
&- \rho_2 U_{23} \frac{\partial H_2}{\partial x_3} + \rho_1 U_{13} \frac{\partial H_1}{\partial x_3} + \frac{\partial R_2}{\partial t} - \rho_2 \frac{\partial H_2}{\partial t} \\
&+ \rho_1 \frac{\partial H_1}{\partial t} + \rho_2 U_{22} - \rho_1 U_{12}
\end{aligned}$$

Being R , F and G defined by:

$$\mathbf{R} = \int_{H_1}^{x_2} \rho(x_1, \xi, x_3, t) d\xi \quad (\text{Eq. 25})$$

$$\mathbf{F} = \frac{1}{J_2} \int_{H_1}^{H_2} \frac{\mathbf{R}}{\mu} dx_2 \quad (\text{Eq.26})$$

$$\mathbf{G} = \int_{H_1}^{H_2} \frac{\mathbf{R}}{\mu} \left(x_2 - \frac{I_2}{J_2} \right) dx_2 = \int_{H_1}^{H_2} \frac{\mathbf{R}x_2}{\mu} dx_2 - I_2 \mathbf{F} \quad (\text{Eq. 27})$$

The thin viscous film equation is the most general form of the Reynolds equation and to be able to obtain it was necessary to take some consideration into account[10]:

- A continuous environment;
- the fluid is Newtonian;
- mass exterior forces were neglected;
- inertia forces were neglected;
- no sliding between the fluid and contact surfaces;
- the thickness in Ox_2 axis is always much smaller compared to other dimension of contact (basic hypotheses of contact mechanics).

Table 30 – Nomenclature of the thin viscous fluid mechanics equation.

Nomenclature	
Symbol	Designation
$x_{i,j}$	Space variable
t	Time variable
$u_{i,j}$	Speed components
ρ	Density
f_i	Mass exterior forces
$\sigma_{i,j}$	Stress tensor
E	Internal energy
K	Fluid Thermal Conductibility coefficient
T	Temperature
P	Pressure
$\epsilon_{i,j}$	Deformation tensor
θ	Cubic dilatation coefficient
$\delta_{i,j}$	Kronecker symbol
λ	Space Navier coefficient
μ	Time Navier coefficient
C_p	Mass heat(const. Pressure)
$A=(1-\rho)(\partial\rho/(\partial t))_p$	Calorimetric dilatation coefficient(const. Pressure)

B. Hydrodynamic Lubrication

Hydrodynamic lubrication has mentioned before, relies on relative motion between two surfaces to form a film layer strong enough to bear the loads transferred from the surfaces[9]. In order to do so there are two possibilities, one is by wedging the lubricant into a convergent gap with the tangential surface velocities, known as “wedging film action”, or squeezing the lubricant out of the contact, using the relative normal velocity between the surfaces, known as “squeeze film action” [15].

In a converging hydrodynamic slider the inlet section has a higher film thickness than the outlet section allowing this section to have a larger amount of lubricant entering, therefore considering the slider to be infinitely wide and in order to have a constant flow along the slider section, the lubricant should have an increasing pressure and low speed on the inlet section and low pressure and high speed in the outlet section[15], has you can see in Figure 86.

This type of behavior is typical of hydrodynamic lubrication, but doesn't happens just in flat sliders, it is present in curve and spherical sliders lubricant rollers, journal bearings, ball bearings, etc. For the case where the surfaces are parallel formation of a hydrodynamic film is compromised due mainly to the lack of the wedging effect. This problem can be solved if instead of a pressure and speed differential caused by wedging action we generate this using a downward movement of the slider with a velocity normal to the surface, being generated a pressure differential by squeezing, leading the lubricant to escape for both sides generating a parabolic pressure profile similar to the one formed in the wedging film action[15](Figure 87).

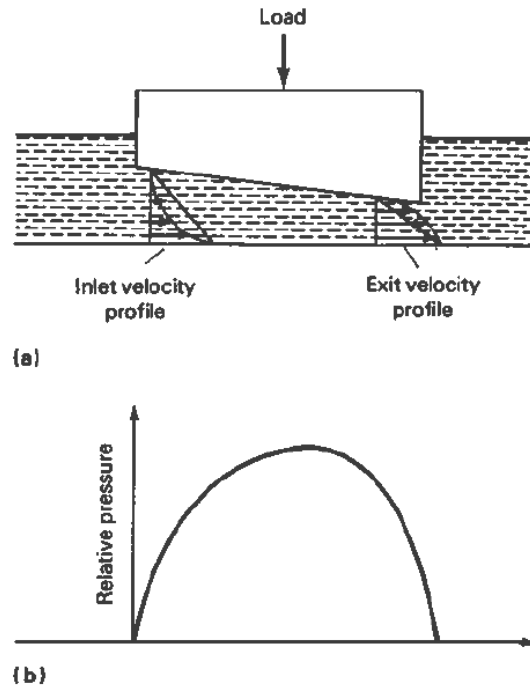


Figure 86 – Wedging film action in a hydrodynamic slider. a) Velocity profiles at inlet and outlet region in wedge shape load. b) Pressure distribution beneath the wedge[15].

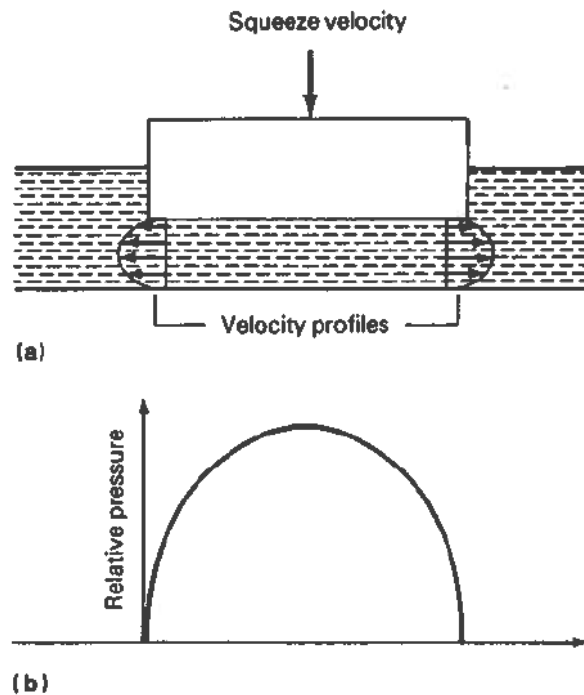


Figure 87 – Squeeze film action in a hydrodynamic slider. a) Equal velocity profiles generated at each end of a flat slider that moves downward due to a squeeze velocity in a normal direction to the slider surface. b) Pressure distribution beneath flat slider[15].

Bearings operating under the effect of dynamic loads can have squeeze film action at the same time as wedging film action, being the pressure generated by squeeze film action able to reach significant levels to provide an effective damping component for high-speed rotor-bearing systems stabilization[15].

C. Hydrostatic Lubrication

In hydrodynamic mechanisms load supporting pressure is generated due to the relative movement of the contact surfaces in the presence of a wedge. If for some reason the movement necessary to generate pressure don't exists or is not enough to bear the entire load, there comes the need to resort to the hydrostatic lubrication[10], which consists in injecting pressurized fluid between the contacting surfaces(Figure 88) in order to generate fluid film[15]. This type of lubrication is present in bearings per example, being the most common ways to introduce fluid inside a bearing (assuming liquid lubricants only):

Constant pressure feed;

Constant debt feed.

In constant pressure systems, the bearing is feed through as hydraulic resistance whose load loss is in function of the debt, which ensures good system stiffness.

In constant debt systems, a constant debt pump is placed between the reservoir and the lubricant admission hole in the bearing. These types of systems are generally very complex and expensive, therefore not much used in practical applications.[10]

The main advantages of hydrostatic lubrication and hydrostatic bearings are:

1. Both surfaces are always separated by a lubricant film even when there is surfaces are stopped which leads to virtually no wear;
2. Pressure is spread by a wide surface avoiding pressure concentration areas;
3. Because the pressure force is generated by surface action, manufacture defects effect is reduced.

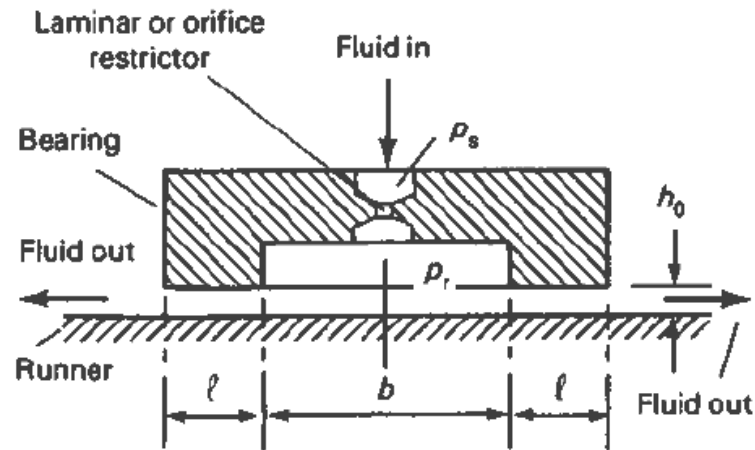


Figure 88 – schematics showing the key parameters that determine the operation of a hydrostatic bearing. Nomenclature: p_s , supply pressure; p_r , recess pressure; h_0 , film thickness; b , bearing pocket diameter; l , bearing load thickness[15].

In a hydrostatic bearing (Figure 88) the pocket pressure, the film thickness and the lubricant flow depends directly on the bearing load, therefore for a heavy load, the pocket pressure comes closer to the supply pressure, yielding a very small flow and consequently, a low film thickness, happening the exact opposite for a light load.